PHOSPHORYLATION AND BEYOND: EXPLORATION OF TOR-MEDIATED PTM SIGNALING IN *CHLAMYDOMONAS REINHARDTII*

Megan M. Ford

A dissertation submitted to the faculty at the University of North Carolina at Chapel Hill in partial fulfillment of the requirements for the degree of Doctor of Philosophy in the Department of Chemistry in the School of Arts and Sciences.

Chapel Hill
2021

Approved by:

Leslie M. Hicks

Gary L. Glish

Lee M. Graves

Matthew R. Lockett

Marcey L. Waters

ABSTRACT

Megan M. Ford: Phosphorylation and Beyond: Exploration of TOR-mediated PTM Signaling in *Chlamydomonas reinhardtii*
(Under the direction of Leslie M. Hicks)

Target of rapamycin (TOR) is a highly conserved master regulatory kinase involved in the control of most essential biological processes including cell growth, nutrient sensing, and autophagy. While TOR is well-studied in mammalian species and yeast, comparatively little is known about its regulatory roles in other organisms, particularly in phototrophs. To fill this knowledge gap, the plant community is applying -omic strategies to assess the role of TOR in regulating metabolic pathways, particularly proteomics, which provides insight into expression levels and modifications that is missing in other techniques. Post-translational modifications (PTMs) to activate/deactivate functional proteins are an essential component of cellular signaling used by TOR and other regulators. This has propelled innovations in PTM analysis to probe metabolic pathways. *Chlamydomonas reinhardtii* is a model phototroph that is easily culturable and has a fully sequenced genome, making it an attractive organism for studying algal TOR signaling. The aim of this dissertation is to establish and apply PTM-focused proteomic methods in *Chlamydomonas* to characterize the role of protein phosphorylation and reversible oxidation in TOR's regulation of signaling networks.

First, this work investigates reversible oxidation sites under the control of TOR in *Chlamydomonas* through a quantitative inhibition study (Chapter 2). Next, a quantitative workflow for phosphopeptide analysis in *Chlamydomonas* that can be used to assess phosphorylative TOR signaling is described in detail with technical replicates to assess its

overall reproducibility (Chapter 3). Application of the quantitative phosphoproteomic pipeline was then employed to study the impact of inositol polyphosphates on TOR signaling (Chapter 4). Techniques for performing *in vitro* kinase screening to identify direct targets of phosphorylation, are discussed including heterologous expression of kinase samples, preparation of a library of potential targets, screening parameters, and sample preparation for LC-MS/MS analysis (Chapter 5). This workflow provides insight into signaling pathways that cannot be gleaned from proteomic *in vivo* studies alone. Using these techniques, this kinase screening platform was validated using the pyruvate dehydrogenase kinase of *Arabidopsis thaliana*, and then applied to attempt to identify putative direct targets of *Chlamydomonas* TOR (Chapter 6). While this technique was unable to identify direct TOR targets, the success of the validation suggests that with further optimization of the expression and purification of the kinase construct, screening of TOR may be possible. Combined, the work shared herein highlights the importance of TOR in algal signaling and provides valuable information on the regulatory modifications under TOR control.

Soli Deo gloria

ACKNOWLEDGMENTS

I would like to begin by thanking Leslie M. Hicks, who has been not only my advisor, but a mentor and advocate. Her leadership helped to shape the Hicks laboratory into a special place to work and it has been a privilege to be a part of such an exceptional group of researchers. I want to thank all of the members of the Hicks group that I have spent countless hours working with. I will always be grateful for your support, encouragement, honest editing, and humor. Special thanks to my fellow classmates who made my experience in graduate school, particularly those early years, so enjoyable and memorable. I also want to thank all of my friends in the math and computer science departments for the many nights of trivia, board games, and fun!

My husband Andrew and I made a home in North Carolina thanks in large part to the wonderful people we met at Church of the Good Shepherd. Through this community, we found more than just friendship, we found family. Thank you to our young adult friends for the countless board game nights, Monday Growler Grlz hangouts, and potlucks. In particular, I want to thank the members of our small group who have been there for the ups and downs of graduate school, new marriages, and pet parenting.

Above all, I need to thank my family and friends for their endless support and encouragement. Thank you for all the cards, care packages, and trips to NC to come see us! I want to thank my in laws for their love, kindness, and generosity. To my sister, I could not have imagined how close we would become as adults. You, Hunter, and Baby J mean the world to me. To my mom and dad, you never let myself or others set limits on who I can become. Without your unwavering love and support this would not have been possible. Thank you. I need to thank

Gonzo, my lovable dog, who knows the true healing that a good cuddle can bring and that any situation can be made better if snacks are included. But most importantly, I thank Andrew, my wonderful husband, number one supporter, and partner in life. Words cannot express how much your love and encouragement mean to me. I love you and I like you.

TABLE OF CONTENTS

LIST OF TABLES

LIST OF FIGURES

LIST OF ABBREVIATIONS AND SYMBOLS

Abs	absorbance
ε-ACA	ε-aminocaproic acid
ACN	acetonitrile
AGC	automatic gain control
Akt	Ak strain transforming
AMPK	AMP kinase
ANOVA	analysis of variance
Arg	arginine
Asp	aspartic acid
ATG	autophagy related protein
AtPDK	*Arabidopsis thaliana* PDK
AUC	area under the curve
B_0	number of inactive reducing centers
BH	Benjamini and Hochberg
BLAST	Basic local alignment search tool
BSA	bovine serum albumin
CBBC	Calvin-Benson-Bassham cycle
CDK	cyclin dependent kinase
CDPKK2	calcium/calmodulin dependent kinase kinase
Chl *a*	Chlorophyll *a*
CrTOR-EKD	*Chlamydomonas reinhardtii* TOR – extended kinase domain

CV	coefficient of variation
Cys	cysteine
Da	unified atomic mass unit
DD-MS^2	data dependent MS^2
DMSO	dimethyl sulfoxide
DTT	dithiothreitol
ETC	electron transport chain
EtOH	ethanol
F_M	fluorescence at step P
F_O	fluorescence at step O
F_v	variable fluorescence
FA	formic acid
FDR	false discovery rate
FNR	ferredoxin-NADP reductase
FRB	FKBP12-rapamycin binding
GO	gene ontology
GSK3	glycogen synthase kinase 3
GST	glutathione S-transferase
His	histidine
HRD	His-Arg-Asp
IAM	iodoacetamide
IMAC	ion metal affinity chromatography
IMPK	nositol polyphosphate multikinase

InsP	inositol polyphosphate
IPTG	isopropyl β-D-1-thiogalactopyranoside
IT	injection time
KLD	kinase-ligase-Dpn1
KOG1	kontroller of growth 1
LARP	La-domain RNA-binding protein
LB	lysogeny broth
LC	liquid chromatography
LFQ	label-free quantification
LHC	light-harvesting complex
LST8	lethal with sec-13 protein 8
Lys	lysine
M_0	relative rate of primary Q_A reduction
MBP	maltose binding protein
MEK1	mitogen-activated protein kinase and extracellular signal-related kinase kinase 1
MeOH	methanol
MGF	Mascot generic file
MOAC	metal oxide affinity chromatography
MS	mass spectrometry
MS/MS	tandem mass spectrometry
MTBE	methyl *tert*-butyl ether
MWCO	molecular weight cutoff
m/z	mass-to-charge ratio

NCE	normalized collision energy
NEM	*N*-ethylmaleimide
NPQ	non-photochemical quenching
OD	optical density
OxRAC	oxidized cysteine resin-assisted capture
PAGE	polyacrylamide gel electrophoresis
PAM	pulse amplitude modulated
PAR	photosynthetically active radiation
PBS	phosphate-buffered saline
PCR	polymerase chain reaction
PetA	cytochrome *f*
PetF	ferredoxin
PGRL1	proton-gradient related-like protein 1
PI_{abs}	performance index per absorption
PIKK	phosphatidylinositol kinase-related kinase
PDCelα	pyruvate dehydrogenase complex e1 alpha subunit
PDK	pyruvate dehydrogenase kinase
PDK1	phosphoinositide-dependent protein kinase 1
PGK	phosphoglycerate kinase
PI4K	phosphatidylinositol 4-kinase
PIP	phosphatidyl inositol
PI-PLC	phosphoinositide-specific PLC
PKA	c-AMP dependent protein kinases

PLC	phospholipase C
PP2A	protein phosphatase 2A
PP2C	protein phosphatase 2C
PSI	photosystem I
PSII	photosystem II
PsaC	photosystem I iron-sulfur center
PsbO	PSII oxygen evolution enhancer protein
PsbR	PSII 10kDa polypeptide
PSR1	phosphorus starvation response protein 1
PTM	post-translational modification
R^2	coefficient of determination
RAPTOR	regulatory-associated protein of TOR
RF	radio frequency
RICTOR	companion of TOR
RNS	reactive nitrogen species
ROS	reactive oxygen species
RPM	rotations per minute
RPS6	ribosomal protein S6
RT	room temperature
S6K	ribosomal protein S6 kinase
SDS	sodium dodecyl sulfate
Ser	serine
SIM	selected ion monitoring

Sin1	stress-activated map kinase-interacting protein 1
SOP	standard operating procedure
SPE	solid-phase extraction
SRM	selected reaction monitoring
STL1	sugar transporter-like protein 1
STN	state transition kinase
TAG	triacylglycerol
TAP	Tris-acetate-phosphate
TB	terrific broth
TFA	trifluoroacetic acid
Thr	threonine
TIC	total ion chromatogram
TiO_2	titanium dioxide
TOP	terminal oligopyrimidine
TOR	target of rapamycin
TORC1	TOR complex 1
TORC2	TOR complex 2
TPS6B	Thiopropyl Sepharose 6B
Trp	tryptophan
TR_0/RC	trapped energy flux per PSII reaction center
Tyr	tyrosine
UPLC	ultra-performance liquid chromatography
VIP1	inositol hexakisphosphate and diphosphoinositol-pentakisphosphate kinase 1

WKS1	wheat kinase STARTS1
XIC	extracted ion chromatogram
YII	electron flow through PSII

CHAPTER 1: Introduction

This dissertation investigates the post-translational signaling controlled by the target of rapamycin kinase (TOR) pathway in *Chlamydomonas reinhardtii*. Post-translational modifications (PTMs) are a critical component of the regulation of cellular activity, and are often required to create functional, active proteins. Reversible oxidation and phosphorylation, two of the most common eukaryotic PTMs, are signaling mechanisms used by the master regulatory kinase pathway TOR, in the control of nearly all essential biological processes. This chapter will introduce *Chlamydomonas* as a model organism for the study of TOR in algal species and frame the current knowledge of the TOR pathway, specifically the roles PTMs play in its regulation and signaling. Further, a brief background on the protein kinase enzyme family is included, along with the approaches used to study TOR-regulated PTMs, namely *in vivo* large-scale proteomic profiling and *in vitro* kinase-substrate identification methods.

1.1 Target of Rapamycin

TOR is a master regulator that is part of the phosphatidylinositol kinase-related kinase (PIKK) family, and is conserved across all eukaryotes. It is known to regulate cell growth by controlling protein synthesis and degradation through phases of translation, ribosome biosynthesis, amino acid transport, transcription, and autophagy[1]. Additionally, TOR plays critical roles in response to nutrients, energy, and stress[2–6].

In mammals and yeast where it is well studied, TOR is found in two distinct complexes, target of rapamycin complex 1 (TORC1) and 2 (TORC2)[2]. TORC1 contains three components: TOR, lethal with sec-13 protein 8 (LST8), and regulatory-associated protein of TOR (RAPTOR)

in mammalian cells or the ortholog kontroller of growth 1 (KOG1) in yeast[7]. TORC1 is known to regulate growth in response to nutrients, cellular energy state, and growth factors. TORC2 also contains LST8 and TOR, but also has the unique proteins companion of TOR (RICTOR) and stress-activated map kinase-interacting protein 1 (Sin1). TORC2 regulates Ak strain transforming (Akt) signaling and modulates cytoskeletal polarization[8]. Unlike TORC1, which is inhibited by rapamycin, TORC2is not directly sensitive to rapamycin treatment[8].

Rapamycin is a known indirect inhibitor of TOR that complexes with the protein FKBP12 and binds to the FRB domain of the TORC1 complex to allosterically inhibit the kinase activity[9]. In addition to rapamycin other known inhibitors to TOR include AZD8055 and Torin1, which are both direct inhibitors of TOR, meaning they are ATP-competitive inhibitors. Kinase activity involves the transfer of the γ-phosphate of ATP to a target protein substrate, and ATP competitive inhibitors block this by binding directly to the active site domain[10]. These inhibitors more fully inhibit TOR, resulting in a more pronounced response physiologically and proteomically when compared to rapamycin treatment. Use of these inhibitors in TOR studies allows for a more complete interrogation of the functions of TOR, including those not inhibited by rapamycin.

1.2 TOR in *Chlamydomonas reinhardtii*

Unlike other eukaryotic cells, photosynthetic organisms only contain homologs of TORC1 and no secondary TOR complex has been identified[11]. In *Arabidopsis thaliana* and other higher order plants, little to no TOR inhibition is seen when treated with rapamycin, likely a consequence of the *Arabidopsis* FKBP12 not strongly associating with rapamycin[12]. However, other ATP-competitive inhibitors are still effective in regulating TOR activity[13]. Unlike its higher order counterparts, a homolog for FKBP12 has been identified in the algal organism

Chlamydomonas, making it susceptible to rapamycin treatment[14]. This unique feature of *Chlamydomonas* allows for a more comprehensive investigation of the TOR pathway, and it has been shown that inhibition with these three drugs produce unique phosphorylation changes across the proteome[15].

Chlamydomonas is a model photosynthetic organism, in part due to its simple life cycle, rapid growth rate and fully sequenced genome[16].Microalgal processes such as triacylglycerol (TAG) accumulation[17–19] and cell cycle control[20] have been extensively studied in *Chlamydomonas*. Genomic, transcriptomic, and proteomic efforts have advanced the current understanding of molecular infrastructure and metabolic signaling[18,21–25]. Specifically, previous studies have shown that nutrient deprivation results in triacylglycerol (TAG) and starch accumulation[17–19], but research into algal metabolism regulation is still needed. Similar to nutrient deprivation, inhibition of TOR in *Chlamydomonas* has shown an increase in TAG accumulation[5,26–29], supporting the role of TOR in regulating nutrient response. Investigation of TOR in *Chlamydomonas* could help delineate how microalgae and phototrophs more generally respond to stressors and nutrient loss, providing insight into the fundamentals of algal and plant metabolism.

1.3 Post-Translational Modifications in Algal Signaling

PTMs, like the phosphorylation events controlled by kinases like TOR, are a critical component of the regulation of cellular activity. PTMs are typically catalyzed enzymatically and result in covalent modification of the translated protein. These modifications contribute to the complexity of the proteome, and cannot be predicted based on the genetic makeup of an organism. There are hundreds of known PTMs[30,31], including phosphorylation, reversible oxidation, acetylation, ubiquitination, glycosylation, and sumoylation. These PTMs control

protein folding, structure, and diversify functional proteoforms[32] - unique forms of a protein product from a single gene. Many PTMs, including those used by TOR to regulate cellular processes, are reversible and signal the activation/deactivation of proteins.

Nearly all metabolic responses to environmental stressors in *Chlamydomonas* and other organisms are modulated by PTMs[33]. Regulatory PTMs have been identified on many enzymes involved in primary metabolism including the Calvin-Benson-Bassham cycle, glycolysis, and photosynthesis[34]. Despite their importance, mapping PTMs is a continued challenge due to their complexity and low abundance, requiring targeted experiments or enrichment strategies for reliable identification and quantification. While targeted approaches such as western blots, pull-downs, and selected ion/reaction monitoring (SIM/SRM) provide detailed information on a specific protein, proteoform, or complex, enrichment strategies enable proteome-wide investigation of a modification. Enrichment strategies are well suited to examine TOR signaling pathways because it is involved in regulating diverse biological processes.

The development of robust LC-MS/MS proteomic platforms has enabled large-scale in-depth proteomic profiling of PTMs for studying protein signaling. These workflows assess changes in a modification upon perturbation (*e.g.,* nutrient deprivation, chemical inhibition, biotic stress) by combining a reproducible enrichment strategy with a quantitative proteomics workflow. Studying how PTM events change *in vivo* enables the identification of key proteins and modification sites involved in signaling and other essential biological processes. In particular, reversible oxidation of cysteine thiols and phosphorylation are among the most crucial modifications and known to be regulators of stress response [35–38], nutrient availability[39–41] and the cell cycle[27,42–44].

1.3.1 Reversible Oxidation

Cysteine contains a reactive sulfur group that is susceptible to oxidation by reactive oxygen species (ROS) and reactive nitrogen species (RNS). ROS/RNS are usually produced as toxic byproducts from electron transport, enzymatically from oxidases, or from exogenous stressors. Depending on the ROS reaction(s), cysteine oxidation can be reversible, including sulfenic and sulfinic acid, disulfide bonds, glutathionylation, and nitrosylation, with modifications regulated by enzymes or the presence of ROS/RNS or reductive species. However, when a cysteine reaches an overly oxidized state, sulfonic acid, the modification becomes irreversible, leading to dysfunctionality and eventual protein degradation[45]. Reversible oxidation is a regulatory mechanism, modulating protein activity and participating in stress response signaling cascades. In photosynthetic organisms, reversible oxidation sites have been identified on enzymes involved in signaling, stress response, transcription, translation, and metabolism, reflecting the broad scope and importance of this PTM[26,27,35,46–49].

Measurements of *in vivo* cysteine oxidation can be challenging due to the labile and reactive nature of thiols. Additionally, cysteines only account for ~2% of amino acids in eukaryotes[50]. Given that only a subset is oxidized at any point, enrichment methods are needed in order to stabilize, concentrate, and identify cysteine oxidation sites of biological significance. Generally, these methods can be direct, involving a label or enrichment that targets oxidized cysteines, or indirect where reversibly oxidated sites are chemically reduced and these newly free thiols are identified. Many probes for direct detection are limited by reaction rate and efficiency, making them unappealing for proteome-wide experiments[51–53]. Indirect detection methods typically involve blocking free thiols with an alkylating agent, followed by reduction of the oxidatively modified cysteines. This reduction can be modification specific, such as arsenite for

reduction of sulfenylation[54,55], or can reduce all reversible oxidation using reagents like dithiothreitol (DTT). The previously oxidized cysteines can then be modified using a marker such as a fluorophore or isotope-coded affinity tag[56,57], or enriched via biotin-avidin or thiol affinity purification[58,59] as part of a quantitative proteomic workflow.

1.3.2 Phosphorylation

Phosphorylation is the most common PTM and an estimated one third of proteins are predicted to be targets of phosphorylation in eukaryotes [60]. It is known to impact essential cellular processes in phototrophs including cell cycle, autophagy metabolism, stress response, photosynthesis and signaling transduction[61–63]. Protein kinases catalyze phosphorylation by transferring the γ-phosphate group from ATP to an amino acid on a target protein. This modification is reversible, with removal of the phosphate group catalyzed by phosphatases. While phosphorylation occurs on many different residues[64–66], it is most commonly found on the hydroxyl group of serine, threonine, or tyrosine.

While this phosphorylation is one of the most well-studied PTMs, many known phosphosites, particularly in phototrophs, are not yet associated with a biological function or process. A major cause of this ambiguity is the relatively low abundance of phosphorylated peptides after digestion of a eukaryotic cell lysate. In addition to their substoichiometric levels, phosphopeptides tend to have decreased ionization efficiency in positive electrospray ionization compared to their non-phosphorylated counterparts resulting in reduced signal during MS-based whole proteome analysis [67]. To address these issues in large-scale proteomic analyses, an efficient and selective enrichment method is usually implemented. While many different methods for phosphopeptide enrichment have been developed, the two most common techniques include ion metal affinity chromatography[68] (IMAC) and metal oxide affinity chromatography

(MOAC), specifically TiO_2[69]. When combined with careful sample preparation, enrichment allows for the identification/quantification of thousands of phosphorylation events in a single analysis.

1.4 Kinases

Protein kinases, the enzymes responsible for protein phosphorylation, are one of the largest enzyme families in eukaryotes[70]. Generally, they have a highly conserved active region called the kinase domain, which has a number of conserved motifs. These include an activation loop that interacts with the residues adjacent to the phosphosite, and a His-Arg-Asp (HRD) motif directly involved in the transfer of the γ-phosphate from ATP to the substrate. *Chlamydomonas* is known to have nearly 16,000 phosphorylation events catalyzed by 355 kinases[71,72]. Generally, kinases are site-specific enzymes, likely due to the importance of phosphorylation in controlling essential biological processes, but the number of targets for a given kinase can vary greatly. For example, the mammalian protein mitogen-activated protein kinase and extracellular signal-related kinase kinase 1 (MEK1) is known to phosphorylate only four proteins while cyclin dependent kinases (CDKs) are predicted to phosphorylate hundreds of substrates [73,74]. However, given the estimated 700,000 potential phosphorylation sites based on the prevalence of Ser, Thr, and Tyr residues, the average size of proteins, and the average number of proteins in a typical mammalian cell, even the most promiscuous kinases, like CDKs, are relatively specific with their targets[73].

A number of factors contribute to kinase specificity[73,75]. Broadly speaking, most protein kinases are classified by their target residues (either Ser/Thr or Tyr). In the active domain of many kinases, the conserved activation loop interacts with adjacent residues and certain motifs, distinctive sequences of amino acids, are required in order to complete phosphorylation. This

results in a consensus sequence motif that is conserved across a kinase's substrates. Some kinases require phosphorylation on an adjacent residue to be present, called priming phosphorylation, in order to phosphorylate their target residue. Outside of the kinase domain, the kinase can interact with its substrate at other locations on the protein, called docking sites, or interact with a third scaffolding protein, that brings together the kinase and substrate in the correct orientation.

Phosphorylation events can also be categorized based on the substrate. In trans-phosphorylation, a kinase phosphorylates a protein translated from a different gene, while auto-phosphorylation occurs when a kinase phosphorylates a protein that is translated from the same gene[76]. Autophosphorylation can occur between two of the same kinase (kinase A_1 phosphorylates kinase A_2) or as self-phosphorylation wherein a kinase phosphorylates itself[77]. Many kinases are themselves phosphorylated through one of these modes, and when combined, kinases form signaling cascades that regulate cellular functions. By characterizing kinases and identifying their substrates, these signaling pathways can be delineated, providing more information on how biological processes are regulated.

1.4.1 Kinase-Substrate Identification

As described previously, the use of enrichment techniques combined with LC-MS-based phosphoproteomics enables identification and quantification of thousands of phosphorylation events. However, the precise connections between the identified phosphorylation sites and protein kinases are missing. A common approach to investigating phosphorylation signaling is *in vivo* studies using kinase inhibitors or kinase knockout strains with differential phosphoproteomic analysis. Using this technique phosphorylation sites related to a kinase can be identified, but there is no way to differentiate between direct substrates, which are

phosphorylated by the kinase being investigated, and indirect substrates, which are targets of kinases downstream of the kinase of interest. Additionally, this technique is limited to kinases with inhibitors, or it requires the creation of a mutant strain, which can be time intensive and is infeasible for some essential enzymes. For many kinases with known consensus sequence motifs and docking domains, there are tools that can predict potential substrates from protein databases for a given kinase[78–80]. This generates a subset of potential substrates that can be further characterized with additional studies to confirm which proteins are valid kinase targets. These tools can help reduce a potential substrate pool, yet are limited to kinases that are at least partially characterized or part of a family of well-studied kinases with known consensus sequences and conserved substrate domains.

Given the limitations of these techniques, many studies are using *in vitro* approaches to investigate kinase-substrate pairings. These studies generally take a high-throughput approach to screening kinases where a kinase is incubated with tens to thousands of potential substrates and then phosphorylated substrates are identified using mass spectrometric approaches very similar to those used for quantitative phosphoproteomic studies[81–84]. Most screening approaches can be broken down into four steps: generation of an active kinase sample, creation of a substrate library, screening of the kinase, and analysis of the screening. Kinase samples are purified from their native organism, or heterologously expressed and purified using a protein expression system. Kinase purification strategy is dependent on abundance in the native organism, molecular weight, and knowledge of complex PTMs or scaffolds needed for activity. Substrate libraries are created either synthetically or produced from the proteome of the native organism. They can vary in their complexity depending on how they are prepared and contain peptides or intact proteins as potential substrates. Peptide libraries can provide information on a kinase's

consensus sequence and can potentially give a larger number of putative substrates that could be further validated. Protein libraries provide additional modes of specificity that result in a more targeted screening. Optimization of screening and analysis is also an important part of the screening process, taking into account any additional cofactors needed for the kinase activity as well as any enrichment or library preparation needed post-screening in order to identify putative targets.

1.5 Scope of Dissertation

This dissertation uses the study of PTMs to investigate the TOR pathway in *Chlamydomonas* to better understand the signaling mechanisms that drive essential cellular functions. This work uses label-free proteomics combined with specific PTM enrichment strategies optimized for studying reversible oxidation and phosphorylation. First, **Chapter 2** investigates the crosstalk between TOR kinase signaling and reversible oxidation by performing differential redox analysis in TOR-inhibited *Chlamydomonas*. **Chapter 3** is a comprehensive explanation of the label-free quantitative phosphoproteomic workflow for experiments in *Chlamydomonas* used in the Hicks laboratory. This also includes assessment strategies for determining reproducibility and quality of the proteomic data. This platform is then applied (**Chapter 4**) to study the differential phosphoproteomes of a rapamycin hypersensitive mutant of *Chlamydomonas* after TOR inhibition and rapamycin-treated wild-type cells. Then standard operating procedures (SOPs) are detailed for an *in vitro* screening platform for identifying putative kinase-substrate relationships (**Chapter 5**). These SOPS are optimized to heterologously express kinases of interest and prepare a substrate library from a *Chlamydomonas* cell lysate. Finally, in **Chapter 6**, the screening platform is validated using a well-studied, highly specific kinase from *Arabidopsis*, the

pyruvate dehydrogenase kinase (AtPDK) and applied in the identification of putative targets of *Chlamydomonas* TOR (CrTOR).

REFERENCES

1. Raught, B.; Gingras, A. C.; Sonenberg, N. The Target of Rapamycin (TOR) Proteins. *Proc. Natl. Acad. Sci. U.S.A.* **2001**, *98* (13), 7037–7044.

2. Loewith, R.; Hall, M. N. Target of Rapamycin (TOR) in Nutrient Signaling and Growth Control. *Genetics* **2011**, *189* (4), 1177–1201.

3. Wullschleger, S.; Loewith, R.; Hall, M. N. TOR Signaling in Growth and Metabolism. *Cell* **2006**, *124* (3), 471–484.

4. Dobrenel, T.; Caldana, C.; Hanson, J.; Robaglia, C.; Vincentz, M.; Veit, B.; Meyer, C. TOR Signaling and Nutrient Sensing. *Annu. Rev. Plant Biol.* **2016**, *67* (1), 261–285.

5. Pérez-Pérez, M. E.; Couso, I.; Crespo, J. L. The TOR Signaling Network in the Model Unicellular Green Alga Chlamydomonas reinhardtii. *Biomolecules* **2017**, *7* (3), 54.

6. González, A.; Hall, M. N. Nutrient Sensing and TOR Signaling in Yeast and Mammals. *EMBO J.* **2017**, *36* (4), 397–408.

7. Loewith, R.; Jacinto, E.; Wullschleger, S.; Lorberg, A.; Crespo, J. L.; Bonenfant, D.; Oppliger, W.; Jenoe, P.; Hall, M. N. Two TOR Complexes, Only One of Which is Rapamycin Sensitive, Have Distinct Roles in Cell Growth Control. *Mol. Cell* **2002**, *10* (3), 457–468.

8. Rosel, D.; Khurana, T.; Majithia, A.; Huang, X.; Bhandari, R.; Kimmel, A. R. TOR Complex 2 (TORC2) in Dictyostelium Suppresses Phagocytic Nutrient Capture Independently of TORC1-Mediated Nutrient Sensing. *J. Cell Sci.* **2012**, *125* (1), 37–48.

9. Yang, H.; Rudge, D. G.; Koos, J. D.; Vaidialingam, B.; Yang, H. J.; Pavletich, N. P. MTOR Kinase Structure, Mechanism and Regulation by the Rapamycin-Binding Domain. *Nature* **2013**, *497* (7448), 217–223.

10. Liu, Q.; Kirubakaran, S.; Hur, W.; Niepel, M.; Westover, K.; Thoreen, C. C.; Wang, J.; Ni, J.; Patricelli, M. P.; Vogel, K.; Riddle, S.; Waller, D. L.; Traynor, R.; Sanda, T.; Zhao, Z.; Kang, S. A.; Zhao, J.; Look, A. T.; Sorger, P. K.; Sabatini, D. M.; Gray, N. S. Kinome-Wide Selectivity Profiling of ATP-Competitive Mammalian Target of Rapamycin (MTOR) Inhibitors and Characterization of Their Binding Kinetics. *J. Biol. Chem.* **2012**, *287* (13), 9742–9752.

11. Xiong, Y.; Sheen, J. The Role of Target of Rapamycin Signaling Networks in Plant Growth and Metabolism. *Plant Physiol.* **2014**, *164* (2), 499–512.

12. Xu, Q.; Liang, S.; Kudla, J.; Luan, S. Molecular Characterization of a Plant FKBP12 That Does Not Mediate Action of FK506 and Rapamycin. *Plant J.* **1998**, *15* (4), 511–519.

13. Montané, M. H.; Menand, B. ATP-Competitive MTOR Kinase Inhibitors Delay Plant Growth by Triggering Early Differentiation of Meristematic Cells but No Developmental Patterning Change. *J. Exp. Bot.* **2013**, *64* (14), 4361–4374.

14. Crespo, J. L.; Díaz-Troya, S.; Florencio, F. J. Inhibition of Target of Rapamycin Signaling by Rapamycin in the Unicellular Green Alga Chlamydomonas reinhardtii. *Plant Physiol.* **2005**, *139* (4), 1736–1749.

15. Werth, E. G.; McConnell, E. W.; Lianez, I. C.; Perrine, Z.; Crespo, J. L.; Umen, J. G.; Hicks, L. M. Investigating the Effect of Target of Rapamycin Kinase Inhibition on the Chlamydomonas reinhardtii Phosphoproteome: From Known Homologs to New Targets. *New Phytol.* **2019**, *221* (1), 247–260.

16. Harris, E. H. Chlamydomonas as a Model Organism. *Annu. Rev. Plant Physiol. Plant Mol. Biol.* **2001**, *52* (1), 363–406.

17. Siaut, M.; Cuiné, S.; Cagnon, C.; Fessler, B.; Nguyen, M.; Carrier, P.; Beyly, A.; Beisson, F.; Triantaphylidès, C.; Li-Beisson, Y.; Peltier, G. Oil Accumulation in the Model Green Alga Chlamydomonas reinhardtii: Characterization, Variability between Common Laboratory Strains and Relationship with Starch Reserves. *BMC Biotechnol.* **2011**, *11*, 7.

18. Park, J.-J.; Wang, H.; Gargouri, M.; Deshpande, R. R.; Skepper, J. N.; Holguin, F. O.; Juergens, M. T.; Shachar-Hill, Y.; Hicks, L. M.; Gang, D. R. The Response of Chlamydomonas reinhardtii to Nitrogen Deprivation: A Systems Biology Analysis. *Plant J.* **2015**, *81* (4), 611–624.

19. Merchant, S. S.; Kropat, J.; Liu, B.; Shaw, J.; Warakanont, J. TAG, You're It! Chlamydomonas as a Reference Organism for Understanding Algal Triacylglycerol Accumulation. *Curr. Opin. Biotechnol.* **2012**, *23* (3), 352–363.

20. Cross, F. R.; Umen, J. G. The Chlamydomonas Cell Cycle. *Plant J.* **2015**, *82* (3), 370–392.

21. Merchant, S. S.; Prochnik, S. E.; Vallon, O.; Harris, E. H.; Karpowicz, S. J.; Witman, G. B.; Terry, A.; Salamov, A.; Fritz-Laylin, L. K.; Maréchal-Drouard, L.; Marshall, W. F.; Qu, L.-H.; Nelson, D. R.; Sanderfoot, A. A.; Spalding, M. H.; Kapitonov, V. V.; Ren, Q.; Ferris, P.; Lindquist, E.; Shapiro, H.; Lucas, S. M.; Grimwood, J.; Schmutz, J.; Cardol, P.; Cerutti, H.; Chanfreau, G.; Chen, C.-L.; Cognat, V.; Croft, M. T.; Dent, R.; Dutcher, S.; Fernández, E.; Ferris, P.; Fukuzawa, H.; González-Ballester, D.; González-Halphen, D.; Hallmann, A.; Hanikenne, M.; Hippler, M.; Inwood, W.; Jabbari, K.; Kalanon, M.; Kuras, R.; Lefebvre, P. A.; Lemaire, S. D.; Lobanov, A. V.; Lohr, M.; Manuell, A.; Meier, I.; Mets, L.; Mittag, M.; Mittelmeier, T.; Moroney, J. V.; Moseley, J.; Napoli, C.; Nedelcu, A. M.; Niyogi, K.; Novoselov, S. V.; Paulsen, I. T.; Pazour, G.; Purton, S.; Ral, J.-P.; Riaño-Pachón, D. M.; Riekhof, W.; Rymarquis, L.; Schroda, M.; Stern, D.; Umen, J.; Willows, R.; Wilson, N.; Zimmer, S. L.; Allmer, J.; Balk, J.; Bisova, K.; Chen, C.-J.; Elias, M.; Gendler, K.; Hauser, C.; Lamb, M. R.; Ledford, H.; Long, J. C.; Minagawa, J.; Page, M. D.; Pan, J.; Pootakham, W.; Roje, S.; Rose, A.; Stahlberg, E.; Terauchi, A. M.;

Yang, P.; Ball, S.; Bowler, C.; Dieckmann, C. L.; Gladyshev, V. N.; Green, P.; Jorgensen, R.; Mayfield, S.; Mueller-Roeber, B.; Rajamani, S.; Sayre, R. T.; Brokstein, P.; Dubchak, I.; Goodstein, D.; Hornick, L.; Huang, Y. W.; Jhaveri, J.; Luo, Y.; Martínez, D.; Ngau, W. C. A.; Otillar, B.; Poliakov, A.; Porter, A.; Szajkowski, L.; Werner, G.; Zhou, K.; Grigoriev, I. V.; Rokhsar, D. S.; Grossman, A. R. The Chlamydomonas Genome Reveals the Evolution of Key Animal and Plant Functions. *Science* **2007**, *318* (5848), 245–250.

22. Zones, J. M.; Blaby, I. K.; Merchant, S. S.; Umen, J. G. High-Resolution Profiling of a Synchronized Diurnal Transcriptome from Chlamydomonas reinhardtii Reveals Continuous Cell and Metabolic Differentiation. *Plant Cell* **2015**, *27* (10), 2743–2769.

23. Miller, R.; Wu, G.; Deshpande, R. R.; Vieler, A.; Gartner, K.; Li, X.; Moellering, E. R.; Zauner, S.; Cornish, A.; Liu, B. Changes in Transcript Abundance in Chlamydomonas reinhardtii Following Nitrogen Deprivation Predict Diversion of Metabolism. *Plant Physiol.* **2010**, *154*, 1737–1752.

24. Förster, B.; Mathesius, U.; Pogson, B. J. Comparative Proteomics of High Light Stress in the Model Alga Chlamydomonas reinhardtii. *Proteomics* **2006**, *6* (15), 4309–4320.

25. Atteia, A.; Adrait, A.; Brugière, S.; Tardif, M.; van Lis, R.; Deusch, O.; Dagan, T.; Kuhn, L.; Gontero, B.; Martin, W.; Garin, J.; Joyard, J.; Rolland, N. A Proteomic Survey of Chlamydomonas reinhardtii Mitochondria Sheds New Light on the Metabolic Plasticity of the Organelle and on the Nature of the α-Proteobacterial Mitochondrial Ancestor. *Mol. Biol. Evol.* **2009**, *26* (7), 1533–1548.

26. Rodrigues, S. P.; Alvarez, S.; Werth, E. G.; Slade, W. O.; Gau, B.; Cahoon, E. B.; Hicks, L. M. Multiplexing Strategy for Simultaneous Detection of Redox-, Phospho- and Total Proteome – Understanding TOR Regulating Pathways in Chlamydomonas reinhardtii. *Anal. Methods* **2015**, *7* (17), 7336–7344.

27. Ford, M. M.; Smythers, A. L.; McConnell, E. W.; Lowery, S. C.; Kolling, D. R. J.; Hicks, L. M. Inhibition of TOR in Chlamydomonas reinhardtii Leads to Rapid Cysteine Oxidation Reflecting Sustained Physiological Changes. *Cells* **2019**, *8* (10), 1171.

28. Pérez-Pérez, M. E.; Florencio, F. J.; Crespo, J. L. Inhibition of Target of Rapamycin Signaling and Stress Activate Autophagy in Chlamydomonas reinhardtii. *Plant Physiol.* **2010**, *152* (4), 1874–1888.

29. Pérez-Pérez, M. E.; Couso, I.; Heredia-Martínez, L. G.; Crespo, J. L. Monitoring Autophagy in the Model Green Microalga Chlamydomonas reinhardtii. *Cells* **2017**, *6* (4).

30. Minguez, P.; Parca, L.; Diella, F.; Mende, D. R.; Kumar, R.; Helmer-Citterich, M.; Gavin, A.-C.; van Noort, V.; Bork, P. Deciphering a Global Network of Functionally Associated Post-Translational Modifications. *Mol. Syst. Biol.* **2012**, *8*, 599.

31. Minguez, P.; Letunic, I.; Parca, L.; Bork, P. PTMcode: A Database of Known and Predicted Functional Associations between Post-Translational Modifications in Proteins. *Nucleic Acids Res.* **2013**, *41* (Database issue), D306-311.

32. Smith, L. M.; Kelleher, N. L. Proteoform: A Single Term Describing Protein Complexity. *Nat. Methods* **2013**, *10* (3), 186–187.

33. Hashiguchi, A.; Komatsu, S. Impact of Post-Translational Modifications of Crop Proteins under Abiotic Stress. *Proteomes* **2016**, *4* (4), 42.

34. Friso, G.; Wijk, K. J. van. Posttranslational Protein Modifications in Plant Metabolism. *Plant Physiol.* **2015**, *169* (3), 1469–1487.

35. McConnell, E. W.; Werth, E. G.; Hicks, L. M. The Phosphorylated Redox Proteome of Chlamydomonas reinhardtii: Revealing Novel Means for Regulation of Protein Structure and Function. *Redox Biol.* **2018**, *17*, 35–46.

36. Cai, Z.; Yan, L.-J. Protein Oxidative Modifications: Beneficial Roles in Disease and Health. *J. Biochem. Pharmacol. Res.* **2013**, *1* (1), 15–26.

37. Dunand-Sauthier, I.; Walker, C. A.; Narasimhan, J.; Pearce, A. K.; Wek, R. C.; Humphrey, T. C. Stress-Activated Protein Kinase Pathway Functions to Support Protein Synthesis and Translational Adaptation in Response to Environmental Stress in Fission Yeast. *Eukaryot. Cell* **2005**, *4* (11), 1785–1793.

38. Crespo, J. L. BiP Links TOR Signaling to ER Stress in Chlamydomonas. *Plant Signal Behav.* **2012**, *7* (2), 273–275.

39. Smythers, A. L.; McConnell, E. W.; Lewis, H. C.; Mubarek, S. N.; Hicks, L. M. Photosynthetic Metabolism and Nitrogen Reshuffling Are Regulated by Reversible Cysteine Thiol Oxidation Following Nitrogen Deprivation in Chlamydomonas. *Plants (Basel)* **2020**, *9* (6), 784.

40. Bertoni, G. Phosphorus Sensing by LST8 Acts as a TOR Guide for Cell Growth in Chlamydomonas. *Plant Cell* **2020**, *32* (1), 7.

41. Roustan, V.; Bakhtiari, S.; Roustan, P.-J.; Weckwerth, W. Quantitative in vivo Phosphoproteomics Reveals Reversible Signaling Processes during Nitrogen Starvation and Recovery in the Biofuel Model Organism Chlamydomonas reinhardtii. *Biotechnol. Biofuels* **2017**, *10* (1), 280.

42. Takeuchi, T.; Benning, C. Nitrogen-Dependent Coordination of Cell Cycle, Quiescence and TAG Accumulation in Chlamydomonas. *Biotechnol. Biofuels* **2019**, *12* (1), 292.

43. Olson, B. J. S. C.; Oberholzer, M.; Li, Y.; Zones, J. M.; Kohli, H. S.; Bisova, K.; Fang, S.-C.; Meisenhelder, J.; Hunter, T.; Umen, J. G. Regulation of the Chlamydomonas Cell Cycle by a Stable, Chromatin-Associated Retinoblastoma Tumor Suppressor Complex. *Plant Cell* **2010**, *22* (10), 3331–3347.

44. Marcus, Y.; Schuster, G.; Michaels, A.; Kaplan, A. Adaptation to CO_2 Level and Changes in the Phosphorylation of Thylakoid Proteins during the Cell Cycle of Chlamydomonas reinhardtii. *Plant Physiol.* **1986**, *80* (2), 604–607.

45. Couturier, J.; Chibani, K.; Jacquot, J.-P.; Rouhier, N. Cysteine-Based Redox Regulation and Signaling in Plants. *Front. Plant Sci.* **2013**, *4*, 105.

46. Wang, H.; Wang, S.; Lu, Y.; Alvarez, S.; Hicks, L. M.; Ge, X.; Xia, Y. Proteomic Analysis of Early-Responsive Redox-Sensitive Proteins in Arabidopsis. *J. Proteome Res.* **2012**, *11* (1), 412–424.

47. Zaffagnini, M.; Bedhomme, M.; Groni, H.; Marchand, C. H.; Puppo, C.; Gontero, B.; Cassier-Chauvat, C.; Decottignies, P.; Lemaire, S. D. Glutathionylation in the Photosynthetic Model Organism Chlamydomonas reinhardtii: A Proteomic Survey. *Mol. Cell. Proteom.* **2012**, *11* (2), M111.014142.

48. Liu, P.; Zhang, H.; Wang, H.; Xia, Y. Identification of Redox-Sensitive Cysteines in the Arabidopsis Proteome Using OxiTRAQ, a Quantitative Redox Proteomics Method. *Proteomics* **2014**, *14* (6), 750–762.

49. Slade, W. O.; Werth, E. G.; McConnell, E. W.; Alvarez, S.; Hicks, L. M. Quantifying Reversible Oxidation of Protein Thiols in Photosynthetic Organisms. *J. Am. Soc. Mass Spectrom.* **2015**, *26* (4), 631–640.

50. Pe'er, I.; Felder, C. E.; Man, O.; Silman, I.; Sussman, J. L.; Beckmann, J. S. Proteomic Signatures: Amino Acid and Oligopeptide Compositions Differentiate among Phyla. *Proteins* **2004**, *54* (1), 20–40.

51. Weerapana, E.; Wang, C.; Simon, G. M.; Richter, F.; Khare, S.; Dillon, M. B. D.; Bachovchin, D. A.; Mowen, K.; Baker, D.; Cravatt, B. F. Quantitative Reactivity Profiling Predicts Functional Cysteines in Proteomes. *Nature* **2010**, *468* (7325), 790–795.

52. Gupta, V.; Yang, J.; Liebler, D. C.; Carroll, K. S. Diverse Redoxome Reactivity Profiles of Carbon Nucleophiles. *J. Am. Chem. Soc.* **2017**, *139* (15), 5588–5595.

53. Chang, Y.-C.; Huang, C.-N.; Lin, C.-H.; Chang, H.-C.; Wu, C.-C. Mapping Protein Cysteine Sulfonic Acid Modifications with Specific Enrichment and Mass Spectrometry: An Integrated Approach to Explore the Cysteine Oxidation. *Proteomics* **2010**, *10* (16), 2961–2971.

54. Saurin, A. T.; Neubert, H.; Brennan, J. P.; Eaton, P. Widespread Sulfenic Acid Formation in Tissues in Response to Hydrogen Peroxide. *Proc. Natl. Acad. Sci. U.S.A* **2004**, *101* (52), 17982–17987.

55. Tyther, R.; Ahmeda, A.; Johns, E.; McDonagh, B.; Sheehan, D. Proteomic Profiling of Perturbed Protein Sulfenation in Renal Medulla of the Spontaneously Hypertensive Rat. *J. Proteome Res.* **2010**, *9* (5), 2678–2687.

56. Puljung, M. C.; Zagotta, W. N. Fluorescent Labeling of Specific Cysteine Residues Using CyMPL. *Curr. Protoc. Protein Sci.* **2012**, *70*, 14.14.1-14.14.10.

57. Sethuraman, M.; McComb, M. E.; Huang, H.; Huang, S.; Heibeck, T.; Costello, C. E.; Cohen, R. A. Isotope-Coded Affinity Tag (ICAT) Approach to Redox Proteomics: Identification and Quantitation of Oxidant-Sensitive Cysteine Thiols in Complex Protein Mixtures. *J. Proteome Res.* **2004**, *3* (6), 1228–1233.

58. Murray, C. I.; Van Eyk, J. E. Chasing Cysteine Oxidative Modifications: Proteomic Tools for Characterizing Cysteine Redox-Status. *Circ. Cardiovasc. Genet.* **2012**, *5* (5), 591.

59. Guo, J.; Gaffrey, M. J.; Su, D.; Liu, T.; Camp, D. G.; Smith, R. D.; Qian, W.-J. Resin-Assisted Enrichment of Thiols as a General Strategy for Proteomic Profiling of Cysteine-Based Reversible Modifications. *Nat. Protoc.* **2014**, *9* (1), 64–75.

60. Olsen, J. V.; Blagoev, B.; Gnad, F.; Macek, B.; Kumar, C.; Mortensen, P.; Mann, M. Global, in Vivo, and Site-Specific Phosphorylation Dynamics in Signaling Networks. *Cell* **2006**, *127* (3), 635–648.

61. Hubbard, M. J.; Cohen, P. On Target with a New Mechanism for the Regulation of Protein Phosphorylation. *Trends Biochem. Sci.* **1993**, *18* (5), 172–177.

62. Hunter, T. Protein Kinases and Phosphatases: The Yin and Yang of Protein Phosphorylation and Signaling. *Cell* **1995**, *80* (2), 225–236.

63. Allen, J. F. Protein Phosphorylation in Regulation of Photosynthesis. *Biochim. Biophys. Acta* **1992**, *1098* (3), 275–335.

64. Hardman, G.; Perkins, S.; Brownridge, P. J.; Clarke, C. J.; Byrne, D. P.; Campbell, A. E.; Kalyuzhnyy, A.; Myall, A.; Eyers, P. A.; Jones, A. R.; Eyers, C. E. Strong Anion Exchange-mediated Phosphoproteomics Reveals Extensive Human Non-Canonical Phosphorylation. *EMBO J.* **2019**, *38* (21).

65. Fuhs, S. R.; Hunter, T. PHisphorylation; The Emergence of Histidine Phosphorylation as a Reversible Regulatory Modification. *Curr. Opin. Cell Biol.* **2017**, *45*, 8–16.

66. Cieśla, J.; Frączyk, T.; Rode, W. Phosphorylation of Basic Amino Acid Residues in Proteins: Important but Easily Missed. *Acta Biochim. Pol.* **2011**, *58* (2), 137-148.

67. Solari, F. A.; Dell'Aica, M.; Sickmann, A.; Zahedi, R. P. Why Phosphoproteomics Is Still a Challenge. *Mol. BioSyst.* **2015**, *11* (6), 1487–1493.

68. Neville, D. C.; Rozanas, C. R.; Price, E. M.; Gruis, D. B.; Verkman, A. S.; Townsend, R. R. Evidence for Phosphorylation of Serine 753 in CFTR Using a Novel Metal-Ion Affinity Resin and Matrix-Assisted Laser Desorption Mass Spectrometry. *Protein Sci.* **1997**, *6* (11), 2436–2445.

69. Larsen, M. R.; Thingholm, T. E.; Jensen, O. N.; Roepstorff, P.; Jørgensen, T. J. D. Highly Selective Enrichment of Phosphorylated Peptides from Peptide Mixtures Using Titanium Dioxide Microcolumns. *Mol. Cell Proteomics* **2005**, *4* (7), 873–886.

70. Hanks, S. K.; Hunter, T. The Eukaryotic Protein Kinase Superfamily: Kinase (Catalytic) Domain Structure and Classification1. *FASEB J.* **1995**, *9* (8), 576–596.

71. Wang, H.; Gau, B.; Slade, W. O.; Juergens, M.; Li, P.; Hicks, L. M. The Global Phosphoproteome of Chlamydomonas reinhardtii Reveals Complex Organellar Phosphorylation in the Flagella and Thylakoid Membrane. *Mol. Cell Proteomics* **2014**, *13* (9), 2337–2353.

72. Wheeler, G. L.; Miranda-Saavedra, D.; Barton, G. J. Genome Analysis of the Unicellular Green Alga Chlamydomonas reinhardtii Indicates an Ancient Evolutionary Origin for Key Pattern Recognition and Cell-Signaling Protein Families. *Genetics* **2008**, *179* (1), 193–197.

73. Ubersax, J. A.; Ferrell, J. E. Mechanisms of Specificity in Protein Phosphorylation. *Nat. Rev. Mol. Cell Biol.* **2007**, *8* (7), 530–541.

74. Ubersax, J. A.; Woodbury, E. L.; Quang, P. N.; Paraz, M.; Blethrow, J. D.; Shah, K.; Shokat, K. M.; Morgan, D. O. Targets of the Cyclin-Dependent Kinase Cdk1. *Nature* **2003**, *425* (6960), 859–864.

75. Pinna, L. A.; Ruzzene, M. How Do Protein Kinases Recognize Their Substrates? *Biochim. Biophys. Acta - Mol. Cell Res.* **1996**, *1314* (3), 191–225.

76. Beenstock, J.; Mooshayef, N.; Engelberg, D. How Do Protein Kinases Take a Selfie (Autophosphorylate)? *Trends Biochem. Sci.* **2016**, *41* (11), 938–953.

77. Bertics, P. J.; Gill, G. N. Self-Phosphorylation Enhances the Protein-Tyrosine Kinase Activity of the Epidermal Growth Factor Receptor. *J. Biol. Chem.* **1985**, *260* (27), 14642–14647.

78. Song, J.; Wang, H.; Wang, J.; Leier, A.; Marquez-Lago, T.; Yang, B.; Zhang, Z.; Akutsu, T.; Webb, G. I.; Daly, R. J. PhosphoPredict: A Bioinformatics Tool for Prediction of Human Kinase-Specific Phosphorylation Substrates and Sites by Integrating Heterogeneous Feature Selection. *Sci. Rep.* **2017**, *7* (1), 6862.

79. Neuberger, G.; Schneider, G.; Eisenhaber, F. PkaPS: Prediction of Protein Kinase A Phosphorylation Sites with the Simplified Kinase-Substrate Binding Model. *Biol. Direct* **2007**, *2* (1), 1.

80. Yang, P.; Humphrey, S. J.; James, D. E.; Yang, Y. H.; Jothi, R. Positive-Unlabeled Ensemble Learning for Kinase Substrate Prediction from Dynamic Phosphoproteomics Data. *Bioinformatics* **2016**, *32* (2), 252–259.

81. Huang, Y.; Houston, N. L.; Tovar-Mendez, A.; Stevenson, S. E.; Miernyk, J. A.; Randall, D. D.; Thelen, J. J. A Quantitative Mass Spectrometry-Based Approach for Identifying Protein Kinase Clients and Quantifying Kinase Activity. *Anal. Biochem.* **2010**, *402* (1), 69–76.

82. Vlad, F.; Turk, B. E.; Peynot, P.; Leung, J.; Merlot, S. A Versatile Strategy to Define the Phosphorylation Preferences of Plant Protein Kinases and Screen for Putative Substrates. *Plant J* **2008**, *55* (1), 104–117.

83. Wang, P.; Hsu, C.-C.; Du, Y.; Zhu, P.; Zhao, C.; Fu, X.; Zhang, C.; Paez, J. S.; Macho, A. P.; Tao, W. A.; Zhu, J.-K. Mapping Proteome-Wide Targets of Protein Kinases in Plant Stress Responses. *Proc. Natl. Acad. Sci. U.S.A.* **2020**, 201919901.

84. Xue, L.; Wang, W.-H.; Iliuk, A.; Hu, L.; Galan, J. A.; Yu, S.; Hans, M.; Geahlen, R. L.; Tao, W. A. Sensitive Kinase Assay Linked with Phosphoproteomics for Identifying Direct Kinase Substrates. *Proc. Natl. Acad. Sci. U.S.A.* **2012**, *109* (15), 5615–5620.

CHAPTER 2: Inhibition of TOR in *Chlamydomonas reinhardtii* Leads to Rapid Cysteine Oxidation Reflecting Sustained Physiological Changes[1]

2.1 Introduction

Target of rapamycin (TOR) is a conserved Ser/Thr kinase and master regulator of cellular growth and homeostasis in eukaryotes, with significant control over nutrient-responsive pathways including macromolecular anabolism and catabolism as well as vacuole formation and autophagy[1–7]. In yeast, mammals, and other complex eukaryotes, TOR has been identified in two distinct complexes, TORC1 and TORC2[2,8–11], but in photosynthetic organisms only the components of TORC1 have been identified[2,4]. While the role of TOR in mammalian species and yeast has been studied extensively[2,12,13], its role in photosynthetic organisms is less established[4,5].

Specific chemical inhibitors of TOR have been used to delineate some of the targets of the TOR pathway in mammalian cells[14], yeast[15], and photosynthetic organisms[16–18] through proteomics and transcriptomic analyses as well as physiological characterization. Directly inhibiting TOR results in similar phenotypic changes observed under nitrogen deprivation[19,20], including an increase in triacylglycerol (TAG) content and a decrease in protein synthesis[21]. This suggests that the eukaryotic "lipid switch"—the protein(s) responsible for upregulating lipid formation under nutrient limitation—is regulated by the TOR pathway[19–23]. TAG induction is a response to autophagy[24,25], a process highly regulated by TOR in algae. TOR inhibition of the model algal species *Chlamydomonas reinhardtii* (*C. reinhardtii*) induces vacuolization, cell

[1] Reprinted with permission from Ford, M. M.; Smythers, A. L.; McConnell, E. W.; Lowery, S. C.; Kolling, D. R. J; Hicks, L. M. Inhibition of TOR in *Chlamydomonas reinhardtii* Leads to Rapid Cysteine Oxidation Reflecting Sustained Physiological Changes. *Cells* **2019**, *8*(10), 1171.

bleaching, and production of autophagy-specific cell markers[1,26]. Additionally, TOR is involved in the regulation of protein synthesis, with the small molecule inhibitor rapamycin decreasing protein synthesis through the phosphorylation of BiP, an endoplasmic reticulum chaperone and member of the HSP70 superfamily involved in post-translational protein folding[27]. Furthermore, TOR has a significant role in the overall nutrient metabolism of the cell, including the aforementioned TAG synthesis pathways as well as the tricarboxylic acid cycle, which is downregulated under TOR inhibition and decreases carbohydrate catabolism[18,28].

In addition to phosphorylation, protein oxidation can play an important role in the regulation of stress response, as studied previously using exogenous H_2O_2 in algae[29]. However, little work has been done to look at the role of oxidative signaling in response to the TOR pathway, either through regulation of the TOR pathway via oxidation or the TOR pathway controlling oxidative stress response in the cell. Oxidative stress can cause increased protein oxidation on the reactive thiol groups of cysteines (Cys) in the form of disulfide bonds, S-glutathionylation, S-nitrosylation, and S-sulfenylation, all of which can leverage a reversible regulatory mechanism. TOR itself has been shown in mammalian cells to be regulated by the reversible formation of disulfide bonds by thioredoxin-1[30]. In photosynthetic organisms, reversible oxidation sites have been previously identified on enzymes involved in signaling, stress response, transcription and translational control, and metabolism[22,31–35]; all of these are pathways also known to be regulated by TOR, indicating that TOR is likely utilizing reversible oxidative signaling. While many targets of the TOR pathway have known sites of reversible oxidation, the extent to which reversible oxidation is implemented in TOR signaling is unknown, as are the resulting physiological responses.

Herein, quantitative proteomics of TOR inhibition in *C. reinhardtii* via enrichment of reversibly oxidized Cys (Figure 2.1) reveals significant increases in reversible oxidation throughout the proteome over the first hour of inhibition, including sites related to lipid synthesis, carbohydrate synthesis and catabolism, and photosynthesis. Physiological changes measured up to 48 h, including increases in TAG and carbohydrate content, correlate with oxidative changes, delineating the impact of TOR inhibition on changing cell metabolism. Additionally, inhibition of photosynthesis in response to TOR inhibition was characterized for the first time. This analysis demonstrates the overlap of physiological control and signaling regulation of the TOR pathway through reversible oxidation of thiols.

2.2 Materials and Methods

2.2.1 Strain, Culture Growth and Treatment Conditions

Wild-type *C. reinhardtii* strain CC-2895 6145c mt- and Hutner's trace elements were purchased from the Chlamydomonas Resource Center (St. Paul, MN, USA) and batch cultures were maintained photoheterotrophically on Tris-acetate-phosphate (TAP) agar plates. For physiological experiments, *C. reinhardtii* was inoculated into 25 mL of TAP medium using a 250 µL inoculum in a 50 mL Erlenmeyer flask top capped with aluminum foil. For proteomic experiments, cells were inoculated into 250 mL of TAP liquid medium[36] in 500 mL sterile Erlenmeyer flasks. Cultures were grown photoheterotrophically in quadruplicate, using a 2.5 mL inoculum from a mid-exponential-phase ($OD_{750\ nm}$ 0.4–0.5) culture and grown under constant white-light conditions of 30 µmol photons m^{-2} s^{-1} at 25 °C and at an orbital rotational speed of 120 rpm on a VWR International model 1000 standard orbital shaker (Radnor, PA, USA).

AZD8055 (MedChem Express; Monmouth Junction, NJ, USA) dissolved in dimethyl sulfoxide (DMSO; Fisher Scientific, Waltham, MA, USA) was added when cells reached an

$OD_{750\ nm}$ of 0.4 ± 0.1 to the saturating concentration of 700 nM[16]. Control cultures were given an equal volume of DMSO without AZD8055. For physiological measurements, the cells were harvested immediately after dosing and then every 12 h through 48 h of treatment (Figure 2.2a). For proteomics experiments, the cells were harvested immediately after dosing as well as 15 min, 30 min, and 1 h post-dosing (Figure 2.2b). Cells were harvested by centrifuging for 2 min at 3220× *g* and discarding the supernatant. Cell pellets were flash-frozen using liquid nitrogen and stored at −80 °C until use.

2.2.2 Spectroscopic Cell Density and Cell Diameter

Spectroscopic cell density (turbidity) was measured using a Shimadzu UV-1800 spectrophotometer (Shimadzu Corp., Kyoto, Japan) at 750 nm as previously described[37,38]. Cell diameter was determined using a micrometer slide on a VistaVision light microscope (VWR International), at 1000× magnification. FIJI software was used for image analysis[39].

2.2.3 Pigment Extraction

Pigments were extracted as previously described and measured from 470 to 700 nm[37]. Chlorophyll *a* content (Chl *a*) was calculated using the following equation[40]: [Chl *a*] = (12.47 × $Abs_{665.1}$) – (3.62 × $Abs_{649.1}$).

2.2.4 Cell Dry Weight Measurement

Dry mass was measured as previously reported[38]. Briefly, 1 mL of cells were pelleted and rinsed with H_2O and filtered onto pre-weighed 1 μm, 25 mm GF/B Whatman glass microfiber filters (Whatman International Ltd., Maidstone, UK) using a Büchner funnel. Filters and cells were dried in an incubator at 75 °C for 24 h before being weighed on a Secura 125-1S analytical balance (Sartorius, Göttingen, Germany).

2.2.5 Lipid Analysis

Lipid extractions were performed as previously described using a modified methyl *tert*-butyl ether (MTBE) extraction[41]. A 10 mL sample was pelleted and the supernatant discarded. Cell pellets were lysed with 1 mL of methanol (Fisher Scientific) and incubated in a 9 mL tube with 4 mL of MTBE (Fisher Scientific) for 1 h before adding 1 mL H_2O and incubating for another 15 min. Suspensions were centrifuged for 15 min at 10,000× *g* and the organic layer was removed by a Pasteur pipette into a pre-weighed 4 cm tube and dried under vacuum. The extraction was completed twice to ensure near-complete recovery of lipid mass. Tubes were weighed on a 125-1S Secura analytical balance. Neutral lipids were measured using Nile Red (Sigma-Aldrich, St. Louis, MO, USA) fluorescent staining[42]. Cells were incubated in the dark for 10 min following a 1:1 dilution in 2 $\mu g \cdot mL^{-1}$ Nile Red in DMSO. Fluorescence was measured using a SpectraMax M2 (Molecular Devices, LLC, San Jose, CA, USA) with a nine-point well scan and an excitation wavelength of 530 nm and emission wavelength of 580 nm.

2.2.6 Biochemical Composition

Terminal carbohydrates were assayed as previously described using the acid-phenol assay[38,43]. Briefly, 100 µL of sample was collected in triplicate from each culture and pelleted, discarding the supernatant. The pellet was then resuspended with 100 µL H_2O before adding 500 µL concentrated H_2SO_4 (Fisher Scientific) and vortexing. After a 15 min incubation at room temperature (RT), 100 µL of 5% (*w*/*v*) phenol (Fisher Scientific) in H_2O was added and vortexed. After 15 min, the absorbance of each sample was measured at 490 nm using a Shimadzu UV-1800 spectrophotometer. Calibration curves were prepared daily using a freshly prepared 0.05 mg/mL D-glucose (Sigma-Aldrich) stock solution.

Terminal proteins were extracted following a previously described method [44] and were assayed using a modified Lowry assay[45,46]. A stock of Lowry Reagent D was prepared daily in a 48:1:1 ratio of Lowry Reagents A (2% *w*/*v* Na_2CO_3 in 0.1N NaOH; Fisher Scientific), B (1% *w*/*v* NaK tartrate; Fisher Scientific), and C (0.5% *w*/*v* $CuSO_4 \cdot 5H_2O$; Fisher Scientific) and the Folin-Ciocalteu reagent (Sigma-Aldrich) was prepared daily with a 1:1 ratio of H_2O. All biological replicates were measured in triplicate by adding 50 µL of protein extract to 950 µL of Lowry Reagent D before vortexing and incubating at RT for 10 min. Following incubation, 100 µL of diluted Folin-Ciocalteu reagent was added before thoroughly vortexing and incubating at RT for 30 min. The absorbance of each sample was measured at 600 nm using a Shimadzu UV-1800 spectrophotometer and quantified daily using a five-point calibration curve prepared from a 2 mg $\cdot$ mL^{-1} bovine serum albumin stock solution (Fisher Scientific).

2.2.7 Chlorophyll Fluorescence Induction *in vivo*

The Chl *a* OJIP transient is a highly sensitive measurement of photosynthesis that is used to infer information about the efficiency of electron transport through photosystem II (PSII)[47]. When a dark-adapted phototrophic sample is exposed to actinic light, the Chl *a* fluorescence emits in a polyphasic rise with four characteristic 'steps,' O, J, I, and P. The O step corresponds with the origin, or minimal fluorescence, the J and I are for the inflections at 2 and 30 ms, respectively, and the P is the maximum fluorescence output. Using the O and P steps, it is possible to calculate the F_V/F_M, in which F_V denotes the variable fluorescence calculated by taking the difference between F_M and F_O and F_M is the fluorescence at the P step (Table 2.1). F_V/F_M is a measure of the maximum quantum yield of primary photochemistry in a dark-adapted state and is frequently used to express overall photosynthetic efficiency. The steps of the OJIP

transient have also been shown to correspond to the oxidation state of the plastoquinone pool; as the steps increase in intensity, the overall oxidation state of the pool also increases[48].

Photosynthetic electron transfer fluxes were inferred from Chl *a* fluorescence using a Photon Systems Instruments FL 3500 fluorometer (Drasov, Czech Republic) as previously described[38]. The OJIP protocol included a 1s actinic illumination using a 630 nm light at an intensity of 2,400 μmole photons · m^{-2} · s^{-1}. Fluorometry OJIP parameters (JIP test) were calculated as outlined by Stirbet[47].

Additionally, Chl *a* fluorescence was used to determine the proportion of active reducing centers, as using two subsequent actinic pulses separated by 1 s of darkness allows further information regarding the redox state of the Q_B reducing centers of PSII. While the first pulse was conducted following dark adaptation, meaning that all the reaction centers were open, the second pulse only excited so-called 'fast-opening' reaction centers, allowing for the calculation of non-reducing centers (centers which are unable to open in time for the second pulse) through the equation:

where F_V/F_M is derived from the first pulse and F_V*/F_M* is derived from the second pulse.

2.2.8 Pulse Amplitude Modulated (PAM) Fluorescence

When photons (or excitons) reach PSII reaction centers, they have one of three fates: they may be used for photochemistry, emitted as fluorescence, or dissipated as heat via an internal conversion phenomenon called non-photochemical quenching (NPQ). These three fates combine to be unity, meaning that a change in the abundance of one will result in proportional changes in

the others. Thus by determining the amount of NPQ and photochemistry through fluorescence techniques, a total picture of photon fate can be generated[49].

To measure NPQ, a quenching analysis of PAM fluorescence was used on dark-adapted cells with an actinic intensity of 300 µmol photons · m^{-2} · s^{-1}, a saturating pulse intensity of 64,000 µmol photons · m^{-2} · s^{-1}, and a measuring flash voltage of 80%. There was a dark relaxation duration of 20 s between pulses[50]. Photochemical coefficients were calculated as previously reported[48].

2.2.9 Protein Extraction for Proteomics Analyses

Frozen cell pellets (0.3 g FW from 50 mL of culture) were lysed in 10 mL of phosphate-buffered saline (PBS) with 0.5% SDS (Sigma-Aldrich), 0.1% Triton X-100 (Sigma-Aldrich), and ¼ tablet of cOmplete, EDTA-free protease inhibitor cocktail (Roche, Basel, Switzerland). Reduced Cys were blocked using 100 mM *N*-ethylmaleimide (NEM; Sigma-Aldrich) by adding 1 mL of 1 M NEM dissolved in 50% ethanol (Fisher Scientific). The reaction was incubated for 2 h at RT protected from light before centrifuging for 5 min at 3220× *g* and 4 °C to form a white pellet of cell debris. The supernatant was added to 10 mL of cold acetone (Fisher Scientific) and incubated for 30 min at –20 °C before centrifuging to pellet proteins. Samples were resuspended in 10 mL of PBS with 0.25% SDS and 4 M urea (Sigma-Aldrich) by aspirating back and forth with a 1 mL pipette tip. Protein concentration was estimated using the CB-X Protein Assay (G-Biosciences, St. Louis, MO, USA) and normalized to 1 mg/mL with resuspension buffer. Aliquots were taken for global proteomic (100 µg) and oxidized Cys enrichment analysis (1 mg).

2.2.10 Global Proteomics

Sample lysates (100 µg) were incubated on a covered ThermoMixer (Eppendorf, Hamburg, Germany) set to 25 °C and 1000 rpm. Disulfide bonds were reduced with 10 mM dithiothreitol

(DTT; Sigma-Aldrich) for 30 min before directly adding 30 mM NEM for 30 min to alkylate Cys residues. Samples were mixed with 1 mL of cold acetone to precipitate proteins and centrifuged for 5 min at 10,000× *g* and 4 °C. Pellets were resuspended (500 µL) in 50 mM Tris, pH 8 with 2 M urea and digested with 2.5 µg of Trypsin Gold (Promega, Madison, WI, USA) overnight (> 16 h). The digestion was quenched (20 µL) with 5% trifluoroacetic acid (TFA; Fisher Scientific) and desalted with solid-phase extraction (SPE).

2.2.11 Oxidized Cys Enrichment

Reversible oxidation changes were measured using an oxidized Cys resin-assisted capture enrichment strategy, abbreviated as OxRAC, that has been described previously (Figure 2.1)[35,51]. Briefly, protein lysates (1 mg) were incubated with 10 mM DTT for 1 h at RT to reduce all reversibly oxidized Cys before precipitating proteins with 10 mL of cold acetone. Samples were incubated for 30 min at –20 °C before centrifuging for 5 min at 3220× *g* and 4 °C to collect proteins. Samples were resuspended in 1 mL of 50 mM Tris, pH 8 with 0.5% SDS and 4 M urea by aspirating back and forth with a 1 mL pipette.

Thiopropyl Sepharose 6B (TPS6B; GE Healthcare, Pittsburgh, PA, USA) resin was rehydrated in water and washed with 50 mM Tris, pH 8 before suspending to a 100 mg/mL slurry. Each sample was mixed with 50 mg of TPS6B resin (0.5 mL slurry) and incubated with end-over-end rotation for 2 h to covalently enrich proteins with reduced Cys. Samples were transferred to a MobiSpin column (Boca Scientific, Westwood, MA, USA) and nonspecifically bound proteins were removed by washing the resin (400 µL each) in 50 mM Tris, pH 8 with 0.5% SDS, 50 mM Tris, pH 8 with 2 M NaCl (Sigma-Aldrich), 80% acetonitrile (Fisher Scientific) with 0.1% TFA, and 50 mM Tris, pH 8. On-resin digestion of Cys-bound proteins was performed in 250 µL of 50 mM Tris, pH 8 with 2.5 µg of Trypsin Gold (Promega) and

incubated overnight (> 16 h) with agitation at RT. The unbound peptide flow-through was separated from the Cys-bound peptides by briefly centrifuging the spin columns. Samples were washed (400 µL) using 50% acetonitrile and subsequently water. Bound Cys-containing peptides were eluted from the resin using 50 mM DTT (250 µL) for 15 min with agitation at RT and centrifuged to collect. The resin was washed twice with 50% acetonitrile (200 µL) and collected with the eluate. Samples were dried by vacuum centrifugation and SPE desalted as described below.

2.2.12 Solid-Phase Extraction

Desalting of samples was performed using 50 mg/1.0 mL Sep-Pak C18 cartridges (Waters, Milford, MA, USA) held in a SPE 24-position vacuum manifold (Phenomenex, Torrance, CA, USA) at a maximum flow rate of 1 drop/s. Resin was first pre-eluted using 1 mL of 80% acetonitrile with 0.1% TFA before equilibration with 1 mL of water with 0.1% TFA. Samples were acidified to pH 3 using 5% TFA and loaded onto the cartridges in two passes before washing with 1 mL of water with 0.1% TFA. Peptides were eluted using 1 mL of 80% acetonitrile with 0.1% TFA and dried by vacuum centrifugation.

2.2.13 LC-MS/MS Analysis

Samples were analyzed using a nanoAcquity UPLC (Waters) coupled to a TripleTOF 5600 mass spectrometer (AB Sciex, Framingham, MA, USA). Mobile phase A consisted of water with 0.1% formic acid (Fisher Scientific) and mobile phase B was acetonitrile with 0.1% formic acid. Injections (5 µL) were made to a Symmetry C_{18} trap column (100 Å, 5 µm, 180 µm x 20 mm; Waters) with a flow rate of 5 µL/min for 3 min using 99% A and 1% B. Peptides were then separated on a HSS T3 C_{18} column (100 Å, 1.8 µm, 75 µm x 250 mm; Waters) using a linear gradient of increasing mobile phase B at a flow rate of 300 nL/min. Mobile phase B increased

from 5% to 35% in 90 min before ramping to 85% in 5 min, where it was held for 5 min before returning to 5% in 2 min and re-equilibrating for 13 min. The mass spectrometer was operated in positive polarity and the NanoSpray III source had ion source gas 1 set to 15, curtain gas at 25, IonSpray voltage floating at 2400, and interface heater temperature at 150. MS survey scans were accumulated across *m/z* range of 350–1600 for 250 ms. For data-dependent acquisition, the mass spectrometer was set to automatically switch between MS and MS/MS experiments for the first 20 features above 150 counts having +2 to +5 charge state. Precursor ions were fragmented using rolling collision energy and accumulated in high sensitivity mode across *m/*z range 100–1800 for 85 ms. Dynamic exclusion for precursor *m/z* was set to 8 s. Automatic calibration was performed every 8 h using a tryptic digest of BSA protein standard (Thermo Scientific) to maintain high mass accuracy in both MS and MS/MS acquisition.

2.2.14 Database Searching and Label-Free Quantification

Acquired spectral files (*.wiff) were imported into Progenesis QI for proteomics (Nonlinear Dynamics, version 2.0; Northumberland, UK). Peak picking sensitivity was set to maximum of five and a reference spectrum was automatically assigned. Total ion chromatograms (TICs) were then aligned to minimize run-to-run differences in peak retention time. Each sample received a unique factor to normalize all peak abundance values resulting from systematic experimental variation. Alignment was validated (> 80% score) and a combined peak list (*.mgf) was exported for peptide sequence determination and protein inference by Mascot (Matrix Science, version 2.5.1; Boston, MA, USA). Database searching was performed against the *Chlamydomonas reinhardtii* UniProt database (https://www.uniprot.org/proteomes/UP000006906, 18,828 canonical entries) with sequences for common laboratory contaminants (https://www.thegpm.org/cRAP/, 116 entries) appended. Searches of MS/MS data used a trypsin

protease specificity with the possibility of two missed cleavages, peptide/fragment mass tolerances of 15 ppm/0.1 Da, and variable modifications of protein *N*-terminus acetylation, and methionine oxidation. Alkylation of Cys with NEM (+125.0477 Da, $C_6H_7NO_2$) was set as a fixed modification for global proteomic samples and variable for oxidized Cys enrichments. Significant peptide identifications above the identity or homology threshold were adjusted to less than 1% peptide FDR using the embedded Percolator algorithm[52] and imported to Progenesis for peak matching. Identifications with a Mascot score less than 13 were removed from consideration in Progenesis before exporting both "Peptide Measurements" and "Protein Measurements" from the "Review Proteins" stage.

2.2.15 Data Analysis and Statistics

For physiological measurements, the data were analyzed through multiple comparisons of means conducted using Welch's t-tests. The family-wise error rate for each figure was maintained at 0.05 through the use of the Holm-Bonferroni method, unless stated otherwise. To determine statistical significance of changes over time, data was analyzed through one-way repeated measures analysis of variance (ANOVA) conducted with Graphpad Prism (Graphpad Software, v7.01;San Diego, CA, USA). Statistical significance is indicated numerically through increasing asterisks, where * indicates $p \leq 0.05$, ** indicates $p \leq 0.01$, *** indicates $p \leq 0.005$, and **** indicates $p \leq 0.001$. Figures show the means of quadruplicate data and the error bars denote the standard error of the measurement.

For LC-MS/MS-based proteomics, data were parsed using custom scripts written in R for pre-processing and statistical analysis (https://github.com/hickslab/QuantifyR).

For global proteomic analysis, leading protein accessions were considered from the "Protein Measurements" data and kept if there were ≥ 2 shared peptides and ≥ 1 unique peptide assigned.

Proteins were removed if there was not at least one condition with 3/4 nonzero values across the Progenesis-normalized abundance columns. Values were $\log_2$-transformed and we applied a conditional imputation strategy using the imp4p package[53], where conditions with at least one nonzero value had missing values imputed using the *impute.rand* function with default parameters. For cases where a condition had only missing values, the *impute.pa* function was used to impute small numbers centered on the lower 2.5% of values in each replicate. Statistical significance was determined using a two-tailed, equal variance *t*-test and the method of Benjamini and Hochberg (BH) was used to correct *p*-values for multiple comparisons[54]. Fold change was calculated by the difference of the mean abundance values between conditions being compared. Only observations with FDR-adjusted $p < 0.05$ and $\log_2$-transformed fold change +/– 1.5 were considered significantly different.

For the OxRAC experiment, we summarized the "Peptide Measurements" data, which contains peak features with distinct precursor mass and retention time coordinates matched with a peptide sequence identification from the database search results.

Some features were duplicated and matched with peptides having identical sequence, modifications, and score, but alternate protein accessions. These groups were reduced to satisfy the principle of parsimony and represented by the protein accession with the highest number of unique peptides found in the "Protein Measurements" data for this experiment, else the protein with the largest confidence score assigned by Progenesis. Some features were also duplicated with differing peptide identifications and were reduced to just the peptide with the highest Mascot ion score.

Results were then filtered for reversibly oxidized Cys-peptides only, defined here by the absence of NEM modification on at least one Cys residue in the peptide sequence. An identifier

was created by joining the protein accession of each peptide to the particular site(s) of modification in the protein sequence. Each dataset was reduced to unique identifiers by summing the abundance of all contributing peak features (i.e., different peptide charge states, missed cleavages, and combinations of additional variable modifications). Identifiers were represented by the peptide with the highest Mascot score in each group.

Identifiers were removed if there was not at least one condition with 3/4 nonzero values across the Progenesis-normalized abundance columns. Values were $\log_2$-transformed and we applied the same conditional imputation strategy as used for the global proteomic analysis.

Statistical significance was determined using one-way analysis of variance (ANOVA) and *p*-values were BH-corrected. Only observations with FDR-adjusted $p < 0.05$ and $\log_2$-transformed fold change +/– 2 in the 60 min condition relative to the 0 min control were considered significantly different. Unsupervised hierarchical clustering was performed on significantly different identifiers to group together similarly changing abundance trends across conditions (i.e., with time). Gene ontology (GO) annotations were pulled from UniProt and summarized/visualized for each cluster.

2.2.16 Data Availability

The mass spectrometry proteomics data have been deposited to the ProteomeXchange Consortium via the PRIDE partner repository[55] and can be accessed with the identifier PXD014819.

2.3 Results

2.3.1 Cell Growth

Cell growth of both control and TOR inhibitor-treated cultures increased by 142 and 68%, respectively, from the point of dosage until 48 h (Figure 2.3a). However, treatment with AZD8055 inhibited the amount of overall growth when compared to the control, with a final turbidity 32% less than the control cultures, showing that while AZD8055 treatment did not completely result in the stagnation of cell density, it did lead to a severe decrease in rate of cell growth. Dry mass measurements were congruent with the $OD_{750\ nm}$ measurements (Figure 2.3b). While the optical density of AZD8055-exposed cells was increasing, the cell size also significantly increased over time, whereas the cell size of control cultures did not change significantly (Figure 2.3c). This suggests that the increasing optical density of AZD8055-treated cultures is due to an increase in cell size rather than cell number, which is further supported by cell counting (Figure 2.4). Additionally, while Chl *a* in AZD8055-treated cells was significantly less than in non-inhibited cells, this accumulation did not change significantly in treated cells over time, indicating that the cells are not chlorotic - the penultimate step in photoautotrophic autophagy (Figure 2.3d)[56].

Rather, it appears as though Chl *a* synthesis is inhibited without a subsequent increase in chlorophyll degradation. Thus, cell division of AZD8055-dosed cells was significantly inhibited in comparison with the control cultures, but cell death does not appear to be initiated as a result of TOR inhibition.

2.3.2 Bulk Cell Composition

Cells were assayed for protein, lipid, and carbohydrate content every 12 h (Figure 2.5a–c). No differences between control and AZD8055-treatment were observed in total protein or total

lipids, with the overall compositional percent staying within error throughout the time points measured (Figure 2.5a, b). However, neutral lipids had significant increases in AZD8055-exposed cells, with 2.6x the control at 48 h (Figure 2.5d).

Carbohydrates also significantly increased by 36 h post-dosage, with AZD8055-treated cultures accumulating 2.4x the carbohydrates vs. control cultures when normalized to dry mass (Figure 2.5c).

This is likely due to an increase in starch accumulation, as previous work has shown TOR-inhibition to favor lipid cycling to storage macromolecules[57]. This also could explain the increase in AZD8055-treated cell size, as cells with higher accumulations of starch are likely to have higher water accumulation that could increase the overall cell diameter[58,59].

2.3.3 Photosynthetic Output

In order to determine if TOR inhibition affects photosynthetic productivity, Chl *a* (OJIP) fluorescence and PAM fluorescence were used *in vivo* following AZD8055 treatment (Figure 2.6). Analysis of the OJIP transient following TOR inhibition revealed a decrease in PI_{abs}, the performance index on a per absorption basis, to 47% of its pre-AZD8055 productivity after just 1 h of exposure, showing that TOR has a significant and quick effect on photosynthetic electron transport (Figure 2.6a). Over time, this decrease in photosynthetic activity becomes more pronounced. The decrease in F_V/F_M (which shows that PSII is affected by AZD8055 even in a dark-adapted state) when compared to the control paired with the increase in the overall amplitude of the OJ phase of the transient indicates that the decline in photosynthetic efficiency is the result of a decrease in the overall reduction of Q_A centers in PSII[60] (Figure 2.6b). Furthermore, the averaged trapped energy flux per PSII reaction center (TR_0/RC), the relative

number of photons absorbed through the antenna that are trapped by PSII reaction centers, decreases to 60% of the control by 36 h post-dosage (Table 2.1).

Additionally, the two-pulse method of collecting OJIP traces indicated that the AZD8055-treated cultures decreased in reduction capacity (when compared to the control) only at 12 and 24 h after treatment, after which it was not statistically different from the control (Figure 2.7). This shows that the lack of electron flux was not a result of damage to the acceptor side of PSII, as the increase in B_0 does not explain the continuing decrease in photoactivity following the 24 h measurement[61]. However, while PAM fluorescence indicated that the electron flow through PSII (YII) was significantly diminished with a decrease of 1.8x after 1 h of AZD8055 treatment, the NPQ parameter was not increased (Figure 2.6c, d). As all absorbed photons must be accounted for through photochemistry, NPQ, or fluorescence, the decrease in photochemical flow in this case must be reallocated to fluorescence, showing a decrease in available PSII to further reduce the plastoquinone pool.

However, the M_0 parameter of the OJIP analysis, representative of the relative rate of primary Q_A reduction, increases over the first hour of AZD8055 inhibition, suggesting that the plastoquinone pool is being reduced more rapidly after TOR inhibition (Figure 2.6a). An increase in fluorescence paired with the increase in M_0 suggests that the plastoquinone pool is either not being sufficiently oxidized downstream or being re-reduced via cyclic electron transport, decreasing the availability of plastoquinone for the Q_A site of PSII and increasing the likelihood of charge recombination and subsequent fluorescence.

2.3.4 Coverage and Differential Analysis of the Reversibly Oxidized Thiol Proteome Upon TOR Inhibition

A total of 16 *C. reinhardtii* cultures, four biological replicates for each time point, were grown to mid-exponential phase before treatment. Previous TOR inhibition studies have shown that changes in signaling occur rapidly after treatment, in as little as two min[62]. Previous work in both *C. reinhardtii* and *Arabidopsis thaliana* has shown that after treatment with H_2O_2, changes in reversible oxidation are seen in as little as ten min[34,63]. Given these documented rapid changes and to minimize the impact of protein turnover in the experiment, time points of 0, 15, 30, and 60 min were selected to assess reversible oxidation upon TOR inhibition. Global differential proteomic analysis was performed between the 0- and 60-min time points to confirm the absence of protein turnover. Of the 1346 proteins identified across these samples, only one (A0A2K3DLA1, Ubiquinol oxidase) was shown to be significantly changing in abundance. 732 of these proteins identified in this global analysis, or 54%, were also measured in the oxidized Cys analysis. Thus, the observed changes in oxidation of the identified Cys sites in the time course can be confidently assessed and with little to no false positives resulting from protein turnover or expression changes.

Identification and site-specific quantification of reversible thiol oxidation has been readily performed via differential alkylation-based methods utilizing thiol-disulfide exchange chromatography[64,65] that have been tailored for specific modifications including S-nitrosylation[66,67], S-glutathionylation[68,69], and S-acylation[70]. By using DTT rather than a modification-specific reductant, it is possible to map the entirety of the cellular redox proteome. Herein, we have applied this strategy for quantitative profiling of reversible Cys oxidation using OxRAC in the *C. reinhardtii* proteome following *in situ* TOR inhibition with exogenous AZD8055.

Cys reactivity was quenched during cell lysis under denaturing conditions in the presence of NEM to block reduced thiols, which has been shown to be rapid and efficient in alkylation[71,72]. All reversibly oxidized Cys-residues were later reduced by DTT and nascent thiols enriched at the protein-level using Thiopropyl Sepharose 6B (TPS6B) resin. On-resin trypsin digestion of Cys-bound proteins was performed and unbound peptides were washed away. Cys-bound peptides were eluted from the resin and analyzed by LC-MS/MS.

Overall, 5177 unique oxidized Cys sites were identified, quantified by 4755 peptides, referred to as identifiers, from 2234 proteins. Most of these peptides had only one modification site (85% of 4755), which was most likely due to Cys being particularly rare. Most proteins in the *C. reinhardtii* proteome have Cys residues (93%, 17571/18828), but there are relatively fewer Cys compared to other amino acids (i.e., on average 1.6% Cys per protein compared to 11% Gly and 16% Ala), making peptides with multiple Cys residues a less frequent occurrence. Nearly half the proteins identified had only one modified site (48% of 2234).

These sites were compared with literature where specific redox modifications were targeted in *C. reinhardtii* including S-glutahionylation[32], S-nitrosylation[73], and thioredoxin-dependent reduction[74]. Of the proteins identified in this dataset, 22 were shown previously to be S-glutathionylated, 100 were S-nitrosylated, and 188 were thioredoxin-dependent.

The most modified protein had 41 oxidized Cys sites quantified by 36 identifiers and was a large (870 residues), predicted protein (A8JFZ2_CHLRE) localized to the Golgi membrane (GO:0000139) with a Cys-rich repeat (PF00839) known to form intra-chain disulfide bonds[75]. While most Cys sites on this protein were unchanged during the treatment, one Cys identifier (C632–646) increased 2.3-fold by 60 min and could provide mechanistic insight to this otherwise uncharacterized protein.

To assess overall change in oxidation across all four time points, a one-way ANOVA test was performed. After FDR-correction, 510 identifiers from 401 proteins had a significant 0–60 min fold change, with 135 identifiers decreasing in oxidation and 375 identifiers increasing in oxidation following TOR inhibition. A $p < 0.05$ after FDR correction and at least a two-fold change in oxidation was needed for an identifier to be considered significantly changing. Hierarchical clustering was performed on the identifiers that were significantly changing with AZD8055 treatment (Figure 2.8a). These identifiers, when sorted into two clusters, separate based on those identifiers that generally increase in oxidation (361 identifiers), and those that decrease (149 identifiers), suggesting the most pronounced change in oxidative state occurs after 60 min of treatment. However, there are identifiers within these data that, when a four-cluster analysis is used, show that some Cys sites have a maximum fold change before 60 min (Figure 2.9). This implies either a recovery of the oxidation state prior to treatment, or oxidation of the site to an extent that it becomes irreversibly oxidized. GO analysis revealed that proteins within cluster A from the two-cluster analysis, which are generally increasing in oxidation, include many physiologically important processes including translation, photosynthesis, and transcription (Figure 2.8b), as well as proteins with inorganic binding sites such as metal ion and ATP-binding enzymes. Many proteins in cluster B, which generally decrease in reversible oxidation, are involved with cell redox homeostasis. This finding suggests that these proteins may be highly reactive to oxidation under TOR inhibition, and rather than seeing a decrease in reversible oxidation through reduction, these Cys residues instead might be hyper-oxidized to an irreversible sulfinyl or sulfonyl modification.

2.4 Discussion

While previous research has shown the connection between TOR inhibition, lipid accumulation, and the similar phenotypic response seen with H_2O_2 treatment[29], this study indicates that large-scale reversible oxidative signaling is part of TOR pathway regulation and impacts all major aspects of metabolism. By investigating the 401 proteins with statistically significant changes in oxidation, focusing specifically on the proteins involved in lipid synthesis, protein translation, carbohydrate metabolism, the TOR pathway, and photosynthesis, it was possible to integrate observed physiological changes with the oxidized Cys-containing peptides, providing a framework for determining how TOR impacts the changing phenotype of *C. reinhardtii*.

2.4.1 Lipid Metabolism

The physiological response following TOR inhibition shows an increase in neutral lipids while overall lipid content remains steady. These data, when paired with the increase in cell size of AZD8055-treated cultures, is indicative of carbon reallocation in which the cells are redistributing lipids from phospholipids into TAGs for long-term storage—a phenomenon that has been characterized in *C. reinhardtii* following nitrogen deprivation[20]. These results are supported by the regulation of 48 lipid-related proteins through changes in reversible oxidation upon TOR inhibition. Of the 106 identifiers, eight were seen to significantly increase in oxidation upon inhibition including Cys302 on glycerol-3-phosphate acyltransferase (H9CTH0, FC: 49.67), Cys35-Cys39-Cys44 on phospholipase A2 (A8I2I2, FC: 9.59), Cys387-Cys390 on chloroplast ω6 desaturase (O48663, FC: 5.82), Cys653 on phospholipase B-like (A0A2K3DXV3, FC: 4.86), and C278 on phosphoglycerate kinase (A8JC04, FC: 2.74). Both phospholipases are involved in the cleavage of fatty acids in phospholipids, hydrolyzing the

major component of the cell membrane. It has been previously shown that under nitrogen deprivation there is an increase in phospholipase abundance and other components responsible for membrane remodeling, reflecting a similar response in regulation between these two stressors[20]. Phospholipases are also known to be Cys-rich, with many of these Cys residues involved in disulfide bonds[76]. While the impact of these oxidation sites is unknown, previous work has shown that oxidized Cys in mammalian cells regulate the activity of phospholipases[76]. Conversely, chloroplast ω6 desaturase is involved in lipid synthesis, introducing a double bond in the biosynthesis of 16:3 and 18:3 fatty acids, an important component of plant membranes[77]. The diversion of lipids from membrane components to TAGs suggests that this oxidation site may regulate the activity of this desaturase. Phosphoglycerate kinase (PGK) is involved in glycolysis and in carbon metabolism, catalyzing the reaction of 1,3-bisphosphoglycerate into 3-phosphoglycerate in glycolysis and the reverse reaction in the Calvin-Benson-Bassham Cycle (CBBC)[78]. This enzyme is known to be highly regulated by oxidation, with previous work in cyanobacteria showing that the conserved Cys residue found in this study plays an important role in regulating the activity of this kinase[78]. This previous work showed that oxidation of this Cys greatly diminished the activity of PGK, suggesting that the increase in oxidation seen in this study could be inhibiting the kinase, demonstrating regulation of glycolysis/CBBC by the TOR pathway via reversible oxidation[78].

2.4.2 Protein Translation

Although there was not a significant physiological change in total protein due to treatment, a number of translation-related proteins were identified as being regulated by reversible oxidation upon TOR inhibition. The latter better correlates to previous research studying physiological changes in *C. reinhardtii* following TOR inhibition[27]. A total of 204 identifiers were quantified

on 101 unique proteins involved in translation. Of these identifiers, 17 were found to increase in oxidation, while three significantly decreased. One of these identifiers is Cys82 on elongation factor Tu (P17746, FC: 3.23), a protein that promotes binding of aminoacyl-tRNA to the ribosomal A-site during protein synthesis. This protein has been shown to be oxidized in a number of different bacteria[79–81], and although the exact function of this oxidation is unknown, the conservation across multiple bacterial strains as well as in *C. reinhardtii* suggests this post-translational modification may be important for regulation of its activity.

Many ribosomal proteins were shown to contain reversible oxidation sites, including 121 identifiers on 62 proteins, nine of which significantly increased and two that significantly decreased. Ribosomal proteins in yeast have been shown to be regulated by reversible oxidation with many of these proteins containing a conserved CX_2C-$X_{9\text{-}47}$-$CX_{2,4}C$ site where oxidation occurs on one of these Cys residues[82]. These conserved motifs have been shown to be Zn^{+2} binding, stabilizing in protein folding, and their activity is redox-regulated. Two of the proteins in this study, ribosomal protein L37a (A8HY08) and ribosomal protein L36a (A8IM74), have this conserved motif. Ribosomal protein L37a demonstrated reversible oxidation on Cys39, the first Cys in the conserved motif, although it was not shown to be significantly changing. Ribosomal protein L36a had significantly changing oxidation on Cys86 (FC: 2.05), a Cys outside the conserved motif. Ribosomal protein L10 (A8IZK3) also has an identifier, Cys140, that significantly increases 2.07-fold in oxidation upon inhibition of TOR. This site is conserved in yeast, and is shown to be oxidized with H_2O_2 treatment, suggesting this site is involved in the response to chemical stressors[82].

2.4.3 Carbohydrate Metabolism

The assessment of cell composition after treatment with AZD8055 showed a significant increase in the percentage of carbohydrates as a function of dry mass in the cells beginning 36 h after treatment (Figure 2.5c). Previous work in plants and a red alga supports this, also showing an increase in starch accumulation with inactivity of TOR[83,84]. This result is further reflected in the changes in thiol oxidation found in this study, with 214 identifiers on 74 proteins showing reversible oxidation, 15 of these identifiers increasing in oxidation and one decreasing. The increase in carbohydrate content is supported more specifically by the oxidative regulation of several important enzymes involved in carbohydrate metabolism. NADP-malate dehydrogenase (Q9FNS5), has one site, Cys389, increasing in oxidation upon treatment (FC: 3.20). This is the chloroplastic isoform of the dehydrogenase, and is well-known to be redox-regulated in higher-order plants[85] and *C. reinhardtii*[86], but this is the first time it has been linked to TOR regulation. This Cys residue is conserved in sorghum and has been shown to be part of a regulatory disulfide bond, with the enzyme being fully active when it is completely reduced[87], suggesting that the increase in oxidation observed is decreasing the overall activity of the dehydrogenase.

The large subunit of isopropylmalate dehydratase (A8JG03) also has a Cys site significantly increasing in oxidation, Cys444 (FC: 2.47). This is a highly modified site, with previous work identifying S-glutathionylation[32], S-nitrosylation[73], and regulation via thioredoxin[74] on this Cys. Although the exact function of this Cys is unknown, it appears to be an important site for oxidative signaling in the cell.

The identifier with the largest fold change on a carbohydrate-related enzyme is a hypothetical protein (A0A2K3DY10, FC: 20.92) with a sequence almost identical to that of chloroplastic sedoheptulose-1,7-bisphosphatase (P46284), which shares this identifier. This

Cys116 site is known to be part of a disulfide bond controlled by thioredoxin, which activates the enzyme upon reduction of the disulfide[88]. With its important role in carbon fixation, the regulation of this enzyme could be contributing significantly to the increase in carbohydrate content that is seen in the cell.

2.4.4 TOR Pathway-Related Proteins

A total of 28 identifiers on 10 proteins of the known TOR signaling pathway had reversible oxidation identified in this study. Of those identifiers, only one, Cys26 on the TOR complex subunit Lethal with SEC-13 (LST8, A8JDD2), was shown to be significantly changing, with a four-fold increase in oxidation. Although a previous study on mTORC1 has shown that TOR activity is redox regulated[89], this is the first time that an oxidation site has been identified on LST8, which could impact the formation and activity of the TOR complex. While not shown in this dataset, the presence of oxidative sites on the other components of the TORC complex, TOR and Regulatory-associated protein of TOR (RAPTOR), each of which contain several cysteine residues, cannot be excluded; however, more specific enrichment/fractionation methods would need to be used to get the coverage needed for this determination.

A majority of the other TOR-pathway-realted identifiers were from vacuolar ATPases, many of which have been previously shown to be associated with the TOR pathway in mammalian systems[90]. This class of enzymes has high sequence homology, with conserved domains and subunits, and is known to be regulated by Cys oxidation. Although none of these identifiers in this study are changing with TOR inhibition, Cys oxidation was identified on V-type proton ATPase subunits C (A8HYU2), F (A8HZ87), and H (A8HQ97), as well as vacuolar ATP (V-ATP) synthase subunits A (A8I164), B (A8IA45), and E (A8IW47). Interestingly, Cys247 on V-ATP synthase subunit A is a conserved Cys shown to modulate its activity in Arabidopsis[91].

Although not changing, oxidation on this subunit suggests that this site may have a similar mechanism in *C. reinhardtii*, but is not regulated by TOR under the presented conditions. However, Subunit B of V-ATP synthase has been previously shown to be regulated by TOR via phosphorylation on Ser8[16]. With ATPases' important role of maintaining cell homeostasis under stress, this subunit could be an important component of TOR's regulatory pathway, but further studies would be required to assess its exact role.

2.4.5 Photosynthesis

There were 20 photosynthesis-related proteins with 21 significantly changing reversible oxidation identifiers, suggesting that inhibition TOR plays a role in regulating the light reactions of photosynthesis, a novel finding. Looking specifically at the protein components of photosynthetic machinery, 13 proteins were found to have oxidation on Cys with a total of 60 identifiers (Figure 2.10). Two of these proteins, photosystem I iron-sulfur center (PsaC, Q00914) and Ferredoxin—NADP reductase (FNR, A8J6Y8) have an identifier significantly increasing in oxidation (FC: 2.46 and 3.80, respectively) and two proteins, Cytochrome f (PetA, P23577) and Ferredoxin (PetF, A8IV40), have identifiers significantly decreasing in oxidation (FC: 0.39 and 0.36, respectively). OJIP analysis suggests that TOR inhibition results in decreased electron flow through PSII, likely stemming from an overly reduced plastoquinone pool due to downstream effects, resulting in decreased overall turnover of PSII and linear (oxygen-producing) photosynthetic activity. This diminished activity is irreversible and begins within 15 min of inhibition and continues through the full 48 h of treatment. While the lack of chlorosis (degradation of chlorophyll) suggests the photosynthetic apparatus is still intact, these data suggests that TOR inhibition results in a marked inhibition of electron flux through PSII. Furthermore, the increased reduction of the plastoquinone pool downstream of PSII suggests that

either downstream proteins of PSII have been damaged or that PSI is participating in cyclic, rather than linear, electron transport. Cyclic electron transport results in greater production of ATP as FNR is bypassed, resulting in electron transfer to cytochrome b_6f via the stromal side, increasing the proton gradient needed for ATP synthesis while decreasing the production of NADPH. This leads to a more reduced quinone pool, as fewer electrons are transferred to CO_2 via NADPH.

A shift to cyclic electron transport is supported by proteomic analysis, as there is a 3.8x FC in oxidation of FNR (A8J6Y8), showing a decrease in enzyme activity (FNR is reduced by ferredoxin following reduction by PSI)[92]. If FNR was generating NADPH, an increase in reduction, not oxidation, would be expected, as it would be reduced in the process of shuttling electrons. A shift toward cyclic electron transport is further indicated by the pairing of decreased PSII activity with the decrease in oxidation of Cys52-Cys55 of cytochrome *f* (P23577, FC: 0.39), the subunit of cytochrome b_6f responsible for electron transfer to plastocyanin. An increase in the reduction of cytochrome *f* suggests an increased electron load; while the b_6f complex is a rate-limiting step in both linear and cyclic electron transport[93], it would likely be more substantial under cyclic electron transport as electrons are supplied from both plastoquinol and ferredoxin. However, when paired with the increased oxidation of other regulatory Cys, such as PsaC (Q00914, FC: 3.36), a PSI subunit containing one of the iron-sulfur centers, it is also possible that damages downstream of PSII are causing a “traffic jam” for electrons, resulting in a more reduced plastoquinone pool that decreases the available plastoquinone for PSII. It could possibly be a combination of these two phenomena, wherein the ETC converts to cyclic electron transfer due to stress, while simultaneously decreasing capacity due to oxidative changes downstream of PSII.

2.5 Conclusions

While TOR is a known master regulator with significant control over nutrient-responsive pathways, its role in the metabolic regulation of photosynthetic eukaryotes is still not completely understood. By characterizing the physiological effects of AZD8055-mediated TOR inhibition on *C. reinhardtii* and pairing it with label-free quantitative proteomics following OxRAC, a network of reversible thiol oxidation was unveiled. This complex oxidation network was cell-wide, overlapping all major metabolic processes and indicating an essential role for thiol oxidative signaling in TOR regulation. TOR targets for thiol oxidation included important lipases involved in lipid cycling and TAG biosynthesis, directly linking oxidative signaling to upregulation of TAGs following TOR inhibition. Additionally, for the first time, photosynthesis was shown to be regulated by the TOR pathway with inhibition of TOR causing a decrease in the photosynthetic efficiency of PSII, and a shift toward cyclic electron transport. Future studies will benefit from modification-specific redox analysis, through which the individual regulatory mechanisms could be determined.

2.6 Tables

Table 2.1 OJIP parameters for AZD8055-treated and non-treated cells.

	AZD8055-dosed cells					**Control**				
	t0	**12 h**	**24 h**	**36 h**	**48 h**	**t0**	**12 h**	**24 h**	**36 h**	**48 h**
F_V/F_M	0.686	0.627	0.559	0.532	0.53	0.685	0.713	0.703	0.634	0.607
M_0	0.804	1.123	1.091	1.115	1.214	0.872	0.78	0.777	0.832	0.824
Φ_{E0}	0.345	0.269	0.25	0.241	0.23	0.346	0.369	0.346	0.315	0.313
Ψ_0	0.503	0.429	0.446	0.454	0.433	0.505	0.518	0.493	0.497	0.515
Abs/RC	2.351	3.141	3.522	3.829	4.044	2.571	2.273	2.178	2.608	2.802
TR_0/RC	1.614	1.967	1.97	2.038	2.142	1.76	1.619	1.531	1.652	1.701
Et_0/RC	0.81	0.843	0.879	0.924	0.928	0.888	0.839	0.754	0.821	0.877
Piabs	0.946	0.405	0.291	0.248	0.215	0.876	1.187	1.062	0.66	0.59

2.7 Figures

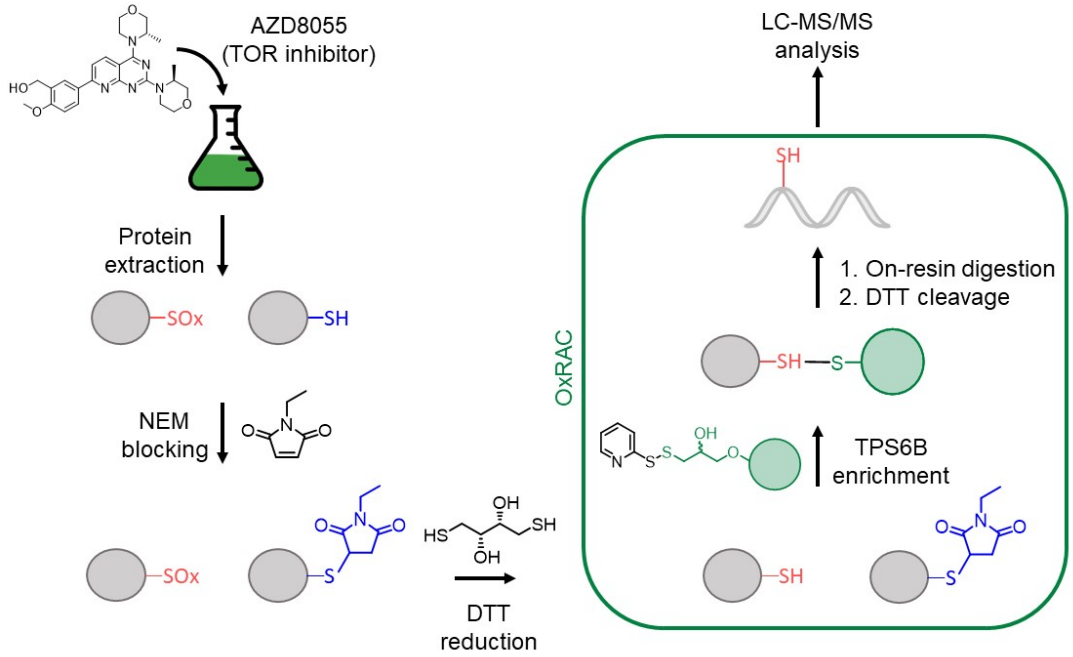

Figure 2.1 Workflow for proteomic oxidative cysteine analysis of *C. reinhardtii* with AZD8055 treatment. After protein extraction, reduced cysteine thiols are blocked with *N*-ethylmalemide (NEM), before reversibly oxidized cysteines are reduced using dithiothreitol (DTT). An oxidized cysteine resin-assisted capture method (OxRAC) is used to enrich proteins containing oxidized cysteines and samples are processed for bottom-up liquid chromatography—tandem mass spectrometry (LC-MS/MS) analysis.

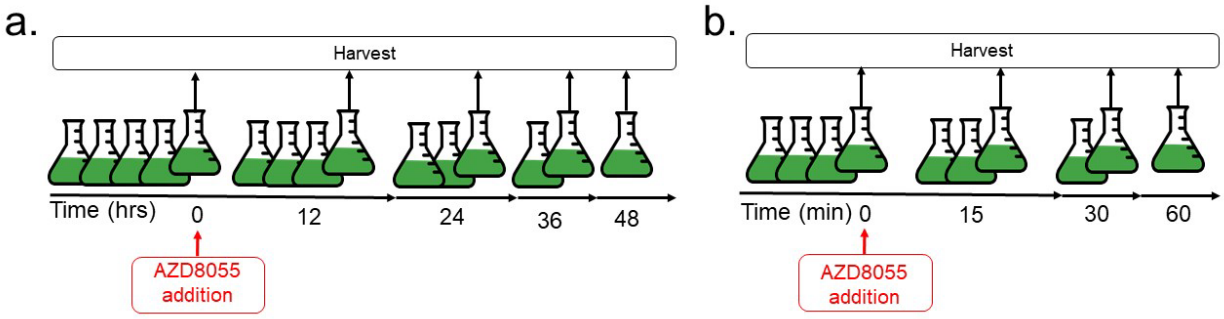

Figure 2.2 a.) Treatment and sampling timeline for physiological measurements. *C. reinhardtii* cultures were grown to stationary phase prior to treatment with AZD8055. b.) Treatment and harvesting timeline for proteomic oxidative cysteine thiol analysis and photosynthetic measurements. Cultures were grown to an OD_{750} of ~0.5 prior to treatment.

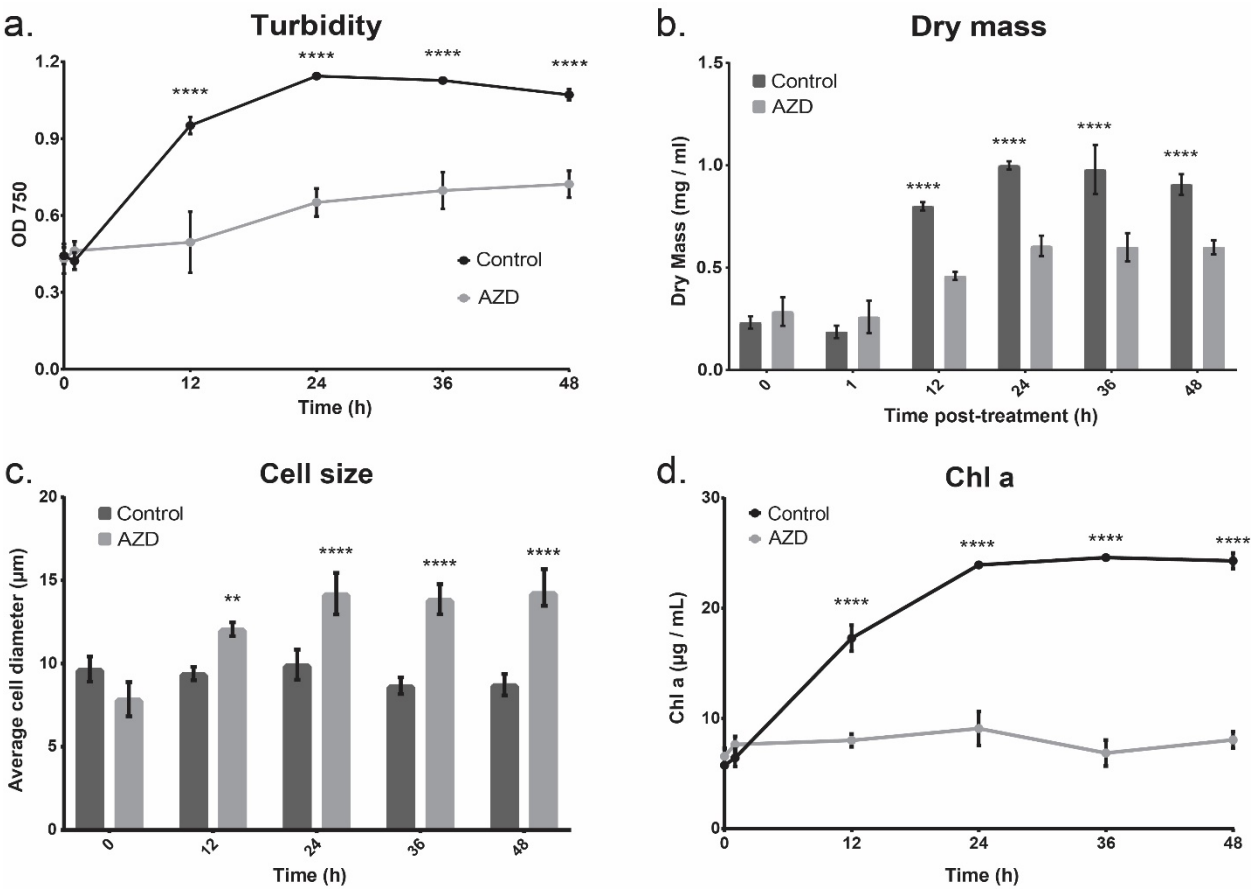

Figure 2.3 The growth curves of cultures with and without AZD8055 exposure. The error bars represent standard deviation and statistical differences indicate a difference between the inhibited and non-inhibited cultures at one time point. Significance is denoted by asterisks, where *** indicates $p \leq 0.001$, and **** indicates $p \leq 0.0001$. a.) The turbidity (optical density) of *C. reinhardtii* following dosing with AZD8055. Cells were dosed in mid-exponential phase. Control cultures were dosed with DMSO, the solvent used for AZD8055. b.) The total dry mass of the cultures with and without AZD8055 treatment. c.) The cell diameter of the cultures with and without AZD8055 treatment. d.) The Chl *a* content of cultures following treatment in mid-exponential phase. Chl *a* is an indication of both organismal health as well as photosynthetic productivity.

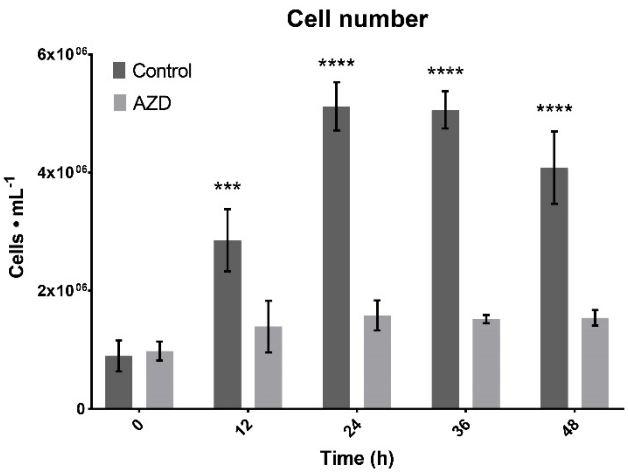

Figure 2.4 The cell number of cultures with and without AZD8055 exposure. The error bars represent standard deviation and statistical differences indicate a difference between the inhibited and non-inhibited cultures at one time point. Significance is denoted by asterisks, where *** indicates $p \leq 0.001$, and **** indicates $p \leq 0.0001$.

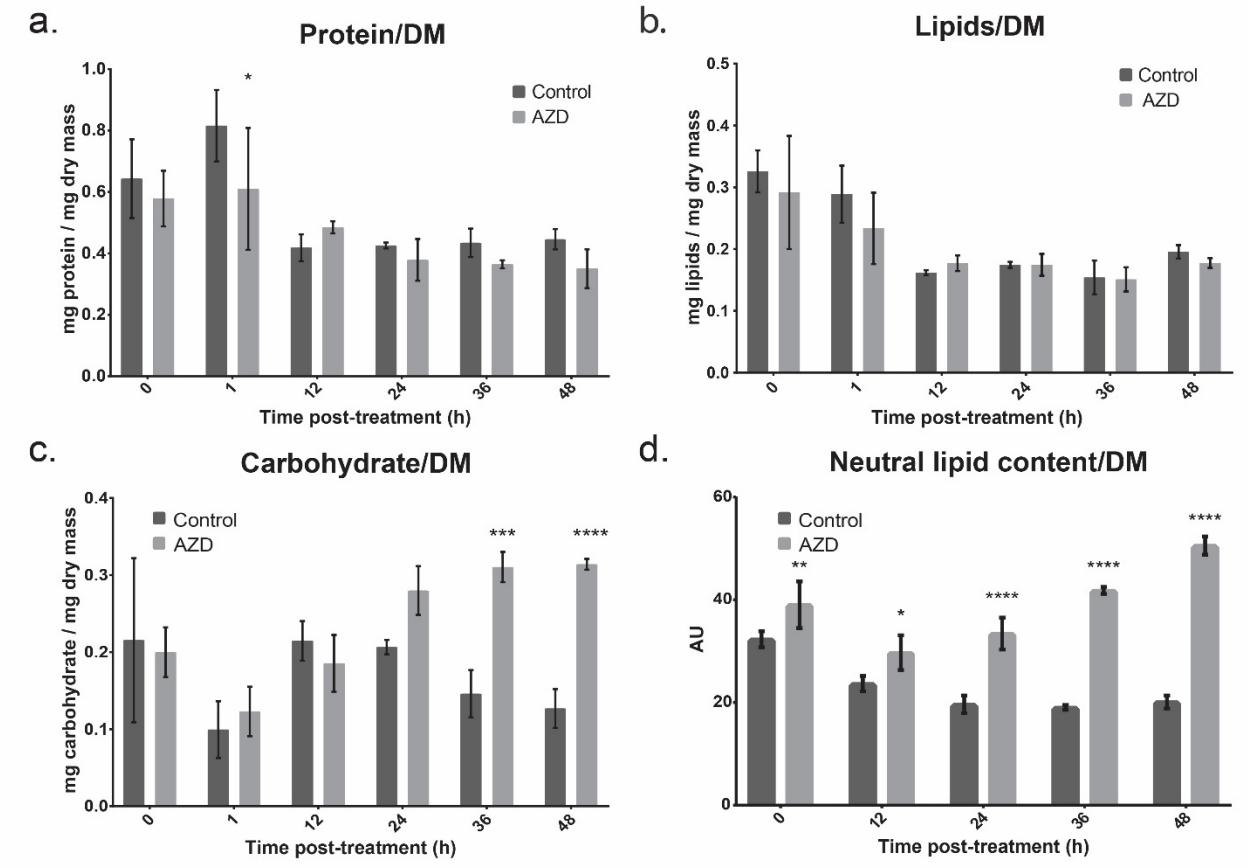

Figure 2.5 Compositional analysis of *C. reinhardtii* cultures with and without AZD8055 treatment, taken over time. The error bars represent standard deviation and statistical differences indicate a difference between the inhibited and non-inhibited cultures at one time point. Significance is denoted by asterisks, where * indicates $p \leq 0.05$, ** indicates $p \leq 0.01$, *** indicates $p \leq 0.001$, and **** indicates $p \leq 0.0001$. a.) The total protein content of the cultures, measured in mg/mg dry mass, with and without AZD8055 treatment. b.) The total lipid content of cultures, measured in mg/mg dry mass. c.) The total carbohydrate content of cultures, measured in mg/mg dry mass. d.) Neutral lipid content of the cultures with and without AZD8055 treatment measured using Nile Red staining.

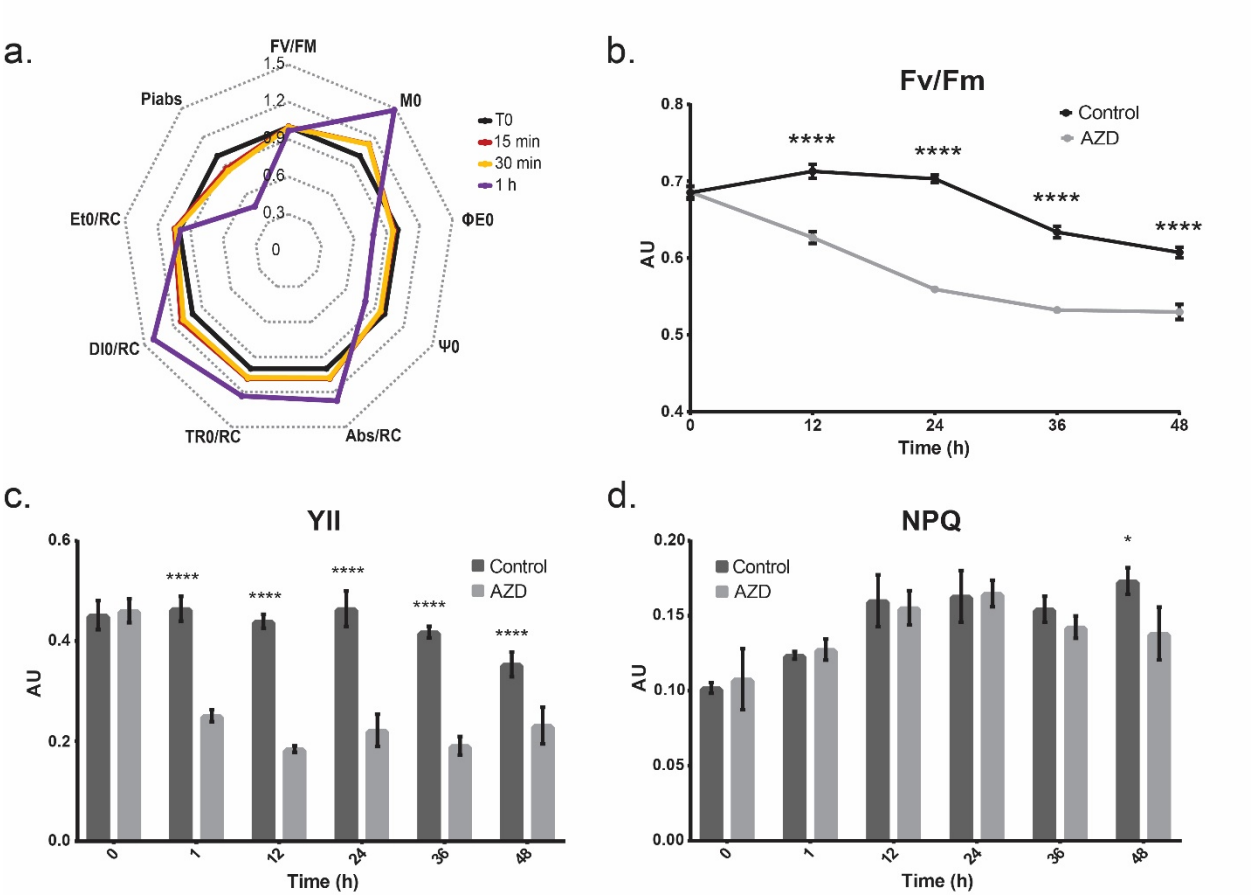

Figure 2.6 Photosynthesis measurements taken after treatment. The error bars represent standard deviation and statistical differences indicate a difference between the inhibited and non-inhibited cultures at one time point. Significance is denoted by asterisks, where * indicates $p \leq 0.05$, and **** indicates $p \leq 0.0001$. a.) Chl *a* fluorescence OJIP parameters of AZD-dosed cultures over the course of 1 h, where t0 is normalized to 1, enabling visualization of rapid changes in the photosynthetic apparatus. Changes in OJIP parameters relative to the control, as well as the derivations and explanations of all parameters, can be found in supplemental materials. b.) F_V/F_M, the measure of quantum efficiency of PSII following dark adaptation, of the cultures with and without AZD treatment. c.) The photochemical yields of photosystem II with and without treatment with AZD8055 measured using PAM fluorescence. d.) The nonphotochemical quenching of the cultures with and without AZD8055 treatment measured using PAM fluorescence.

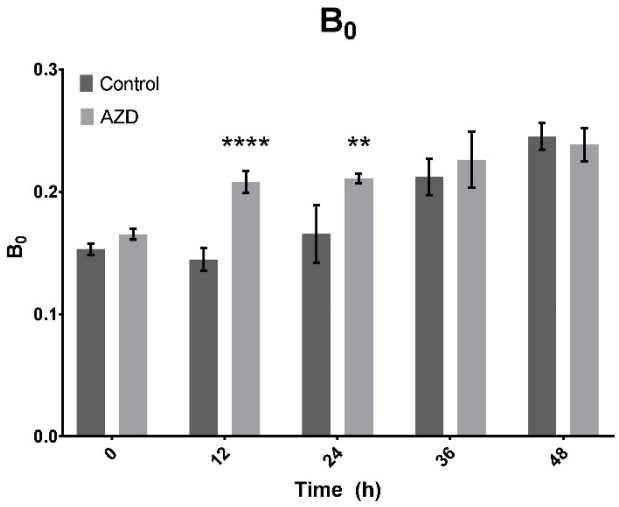

Figure 2.7 The B_0 of cultures with and without AZD8055 inhibition, measured using the double pulse method of OJIP fluorescence. B_0 indicates the relative number of inactive reducing centers; thus, as B_0 increases, the activity decreases. The error bars represent standard deviation and statistical differences indicate a difference between the inhibited and non-inhibited cultures at one time point. Significance is denoted by asterisks, where ** indicates $p \leq 0.01$, and **** indicates $p \leq 0.0001$.

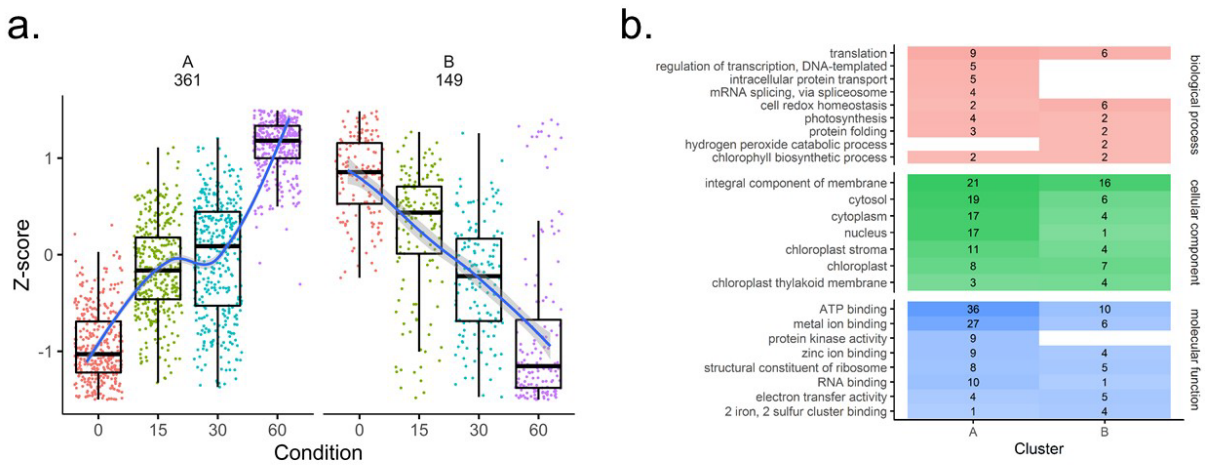

Figure 2.8 Differential analysis of the reversibly oxidized cysteine thiol proteome. a.) Hierarchical clustering of the 510 identifiers significantly changing ($p < 0.05$, FC > ±2) into two clusters. b.) Gene ontology (GO) summary of significantly changing identifiers in clusters A and B from hierarchical clustering analysis. The number and shading correspond to the number of unique proteins in each category for each cluster.

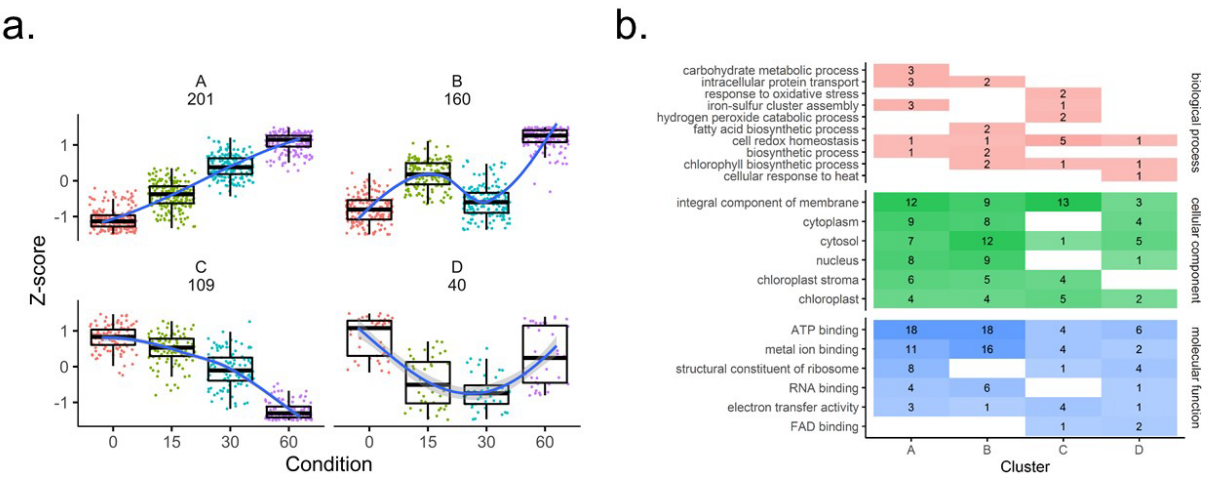

Figure 2.9 Differential analysis of the reversibly oxidized cysteine thiol proteome. a.) Hierarchical clustering of the 510 identifiers significantly changing ($p < 0.05$, FC > ±2) into four clusters. b.) Gene ontology (GO) summary of significantly changing identifiers in clusters from hierarchical clustering analysis. The number and shading correspond to the number of unique proteins in each category for each cluster.

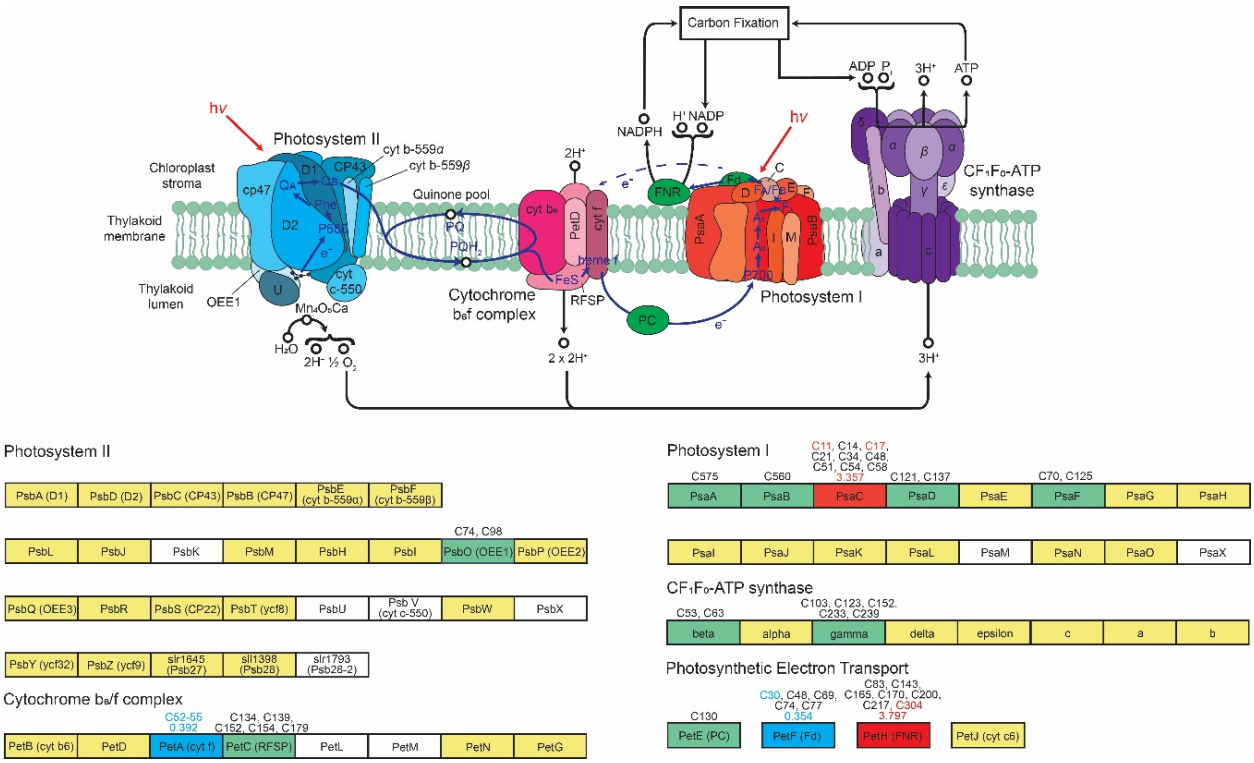

Figure 2.10 Reversible oxidation on photosynthetic machinery. Adapted from KEGG pathway map for photosynthesis (https://www.genome.jp/dbget-bin/www_bget?pathway:map00195). Protein names are labeled in diagram with gene names listed in boxes below. Components with *C. reinhardtii* homologs are in yellow. Proteins with identified reversible oxidation sites are in green with the Cys sites identified listed above. Proteins with significantly increasing (red) or decreasing (blue) identifiers upon inhibition of TOR also include the maximum fold change listed above.

REFERENCES

1. Crespo, J. L.; Díaz-Troya, S.; Florencio, F. J. Inhibition of Target of Rapamycin Signaling by Rapamycin in the Unicellular Green Alga Chlamydomonas reinhardtii. *Plant Physiol.* **2005**, *139* (4), 1736–1749.

2. Wullschleger, S.; Loewith, R.; Hall, M. N. TOR Signaling in Growth and Metabolism. *Cell* **2006**, *124* (3), 471–484.

3. Loewith, R.; Hall, M. N. Target of Rapamycin (TOR) in Nutrient Signaling and Growth Control. *Genetics* **2011**, *189* (4), 1177–1201.

4. Dobrenel, T.; Caldana, C.; Hanson, J.; Robaglia, C.; Vincentz, M.; Veit, B.; Meyer, C. TOR Signaling and Nutrient Sensing. *Annu. Rev. Plant Biol.* **2016**, *67* (1), 261–285.

5. Pérez-Pérez, M. E.; Couso, I.; Crespo, J. L. The TOR Signaling Network in the Model Unicellular Green Alga Chlamydomonas reinhardtii. *Biomolecules* **2017**, *7* (3).

6. González, A.; Hall, M. N. Nutrient Sensing and TOR Signaling in Yeast and Mammals. *EMBO J.* **2017**, *36* (4), 397–408.

7. Ryabova, L. A.; Robaglia, C.; Meyer, C. Target of Rapamycin Kinase: Central Regulatory Hub for Plant Growth and Metabolism. *J. Exp. Bot.* **2019**, *70* (8), 2211–2216.

8. Kunz, J.; Henriquez, R.; Schneider, U.; Deuter-Reinhard, M.; Movva, N. R.; Hall, M. N. Target of Rapamycin in Yeast, TOR2, Is an Essential Phosphatidylinositol Kinase Homolog Required for G1 Progression. *Cell* **1993**, *73* (3), 585–596.

9. Helliwell, S. B.; Wagner, P.; Kunz, J.; Deuter-Reinhard, M.; Henriquez, R.; Hall, M. N. TOR1 and TOR2 Are Structurally and Functionally Similar but Not Identical Phosphatidylinositol Kinase Homologues in Yeast. *Mol. Biol. Cell* **1994**, *5* (1), 105–118.

10. Loewith, R.; Jacinto, E.; Wullschleger, S.; Lorberg, A.; Crespo, J. L.; Bonenfant, D.; Oppliger, W.; Jenoe, P.; Hall, M. N. Two TOR Complexes, Only One of Which Is Rapamycin Sensitive, Have Distinct Roles in Cell Growth Control. *Mol. Cell* **2002**, *10* (3), 457–468.

11. Wedaman, K. P.; Reinke, A.; Anderson, S.; Yates, J.; McCaffery, J. M.; Powers, T. Tor Kinases Are in Distinct Membrane-Associated Protein Complexes in Saccharomyces Cerevisiae. *Mol. Biol. Cell* **2003**, *14* (3), 1204–1220.

12. Dibble, C. C.; Manning, B. D. Signal Integration by MTORC1 Coordinates Nutrient Input with Biosynthetic Output. *Nat. Cell Biol.* **2013**, *15* (6), 555–564.

13. Saxton, R. A.; Sabatini, D. M. MTOR Signaling in Growth, Metabolism, and Disease. *Cell* **2017**, *168* (6), 960–976.

14. Ballou, L. M.; Lin, R. Z. Rapamycin and MTOR Kinase Inhibitors. *J Chem Biol* **2008**, *1* (1–4), 27–36.

15. De Virgilio, C.; Loewith, R. The TOR Signalling Network from Yeast to Man. *Int. J. Biochem. Cell Biol.* **2006**, *38* (9), 1476–1481.

16. Werth, E. G.; McConnell, E. W.; Lianez, I. C.; Perrine, Z.; Crespo, J. L.; Umen, J. G.; Hicks, L. M. Investigating the Effect of Target of Rapamycin Kinase Inhibition on the Chlamydomonas reinhardtii Phosphoproteome: From Known Homologs to New Targets. *New Phytol.* **2019**, *221* (1), 247–260.

17. Ramundo, S.; Casero, D.; Mühlhaus, T.; Hemme, D.; Sommer, F.; Crèvecoeur, M.; Rahire, M.; Schroda, M.; Rusch, J.; Goodenough, U.; Pellegrini, M.; Perez-Perez, M. E.; Crespo, J. L.; Schaad, O.; Civic, N.; Rochaix, J. D. Conditional Depletion of the Chlamydomonas Chloroplast ClpP Protease Activates Nuclear Genes Involved in Autophagy and Plastid Protein Quality Control. *Plant Cell* **2014**, *26* (5), 2201–2222.

18. Kleessen, S.; Irgang, S.; Klie, S.; Giavalisco, P.; Nikoloski, Z. Integration of Transcriptomics and Metabolomics Data Specifies the Metabolic Response of Chlamydomonas to Rapamycin Treatment. *Plant J.* **2015**, *81* (5), 822–835.

19. Valledor, L.; Furuhashi, T.; Recuenco-Muñoz, L.; Wienkoop, S.; Weckwerth, W. System-Level Network Analysis of Nitrogen Starvation and Recovery in Chlamydomonas reinhardtii Reveals Potential New Targets for Increased Lipid Accumulation. *Biotechnol. Biofuels* **2014**, *7*, 171.

20. Park, J.-J.; Wang, H.; Gargouri, M.; Deshpande, R. R.; Skepper, J. N.; Holguin, F. O.; Juergens, M. T.; Shachar-Hill, Y.; Hicks, L. M.; Gang, D. R. The Response of Chlamydomonas reinhardtii to Nitrogen Deprivation: A Systems Biology Analysis. *Plant J.* **2015**, *81* (4), 611–624.

21. Imamura, S.; Kawase, Y.; Kobayashi, I.; Shimojima, M.; Ohta, H.; Tanaka, K. TOR (Target of Rapamycin) Is a Key Regulator of Triacylglycerol Accumulation in Microalgae. *Plant Signal Behav.* **2016**, *11* (3).

22. Rodrigues, S. P.; Alvarez, S.; Werth, E. G.; Slade, W. O.; Gau, B.; Cahoon, E. B.; Hicks, L. M. Multiplexing Strategy for Simultaneous Detection of Redox-, Phospho- and Total Proteome – Understanding TOR Regulating Pathways in Chlamydomonas reinhardtii. *Anal. Methods* **2015**, *7* (17), 7336–7344.

23. Couso, I.; Evans, B. S.; Li, J.; Liu, Y.; Ma, F.; Diamond, S.; Allen, D. K.; Umen, J. G. Synergism between Inositol Polyphosphates and TOR Kinase Signaling in Nutrient Sensing, Growth Control, and Lipid Metabolism in Chlamydomonas. *Plant Cell* **2016**, *28* (9), 2026–2042.

24. Couso, I.; Pérez-Pérez, M. E.; Martínez-Force, E.; Kim, H.-S.; He, Y.; Umen, J. G.; Crespo, J. L. Autophagic Flux Is Required for the Synthesis of Triacylglycerols and Ribosomal Protein Turnover in Chlamydomonas. *J. Exp. Bot.* **2018**, *69* (6), 1355–1367.

25. Fan, J.; Yu, L.; Xu, C. Dual Role for Autophagy in Lipid Metabolism in Arabidopsis. *The Plant Cell* **2019**, *31* (7), 1598–1613.

26. Pérez-Pérez, M. E.; Florencio, F. J.; Crespo, J. L. Inhibition of Target of Rapamycin Signaling and Stress Activate Autophagy in Chlamydomonas reinhardtii. *Plant Physiol.* **2010**, *152* (4), 1874–1888.

27. Díaz-Troya, S.; Pérez-Pérez, M. E.; Pérez-Martín, M.; Moes, S.; Jeno, P.; Florencio, F. J.; Crespo, J. L. Inhibition of Protein Synthesis by TOR Inactivation Revealed a Conserved Regulatory Mechanism of the BiP Chaperone in Chlamydomonas. *Plant Physiol.* **2011**, *157* (2), 730–741.

28. Lee, D. Y.; Fiehn, O. Metabolomic Response of Chlamydomonas reinhardtii to the Inhibition of Target of Rapamycin (TOR) by Rapamycin. *J. Microbiol. Biotechnol.* **2013**, *23* (7), 923–931.

29. Yilancioglu, K.; Cokol, M.; Pastirmaci, I.; Erman, B.; Cetiner, S. Oxidative Stress Is a Mediator for Increased Lipid Accumulation in a Newly Isolated Dunaliella Salina Strain. *PLOS ONE* **2014**, *9* (3), e91957.

30. Oka, S.-I.; Hirata, T.; Suzuki, W.; Naito, D.; Chen, Y.; Chin, A.; Yaginuma, H.; Saito, T.; Nagarajan, N.; Zhai, P.; Bhat, S.; Schesing, K.; Shao, D.; Hirabayashi, Y.; Yodoi, J.; Sciarretta, S.; Sadoshima, J. Thioredoxin-1 Maintains Mechanistic Target of Rapamycin (MTOR) Function during Oxidative Stress in Cardiomyocytes. *J. Biol. Chem.* **2017**, *292* (46), 18988–19000.

31. Wang, H.; Wang, S.; Lu, Y.; Alvarez, S.; Hicks, L. M.; Ge, X.; Xia, Y. Proteomic Analysis of Early-Responsive Redox-Sensitive Proteins in Arabidopsis. *J. Proteome Res.* **2012**, *11* (1), 412–424.

32. Zaffagnini, M.; Bedhomme, M.; Groni, H.; Marchand, C. H.; Puppo, C.; Gontero, B.; Cassier-Chauvat, C.; Decottignies, P.; Lemaire, S. D. Glutathionylation in the Photosynthetic Model Organism Chlamydomonas reinhardtii: A Proteomic Survey. *Mol. Cell Proteomics* **2012**, *11* (2), M111.014142.

33. Liu, P.; Zhang, H.; Wang, H.; Xia, Y. Identification of Redox-Sensitive Cysteines in the Arabidopsis Proteome Using OxiTRAQ, a Quantitative Redox Proteomics Method. *Proteomics* **2014**, *14* (6), 750–762.

34. Slade, W. O.; Werth, E. G.; McConnell, E. W.; Alvarez, S.; Hicks, L. M. Quantifying Reversible Oxidation of Protein Thiols in Photosynthetic Organisms. *J. Am. Soc. Mass Spectrom.* **2015**, *26* (4), 631–640.

35. McConnell, E. W.; Werth, E. G.; Hicks, L. M. The Phosphorylated Redox Proteome of Chlamydomonas reinhardtii: Revealing Novel Means for Regulation of Protein Structure and Function. *Redox Biol.* **2018**, *17*, 35–46.

36. Harris, E. H. *The Chlamydomonas* Sourcebook; Academic Press Inc, San Diego, CA, USA, **1989**.

37. Woodworth, B. D.; Mead, R. L.; Nichols, C. N.; Kolling, D. R. J. Photosynthetic Light Reactions Increase Total Lipid Accumulation in Carbon-Supplemented Batch Cultures of Chlorella Vulgaris. *Bioresour. Technol.* **2015**, *179*, 159–164.

38. Smythers, A. L.; Garmany, A.; Perry, N. L.; Higginbotham, E. L.; Adkins, P. E.; Kolling, D. R. J. Characterizing the Effect of Poast on Chlorella Vulgaris, a Non-Target Organism. *Chemosphere* **2019**, *219*, 704–712.

39. Schindelin, J.; Arganda-Carreras, I.; Frise, E.; Kaynig, V.; Longair, M.; Pietzsch, T.; Preibisch, S.; Rueden, C.; Saalfeld, S.; Schmid, B.; Tinevez, J.-Y.; White, D. J.; Hartenstein, V.; Eliceiri, K.; Tomancak, P.; Cardona, A. Fiji: An Open-Source Platform for Biological-Image Analysis. *Nat. Methods* **2012**, *9* (7), 676–682.

40. Wellburn, A. R. The Spectral Determination of Chlorophylls a and b, as Well as Total Carotenoids, Using Various Solvents with Spectrophotometers of Different Resolution. *J. Plant Physiol.* **1994**, *144* (3), 307–313.

41. Matyash, V.; Liebisch, G.; Kurzchalia, T. V.; Shevchenko, A.; Schwudke, D. Lipid Extraction by Methyl-Tert-Butyl Ether for High-Throughput Lipidomics. *J. Lipid Res.* **2008**, *49* (5), 1137–1146.

42. Greenspan, P.; Mayer, E. P.; Fowler, S. D. Nile Red: A Selective Fluorescent Stain for Intracellular Lipid Droplets. *J. of Cell Biol.* **1985**, *100* (3), 965–973.

43. Dubois, M.; Gilles, K. A.; Hamilton, J. K.; Rebers, P. A.; Smith, F. Colorimetric Method for Determination of Sugars and Related Substances. *Anal. Chem.* **1956**, *28* (3), 350–356.

44. Slocombe, S. P.; Ross, M.; Thomas, N.; McNeill, S.; Stanley, M. S. A Rapid and General Method for Measurement of Protein in Micro-Algal Biomass. *Bioresour. Technol.* **2013**, *129*, 51–57.

45. Lowry, O. H.; Rosebrough, N. J.; Farr, A. L.; Randall, R. J. Protein Measurement with the Folin Phenol Reagent. *J. Biol. Chem.* **1951**, *193* (1), 265–275.

46. Price, C. A. A Membrane Method for Determination of Total Protein in Dilute Algal Suspensions. *Anal. Biochem.* **1965**, *12* (2), 213–218.

47. Stirbet, A.; Lazár, D.; Kromdijk, J.; Govindjee. Chlorophyll a Fluorescence Induction: Can Just a One-Second Measurement Be Used to Quantify Abiotic Stress Responses? *Photosynthetica* **2018**, *56* (1), 86–104.

48. Stirbet, A.; Govindjee. On the Relation between the Kautsky Effect (Chlorophyll a Fluorescence Induction) and Photosystem II: Basics and Applications of the OJIP Fluorescence Transient. *J. Photochem. Photobiol. B* **2011**, *104* (1), 236–257.

49. Müller, P.; Li, X.-P.; Niyogi, K. K. Non-Photochemical Quenching. A Response to Excess Light Energy. *Plant Physiol.* **2001**, *125* (4), 1558–1566.

50. Schansker, G.; Tóth, S. Z.; Strasser, R. J. Dark Recovery of the Chl a Fluorescence Transient (OJIP) after Light Adaptation: The QT-Component of Non-Photochemical Quenching Is Related to an Activated Photosystem I Acceptor Side. *Biochim. Biophys. Acta* **2006**, *1757* (7), 787–797.

51. McConnell, E. W.; Berg, P.; Westlake, T. J.; Wilson, K. M.; Popescu, G. V.; Hicks, L. M.; Popescu, S. C. Proteome-Wide Analysis of Cysteine Reactivity during Effector-Triggered Immunity. *Plant Physiol.* **2019**, *179* (4), 1248–1264.

52. Käll, L.; Canterbury, J. D.; Weston, J.; Noble, W. S.; MacCoss, M. J. Semi-Supervised Learning for Peptide Identification from Shotgun Proteomics Datasets. *Nat. Methods* **2007**, *4* (11), 923–925.

53. Gianetto, Q. G. *Imp4p: Imputation for Proteomics*; 2018. Accessed 03/30/2019.

54. Benjamini, Y.; Hochberg, Y. Controlling the False Discovery Rate: A Practical and Powerful Approach to Multiple Testing. *J. R. Stat. Soc. Series B (Methodological)* **1995**, *57* (1), 289–300.

55. Vizcaíno, J. A.; Deutsch, E. W.; Wang, R.; Csordas, A.; Reisinger, F.; Ríos, D.; Dianes, J. A.; Sun, Z.; Farrah, T.; Bandeira, N.; Binz, P.-A.; Xenarios, I.; Eisenacher, M.; Mayer, G.; Gatto, L.; Campos, A.; Chalkley, R. J.; Kraus, H.-J.; Albar, J. P.; Martinez-Bartolomé, S.; Apweiler, R.; Omenn, G. S.; Martens, L.; Jones, A. R.; Hermjakob, H. ProteomeXchange Provides Globally Coordinated Proteomics Data Submission and Dissemination. *Nat. Biotechnol.* **2014**, *32* (3), 223–226.

56. Ishida, H.; Izumi, M.; Wada, S.; Makino, A. Roles of Autophagy in Chloroplast Recycling. *Biochim. Biophys. Acta Bioenerg.* **2014**, *1837* (4), 512–521.

57. Roustan, V.; Weckwerth, W. Quantitative Phosphoproteomic and System-Level Analysis of TOR Inhibition Unravel Distinct Organellar Acclimation in Chlamydomonas reinhardtii. *Front. Plant Sci.* **2018**, *9*, 1590.

58. Yap, B. H. J.; Crawford, S. A.; Dagastine, R. R.; Scales, P. J.; Martin, G. J. O. Nitrogen Deprivation of Microalgae: Effect on Cell Size, Cell Wall Thickness, Cell Strength, and Resistance to Mechanical Disruption. *J. Ind. Microbiol. Biotechnol.* **2016**, *43* (12), 1671–1680.

59. Jeong, S. W.; Nam, S. W.; HwangBo, K.; Jeong, W. J.; Jeong, B.; Chang, Y. K.; Park, Y.-I. Transcriptional Regulation of Cellulose Biosynthesis during the Early Phase of Nitrogen Deprivation in Nannochloropsis Salina. *Sci. Rep.* **2017**, *7* (1), 5264.

60. Antal, T.; Rubin, A. In Vivo Analysis of Chlorophyll a Fluorescence Induction. *Photosyn. Res.* **2008**, *96* (3), 217–226.

61. Tomek, P.; Lazár, D.; Ilík, P.; Naus, J. Research Note: On the Intermediate Steps between the O and P Steps in Chlorophyll a Fluorescence Rise Measured at Different Intensities of Exciting Light. *Functional Plant Biol.* **2001**, *28* (11), 1151–1160.

62. Rigbolt, K. T.; Zarei, M.; Sprenger, A.; Becker, A. C.; Diedrich, B.; Huang, X.; Eiselein, S.; Kristensen, A. R.; Gretzmeier, C.; Andersen, J. S.; Zi, Z.; Dengjel, J. Characterization of Early Autophagy Signaling by Quantitative Phosphoproteomics. *Autophagy* **2014**, *10* (2), 356–371.

63. Muthuramalingam, M.; Matros, A.; Scheibe, R.; Mock, H.-P.; Dietz, K.-J. The Hydrogen Peroxide-Sensitive Proteome of the Chloroplast in vitro and in vivo. *Front. Plant Sci.* **2013**, *4*.

64. Paulech, J.; Solis, N.; Edwards, A. V. G.; Puckeridge, M.; White, M. Y.; Cordwell, S. J. Large-Scale Capture of Peptides Containing Reversibly Oxidized Cysteines by Thiol-Disulfide Exchange Applied to the Myocardial Redox Proteome. *Anal. Chem.* **2013**, *85* (7), 3774–3780.

65. Guo, J.; Gaffrey, M. J.; Su, D.; Liu, T.; Camp, D. G.; Smith, R. D.; Qian, W.-J. Resin-Assisted Enrichment of Thiols as a General Strategy for Proteomic Profiling of Cysteine-Based Reversible Modifications. *Nat. Protoc.* **2014**, *9* (1), 64–75.

66. Forrester, M. T.; Thompson, J. W.; Foster, M. W.; Nogueira, L.; Moseley, M. A.; Stamler, J. S. Proteomic Analysis of S-Nitrosylation and Denitrosylation by Resin-Assisted Capture. *Nat. Biotechnol.* **2009**, *27* (6), 557–559.

67. Su, D.; Shukla, A. K.; Chen, B.; Kim, J.-S.; Nakayasu, E.; Qu, Y.; Aryal, U.; Weitz, K.; Clauss, T. R. W.; Monroe, M. E.; Camp, D. G.; Bigelow, D. J.; Smith, R. D.; Kulkarni, R. N.; Qian, W.-J. Quantitative Site-Specific Reactivity Profiling of S-Nitrosylation in Mouse Skeletal Muscle Using Cysteinyl Peptide Enrichment Coupled with Mass Spectrometry. *Free Radic. Biol. Med.* **2013**, *57*, 68–78.

68. Lind, C.; Gerdes, R.; Hamnell, Y.; Schuppe-Koistinen, I.; von Löwenhielm, H. B.; Holmgren, A.; Cotgreave, I. A. Identification of S-Glutathionylated Cellular Proteins during Oxidative Stress and Constitutive Metabolism by Affinity Purification and Proteomic Analysis. *Arch. Biochem. Biophys.* **2002**, *406* (2), 229–240.

69. Su, D.; Gaffrey, M. J.; Guo, J.; Hatchell, K. E.; Chu, R. K.; Clauss, T. R. W.; Aldrich, J. T.; Wu, S.; Purvine, S.; Camp, D. G.; Smith, R. D.; Thrall, B. D.; Qian, W.-J. Proteomic Identification and Quantification of S-Glutathionylation in Mouse Macrophages Using Resin-Assisted Enrichment and Isobaric Labeling. *Free Radic. Biol. Med.* **2014**, *67*, 460–470.

70. Forrester, M. T.; Hess, D. T.; Thompson, J. W.; Hultman, R.; Moseley, M. A.; Stamler, J. S.; Casey, P. J. Site-Specific Analysis of Protein S-Acylation by Resin-Assisted Capture. *J. Lipid Res.* **2011**, *52* (2), 393–398.

71. Hansen, R. E.; Winther, J. R. An Introduction to Methods for Analyzing Thiols and Disulfides: Reactions, Reagents, and Practical Considerations. *Anal. Biochem.* **2009**, *394* (2), 147–158.

72. Paulech, J.; Solis, N.; Cordwell, S. J. Characterization of Reaction Conditions Providing Rapid and Specific Cysteine Alkylation for Peptide-Based Mass Spectrometry. *Biochim. Biophys. Acta* **2013**, *1834* (1), 372–379.

73. Morisse, S.; Zaffagnini, M.; Gao, X.-H.; Lemaire, S. D.; Marchand, C. H. Insight into Protein S-Nitrosylation in Chlamydomonas reinhardtii. *Antioxid. Redox Signal* **2014**, *21* (9), 1271–1284.

74. Pérez-Pérez, M. E.; Mauriès, A.; Maes, A.; Tourasse, N. J.; Hamon, M.; Lemaire, S. D.; Marchand, C. H. The Deep Thioredoxome in Chlamydomonas reinhardtii: New Insights into Redox Regulation. *Mol. Plant* **2017**, *10* (8), 1107–1125.

75. Burrus, L. W.; Zuber, M. E.; Lueddecke, B. A.; Olwin, B. B. Identification of a Cysteine-Rich Receptor for Fibroblast Growth Factors. *Mol. Cell. Biol.* **1992**, *12* (12), 5600–5609.

76. Song, H.; Bao, S.; Ramanadham, S.; Turk, J. Effects of Biological Oxidants on the Catalytic Activity and Structure of Group VIA Phospholipase A2. *Biochem.* **2006**, *45* (20), 6392–6406.

77. Sato, N.; Fujiwara, S.; Kawaguchi, A.; Tsuzuki, M. Cloning of a Gene for Chloroplast Ω6 Desaturase of a Green Alga, Chlamydomonas reinhardtii. *J. Biochem.* **1997**, *122* (6), 1224–1232.

78. Tsukamoto, Y.; Fukushima, Y.; Hara, S.; Hisabori, T. Redox Control of the Activity of Phosphoglycerate Kinase in Synechocystis Sp. PCC6803. *Plant Cell Physiol.* **2013**, *54* (4), 484–491.

79. Liebeke, M.; Pöther, D.-C.; van Duy, N.; Albrecht, D.; Becher, D.; Hochgräfe, F.; Lalk, M.; Hecker, M.; Antelmann, H. Depletion of Thiol-Containing Proteins in Response to Quinones in *Bacillus Subtilis*. *Mol. Microbiol.* **2008**, *69* (6), 1513–1529.

80. Loi, V. V.; Rossius, M.; Antelmann, H. Redox Regulation by Reversible Protein S-Thiolation in Bacteria. *Front. Microbiol.* **2015**, *6*.

81. Imber, M.; Pietrzyk-Brzezinska, A. J.; Antelmann, H. Redox Regulation by Reversible Protein S-Thiolation in Gram-Positive Bacteria. *Redox Biol.* **2019**, *20*, 130–145.

82. Topf, U.; Suppanz, I.; Samluk, L.; Wrobel, L.; Böser, A.; Sakowska, P.; Knapp, B.; Pietrzyk, M. K.; Chacinska, A.; Warscheid, B. Quantitative Proteomics Identifies Redox

Switches for Global Translation Modulation by Mitochondrially Produced Reactive Oxygen Species. *Nat. Comm.* **2018**, *9* (1), 324.

83. Xiong, Y.; Sheen, J. The Role of Target of Rapamycin Signaling Networks in Plant Growth and Metabolism. *Plant Physiol.* **2014**, *164* (2), 499–512.

84. Pancha, I.; Shima, H.; Higashitani, N.; Igarashi, K.; Higashitani, A.; Tanaka, K.; Imamura, S. Target of Rapamycin-Signaling Modulates Starch Accumulation via Glycogenin Phosphorylation Status in the Unicellular Red Alga Cyanidioschyzon Merolae. *Plant J.* **2019**, *97* (3), 485–499.

85. Miginiac-Maslow, M.; Lancelin, J.-M. Intrasteric Inhibition in Redox Signalling: Light Activation of NADP-Malate Dehydrogenase. *Photosynth. Res.* **2002**, *72* (1), 1.

86. Lemaire, S. D.; Quesada, A.; Merchan, F.; Corral, J. M.; Igeno, M. I.; Keryer, E.; Issakidis-Bourguet, E.; Hirasawa, M.; Knaff, D. B.; Miginiac-Maslow, M. NADP-Malate Dehydrogenase from Unicellular Green Alga Chlamydomonas reinhardtii. A First Step toward Redox Regulation? *Plant Physiol.* **2005**, *137* (2), 514–521.

87. Issakidis, E.; Saarinen, M.; Decottignies, P.; Jacquot, J. P.; Crétin, C.; Gadal, P.; Miginiac-Maslow, M. Identification and Characterization of the Second Regulatory Disulfide Bridge of Recombinant Sorghum Leaf NADP-Malate Dehydrogenase. *J. Biol. Chem.* **1994**, *269* (5), 3511–3517.

88. Raines, C. A.; Lloyd, J. C.; Dyer, T. A. New Insights into the Structure and Function of Sedoheptulose-1,7-Bisphosphatase; an Important but Neglected Calvin Cycle Enzyme. *J. Exp. Bot.* **1999**, *50* (330), 1–8.

89. Yoshida, S.; Hong, S.; Suzuki, T.; Nada, S.; Mannan, A. M.; Wang, J.; Okada, M.; Guan, K.-L.; Inoki, K. Redox Regulates Mammalian Target of Rapamycin Complex 1 (MTORC1) Activity by Modulating the TSC1/TSC2-Rheb GTPase Pathway. *J. Biol. Chem.* **2011**, *286* (37), 32651–32660.

90. Marshansky, V.; Rubinstein, J. L.; Grüber, G. Eukaryotic V-ATPase: Novel Structural Findings and Functional Insights. *Biochim. Biophys. Acta* **2014**, *1837* (6), 857–879.

91. Seidel, T.; Scholl, S.; Krebs, M.; Rienmüller, F.; Marten, I.; Hedrich, R.; Hanitzsch, M.; Janetzki, P.; Dietz, K.-J.; Schumacher, K. Regulation of the V-Type ATPase by Redox Modulation. *Biochem. J.* **2012**, *448* (2), 243–251.

92. Cassan, N.; Lagoutte, B.; Sétif, P. Ferredoxin-NADP+ Reductase kinetics of electron transfer, transient intermediates, and catalytic activities studied by flash-absorption spectroscopy with isolated Photosystem I and Ferredoxin. *J. Biol. Chem.* **2005**, *280* (28), 25960–25972.

93. Hasan, S. S.; Cramer, W. A. On Rate Limitations of Electron Transfer in the Photosynthetic Cytochrome B6f Complex. *Phys. Chem. Chem. Phys.* **2012**, *14* (40), 13853–13860.

CHAPTER 3: Label-Free Quantitative Phosphoproteomics for Algae[1]

3.1 Introduction

The unicellular alga *Chlamydomonas reinhardtii* is a model organism for the study of microalgal processes, particularly photosynthesis due to its photoheterotrophic growth[1]. More recently, *Chlamydomonas* research has expanded to include the utilization of microalgae for biofuel production due to their ability to produce large amounts of triacylglycerol while having rapid growth potential and tolerance to environmental conditions[2]. Along with genomic and transcriptomic studies[3–5], proteomic analysis of *Chlamydomonas* has led to an increased understanding of its metabolic signaling as well as a growing interest in the elucidation of its phosphorylation networks, particularly those related to biofuel production[6,7].

Protein phosphorylation is a post-translational modification (PTM) that serves as a rapid and reversible means to modulating protein activity and signal transduction in the cell. This modification involves the addition of a phosphate group to an amino acid by a protein kinase, which together with phosphatases, can act as a molecular switch to regulate complex signaling networks. Protein phosphorylation has been extensively studied for more than 60 years due to its widespread prevalence and its critical involvement in the regulation of nearly all basic cellular processes[8,9]. Dynamic protein phosphorylation plays a central role in cell proliferation, metabolism, signaling, and survival, emphasizing the need for an efficient and selective method of analysis. However, studying these events remains an analytical challenge.

[1] Reprinted with permission from Ford, M. M.; Lawrence, S. R., II.; Werth, E. G.; McConnell, E. W.; Hicks, L. M. Label-Free Quantitative Phosphoproteomics for Algae. In: Jorrin-Novo, J.; Valledor, L.; Castillego, M.; Rey, M. D. (eds) Plant Proteomics *Methods in Molecular Biology* **2020***,* 2139. Humana, New York, NY.

One important challenge stems from the labile nature of phosphorylation. As a PTM that is tightly linked to protein function, the phosphorylation status of proteins continually changes in response to specific conditions and stimuli. Thus, understanding phosphorylation requires detection and quantification of the same phosphoprotein(s) in multiple states, or proteoforms, across different conditions while using sample preparation techniques, such as flash freezing and the use of phosphatase inhibitors, to ensure the signal being analyzed is answering the biological question of interest. An additional challenge arises from the large dynamic range of phosphorylation events in the cell, which is dependent on the abundance of the protein in the cell, that can span many orders of magnitude[10], and the occupancy of the phosphorylation site, which is generally low at any given time[10]. Also, while phosphorylation occurs on thousands of proteins, many of them share little sequence homology, increasing the difficulty in identifying dynamic changes in phosphorylation across an entire phosphoproteome[11].

To date several enrichment approaches have been employed to address the challenges in assessing protein phosphorylation[12]. Among these, titanium dioxide metal oxide affinity chromatography (TiO_2-MOAC) is one of the most common shotgun enrichment methods for phosphopeptides from complex biological samples[13–15]. TiO_2-based enrichments have been shown to be more selective[15], and are less sensitive to interferents such as salts and detergents than immobilized metal affinity chromatography[16,17]. However, they show preference to singly phosphorylated peptides over those with multiple phosphosites, potentially due to stronger interactions between TiO_2 and multi-phosphorylated peptides making elution of these peptides challenging[18]. At acidic pH, TiO_2 has a high affinity for phosphorylated species, forming a bidentate bond with the titanium surface and two of the oxygen atoms[18]. To minimize co-purification of acidic peptides, the use of organic acids, such as phthalic, 2,5-dihydroxybenzoic,

or lactic acid, as an additive for binding enhances the overall selectivity of this enrichment method[12].

LC-MS/MS offers highly reproducible and accurate systems-level analysis that can be paired with enrichment for the study of large-scale protein phosphorylation[19]. For quantification, a label-free approach can provide advantages over label-based techniques, primarily in experimental design flexibility[20]. Label-free quantitation (LFQ), with a number of software programs available to aid in data analysis[20], allows for rapid, straight-forward, and cost-effective measurements of a wide range of protein abundances. Typically, LFQ is employed via one of two approaches: changes in ion intensity from LC-peak areas [i.e., area under the curve (AUC)] of the peptides, or based on spectral counting of peptides from MS^2 analysis. The latter approach is limited in its ability to quantify proteins of low abundance[6] due in part to the variability in spectral count response for each peptide making it necessary to observe many spectra for a given protein to assume a linear response between counts and abundance. Additionally, many experiments employ a dynamic exclusion of ions already selected for fragmentation, making accurate quantitation with this method challenging[21]. In phosphoproteomics, quantitation is performed on a single peptide for each phosphorylation site, making AUC quantitation generally preferable for these studies. However, AUC requires highly reproducible chromatography and high mass accuracy because it relies on accurate peak alignment and mass measurement for quantification.

Here we present a method to quantify the phosphoproteome of Chlamydomonas that uses a combination of efficient extraction, TiO_2-based phosphopeptide enrichment and LFQ to provide in depth coverage of the phosphoproteome (Figure 3.1). Using this method, analysis of replicate samples resulted in the quantification of 3595 phosphosites on 1775 phosphoproteins.

Assessment of the reproducibility of this method shows the technical replicates are highly similar, with a 21 % median CV. These results are similar to previous studies performed using a similar approach that uses identical sample preparation and LC separation with a different make/model of mass spectrometer[19,22]. While our quantitative breadth of coverage is extensive, qualitative studies have shown that the global phosphoproteome is still drastically larger than can be obtained in a shotgun LFQ approach. A previous study[23], which used two enrichment methods and additional fractionation to create a total of 60 samples subjected to LC-MS/MS, identified over 4500 phosphoproteins from nearly 16,000 phosphosites, showing that there is room for improvement in the depth of coverage obtained in these phosphoproteomic studies. Implementation of an orthogonal fractionation prior to analysis would help improve this depth of coverage, but at the cost of increased instrument time and variability from the added sample preparation. Although providing moderate depth of coverage, the method outlined here provides an accurate and high-throughput approach for analyzing algal phosphoproteomic samples.

3.2 Materials

3.2.1 Cell Culture

1. Hutner's Trace Elements stock[24]. This can be purchased as a stock solution or prepared in lab (*see* Note 1).
2. TRIS-Acetate-Phosphate (TAP) Media: 20 mM TRIS Base, 17.5 mM acetic acid, 1.65 mM K_2HPO_4, 945 µM KH_2PO_4, 287 µM $CaCl_2$, 405 µM $MgSO_4$, 7.01 mM NH_4Cl, and Hutner's Trace Elements. Stock solutions can be made for easy preparation of TAP media (*see* Note 2).
3. TAP agar media plates, 1.5% agar: To TAP media (see 3.2.1 step 2), add Bacto Agar and autoclave. Cool media to 52 °C and pour plates into petri dishes, 100 x 15 mm, in

biosafety cabinet, about 10 mL per plate. Let plates solidify overnight, parafilm to seal each plate and store at 4 °C.

4. *Chlamydomonas reinhardtii,* strain CC-2895 (6145c *mt*-).
5. 100 μE m^{-2} sec^{-1} white light source.
6. Platform shaker.
7. Liquid nitrogen, 0.5 L.

3.2.2 Protein Extraction

1. Lysis buffer: 100 mM TRIS, pH 8.0, 1% Sodium dodecyl sulfate (SDS), 1x cOmplete protease inhibitor cocktail (Roche, Risch-Rotkreuz, Switzerland) and 1x phosSTOP phosphatase inhibitor cocktail (Roche). Stock solutions can be made for easy preparation of lysis buffer (*see* Note 3). When preparing the lysis buffer, stir slowly when fully dissolving contents to minimize agitation and bubble formation from the SDS.
2. Covaris 2 mL milliTUBEs and 24 Place milliTUBE rack.
3. 100 mM ammonium acetate in methanol (MeOH).
4. 70% Ethanol (EtOH).
5. 100 mM TRIS, pH 8.0. Using a 1 M TRIS stock (*see* Note 3) is recommended for ease of buffer preparation.
6. Resuspension buffer: 8 M Urea, 100 mM TRIS, pH 8.0.
7. CB-X Protein Assay Kit (G-Biosciences, St. Louis, MO, USA) or equivalent protein quantification assay.

3.2.3 Reduction, Alkylation, and Digestion

1. Reduction buffer: 500 mM dithiothreitol in 100 mM TRIS, pH 8.0.

2. Alkylation buffer: 500 mM iodoacetamide (IAM) in 100 mM TRIS, pH 8.0. Make fresh for each experiment and cover tube with aluminum foil or keep buffer in the dark to prevent degradation of light-sensitive IAM solution.
3. Trypsin resuspension buffer: 50 mM acetic acid.
4. Promega (Madison, WI, USA) Trypsin Gold, Mass Spectrometry grade.
5. 20% trifluoroacetic acid (TFA).

3.2.4 Desalting

1. Waters (Milford, MA, USA) Sep-Pak C18 1 cc Vac Cartridge, 50 mg, 55-105 µm particle size.
2. 0.1% TFA (LC-MS grade).
3. 80% acetonitrile (ACN, LC-MS grade), 0.1% TFA (LC-MS grade).
4. Vacuum manifold with 24-port cover (Phenomenex, Torrance, CA, USA) or equivalent setup.

3.2.5 Phosphopeptide Enrichment

1. Wash Buffer: 80% ACN (LC-MS grade), 1% TFA (LC-MS grade).
2. Resuspension Buffer: 80% ACN (LC-MS grade), 1% TFA (LC-MS grade), 25 mg/mL phthalic acid. This can be made by adding phthalic acid to the Wash Buffer.
3. Elution Buffer: 20% ACN (LC-MS grade), 5% aqueous ammonia.
4. TiO_2 phosphopeptide enrichment tips, 3 mg. Titansphere^{TM} Phos-TiO Spin Columns (GL Sciences, Torrance, CA, USA) recommended.
5. Spin column centrifuge adaptors.

3.2.6 Sample Purification

1. 1% formic acid (FA, LC-MS grade), 2% ACN (LC-MS grade).

2. 0.1% FA (LC-MS grade).
3. 60% ACN (LC-MS grade), 0.1% FA (LC-MS grade).
4. Millipore (Burlington, MA, USA) C18 ZipTips.

3.2.7 LC-MS/MS

1. 5% ACN (LC-MS grade), 0.1% TFA (LC-MS grade).
2. LC-MS total recovery vials.
3. Symmetry C18 trap column (100 Å, 5 µm, 180 µm x 20 mm; Waters).
4. HSS T3 C18 column (100 Å, 1.8 µm, 75 µm x 250 mm; Waters). Mobile Phase A: 0.1% FA. Add 1 mL of Optima LC-MS grade FA to 1 L of Optima LC-MS grade water.
5. Mobile Phase B: 0.1% FA in ACN (LC-MS grade).
6. NanoAcquity UPLC system (Waters).
7. Q Exactive HF-X Hyrid Quadrupole Orbitrap mass spectrometer (ThermoFisher, Waltham, MA, USA).

3.2.8 Data Analysis

1. Progenesis QI for Proteomics v2.0 (Nonlinear Dynamics, Durham, NC, USA).
2. Mascot Daemon v3.5.1 (Matrix Science, Boston, MA, USA).
3. R script for processing phosphoproteome data. The code used for processing these data is available on GitHub (https://github.com/hickslab/QuantifyR).

3.3 Methods

3.3.1 Culturing

1. Maintain Chlamydomonas strain on TAP agar plates under continuous light, streaking a fresh plate from a single colony on a previous plate every 1-2 weeks.

2. Grow a 100 mL starter culture of Chlamydomonas using TAP media in a 250 mL flask. In a biosafety cabinet, select a single colony from a TAP agar plate and suspend it in the TAP media. Grow the culture 4-5 days shaking at 120 rpm and under continuous light until a growth density of OD_{750} 0.4-0.5 is reached.
3. Prepare 6x350 mL liquid culture of Chlamydomonas in TAP media. Transfer 3.5 mL of a starter culture to fresh TAP media. Use a 1 L flask for 350 mL of culture to provide sufficient room for consistent mixing. Shake at 120 rpm with 100 μmol m^{-2} s^{-1} white light at room temperature. Grow for 3-4 days until an OD_{750} of 0.4-0.5 is reached (*see* Note 4).
4. Centrifuge each culture for 5 min at 6,000 x *g* at 4 °C in a 1 L centrifuge bottle to harvest.
5. Decant the supernatant from each culture while not disturbing the cell pellet in the centrifuge bottle.
6. Resuspend the *Chlamydomonas* pellets in 10 mL of fresh TAP media and transfer each solution to a 15 mL conical centrifuge tube.
7. Centrifuge each culture for 2 min at 3,200 x *g*, at 4 °C.
8. Decant the supernatant from each culture while not disturbing the cell pellet in the centrifuge bottle.
9. Place the conical centrifuge tubes containing cell pellets in liquid nitrogen until fully frozen. Store at -80 °C until performing plant-based protein extraction.

3.3.2 Protein Extraction

1. Resuspend cell pellets in 4 mL lysis buffer (*see* Note 5) and transfer to Covaris 2 mL tubes. Keep samples on ice during resuspension.
2. Sonicate samples in a 4°C water bath for 3 min at 200 cycles/burst, 100 W power, and 13% duty cycle using an E220 focused ultra-sonicator (Covaris, Woburn, MA, USA).

3. Transfer samples from Covaris tubes to 2 mL centrifuge tubes, keeping the samples on ice.
4. Centrifuge cell lysates at 16,000 x *g* for 10 min at 4 °C and collect the supernatant into a 50 mL conical tube.
5. Add 1 mL of fresh lysis buffer to the pelleted cell debris and vortex.
6. Centrifuge this sample again at 16,000 x *g* for 10 min at 4 °C. Collect the supernatant and combine with the first extraction in a 15 mL conical tube.
7. Precipitate proteins by adding 5 volumes (about 30 mL) of cold 100 mM ammonium acetate in MeOH. Incubate samples overnight at -80 °C.
8. Collect protein pellet by centrifuging for 5 min at 2,000 x *g*. Decant the supernatant without disturbing the pellet.
9. Perform two additional washes with 30 mL fresh 100 mM ammonium acetate in MeOH followed by a wash with 30 mL 70% EtOH. For each wash, resuspend the pellet by vortexing before centrifuging for 5 min at 2,000 x *g*.
10. Allow protein pellets to dry for 5 min in a fume hood at room temperature.
11. Resolubilize the pellets in 1-2 mL minimal resuspension buffer. Incubate for 1 h to ensure protein is fully dissolved.
12. Use a 10 μL aliquot of each replicate to perform protein quantification using the CB-X Protein Assay. Complete assay using manufacturer's protocol (*see* Note 6).
13. Normalize each replicate to 4 mg/ml and use a 0.5 ml aliquot (2 mg) of each sample to continue through the remaining steps in the protocol.

3.3.3 Reduction, Alkylation, and Digestion

1. Reduce samples using 10 mM DTT. Add 10 µL reduction buffer to each sample. Incubate for 30 minutes at room temperature while shaking (500-850 rpm).
2. Alkylate samples using 40 mM IAM (*see* Note 7). Add 40 µL of alkylation buffer to each sample. Incubate for 45 min in the dark at room temperature while shaking.
3. Following alkylation, diluted the samples 5-fold using 100 mM TRIS, pH 8.0 so the concentration of urea is <2 M, which is a requirement for effective tryptic protein digestion. For 0.5 ml samples, add 2 ml of 100 mM TRIS, pH 8.0.
4. Perform overnight digestion using mass spectrometry-grade trypsin (Trypsin Gold from Promega is recommended) at a protease to protein ratio of 1:50 at 25 °C. For 2 mg lysate, 40 µg trypsin is needed. Gently invert or shake the samples during digestion.
5. Following digestion, quench the reaction by adding 20% TFA to the samples until their pH is less than 3 when measured with a pH test strip. Usually 0.2-0.4% final volume TFA, or 5-10 µL for 2.5 ml samples, is sufficient.
6. Freeze samples at -80 °C following digestion until desalting using 50 mg SepPak (Waters) cartridges is performed.

3.3.4 Desalting

1. Thaw samples on ice and centrifuge them for 5 min at 10,000 x *g* to pellet. Remove undigested protein pellet from soluble peptide mixture to avoid clogging the cartridges.
2. Set up one cartridge for each sample on a vacuum manifold using test tubes to collect the flow through from the cartridges.
3. Wet cartridges by adding 1 mL of 80% ACN, 0.1% TFA (*see* Note 8).
4. Equilibrate cartridges using 2 mL of 0.1% TFA.

5. Load peptide samples onto the cartridge and recover the flow through in a new test tube.
6. Reapply this flow through to the cartridge.
7. After the flow through passes through, switch to a new test tube and flow 2 mL of 0.1% TFA are added to the cartridges to remove salts.
8. Elute desalted peptides into a new 2 mL tube by adding 1.5 mL of 80% ACN, 0.1% TFA to the cartridge. Once the elution flows all the way through the cartridge, apply vacuum for about 5 seconds to collect the remaining solvent from the packed bed.
9. Following peptide elution, freeze the samples and vacuum centrifuge to dryness.

3.3.5 Phosphopeptide Enrichment

1. Each sample uses one TiO_2 tip placed in a microcentrifuge tube using an adaptor. Pre-elute the tips using 100 µL of elution buffer (*see* Note 9).
2. Condition each tip with 100 µL of wash buffer twice, for a total of 200 µL, followed by 3 washes using 100 µL of resuspension buffer.
3. Resuspend the dried peptides in 150 µL of resuspension buffer. Centrifuge the samples at 10,000 x *g* for 5 min to prevent clogging and load onto the tips. Use a new centrifuge tube to recover the sample flow through.
4. Reapply the flow through five times.
5. Following binding using a new centrifuge tube, wash the tips using 100 µL of resuspension buffer twice and then wash three times with 100 µL of wash buffer.
6. Using a new centrifuge tube to collect the buffer, elute the phosphopeptide-enriched samples using 2 aliquots of 100 µL of elution buffer, combining them for a total of 200 µL of elution.

7. Flash-freeze the elution with liquid nitrogen and vacuum centrifuge to dryness with the concentrator set to room temperature.

3.3.6 Sample Purification

1. Resuspend phosphopeptide-enriched samples in 15 µL 1% FA, 2% ACN.
2. Centrifuge the samples at 15,000 x *g* for 5 min and transfer to a new tube, taking care not to disturb the pellet if present, to remove any insoluble portion of the sample.
3. Aliquot 15 µL 60% ACN, 0.1% FA for each sample into its own tube to elute samples from the ZipTip.
4. Perform a C18 ZipTip purification on each sample, using a new tip each time (*see* Note 10).
5. Attach a ZipTip to a 10 µL pipette. With pipette set to 10 µL, draw up LC-MS grade ACN to wet the tip. Discard the ACN while keeping the resin wet. Repeat twice for a total of three pre-elution steps.
6. Equilibrate the ZipTip by pipetting 0.1% FA three times, discarding the solvent each time while keeping the resin wet.
7. Pipette the sample 10 times to load the peptides onto the ZipTip.
8. Wash six times with 0.1% FA.
9. Elute the peptides by pipetting 10 times using aliquoted elution solvent from step 4, expelling all of the solvent from the pipette tip.
10. Dry down all of the eluted peptide samples.

3.3.7 LC-MS/MS

1. Resuspend phosphopeptide samples in 20 µL and whole cell samples in 40 µL of 5% acetonitrile, 0.1% TFA and transfer to a Total Recovery Vial (Waters).

2. Inject 5 µL of each sample and perform LC-MS/MS analysis on each sample using a NanoAcquity UPLC system (Waters) coupled to a Q Exactive HF-X Hybrid Quadrupole Orbitrap mass spectrometer (ThermoFisher) via a Nanospray Flex Ion Source (ThermoFisher). Inject the peptide mixture to a Symmetry C18 trap column (100 Å, 5 µm, 180 µm x 20 mm; Waters) with a flow rate of 5 µL/min for 3 min using 99% A and 1% B, then separate on a HSS T3 C18 column (100 Å, 1.8 µm, 75 µm x 250 mm; Waters) using a gradient of increasing mobile phase B at a flow rate of 300 nL/min for 120 min total. Increase mobile phase B from 5-35% in 90 min, ramp to 85% in 5 min, hold for 5 min, return to 5% mobile phase B in 2 min, and re-equilibrate for 13 min.
3. Use the following MS parameters: Use a tune file set with positive polarity, 2.2 kV spray voltage, 325 °C capillary temperature, and 40 S-lens RF level. In the instrument method, include lock masses best of 371.10124 and 445.12003 background polysiloxane ions. Select full MS/DD-MS^2 scan type and set method duration to 120 min and default charge state to 2. Perform MS survey scan in profile mode across 350-1600 *m/z* at 120,000 resolution until 50 ms maximum IT or $3x10^6$ AGC target is reached. Select the top 20 features above 5000 counts excluding ions with unassigned, +1, or > +8 charge state. Collect MS^2 scans at 45,000 resolution with NCE at 32 until 100 ms maximum IT or $1x10^5$ AGC target. Set the dynamic exclusion window for precursor *m/z* to 10 s and an isolation window of 0.7 *m/z*. Check the system's performance every 8 h using an injection of BSA tryptic digest run with the same instrument method.

3.3.8 Data Analysis

1. Upload acquired spectral files (*.raw) into Progenesis QI for Proteomics (Nonlinear Dynamics). Use automatically assigned reference spectrum to align the total ion

chromatograms to minimize run-to-run differences in retention time and normalize peak abundances. Design experiment so that replicates are grouped together as one subject. Export a combined peak list (*.mgf).

2. Upload and determine peptide sequence and protein inference using Mascot (Matrix Science). Use the following search parameters: Search against the database containing the proteome for the organism of interest, in this case the Phytozome *Chlamydomonas* proteome (https://phytozome.jgi.doe.gov/pz/portal.html#!info?alias=Org_Creinhardtii; 19,526 entries) appended with the NCBI mitochondrial (NC_001638.1; 8 entries) and chloroplast databases (BK000554.2; 68 entries) along with the sequence for common laboratory contaminants (www.thegpm.org/cRAP; 116 entries). Use a target decoy MS/MS search with trypsin protease specificity with up to two missed cleavages, a peptide mass tolerance of 15 ppm, and a fragment mass tolerance of 0.1 Da. Set a fixed modification of carbamidomethylation at cysteine and include the following variable modifications: acetylation at the protein N-terminus, oxidation at methionine, and phosphorylation at serine, threonine, and tyrosine. After the search is complete, adjust the false discovery rate of the significant peptide identifications to be less than 1% using the embedded Percolator algorithm. Export matches (*.xml) and reupload data to Progenesis.
3. From Progenesis, export the “Peptide Measurements” from the “Review Proteins” tab. These data can be used to determine the number of phosphosites and phosphoproteins identified in each replicate (Figure 3.2A) and the reproducibility can be assessed (Figure 3.3).

4. The proteomics data have been deposited to the ProteomeXchange Consortium (www.proteomexchange.org) via the PRIDE partner repository[25] with the dataset identifiers PXD012261.
5. Parse data using custom R script found at GitHub (https://github.com/hickslab/QuantifyR) or using similar parsing technique. This script groups together features matched with identical sequence, modifications, and score with differing protein accessions, representing them by the protein accession with the highest number of unique peptides and largest confidence score assigned by Progenesis. Features duplicated by multiple peptide identifications are reduced to a single peptide with the highest Mascot ion score. The results are then limited to only peptide with one or more phosphosites. Identifiers are made by joining the protein accession of each feature with the single-letter amino acid code of the modified residue and location of the modification. The data are then reduced to unique identifiers by summing the abundance of all contributing features (charge states, missed cleavages, etc.). Each identifier group is represented in the final dataset by the peptide with the highest Mascot score. Using these parsed results, the total number of phosphosites, phosphoproteins, and %CV can be calculated for the three replicates (Figure 3.2A, B).

3.4 Notes

1. Hutner's Trace Elements stock preparation taken from Chlamydomonas Resource Center (www.chlamycollection.org). Stock preparation is extensively described on the Chlamydomonas Resource Center Website and by Hutner, *et al*[24].
2. TAP Salts Stock (40x): Add 15.00 g of NH_4Cl, 4.00 g $MgSO_4 \cdot 7H_2O$, and 2.00 g $CaCl_2 \cdot 2H_2O$ to 1 L water. Stir until dissolved and autoclave. TAP Phosphate Stock

(1000x): Add 288.00 g K_2HPO_4 and 144.00 g KH_2PO_4 to 1 L of water. Stir until dissolved and autoclave. TAP Acetate Stock, pH 7.0 (50x): Add 121.00 g TRIS base and 50 mL of glacial acetic acid to 950 mL water. Stir to dissolve and filter sterilize. For 1 L of media combine the following amounts of stock solutions and autoclave: 25 mL TAP Salts Stock, 1 mL TAP Phosphate Stock, 20 mL of TAP Acetate Stock, 1 mL of Hutner's Trace Elements.

3. 1 M TRIS Stock (10x), pH 8.0: Dissolve 121.10 g of TRIS base in 800 mL of water, adjust the pH to 8.0 by adding concentrated HCl, and add water to a final volume of 1 L. 20% SDS Stock: Add 20.00 g SDS to 80 mL water, slowly mix to dissolve keeping the speed low to prevent frothing and heating if needed to no higher than 68°C, and adjust to final volume of 100 mL with water. For 10 mL of buffer, add 1 mL 1 M TRIS Stock solution, 1 protease inhibitor tablet, 1 phosphatase inhibitor tablet, and 0.5 mL 20% SDS stock solution to 8.5 mL of distilled water.
4. An OD_{750} of 0.4-0.5 was identified as mid-log phase growth for this strain of Chlamydomonas based on the known growth patterns[22]. Growth curves should be measured and used to identify the optical density where mid-log growth occurs when using this method to study other strains or algal species. This ensures that the cells are actively growing, there is no shortage of any nutrients, and enough material is harvested for each sample to perform phosphoproteomic analysis.
5. Three *Chlamydomonas* cultures were harvested, resuspended in lysis buffer, combined and re-aliquoted into three technical replicates to assess the reproducibility of this method and normalize any biological variability in the samples. When using this method for

differential studies, each culture should be a biological replicate, with no recombination step.

6. For CB-X protein assay, take a 10 µL aliquot of the protein sample and perform the assay according to the manufacturer's instructions. Briefly, add 1 mL of CB-X reagent and vortex. Centrifuge the sample at 15,000 x *g* for 5 min. Remove the supernatant without disturbing the pelleted protein. Add 50 µL of Solubilization Buffer 1 and 50 µL Solubilization Buffer 2 and pipette to resuspend the pellet. Incubate for one minute before adding 1 ml CB-X Assay Dye. Incubate for 5 minutes before measuring the absorbance of the sample at 595 nm.
7. IAM in solution is unstable and light sensitive. Keep IAM solution in the dark before and during alkylation to prevent degradation. Covering the tubes or mixer with aluminum foil works well for this.
8. When using C18 SepPak cartridges, a manifold can be used to apply vacuum to the samples to increase the flow rate through the cartridges. Vacuum can be used for all of the steps in the procedure except for the initial loading of the peptides onto the cartridge and the elution of the peptides. Flow rate should not exceed 1 mL/min when vacuum is used. The bed of the cartridges should stay wet throughout the procedure by keeping a small amount of solvent above the packed bed at all times.
9. For each step in the enrichment, centrifuge the tips at 1000 x *g* at room temperature to pass buffer through the column. For steps using 100 µL and 150 µL buffer, centrifuge the tips for 3 min and 5 min, respectively.
10. ZipTips work by drawing solvent through the resin using a micropipette to aspirate up and down. It is important that the resin remains wet throughout the purification by

leaving a small amount of solvent visible above the resin bed at all times until the sample is ready for elution.

3.5 Figures

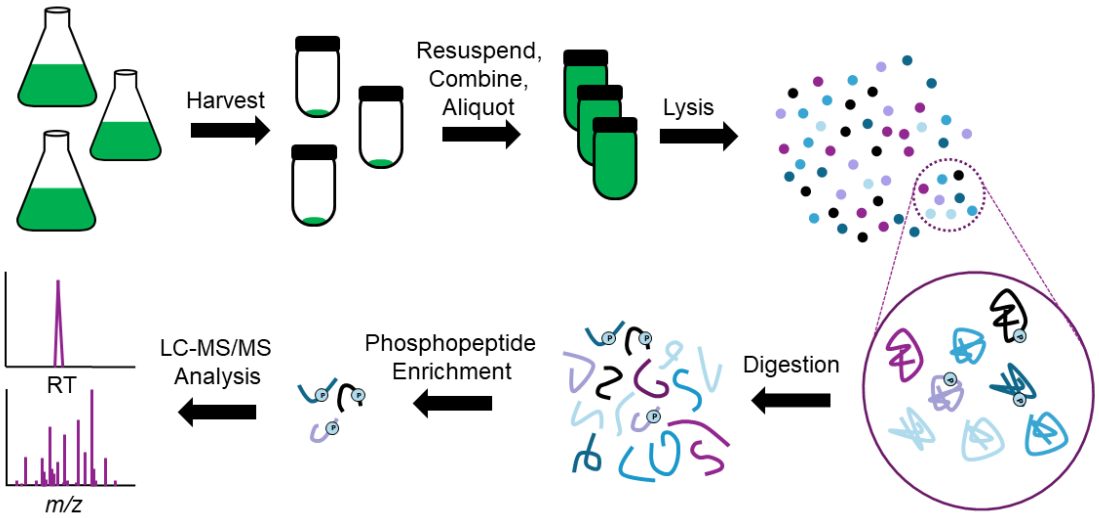

Figure 3.1 Phosphoproteomic workflow for *Chlamydomonas reinhardtii* cells. Briefly, Chlamydomonas cultures are harvested, resuspended in lysis buffer and sonicated. The lysate is collected and soluble proteins are reduced, alkylated and digested with trypsin. Phosphopeptides are enriched for using a titanium dioxide-based (TiO_2) enrichment before being subjected to LC-MS/MS analysis. For the data reported here, samples were pooled after resuspension and aliquoted into three technical replicates to remove any biological variation.

A.

	Replicate 1	Replicate 2	Replicate 3	Combined
Phosphosites	4692	4689	4675	3595
Phosphoproteins	1775	1775	1772	1775
Mean CV				28.3
Median CV				21.7
90% CV				54.9

B.

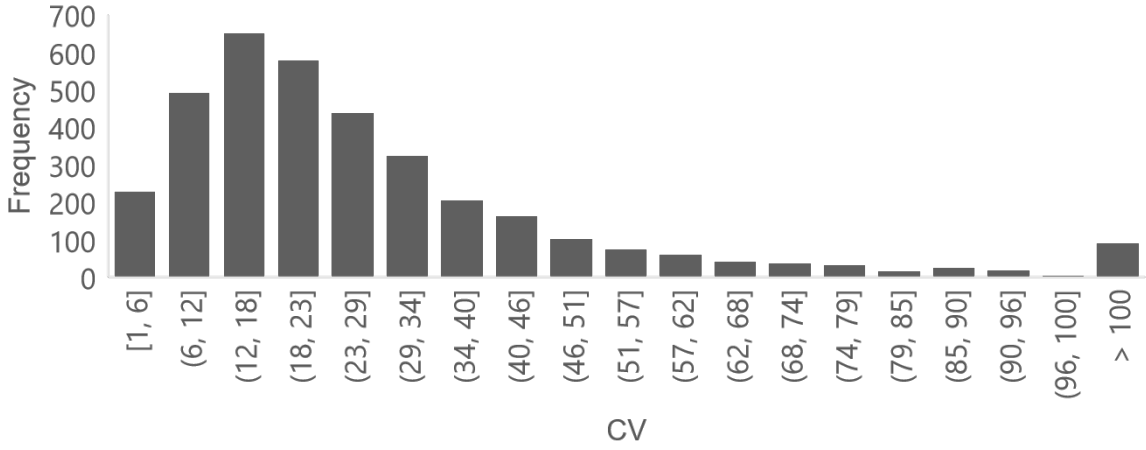

Figure 3.2 Summary of quantitation results between three replicate samples. A.) Number of phosphopeptides, phosphoproteins, and statistics for each individual replicate and combined data with filtered and imputed data. B.) Histogram of the % CV for quantitated phosphosites.

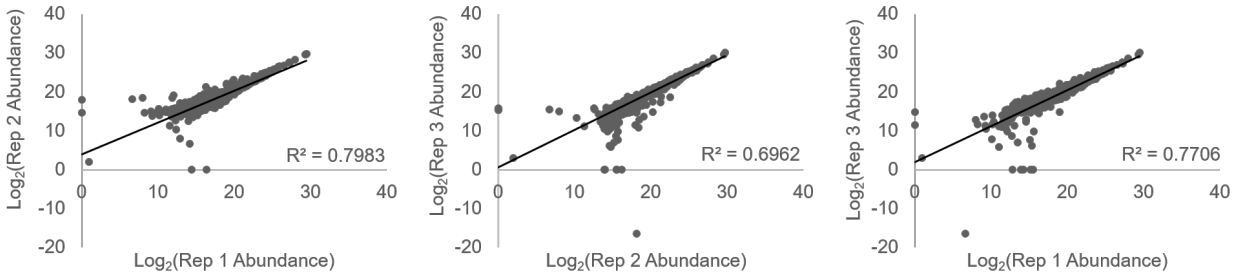

Figure 3.3 Plots comparing the $\log_2$ transformed abundances between replicate samples.

REFERENCES

1. Harris, E. H. Chlamydomonas as a Model Organism. *Annu. Rev. Plant Physiol. Plant Mol. Biol.* **2001**, *52* (1), 363–406.

2. Hu, Q.; Sommerfeld, M.; Jarvis, E.; Ghirardi, M.; Posewitz, M.; Seibert, M.; Darzins, A. Microalgal Triacylglycerols as Feedstocks for Biofuel Production: Perspectives and Advances. *Plant J.* **2008**, *54* (4), 621–639.

3. Merchant, S. S.; Prochnik, S. E.; Vallon, O.; Harris, E. H.; Karpowicz, S. J.; Witman, G. B.; Terry, A.; Salamov, A.; Fritz-Laylin, L. K.; Maréchal-Drouard, L.; Marshall, W. F.; Qu, L.-H.; Nelson, D. R.; Sanderfoot, A. A.; Spalding, M. H.; Kapitonov, V. V.; Ren, Q.; Ferris, P.; Lindquist, E.; Shapiro, H.; Lucas, S. M.; Grimwood, J.; Schmutz, J.; Cardol, P.; Cerutti, H.; Chanfreau, G.; Chen, C.-L.; Cognat, V.; Croft, M. T.; Dent, R.; Dutcher, S.; Fernández, E.; Ferris, P.; Fukuzawa, H.; González-Ballester, D.; González-Halphen, D.; Hallmann, A.; Hanikenne, M.; Hippler, M.; Inwood, W.; Jabbari, K.; Kalanon, M.; Kuras, R.; Lefebvre, P. A.; Lemaire, S. D.; Lobanov, A. V.; Lohr, M.; Manuell, A.; Meier, I.; Mets, L.; Mittag, M.; Mittelmeier, T.; Moroney, J. V.; Moseley, J.; Napoli, C.; Nedelcu, A. M.; Niyogi, K.; Novoselov, S. V.; Paulsen, I. T.; Pazour, G.; Purton, S.; Ral, J.-P.; Riaño-Pachón, D. M.; Riekhof, W.; Rymarquis, L.; Schroda, M.; Stern, D.; Umen, J.; Willows, R.; Wilson, N.; Zimmer, S. L.; Allmer, J.; Balk, J.; Bisova, K.; Chen, C.-J.; Elias, M.; Gendler, K.; Hauser, C.; Lamb, M. R.; Ledford, H.; Long, J. C.; Minagawa, J.; Page, M. D.; Pan, J.; Pootakham, W.; Roje, S.; Rose, A.; Stahlberg, E.; Terauchi, A. M.; Yang, P.; Ball, S.; Bowler, C.; Dieckmann, C. L.; Gladyshev, V. N.; Green, P.; Jorgensen, R.; Mayfield, S.; Mueller-Roeber, B.; Rajamani, S.; Sayre, R. T.; Brokstein, P.; Dubchak, I.; Goodstein, D.; Hornick, L.; Huang, Y. W.; Jhaveri, J.; Luo, Y.; Martínez, D.; Ngau, W. C. A.; Otillar, B.; Poliakov, A.; Porter, A.; Szajkowski, L.; Werner, G.; Zhou, K.; Grigoriev, I. V.; Rokhsar, D. S.; Grossman, A. R. The Chlamydomonas Genome Reveals the Evolution of Key Animal and Plant Functions. *Science* **2007**, *318* (5848), 245–250.

4. Zones, J. M.; Blaby, I. K.; Merchant, S. S.; Umen, J. G. High-Resolution Profiling of a Synchronized Diurnal Transcriptome from Chlamydomonas reinhardtii Reveals Continuous Cell and Metabolic Differentiation. *Plant Cell* **2015**, *27* (10), 2743–2769.

5. Miller, R.; Wu, G.; Deshpande, R. R.; Vieler, A.; Gartner, K.; Li, X.; Moellering, E. R.; Zauner, S.; Cornish, A.; Liu, B. Changes in Transcript Abundance in Chlamydomonas reinhardtii Following Nitrogen Deprivation Predict Diversion of Metabolism. *Plant Physiol.* **2010**, *154*, 1737–1752.

6. Wang, H.; Alvarez, S.; Hicks, L. M. Comprehensive Comparison of ITRAQ and Label-Free LC-Based Quantitative Proteomics Approaches Using Two Chlamydomonas reinhardtii Strains of Interest for Biofuels Engineering. *J. Proteome Res.* **2012**, *11* (1), 487–501.

7. Roustan, V.; Bakhtiari, S.; Roustan, P.-J.; Weckwerth, W. Quantitative in vivo Phosphoproteomics Reveals Reversible Signaling Processes during Nitrogen Starvation

and Recovery in the Biofuel Model Organism Chlamydomonas reinhardtii. *Biotechnol. Biofuels* **2017**, *10* (1), 280.

8. Krebs, E. G.; Fischer, E. H. Phosphorylase Activity of Skeletal Muscle Extracts. *J. Biol. Chem.* **1955**, *216* (1), 113–120.

9. Fischer, E. H.; Krebs, E. G. Conversion of Phosphorylase b to Phosphorylase a in Muscle Extracts. *J. Biol. Chem.* **1955**, *216* (1), 121–132.

10. Eriksson, J.; Fenyö, D. Modeling Experimental Design for Proteomics. *Methods Mol. Biol.* **2010**, *673*, 223–230.

11. Blackburn, K.; Goshe, M. B. Challenges and Strategies for Targeted Phosphorylation Site Identification and Quantification Using Mass Spectrometry Analysis. *Brief Funct. Genomic Proteomic* **2009**, *8* (2), 90–103.

12. Dunn, J. D.; Reid, G. E.; Bruening, M. L. Techniques for Phosphopeptide Enrichment Prior to Analysis by Mass Spectrometry. *Mass Spectrom. Rev.* **2010**, *29* (1), 29–54.

13. Kokubu, M.; Ishihama, Y.; Sato, T.; Nagasu, T.; Oda, Y. Specificity of Immobilized Metal Affinity-Based IMAC/C18 Tip Enrichment of Phosphopeptides for Protein Phosphorylation Analysis. *Anal. Chem.* **2005**, *77* (16), 5144–5154.

14. Ruprecht, B.; Koch, H.; Medard, G.; Mundt, M.; Kuster, B.; Lemeer, S. Comprehensive and Reproducible Phosphopeptide Enrichment Using Iron Immobilized Metal Ion Affinity Chromatography (Fe-IMAC) Columns. *Mol. Cell Proteomics* **2015**, *14* (1), 205–215.

15. Larsen, M. R.; Thingholm, T. E.; Jensen, O. N.; Roepstorff, P.; Jørgensen, T. J. D. Highly Selective Enrichment of Phosphorylated Peptides from Peptide Mixtures Using Titanium Dioxide Microcolumns. *Mol. Cell Proteomics* **2005**, *4* (7), 873–886.

16. Tsai, C.-F.; Wang, Y.-T.; Chen, Y.-R.; Lai, C.-Y.; Lin, P.-Y.; Pan, K.-T.; Chen, J.-Y.; Khoo, K.-H.; Chen, Y.-J. Immobilized Metal Affinity Chromatography Revisited: PH/Acid Control toward High Selectivity in Phosphoproteomics. *J. Proteome Res.* **2008**, *7* (9), 4058–4069.

17. Ye, J.; Zhang, X.; Young, C.; Zhao, X.; Hao, Q.; Cheng, L.; Jensen, O. N. Optimized IMAC Protocol for Phosphopeptide Recovery from Complex Biological Samples. *J. Proteome Res.* **2010**, *9* (7), 3561–3573.

18. Aryal, U. K.; Ross, A. R. S. Enrichment and Analysis of Phosphopeptides under Different Experimental Conditions Using Titanium Dioxide Affinity Chromatography and Mass Spectrometry. *Rapid Commun. Mass Spectrom.* **2010**, *24* (2), 219–231.

19. Werth, E. G.; McConnell, E. W.; Lianez, I. C.; Perrine, Z.; Crespo, J. L.; Umen, J. G.; Hicks, L. M. Investigating the Effect of Target of Rapamycin Kinase Inhibition on the Chlamydomonas reinhardtii Phosphoproteome: From Known Homologs to New Targets. *New Phytol.* **2019**, *221* (1), 247–260.

20. Karlie A Neilson, N. A. A. Less Label, More Free: Approaches in Label-Free Quantitative Mass Spectrometry. *Proteomics* **2011**, *11* (4), 535–553.

21. Bantscheff, M.; Schirle, M.; Sweetman, G.; Rick, J.; Kuster, B. Quantitative Mass Spectrometry in Proteomics: A Critical Review. *Anal. Bioanal. Chem.* **2007**, *389* (4), 1017–1031.

22. Werth, E. G.; McConnell, E. W.; Gilbert, T. S. K.; Couso Lianez, I.; Perez, C. A.; Manley, C. K.; Graves, L. M.; Umen, J. G.; Hicks, L. M. Probing the Global Kinome and Phosphoproteome in Chlamydomonas Reinhardtii via Sequential Enrichment and Quantitative Proteomics. *Plant J.* **2017**, *89* (2), 416–426.

23. Wang, H.; Gau, B.; Slade, W. O.; Juergens, M.; Li, P.; Hicks, L. M. The Global Phosphoproteome of Chlamydomonas reinhardtii Reveals Complex Organellar Phosphorylation in the Flagella and Thylakoid Membrane. *Mol. Cell Proteomics* **2014**, *13* (9), 2337–2353.

24. Hutner, S. H.; Provasoli, L.; Schatz, A.; Haskins, C. P. Some Approaches to the Study of the Role of Metals in the Metabolism of Microorganisms. *Proc. Am. Philos. Soc.* **1950**, *94* (2), 152–170.

25. Vizcaíno, J. A.; Côté, R. G.; Csordas, A.; Dianes, J. A.; Fabregat, A.; Foster, J. M.; Griss, J.; Alpi, E.; Birim, M.; Contell, J.; O'Kelly, G.; Schoenegger, A.; Ovelleiro, D.; Pérez-Riverol, Y.; Reisinger, F.; Ríos, D.; Wang, R.; Hermjakob, H. The Proteomics Identifications (PRIDE) Database and Associated Tools: Status in 2013. *Nucleic Acids Res.* **2013**, *41* (D1), D1063–D1069.

CHAPTER 4: Investigating the Interdependence of Insp and TOR Signaling in *Chlamydomonas*

4.1 Introduction

Inositol polyphosphates (InsPs) are versatile metabolites that store and rapidly proliferate inorganic phosphate throughout the cell[1]. With a *myo*-inositol ring that can be sequentially and reversible phosphorylated on all six carbons, InsP derivatives have distinct properties that allow them to be used across signaling cascades for the regulation of biological processes throughout the cell, including nutritional sensing, metal transport, and hormone signaling[2–4]. The pervasiveness of InsP signaling is in part due to their multitude of signaling mechanisms, as InsPs can influence protein-protein interactions, allosterically regulate via conformational changes, compete with phosphoinositide substrates, and non-enzymatically pyrophosphorylate phospho-serine residues[1]. While InsP signaling has been widely researched in animals and yeast, the study of its regulation in photosynthetic eukaryotes is in its infancy, despite the identification of plant-specific InsP modulated pathways[5–7] and high accumulation of $InsP_6$[8,9]. $InsP_7$ and $InsP_8$, generated from the phosphorylation of $InsP_6$, are unique InsPs that contain high-energy pyrophosphate bonds serve as energy storage molecules[9]. However, their low abundance and high turnover rates imply other unknown roles beyond this[10,11].

Recently, InsP signaling was shown to operate synergistically with Target of Rapamycin (TOR) kinase, a master regulator that influences protein translation, cell proliferation, carbon metabolism, and autophagy[12–16]. TOR's network extends throughout cellular processes combining phosphorylation signaling with reversible oxidation for rapid response and

acclimation to changing conditions[17–20]. The components of TORC1 are conserved across eukaryotes, including the model algal organism *Chlamydomonas reinhardtii*, and include TOR (Cre09.g400553.t1.1), regulatory associate protein target of rapamycin (RAPTOR, Cre08.g371957.t1.1), and lethal with sec-13 protein 8 (LST8, Cre17.g713900.t1.2)[21,22]. While quantification of differentially phosphorylated proteins following TOR inhibition has provided some insights[19], a map of the signaling network throughout the TOR pathway has still not been realized.

TOR is partly regulated by phosphate availability, as phosphate deprivation results in a decreased abundance of LST8 that subsequently downregulates TORC1 activity[23]. This suggests that InsPs, which have a proposed role in the buffering of intracellular phosphate concentrations as well as metal ion homeostasis via chelation[2], may be able to directly modulate TOR activity through the flux of intracellular phosphate. However, studies in yeast have shown contradictory effects of phosphate deprivation on the accumulation of InsPs[4,24,25]. This suggests that the overlap of metabolic signaling in *C. reinhardtii* is likely highly complex and dependent on growth and stress conditions, as shown through the influence of acetate on the physiological state of a hexakisphosphate kinase insertional mutant of *C. reinhardtii*[26].

This study seeks to characterize the relationship between TOR and InsP signaling in *C. reinhardtii*. A previously characterized rapamycin-hypersensitive mutant (*vip1-1*)[26] with an established loss of function for a conserved inositol hexakisphosphate kinase is used to differentially analyze the phosphoproteome during TOR inhibition. Through this work we can begin to deconvolute the mechanistic roles InsPs play in the regulation and proliferation of TOR signaling. These data suggest a prominent role of InsP signaling in cellular metabolism, specifically the regulation of energy transformation via photosynthesis.

4.2 Materials and Methods

4.2.1 Cell Culturing and Rapamycin Treatment

Generation of the *vip1-1* mutant is described previously[26]. Briefly, the parental strain CC-1690 mt+ (Sager 21 gr) (Chlamydomonas Resource Center, St. Paul, MN, USA) was used to generate the rapamycin-hypersensitive strain via insertional mutagenesis[27] of the hygromycin resistance gene, *aph7"*[28]. Transformation was performed as described previously[29] and rapamycin-hypersensitive mutants were identified via differences in growth on Tris-Acetate-Phosphate (TAP) and TAP with 500 nM rapamycin agar plates. For phosphoproteomic studies, as previously described[19,30], *vip1-1* and wild-type cultures were maintained photoheterotrophically on TAP agar plates. 3.5 mL cells from a culture grown to exponential phase (1–2 x 10^6 cells ml $^{-1}$) were inoculated into 350 mL TAP in 1 L Erlenmeyer flasks. Triplicate cultures were grown photoheterotrophically to mid-exponential phase (1–2 x 10^6 cells ml $^{-1}$) under constant light. When the cultures reached mid-exponential phase, rapamycin (Research Products International, Mt Prospect, IL, USA) in dimethyl sulfoxide (DMSO, Sigma Aldrich, St. Louis, MO, USA) was added to a concentration of 500 nM[26] for treated cultures and an equal volume of DMSO was added to the control cultures. Cells were treated for 15 min and then quenched with 40% methanol and then harvested via centrifugation as previously described[19]. The supernatant was discarded, and the pellets were flash-frozen using liquid nitrogen and stored at -80 °C until extraction.

4.2.2 Protein Extraction

Frozen cell pellets were lysed in 4 mL of buffer containing 100 mM Tris, pH 8.0, 1% sodium dodecyl sulfate, 1x cOmplete EDTA-free protease inhibitor cocktail (Roche, Basel, Switzerland), and 1x PhosSTOP phosphatase inhibitor cocktail (Roche). Cell were lysed via

sonication using an E220 focused ultrasonicator (Covaris, Woburn, MA, USA) for 180 s at 200 cycles/burst, 100 W power, and 13% duty cycle. After sonication, samples were centrifuged at 15,000 x *g* for 10 min at 4 °C and the supernatant was collected. The cell pellet was resuspended in 1 mL of fresh lysis buffer, incubated for 30 min at 4 °C, and centrifuged again. Supernatants were combined and proteins were precipitated using four volumes of cold 100 mM ammonium acetate in methanol, incubating overnight at -80 °C. Proteins were pelleted by centrifugation at 3220 x *g* for 5 min and washed twice with fresh 100 mM ammonium acetate in methanol. Proteins were allowed to dry for 5 min before resuspension in 2 mL 8 M urea in 100 mM Tris, pH 8.0. Protein concentration was measured using the CB-X Protein assay (G-Biosciences, St. Louis, MO, USA) according to the manufacturer's protocol, and samples were normalized to the same concentration (0.5 mg/mL) and volume (2 mL) using resuspension buffer.

4.2.3 Protein Reduction, Alkylation, and Digestion

Protein thiols were reduced using 10 mM dithiothreitol at room temperature for 30 min followed by alkylation with 40 mM iodoacetamide for 45 min at room temperature while protected from light. Samples were diluted 5-fold after alkylation with 100 mM Tris, pH 8.0 to reduce the concentration of urea to 1.6 M. Samples were then digested with Trypsin Gold (Promega, Madison, WI, USA) at a 1:50 enzyme:protein ratio overnight at room temperature, rotating end-over-end. The digestion was quenched with 20% trifluoroacetic acid (TFA, Fisher Scientific, Waltham, MA, USA) to a final concentration of 0.4% TFA and a pH < 3.0.

4.2.4 Solid-Phase Extraction

After digestion, samples were desalted using 50 mg/1.0 mL Sep-Pak C18 cartridges (Waters, Milford, MA, USA) using a vacuum manifold (Phenomenex, Torrance, CA, USA). Resin was pre-eluted with 1 mL 80% acetonitrile, 0.1% TFA and then equilibrated with 2 mL

0.1% TFA at a flow rate of ~1 drop/s. Samples were first centrifuged at 3220 x *g* for 5 min to pellet undigested protein before loading onto the cartridges using gravity flow. Samples were then reloaded once, and cartridges were washed with 2 mL of 0.1% TFA followed by elution of the peptides in 1.5 mL of 80% acetonitrile, 0.1% TFA. The samples were then dried by vacuum centrifugation and 25 µg aliquots of each sample were reserved for global proteomics.

4.2.5 Phosphopeptide Enrichment and Desalting

Phosphopeptide enrichment was performed on each sample as previously described using 3 mg Titansphere Phos-TiO_2 kit spin columns (GL Sciences, Torrance, CA)[19,30]. Following each step in the enrichment, columns were centrifuged at 1000 x *g* for 5 min until dry. Columns were pre-eluted with 100 µL 20% acetonitrile, 5% aqueous ammonia, and the equilibrated with 100 µL 80% acetonitrile, 1% TFA twice, and 100 µL 80% acetonitrile, 1% TFA with 25 mg/ml phthalic acid three times. Samples were resuspended in 200 µL of 80% acetonitrile, 1% TFA with 25 mg/mL phthalic acid, and then centrifuged at 15,000 x *g* for 5 min to pellet any precipitant and prevent column clogging. Samples were loaded onto the column a total of five times, reapplying the flow through after each centrifugation step. Columns were then washed using 100 µL 80% acetonitrile, 1% TFA with 25 mg/mL phthalic acid twice, and 100 µL 80% acetonitrile, 1% TFA three times. Phosphopeptides were eluted in 100 µL 20% acetonitrile, 5% aqueous ammonia twice, for a total of 200 µL of elution. Samples were then dried using vacuum centrifugation.

Following phosphopeptide enrichment, samples were desalted using 0.6 µL C_{18} ZipTips (MilliporeSigma, Burlington, MA, USA). After drying, samples were resuspended in 15 µL 0.1 TFA and centrifuged for 5 min at 15,000 x *g* to remove any precipitant and prevent tip clogging. Tips were first pre-eluted three times with 10 µL of 80% acetonitrile, 0.1% TFA, followed by

equilibration with 10 µL 0.1% TFA three times. The samples were then loaded on the tip by passing the phosphopeptides through ten times. Following loading, the tips were then washed six times with 10 µL of 0.1% TFA and the eluted by passing 15 µL of 80% acetonitrile, 0.1% TFA through the tip ten times. The samples were then dried down using vacuum centrifugation.

4.2.6 LC-MS/MS Acquisition and Data Processing

Phosphopeptide samples were resuspended in 20 µL of 5% acetonitrile, 0.1% TFA while global samples were resuspended to a concentration of 0.2 µg/µL in 5% acetonitrile, 0.1% TFA. Global and enriched samples were analyzed using an Acquity M-Class UPLC system (Waters) coupled to a Q Exactive HF-X Hybrid Quadrupole Orbitrap mass spectrometer (ThermoFisher, Waltham, MA, USA) via a Nanospray Flex Ion Source (ThermoFisher) with a spray voltage flowting at 2.1 kV. Mobile phase A was water with 0.1% formic acid and mobile phase B was acetonitrile with 0.1% formic acid. 2 µL of each enriched and global sample was injected with a 5 µL/min flow rate for 3 min onto a Symmetry C_{18} trap column (100 Å, 5 µm, 180 µm x 20 mm, Waters) using 99% A. Samples were separated with a 300 nL/min flow rate on an HSS T3 C18 column (100 Å, 1.8 µm, 75 µm x 250 mm, Waters). Separation was performed in a gradient of 5-35% B over 90 min, followed by a ramp to 85% B in 5 min with a 5 min hold and a return to 5% B in 2 min with a re-equilibration time of 13 min, for a 120 min total run time.

The mass spectrometer was operated in positive polarity with a 2.1 kV spray voltage, 325°C capillary temperature and S-lens RF level of 40. Lock masses of background polysiloxane ions were included. Full MS/DD-MS^2 scan type was used with a method duration of 120 min. MS survey scan was performed in profile mode across 350-1600 *m/z* at 120,000 resolution with a 50 ms maximum IT and $3x10^6$ AGC target. The top 20 features with a +2 to +7 charge state above 5000 counts were selected. MS^2 scans were collected at 45,000 resolution with NCE at 32

until 100 ms maximum IT or $1x10^5$ AGC target. The dynamic exclusion window was set to 10 s and an isolation window of 0.7 *m/z* for precursor ions. The mass spectrometry proteomics data and supplemental tables have been deposited to the ProteomeXchange Consortium via the PRIDE partner repository [31] and can be accessed with the Identifier PXD023250 (Username: reviewer_pxd023250@ebi.ac.uk, Password: NqKCEDEV).

The acquired spectral files (*.raw) were uploaded into Progenesis QI for Proteomics (Nonlinear Dynamics, Waters) and data analysis was performed as described previously [20]. Separate experiments were created for the analysis of the global and enriched samples. An automatically assigned reference spectrum was used to align the total ion chromatograms and a peak picking sensitivity was set to the maximum of 5. Alignment was validated with a score >90%, and replicates were grouped based on sample type before being exported as a combined peak list (*.mgf). The peaklist was uploaded into Mascot (Matrix Science, version 2.5.1, Boston, MA, USA) and database searching was performed against the *Chlamydomonas reinhardtii* JGI v5.6 Phytozome database (https://phytozome-next.jgi.doe.gov/info/Creinhardtii_v5_6, 19,523 entries) appended with the entries from the NCBI chloroplast (BK000554.2, 68 entries) and mitochondrial (NC_001638.1, 8 entries) databases. Sequences for common laboratory contaminants (www.thegpm.org/cRAP, 116 entries) were also included in the database. A target decoy MS/MS search was performed with trypsin specificity of up to two missed cleavages, a peptide mass tolerance of 15 ppm, and a fragment mass tolerance of 0.02 Da. Carbamidomethylation of cysteine was included as a fixed modification with acetylation at the protein N-terminus, oxidation of methionine, and phosphorylation of serine, threonine, and tyrosine included as variable modifications. After completion of the search, the false discovery rate was adjusted to be less than 1% using the embedded Percolator algorithm[32], and matches

were exported (*.xml) and reuploaded into Progenesis for peak matching. After matching, identifications with a Mascot score less than 13 were removed before exporting protein measurements for global samples, and the protein and peptide measurements for the enriched samples from the "Review Proteins" stage.

4.2.7 Downstream Bioinformatic Analysis

For proteomic analysis, data were parsed using custom R scripts designed for global and phosphoproteomic data (https://github.com/hickslab/QuantifyR). For global proteomic analysis, leading protein accessions from the protein measurements were used to identify each protein. Proteins were kept if there were at least 2 shared peptides and at least 1 unique peptide assigned. Only proteins identified across all three replicates in at least one condition were kept, and their Progenesis-normalized abundance columns were $\log_2$-transformed and conditional imputation was applied using the imp4p package[33] to fill in any missing values. For conditions with at least one nonzero value, the *impute.rand* function was used with default parameters. For conditions were there were only missing values, the *impute.pa* function was used to impute small numbers centered at the lowest 2.5% of the values in each replicate. Statistical significance was calculated using a two-tailed, equal variance *t*-test with a Benjamini and Hochberg (BH) correction[34]. Fold-change was calculated from the difference of the mean abundance values between conditions. Observations with an FDR-adjusted p-value <0.05 and a $\log_2$ transformed fold change of ± 1 were considered significantly changing.

For phosphoryation-enriched samples, groups in the peptide measurements data were reduced to satisfy the principle of parsimony, removing duplicated and matched peptides with identical sequence, modifications, and score. These were represented by the protein accession with the highest number of unique peptides, which was found in the protein measurements data,

else the protein with the highest confidence score assigned via Progenesis. For identical features with differing peptide identifications, duplicates were reduced to the peptide with the highest Mascot ion score. These results were filtered for only peptides containing phosphorylation. Identifiers were created for each of these features by joining the protein accession for each peptide to the amino acid and location of the site(s) of modification in the protein sequence. The data were then reduced to only unique identifiers by summing all of the contributing peak features which may come from different charge states, missed cleavages, and the presence of additional variable modifications. The peptide with the highest Mascot score in each group represented the corresponding identifier. Identifiers were then removed if they did not have at least one condition where all three replicates had nonzero values for their Progenesis-normalized abundances. These abundances were $\log_2$-transformed and imputation was applied to assign missing values using the same strategy outlined above. Statistical significance was calculated using a two-tailed, equal variance *t*-test and fold-change was calculated from the difference of the mean abundance values between conditions. Observations with a *p*-value <0.05 and a $\log_2$ transformed fold change of ± 1 were considered significantly changing. Protein accessions for each protein listed in the proteomic dataset and each identifier in the phosphoproteomic dataset were matched to their corresponding Uniprot accession using the Basic Local Alignment Search Tool (BLAST)[35]. These accessions were used to assign Gene Ontology (GO) terms for each accession in the global and identifier in the phosphorylation-enriched datasets. GO terms for the proteins and identifiers significantly changing were compared to the GO terms of the entire dataset to determine the fold-change enrichment and number of proteins/identifiers for each term. The top five GO terms for the significantly changing proteins/identifiers with a fold-change of at least 1.5 were identified.

4.3 Results and Discussion

To examine the relationship between protein phosphorylation and inositol polyphosphates, phosphoproteomic differences between *vip1-1* and its parent strain under normal and TOR inhibited (15 min rapamycin treatment) conditions were assessed (Figure 4.1). Phosphorylation changes can be seen in *C. reinhardtii*[19] and other organisms[36–38] with 15 min of TOR inhibition while protein turnover is minimized, ensuring differential measurements are the result of changes in phosphorylation and not overall protein abundance. This experimental design allows investigation of changes (1) in phosphorylation with the loss of inositol hexakisphosphate and diphosphoinositol-pentakisphosphate kinase (VIP1), and (2) in the response of each strain when TOR is inhibited, revealing ties between inositol polyphosphate and TOR signaling.

Differential global proteomics performed between the four conditions quantified a total of 2,460 proteins with a median CV of 23% (Table S4.1**)**. Of these proteins, 646, or 26% had phosphosites detected in the phosphoproteomic analysis. No proteins were significantly changing when a *t*-test was performed between the control and rapamycin treated conditions for each strain (Figure 4.2), confirming that protein turnover is minimal with 15 min treatment.

4.3.1 Phosphoproteomic Analysis

Phosphopeptide enrichment resulted in the quantification of 3986 phosphopeptides with a unique set of phosphorylation modifications, referred to as identifiers, with a median CV of 29% across biological replicates (Table S4.2). These identifiers came from 1935 proteins, with the majority of proteins only having one identifier (57%). Nearly 90% of identifiers contained only one phosphorylation site in this dataset, following the established global phosphoproteome of *C. reinhardtii*[39]. Following rapamycin treatment, 1,029 identifiers were significantly changing in *vip1-1*, 228 decreasing and 801 increasing (Figure 4.3a**)**, while 217 identifiers were significantly

changing in the parent strain, 129 decreasing and 88 increasing (Figure 4.3b). Comparisons between the two strains yielded 1625 identifiers significantly changing between the control wild-type and *vip1-1* conditions (Figure 4.3c) and 346 significantly changing between the rapamycin-treated conditions (Figure 4.3d). The decrease in significantly changing phosphosites with rapamycin treatment is suggestive that the two strains move toward a similar state of phosphorylation in response to the stress of rapamycin treatment, despite having significantly different phosphoproteomes under normal conditions. Given that there are no significant changes in protein expression within a given strain in the global proteomic samples with rapamycin treatment (Table S4.1), the changes quantified here are likely observed changes in phosphorylation rather than changes in protein abundance. This is further supported by previous work showing little change in the global proteome of *C. reinhardtii* after an hour of TOR inhibition[20]. The higher number of identifiers significantly changing in phosphorylation in *vip1-1* (Figure 4.3a) in response to rapamycin treatment compared to that of wild-type (Figure 4.3c), suggests that the loss of VIP1 impacts the TOR signaling cascade, with more phosphorylation-mediated regulation required to circumvent the loss of InsP in the absence of VIP1.

4.3.2 Hierarchical Clustering and Gene Ontology Analysis

Hierarchical clustering was performed on the identifiers significantly changing with rapamycin treatment in *vip1-1* and wild-type (Figure 4.4). Some of these identifiers, when sorted into four clusters, separate based on those that have the same trend with rapamycin treatment between the two strains (B and D in Figure 4.4a, 282 identifiers; A and C in Figure 4.4b, 101 identifiers), while others have the opposite trend with treatment (A and C in Figure 4.4a, 747 identifiers; B in Figure 4.4b, 62 identifiers). This shows there is a distinct delineation between

phosphorylation that is dependent on VIP1 following TOR inhibition, and that the loss of VIP1 generates a phosphoproteomic response distinct from the response seen in the parent strain.

GO analysis of the significantly changing identifiers in *vip1-1* (Figure 4.5) revealed significantly increasing identifiers are enriched in the biological processes of spliceosome mRNA splicing, rRNA processing, and mRNA processing among others, as well as molecular functions of RNA and DNA binding. Identifiers significantly decreasing in *vip1-1* with rapamycin treatment were enriched in photosynthesis-related GO terms, including photosystem II (PSII) assembly, PSII stabilization, and the PSII oxygen evolving complex. Most of the GO terms found to be enriched in the significantly changing identifiers of *vip1-1* are unique to this strain, with a mostly unique set of GO terms enriched in the identifiers significantly changing in wild-type (Figure 4.6).

4.3.3 Phosphosites Modulated by TORC1 Inhibition – Known and Putative TOR Substrates

A total of 42 identifiers from 22 proteins with homology to known TOR signaling pathway components[21] had phosphorylation identified in this study (Table S4.3). Of those identifiers, 12 significantly increased and two significantly decreased in *vip1-1* following rapamycin treatment. In the parent strain, one identifier significantly increased following rapamycin treatment and four significantly decreased. Interestingly, *vip1-1* and the parent strain did not share any of the same significantly changing identifiers, indicating that the loss of InsP signaling resulting from the absence of VIP1 has a fundamental change on the TOR signaling pathway, further demonstrating the previously proposed synergism between TOR and InsPs[26]. This is illustrated by the identification of an uncharacterized phosphosite on TOR (Cre09.g400553.t1.1, S2598), which significantly increased in the *vip1-1* mutant following rapamycin treatment (FC: 4.98), but did not change in the parent strain. This site was previously

identified in a *C. reinhardtii* TOR inhibition study[19], but was not seen significantly changing with inhibition. This site does not align with the known regulatory phosphosites (S2159/T2164) of human mammalian TOR (mTOR, Uniprot P42345) or the autophosphorylation site they promote (S2481)[40], making it hard to determine the exact significance of this site. However, its significant increase in *vip1-1* with rapamycin treatment, along with its position in the kinase domain based on homology with mTOR, suggests that it may play a role in regulating the activity of TOR and possibly connect to InsP signaling, as well as contributing to the hypersensitivity of *vip1-1* to TOR inhibition.

The La-domain RNA-binding protein (LARP, Cre10.g441200.t1.2) had four significantly changing identifiers, with two identifiers (S670, S812) increasing in the *vip1-1* mutant. The parent strain had significantly increased phosphorylation on S958 and significantly decreased phosphorylation on S817, the latter of which was previously identified following TOR inhibition[19]. Despite the identification of LARP as a downstream target of TOR and S6K in both *Chlamydomonas* and *Arabidopsis*[19,41], the role of LARP in phototrophs has not been fully elucidated. However, heat stress in *Arabidopsis* generates LARP-dependent degradation of mRNA[42], connecting stress response – and TOR by association – to LARP, as predicted from mammalian signaling pathways. In mammalian cells, LARP phosphorylation requires TOR activity and is also a target of both mTORC1 and S6K, as mirrored in *Arabidopsis* and *Chlamydomonas*[43–45]. Additionally, studies in mammalian cells have shown that non-phosphorylated LARP interacts with 5' and 3' UTRs of mRNAs, inhibiting their translation[46], while others have shown mTORC1 uses LARP to control Terminal Oligopyrimidine (TOP) mRNA translation[46,47]. In Chlamydomonas, TOR inhibition leads to a decline in protein translation, similar to that shown in mammalian cells[12]. Thus, the significantly decreased

phosphorylation on S817 in the parent strain of *C. reinhardtii* may mirror the mTOR pathway by inhibiting translation of mRNA. However, this site was not significantly decreased in the *vip1-1* mutant following rapamycin treatment, suggesting a potential dependence on InsP signaling on the dephosphorylation event. While mammalian inositol polyphosphate multikinase (IMPK) binds to mTOR and RAPTOR to mediate mTOR signaling via amino acids, no other direct connections between LARP, TOR, and InsPs are currently known[48].

In mammalian cells, RAPTOR can be directly phosphorylated by AMP kinase (AMPK), Glycogen Synthase Kinase 3 (GSK3), and nemo-like kinase, the latter of which has no homologue in *Chlamydomonas*[49–51]. Both AMPK and GSK3 phosphorylation significantly changed in the *vip1-1* mutant, with S29-S32 from the β2 subunit of AMPK (Cre10.g457500.t1.1) significantly decreasing (FC: 0.25) and both S322 (FC: 2.95) and Y323 (FC: 2.28) significantly increasing on GSK3 (Cre12.g511850.t1.2). The β2 subunit of AMPK was previously observed to have an increase of FC 2.27 on S25 following rapamycin inhibition[19]; although this site was observed in the current study, it did not significantly change in either strain. The increase in phosphorylation of S29-S32 on the *vip1-1* mutant, however, suggests an overlap of InsP signaling with either the TOR or AMPK pathway. In mammalian cells, phosphorylated IMPK binds to AMPK as a nutritional sensor, whereby the AMPK pathway is activated following glucose intake[52]. It is possible that cross-talk between AMPK and InsPs performs a similar function to signal changes in nutritional availability to TOR in plants; however, additional studies are needed to fully delineate this role.

GSK3 also experienced changes in phosphorylation in the *vip1-1* mutant not previously identified in the wildtype, further suggesting a dependence on InsPs for a fully functional TOR pathway. The tyrosine phosphorylation on Y323 is located in the activation loop and is

conserved in higher order eukaryotes as a known regulator of GSK3 kinase activity[53,54]. In mammalian cells, GSK3 is a component of a feedback loop with TOR, acting as an upstream regulator of TOR through the tuberous sclerosis complex, but also inhibited indirectly by TOR through S6K phosphorylation[55]. Whereas active TOR promotes protein translation and cell cycle progression, this is inhibited by active GSK3. In the *vip1-1* mutant, the increase in phosphorylation on Y323 suggests GSK3 activation, which would further participate in the feedback loop to inhibit TOR. This elevated secondary inhibition may contribute to the hypersensitivity of the *vip1-1* mutant to rapamycin, compared to the parent strain. Further, this rapid inactivation of GSK3 in the *vip1-1* mutant that is not observed in the parent strain suggests that InsP signaling is used to modulate the effects of nutritional sensing in wild type *Chlamydomonas*, potentially buffering the sensitivity of cells to perturbations that may be an artifact of small-scale environmental changes.

TORC1 is known to regulate autophagy through phosphorylation of ATG13, which in turn prevents the activation of the ATG1 complex and inhibits autophagy [56]. With inhibition of TOR, rapid dephosphorylation of ATG13 is observed, resulting in autophagy induction through the ATG1 complex activation[57]. Following rapamycin treatment, S1176 of ATG17 (Cre16.g651350.t1.1), a scaffolding protein in the ATG1 complex[58], increased by a FC of 3.29 in the *vip1-1* mutant. In mammalian and yeast cells, ATG17 along with ATG13, ATG11, and ATG1 kinase form the ATG1 complex when ATG13 and ATG1 are dephosphorylated, initiating autophagy. This phosphorylation is known to be controlled at least in part by the TOR pathway. While TOR has been implicated in autophagy in *C. reinhardtii*[59], further experimentation is needed to map and compare the algal signal mechanisms to the pathways of other eukaryotes in order to distinguish the role this ATG17 phosphorylation has on the induction or inhibition of

autophagy. However, its increase in phosphorylation in the *vip1-1* mutant may suggest that InsP signaling is required for its activation or deactivation.

4.3.4 Regulation of Photosynthesis Through Phosphorylation

It is well-established that protein phosphorylation plays a pivotal role in the regulation of phosphorylation through changes in molecular recognition, ligand binding, and protein interactions[60–63]. In a previous study, TOR was shown for the first time to regulate photosynthesis based on changes in reversible oxidation[20], but little is known about how TOR and InsP signaling coordinate together to impact the regulatory phosphosites of photosynthetic machinery. In this work, 80 identifiers from 34 photosynthesis-related proteins were quantified, 17 of which have unique differential phosphorylation in *vip1-1* compared to the parent strain following TOR inhibition (Table S4.4). When global proteomic changes between the two strains were analyzed, PSII was particularly prominent in the analysis, with significant decreases to four of its six catalytic subunits, including D1 and D2 (gi|41179021|ref|NP_958377.1 and gi|41179063|ref|NP_958420.1, respectively), both with FCs of 0.23, and the two reaction center proteins, C43 and C47 (gi|41179065|ref|NP_958422.1 and gi|41179032|ref|NP_958388.1, respectively), with FCs of 0.27 and 0.22. Without these subunits, PSII is rendered useless, and can no longer use electrons to oxidize water nor participate in linear electron transfer[64]. When the phosphoproteomic results are combined with global abundances showing severely diminished PSII and, by association, linear electron transport (Table S4.1), these data indicate an expediency toward cyclic electron transport (CET) in the *vip1-1* mutant that supersedes that of the parent strain, indicating a pronounced role for InsP signaling in the maintenance of linear electron transport.

The most well established regulator of CET is proton-gradient related-like protein 1 (PGRL1, Cre07.g340200.t1.1)[65]. In *C. reinhardtii*, PGRL1 combines with photosystem I (PSI), light harvesting complex 1 (LHC1), light harvesting complex II (LHCII), cytochrome b_6f, and ferredoxin-NADPH oxidoreductase (FNR) to form a supercomplex through which the mode of photosynthetic electron flow is determined[66]. PGRL1 is differentially phosphorylated in response to distinct environmental cues, enabling precise modulation of electron flow through which cells can rapidly adjust to exogenous stressors[67]. Following rapamycin treatment, the parent strain had significantly decreased phosphorylation on S50 by a FC of 0.25. This site was also shown to be decreasing in previous work following rapamycin inhibition, but did not meet the threshold for significance[19]. Since we have previously observed changes in photosynthetic electron fluxes reminiscent of CET following TOR inhibition in *Chlamydomonas*[20], it is likely that the decrease in phosphorylation on S50, in addition to the previously shown significant increase in oxidation on C63, is related to the upregulation of CET. This is further demonstrated when comparing the parent strain with *vip1-1* before rapamycin treatment, where the phosphorylation of S50 is decreased by a FC of 0.23 in the mutant strain (Figure 4.7). This decreased phosphorylation, which is of similar magnitude to the change in phosphorylation following rapamycin in the parent strain, occurs in the presence of significant decreases in global abundance of the catalytic components of PSII. Combined, these results suggest that the *vip1-1* strain has already converted to CET, even before rapamycin inhibits TOR.

In *Arabidopsis*, PGRL1 is phosphorylated by state transition kinase 8 (STN8) in order to "fine-tune" the shift between linear and cyclic electron flow and slow the transition back to linear transport following a decrease in stress conditions[68]. While there is no direct homolog in Chlamydomonas, the most similar protein is sugar transporter-like protein 1 (STL1,

Cre12.g483650.t1.2), a functionally uncharacterized thylakoid protein kinase[69]. One novel phosphosite on STL1 significantly increased in the *vip1-1* mutant following rapamycin treatment (T126, FC: 3.52). Previously characterized phosphorylation has shown an increase on T167 via an state transition protein kinase 7 (STN7)-dependent manner only in state 2, suggesting that STN7 acts upstream of STL1 in a phosphorylation-mediated signaling pathway[69]. Phosphorylation on T126 may play a similar role in activating or deactivating STL1 in response to TOR inhibition. Additionally, this identifier increases in wild type with inhibition as well (FC: 1.41), suggesting that the absence of VIP1 upregulates this signaling pathway.

Photosynthetic state transitions involve the reversible shift of light harvesting antennas between PSII and PSI, through which light capture can be modulated to decrease the occurrence of overexcitation on either photosystem[70]. The transition from state 1 to state 2 induces the switch to CET, where the binding of LHCII to PSI initiates CET. This transition is modulated through cross-talk between redox and phosphorylation signaling; imbalances in the excitation between the two photosystems are reflected in a change in redox state, which then modulates the phosphorylation of the LHCs[71]. In this study, phosphorylation was observed on light harvesting minor chlorophyll a/b binding protein of photosystem II (CP26, Cre16.g673650.t1.1), a component of LHCII with several established phosphorylation sites [72]. Of the four identifiers quantified from this protein, one significantly increased in the parent strain following rapamycin treatment (T10, FC: 2.44) while another significantly decreased in *vip1-1* following treatment (S202, FC: 0.22). Phosphorylation on T10 has previously been identified as a target of phosphorylation in Chlamydomonas without the presence of external stressors [39]. However, while both CP26 and CP29, another minor LHC protein, have been shown to be phosphorylated under optimal conditions, both increase in phosphorylation while in state 2[73], further supporting

an enhanced role of CET following TOR inhibition. Thus, while the exact function of T10 phosphorylation is unknown, it may play a role in modulating the antenna complex toward the shift to CET. The decrease in the *vip1-1* mutant on S202, a site that does not differentially change in the parent strain, likely occurs because the *vip1-1* mutant is already shifted toward CET, making this decrease likely related to a further heightened stress condition. This is supported through the rapamycin induced increase in phosphorylation on S43 of the PSII 10 kDa polypeptide (PsbR, Cre06.g261000.t1.2, FC: 2.41), which only occurred in the *vip1-1* mutant. S43 has been previously identified in *C. reinhardtii* phosphoproteomic studies [39,69,74,75], but is only phosphorylated under state 2 conditions[69,76]. Thus, the pronounced increased in *vip1-1* following rapamycin treatment, likely represents heightened stress beyond the established transition of CET.

One of the first indications of stress on the photosynthetic apparatus is the loss of the extrinsic proteins of PSII, through which oxygen production and the corresponding linear electron flow is severely diminished. These extrinsic proteins, particularly photosystem II oxygen evolution enhancer protein 1 (PsbO, Cre09.g396213.t1.1), have been shown to be highly phosphorylated[72], indicating a substantial role for phosphorylation in photoassembly and disassembly. In this work, a total of 15 identifiers were quantified, with four of these identifiers significantly decreasing in phosphorylation following TOR inhibition in the *vip1-1* mutant (Table S4.4). While phosphorylation of PsbO by wheat kinase STARTS1 (WKS1) in wheat reduces photosynthetic efficiency[77], the role of phosphorylation on PsbO in *C. reinhardtii* is still unknown[72]. However, PsbO phosphorylation in *Chlamydomonas* has been proposed to play a role in causing the monomerization of PSII during the PSII repair cycle[78]. Large scale differential changes in global abundance across the PSII repair cycle pathway suggests an overall

increase in damaged PSII in the *vip1-1* mutant. The decrease in phosphorylation on PsbO may therefore indicate an abandonment of the PSII repair pathways, as the photosynthetic apparatus irreversibly shifts to CET. A permanent shift to state 2 conditions following rapamycin treatment could be a contributing factor to the rapamycin hypersensitivity observed in the *vip1-1* mutant.

4.3.5 Phosphorylation of InsP Signaling-Related Proteins

Myo-inositol derivatives perform a variety of essential functions in eukaryotic cells and are present in both water-soluble InsPs as well as water-insoluble phosphatidylinositols (PIPs)[79]. Whereas InsPs are primarily responsible for signaling activity, PIPs and InsPs are inherently linked; signal-activated phospholipase C (PLC) hydrolyzes PIP to generate $InsP_6$ through inositol dual specificity polyphosphate multi-kinases[80]. Additionally, PIP can be converted to PIP_2, which uses PLC to release $InsP_3$ and diacylglycerol, the latter of which is phosphorylated via diacylglycerol kinase to generate phosphatidic acid[81]. The released $InsP_3$ can be further phosphorylated to generate $InsP_6$, which activates a secondary Ca^{2+} signaling cascade and is later phosphorylated to generate $InsP_7$ and $InsP_8$[82]. Hence it is not surprising that the *vip1-1* mutant produced a varied pattern of phosphorylation, both before and after rapamycin treatment, compared to the parent strain.

Before rapamycin treatment, *vip1-1* produced significantly different phosphorylation across 39 identifiers from 23 unique proteins (Table S4.5). Of these 39 identifiers, seven were increasing in phosphorylation including S1079 of calcium/calmodulin dependent kinase kinase (CDPKK2, Cre17.g705350.t1.1, FC: 6.6), and S255-S264 of phosphorus starvation response 1 protein (PSR1, Cre12.g495100.t1.2, FC: 6.0). Both CPDKK2 and PSR1 regulate components of the TOR pathway. CDPKK2 is proposed to relate to nutritional sensing where it is activated via phosphorylation following a depletion in energy reserves[83]. Following nitrogen deprivation,

S1210 increased in phosphorylation by 1.9-fold, which deactivated the protein phosphatase 2A (PP2A) network, activated the AMP kinase signaling network, and led to the downregulation of TOR. Although our study did not identify phosphorylation on S1210, the increase in phosphorylation on S1079 may relate to the hypersensitivity of the *vip1-1* mutant to rapamycin treatment. Similar to CDPKK2, PSR1 operates upstream of TOR, downregulating LST8 and subsequently downregulating TOR activity following phosphorus starvation[23]. This is the first known study to identify phosphorylation on PSR1. However, the phosphorylation of PSR1 may relate to downregulation of TOR via LST8; the loss of InsPs in the *vip1-1* mutant likely decrease the availability of inorganic phosphate in the cell, thus resulting in a pseudo-starvation response, supported through the increase in TAGs observed in *vip1-1*[26].

The remaining 40 identifiers with significant differences in phosphorylation are all decreased in phosphorylation that the parent strain, with fold changes ranging from 0.0067 – 0.38. The largest decrease in phosphorylation was observed on S803 of the phosphoprotein phosphatase 2C-like protein (PP2C, Cre07.g334750.t1.1, FC: 0.0067). In mammalian cells, secondary messengers of insulin activate PP2C in order to inactivate GSK3 and AMPK, thus implicating PP2C in nutritional sensing upstream of mTOR[84]. Although PP2C has not been well characterized in *C. reinhardtii*, it has previously been shown to increase in phosphorylation following both rapamycin and AZD8055 treatment, indicating that it is likely related to nutritional sensing and the TOR pathway in algae as well[19].

Upstream of PP2C, there was a 0.19 FC decrease on T231 of phosphoinositide-specific phospholipase C family protein (PI-PLC, Cre06.g270200.t1.1) in *vip1-1* compared to the parent strain. Plant PI-PLC is involved in signaling transduction for guard cell signaling, biotic and abiotic stress response, systemic acquired resistance, and carbon fixation, but little is known

about the role of phosphorylation in regulating these activities in plants specifically[85]. In mammalian cells, PI-PLC is a known target of phosphorylation by c-AMP dependent protein kinases (PKA) and protein kinase C at multiple sites that impact the enzyme's activity, with phosphorylation by PKA inhibiting the activity of the enzyme while phosphorylation from protein kinase C does not seem to impact PI-PLC activity directly[86]. Protein kinase C does not have a known homolog in phototrophs[80]. However, PI-PLC enzymatically generates $InsP_3$, which can undergo a string of phosphorylations to form the high-energy $InsP_7$ and $InsP_8$, both of which are significantly downregulated in the *vip1-1* mutant compared to the parent strain[26]. Therefore, the decrease in phosphorylation may result in decreased catalysis and subsequent $InsP_3$ in *C. reinhardtii*.

Phosphoprotein phosphatase 2A also contained differential basal phosphorylation in the *vip1-1* mutant compared to the parent strain, demonstrating addition overlap between the TOR pathway and InsP signaling. There was significantly less phosphorylation on three PP2A identifiers in the *vip1-1* mutant including two from the regulatory subunit PR55 (Cre01.g055420.t1.1; S168, FC: 0.21; S159, FC: 0.27) and one from the PP2A regulatory subunit related (Cre06.g260600.t1.2, S108, FC: 0.28). There is a well-defined relationship between TOR signaling and autophagy[13]; PP2A is associated through the dephosphorylation of ATG13, allowing for the formation of the ATG1 complex which initiates autophagy[87,88]. PP2A is a holoenzyme composed of three subunits: a scaffolding subunit (A), catalytic subunit (C), and regulatory subunit (B). Depending on the organism, there can be many types/families of the B type regulatory subunit, which contributes to its specificity[89]. Genomic analysis of *C. reinhardtii* revealed four catalytic subunits, two scaffold units, and five regulatory units of PP2A based on sequence similarity[89]. The catalytic subunit of PP2A is known to be regulated via post-

translational modifications, including phosphorylation of a conserved C-terminal tyrosine that diminishes PP2A activity[90]. However, this is the first evidence that there may also be phosphorylation events on regulatory subunits that could be involved in the activation of autophagy.

Interestingly, rapamycin treatment only significantly changed the phosphorylation of five identifiers from four proteins in the parent strain, none of which significantly changed in the *vip1-1* mutant. However, 25 unique identifiers significantly changed in the *vip1-1* mutant, with four decreasing and 21 increasing. While the loss of VIP1 clearly causes a stressed state in *C. reinhardtii* in addition to an altered pattern of phosphorylation, rapamycin treatment seems to equilibrate the two strains toward a similar state. This is illustrated by S1020 on phosphatidylinositol 4-kinase (PI4K, Cre05.g245550.t1.1), which significantly increased with rapamycin treatment in *vip1-1* by a fold change of 4.08. Additionally, while the protein abundance of PI4K did not significantly change following rapamycin treatment, it was significantly less abundant in the *vip1-1* mutant compared to the parent strain without rapamycin treatment, with a FC of 0.059. As the phosphopeptide abundance is not normalized to the global, the reported increase in phosphorylation is therefore a severe underestimation of the increase in phosphorylation compared to the parent strain. PI4K synthesizes phosphatidylinositol 4-phosphate, an important membrane-bound component of the InsP signaling pathway, which is further phosphorylated to form PIP_2. PIP_2 is hydrolyzed to generate diacylglycerol and $InsP_3$, a precursor to VIP1 target $InsP_6$[91]. Previous work has shown numerous phosphorylation sites on human PI4K, which may weakly impact its activity. However the exact mechanism through which this regulation occurs is not known, and the site identified here is not conserved in the sites identified on mammalian PI4K[92]. Interestingly, this site did not change in the parent strain

following rapamycin treatment. Additionally, comparing the abundance after rapamycin treatment in the *vip1-1* mutant with the parent strain shows that the phosphorylation is not significantly different. This suggests that the *vip1-1* mutant, while under stress before the treatment, reorients to a phosphorylation state similar to that of the parent strain.

4.4 Conclusions

The link between InsP signaling and the TOR pathway has only been recently established. Through the phosphoproteomic characterization of *vip1-1*, it is clear that InsPs are necessary to maintain basal metabolic networks. Differential phosphorylation sites were identified in the TOR pathway that were unique to *vip1-1* with rapamycin treatment, suggesting that VIP1 and InsP signaling is necessary for the regulation of the TOR pathway following inhibition. This work also supports a link between TOR, InsP and autophagy regulation, with several novel regulatory phosphosites identified on critical components of autophagy activation. While more work is still needed to characterize the exact mechanisms by which these phosphorylation events are regulated, this data set provides a preliminary examination into the interplay between InsPs, specifically $InsP_7$ and $InsP_8$ and TOR, providing a list of potential targets for additional validation and mechanistic studies.

4.5 Figures

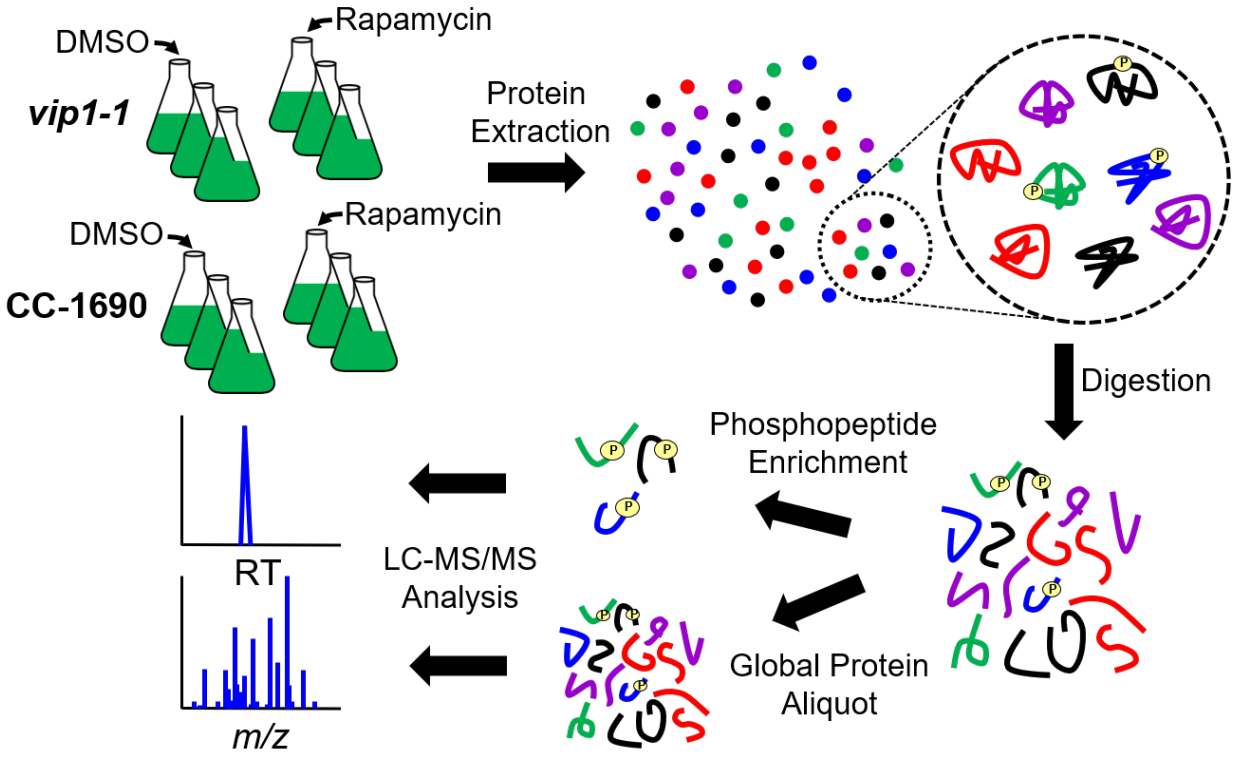

Figure 4.1 Proteomic workflow for analysis of *vip1-1* and wild-type CC-1690 mt+ *C. reinhardtii* cells treated with rapamycin and DMSO (control) for 15 min. After treatment, proteins were extracted and digested with trypsin. A 25 µg global protein aliquot was taken of each sample while 1 mg was enriched for phosphopeptides before all samples were analyzed via LC-MS/MS.

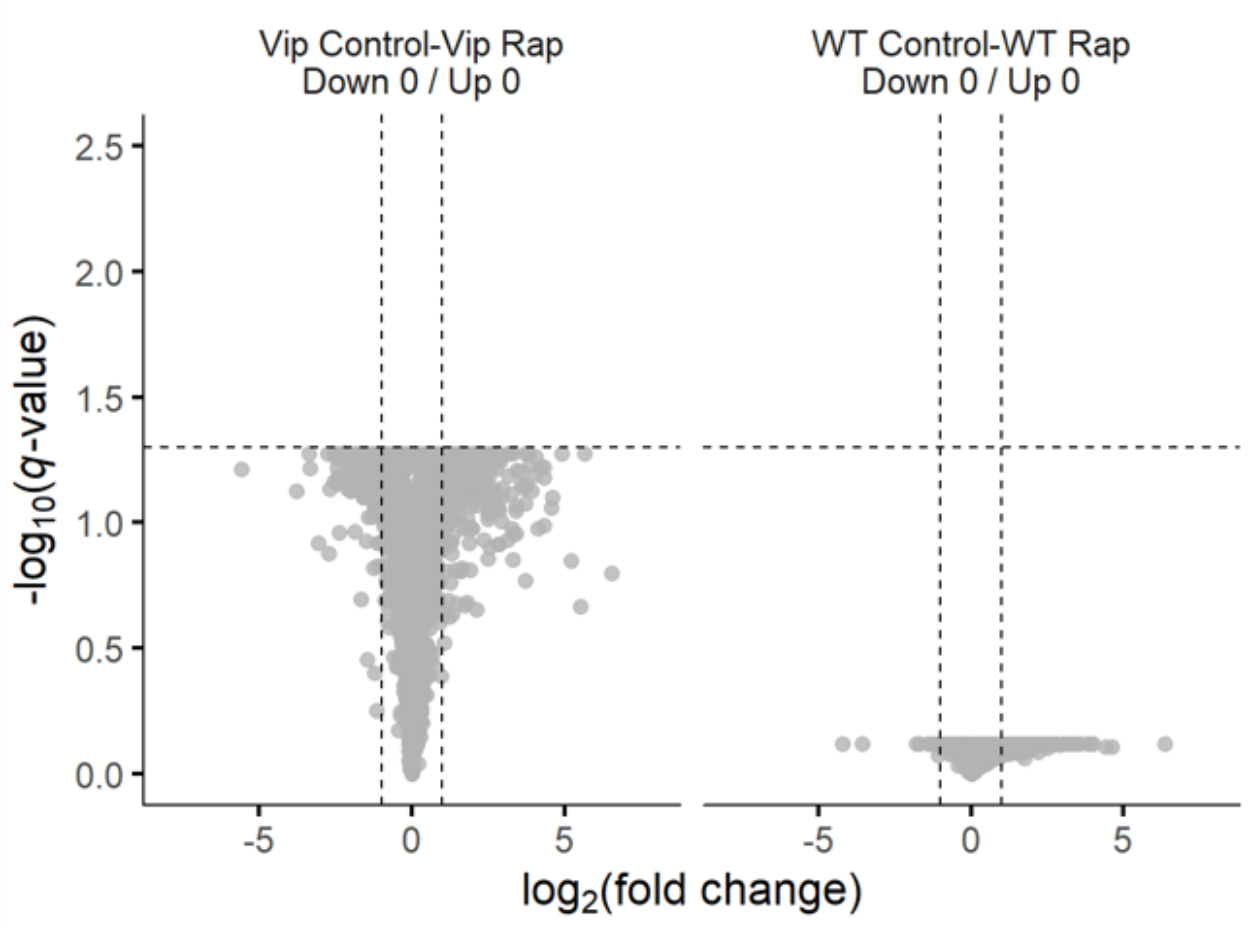

Figure 4.2 Global proteomic results. Volcano plot of two-tailed equal variance *t*-tests between each strain with and without rapamycin (Rap.) treatment with a Benjamani-Hochberg FDR adjustment.

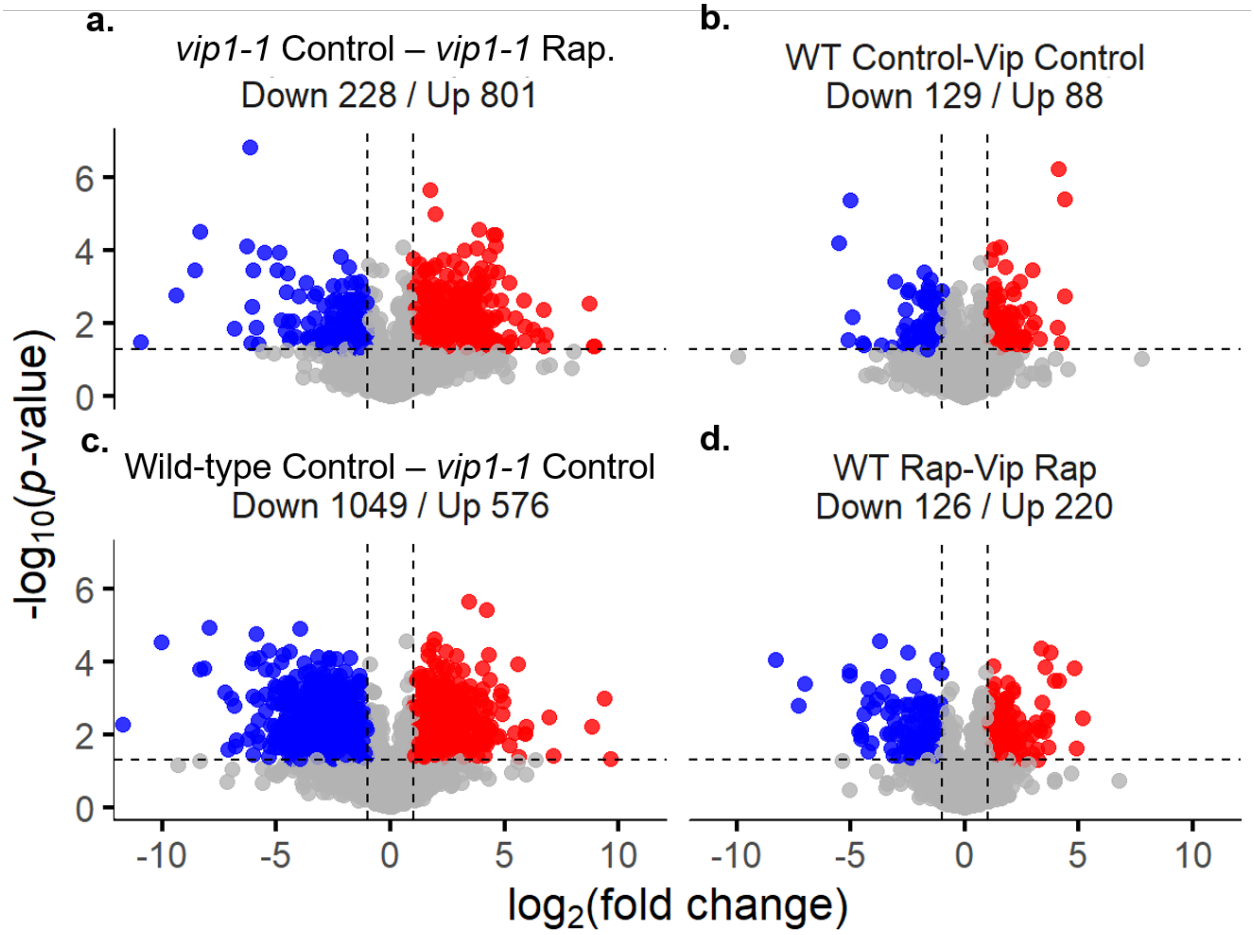

Figure 4.3 Phosphoproteomic results. Volcano plots of two-tailed equal variance *t*-tests between each strain with and without rapamycin (Rap.) treatment (a. and b.) and between strains (c. and d.).

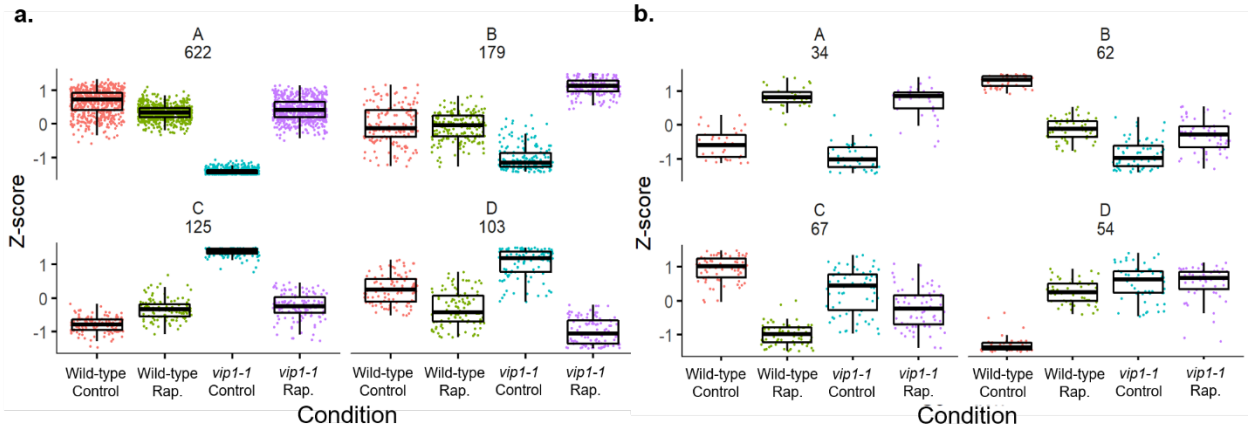

Figure 4.4 Hierarchical clustering of the identifiers significantly changing ($p < 0.05$, FC > ±2) in: a.) *vip1-1* and b.) wild-type.

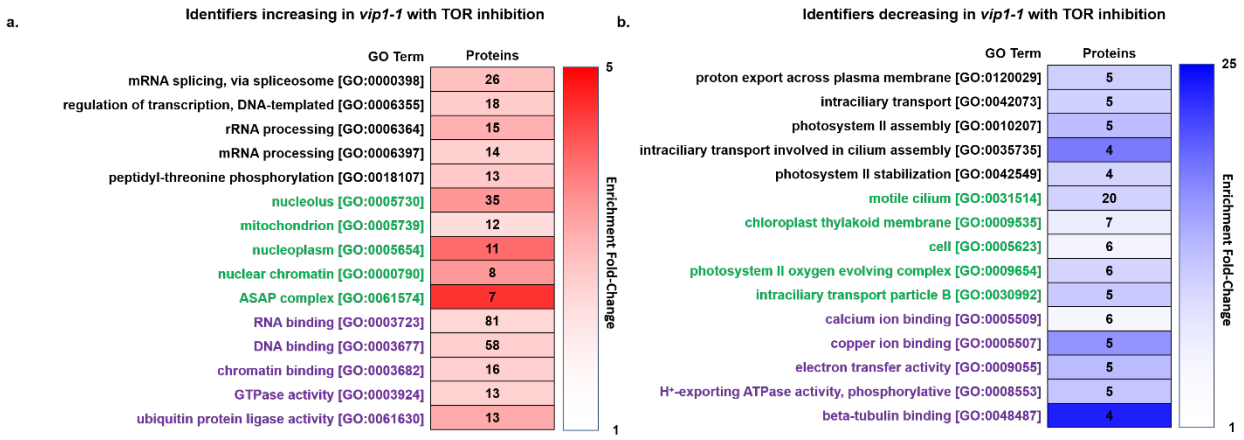

Figure 4.5 *vip1-1* Phosphoproteomic Gene Ontology (GO) Analysis. a.) Count of the number of proteins in the top 5 biological process (black), cellular component (green) and molecular function (purple) GO terms with a fold-change enrichment of at least 1.5 from identifiers significantly more abundant in *vip1-1* with rapamycin treatment. Cells are shaded to reflect fold-change for each GO term. b.) Count of the number of proteins in the top 5 biological process (black), cellular component (green) and molecular function (purple) GO terms with a fold-change enrichment of at least 1.5 from identifiers significantly less abundant in *vip1-1* with rapamycin treatment. Cells are shaded to reflect fold-change for each GO term.

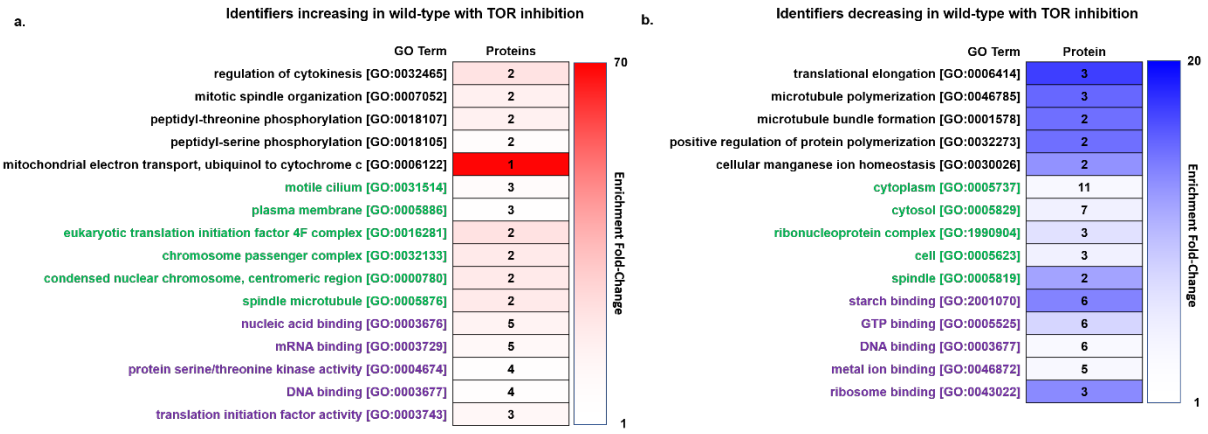

Figure 4.6 Wild-type Phosphoproteomic Gene Ontology (GO) Analysis. a.) Count of the number of proteins in the top 5 biological process (black), cellular component (green) and molecular function (purple) GO terms with a fold-change enrichment of at least 1.5 from identifiers significantly more abundant in the wild-type strain with rapamycin treatment. Cells are shaded to reflect fold-change for each GO term. b.) Count of the number of proteins in the top 5 biological process (black), cellular component (green) and molecular function (purple) GO terms with a fold-change enrichment of at least 1.5 from identifiers significantly less abundant in the wild-type strain with rapamycin treatment. Cells are shaded to reflect fold-change for each GO term.

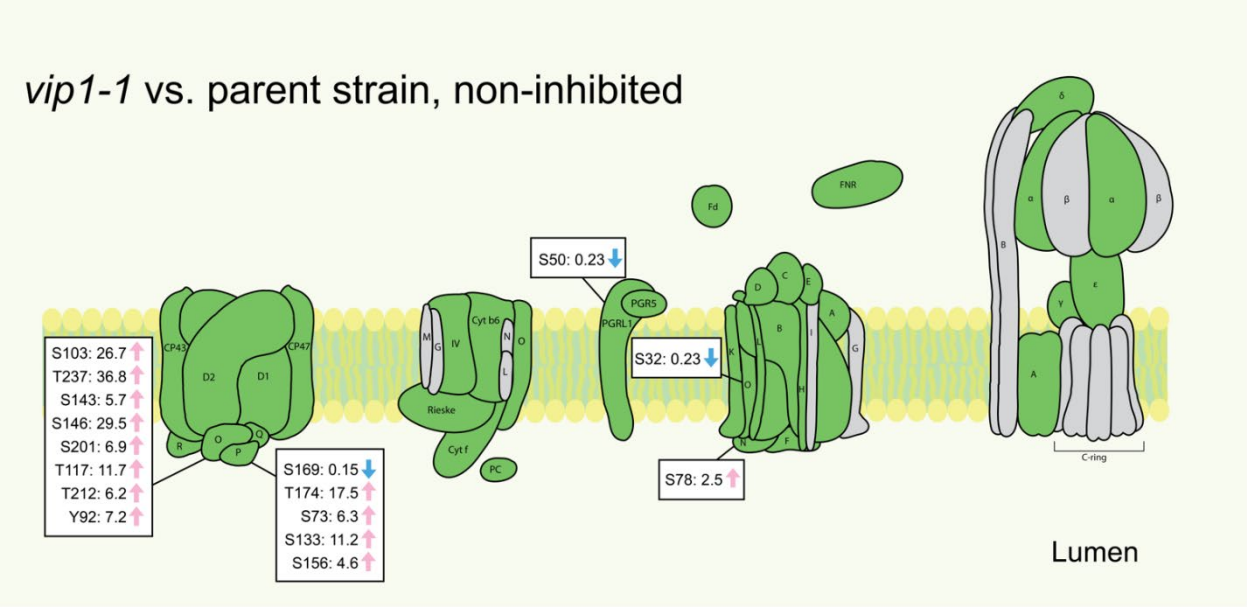

Figure 4.7 The differential phosphorylation of the photosynthetic apparatus in the *vip1-1* mutant compared to the parent strain. Proteins colored green show proteomic coverage in the dataset while proteins colored grey do not. Each significantly changing phosphosite was localized on a unique phosphopeptide. Non-transformed fold changes are reported.

REFERENCES

1. Lorenzo-Orts, L.; Couto, D.; Hothorn, M. Identity and Functions of Inorganic and Inositol Polyphosphates in Plants. *New Phytol.* **2020**, *225* (2), 637–652.

2. Azevedo, C.; Saiardi, A. Eukaryotic Phosphate Homeostasis: The Inositol Pyrophosphate Perspective. *Trends in Biochem. Sci.* **2017**, *42* (3), 219–231.

3. Jia, Q.; Kong, D.; Li, Q.; Sun, S.; Song, J.; Zhu, Y.; Liang, K.; Ke, Q.; Lin, W.; Huang, J. The Function of Inositol Phosphatases in Plant Tolerance to Abiotic Stress. *Int. J. Mol. Sci.* **2019**, *20* (16).

4. Wild, R.; Gerasimaite, R.; Jung, J.-Y.; Truffault, V.; Pavlovic, I.; Schmidt, A.; Saiardi, A.; Jessen, H. J.; Poirier, Y.; Hothorn, M.; Mayer, A. Control of Eukaryotic Phosphate Homeostasis by Inositol Polyphosphate Sensor Domains. *Science* **2016**, *352* (6288), 986–990.

5. Desai, M.; Rangarajan, P.; Donahue, J. L.; Williams, S. P.; Land, E. S.; Mandal, M. K.; Phillippy, B. Q.; Perera, I. Y.; Raboy, V.; Gillaspy, G. E. Two Inositol Hexakisphosphate Kinases Drive Inositol Pyrophosphate Synthesis in Plants. *Plant J.* **2014**, *80* (4), 642–653.

6. Laha, D.; Johnen, P.; Azevedo, C.; Dynowski, M.; Weiß, M.; Capolicchio, S.; Mao, H.; Iven, T.; Steenbergen, M.; Freyer, M.; Gaugler, P.; Campos, M. K. F. de; Zheng, N.; Feussner, I.; Jessen, H. J.; Wees, S. C. M. V.; Saiardi, A.; Schaaf, G. VIH2 Regulates the Synthesis of Inositol Pyrophosphate InsP8 and Jasmonate-Dependent Defenses in Arabidopsis. *Plant Cell* **2015**, *27* (4), 1082–1097.

7. Zhang, W.; Gruszewski, H. A.; Chevone, B. I.; Nessler, C. L. An Arabidopsis Purple Acid Phosphatase with Phytase Activity Increases Foliar Ascorbate. *Plant Physiol.* **2008**, *146* (2), 431–440.

8. Gillaspy, G. E. The Role of Phosphoinositides and Inositol Phosphates in Plant Cell Signaling. *Adv. Exp. Med. Biol.* **2013**, *991*, 141–157.

9. Stephens, L.; Radenberg, T.; Thiel, U.; Vogel, G.; Khoo, K. H.; Dell, A.; Jackson, T. R.; Hawkins, P. T.; Mayr, G. W. The Detection, Purification, Structural Characterization, and Metabolism of Diphosphoinositol Pentakisphosphate(s) and Bisdiphosphoinositol Tetrakisphosphate(s). *J. Biol. Chem.* **1993**, *268* (6), 4009–4015.

10. Glennon, M. C.; Shears, S. B. Turnover of Inositol Pentakisphosphates, Inositol Hexakisphosphate and Diphosphoinositol Polyphosphates in Primary Cultured Hepatocytes. *Biochem. J.* **1993**, *293 (Pt 2)*, 583–590.

11. Menniti, F. S.; Miller, R. N.; Putney, J. W.; Shears, S. B. Turnover of Inositol Polyphosphate Pyrophosphates in Pancreatoma Cells. *J. Biol. Chem.* **1993**, *268* (6), 3850–3856.

12. Díaz-Troya, S.; Pérez-Pérez, M. E.; Pérez-Martín, M.; Moes, S.; Jeno, P.; Florencio, F. J.; Crespo, J. L. Inhibition of Protein Synthesis by TOR Inactivation Revealed a Conserved Regulatory Mechanism of the BiP Chaperone in Chlamydomonas. *Plant Physiol.* **2011**, *157* (2), 730–741.

13. Pérez-Pérez, M. E.; Couso, I.; Crespo, J. L. The TOR Signaling Network in the Model Unicellular Green Alga Chlamydomonas Reinhardtii. *Biomolecules* **2017**, *7* (3).

14. Mubeen, U.; Giavalisco, P.; Caldana, C. TOR Inhibition Interrupts the Metabolic Homeostasis by Shifting the Carbon–Nitrogen Balance in Chlamydomonas reinhardtii. *Plant Signal. Behav.* **2019**, *14* (11), 1670595.

15. Crespo, J. L.; Díaz-Troya, S.; Florencio, F. J. Inhibition of Target of Rapamycin Signaling by Rapamycin in the Unicellular Green Alga Chlamydomonas Reinhardtii. *Plant Physiol.* **2005**, *139* (4), 1736–1749.

16. Pérez-Pérez, M. E.; Florencio, F. J.; Crespo, J. L. Inhibition of Target of Rapamycin Signaling and Stress Activate Autophagy in Chlamydomonas Reinhardtii. *Plant Physiol.* **2010**, *152* (4), 1874–1888.

17. P. Rodrigues, S.; Alvarez, S.; G. Werth, E.; O. Slade, W.; Gau, B.; B. Cahoon, E.; M. Hicks, L. Multiplexing Strategy for Simultaneous Detection of Redox-, Phospho- and Total Proteome – Understanding TOR Regulating Pathways in Chlamydomonas Reinhardtii. *Anal. Methods* **2015**, *7* (17), 7336–7344.

18. Roustan, V.; Weckwerth, W. Quantitative Phosphoproteomic and System-Level Analysis of TOR Inhibition Unravel Distinct Organellar Acclimation in Chlamydomonas Reinhardtii. *Front. Plant Sci.* **2018**, *9*, 1590.

19. Werth, E. G.; McConnell, E. W.; Lianez, I. C.; Perrine, Z.; Crespo, J. L.; Umen, J. G.; Hicks, L. M. Investigating the Effect of Target of Rapamycin Kinase Inhibition on the Chlamydomonas Reinhardtii Phosphoproteome: From Known Homologs to New Targets. *New Phytol.* **2019**, *221* (1), 247–260.

20. Ford, M. M.; Smythers, A. L.; McConnell, E. W.; Lowery, S. C.; Kolling, D. R. J.; Hicks, L. M. Inhibition of TOR in Chlamydomonas Reinhardtii Leads to Rapid Cysteine Oxidation Reflecting Sustained Physiological Changes. *Cells* **2019**, *8* (10), 1171.

21. van Dam, T. J. P.; Zwartkruis, F. J. T.; Bos, J. L.; Snel, B. Evolution of the TOR Pathway. *J. Mol. Evol.* **2011**, *73* (3–4), 209–220.

22. Díaz-Troya, S.; Florencio, F. J.; Crespo, J. L. Target of Rapamycin and LST8 Proteins Associate with Membranes from the Endoplasmic Reticulum in the Unicellular Green Alga Chlamydomonas reinhardtii. *Eukaryot. Cell* **2008**, *7* (2), 212–222.

23. Couso, I.; Pérez-Pérez, M. E.; Ford, M. M.; Martínez-Force, E.; Hicks, L. M.; Umen, J. G.; Crespo, J. L. Phosphorus Availability Regulates TORC1 Signaling via LST8 in Chlamydomonas. *Plant Cell* **2020**, *32* (1), 69–80.

24. Lee, Y.-S.; Mulugu, S.; York, J. D.; O'Shea, E. K. Regulation of a Cyclin-CDK-CDK Inhibitor Complex by Inositol Pyrophosphates. *Science* **2007**, *316* (5821), 109–112.

25. Lonetti, A.; Szijgyarto, Z.; Bosch, D.; Loss, O.; Azevedo, C.; Saiardi, A. Identification of an Evolutionarily Conserved Family of Inorganic Polyphosphate Endopolyphosphatases. *J. Biol. Chem.* **2011**, *286* (37), 31966–31974.

26. Couso, I.; Evans, B. S.; Li, J.; Liu, Y.; Ma, F.; Diamond, S.; Allen, D. K.; Umen, J. G. Synergism between Inositol Polyphosphates and TOR Kinase Signaling in Nutrient Sensing, Growth Control, and Lipid Metabolism in Chlamydomonas. *Plant Cell* **2016**, *28* (9), 2026–2042.

27. Galván, A.; González-Ballester, D.; Fernández, E. Insertional Mutagenesis as a Tool to Study Genes/Functions in Chlamydomonas. *Adv. Exp. Med. Biol.* **2007**, *616*, 77–89.

28. Berthold, P.; Schmitt, R.; Mages, W. An Engineered Streptomyces Hygroscopicus Aph 7" Gene Mediates Dominant Resistance against Hygromycin B in Chlamydomonas Reinhardtii. *Protist* **2002**, *153* (4), 401–412.

29. Shimogawara, K.; Fujiwara, S.; Grossman, A.; Usuda, H. High-Efficiency Transformation of Chlamydomonas Reinhardtii by Electroporation. *Genetics* **1998**, *148* (4), 1821–1828.

30. Werth, E. G.; McConnell, E. W.; Gilbert, T. S. K.; Couso Lianez, I.; Perez, C. A.; Manley, C. K.; Graves, L. M.; Umen, J. G.; Hicks, L. M. Probing the Global Kinome and Phosphoproteome in Chlamydomonas reinhardtii via Sequential Enrichment and Quantitative Proteomics. *Plant J* **2017**, *89* (2), 416–426.

31. Vizcaíno, J. A.; Deutsch, E. W.; Wang, R.; Csordas, A.; Reisinger, F.; Ríos, D.; Dianes, J. A.; Sun, Z.; Farrah, T.; Bandeira, N.; Binz, P.-A.; Xenarios, I.; Eisenacher, M.; Mayer, G.; Gatto, L.; Campos, A.; Chalkley, R. J.; Kraus, H.-J.; Albar, J. P.; Martinez-Bartolomé, S.; Apweiler, R.; Omenn, G. S.; Martens, L.; Jones, A. R.; Hermjakob, H. ProteomeXchange Provides Globally Coordinated Proteomics Data Submission and Dissemination. *Nat. Biotechnol.* **2014**, *32* (3), 223–226.

32. Käll, L.; Canterbury, J. D.; Weston, J.; Noble, W. S.; MacCoss, M. J. Semi-Supervised Learning for Peptide Identification from Shotgun Proteomics Datasets. *Nat. Methods* **2007**, *4* (11), 923–925.

33. Gianetto, Q. G. *Imp4p: Imputation for Proteomics*; 2018.

34. Benjamini, Y.; Hochberg, Y. Controlling the False Discovery Rate: A Practical and Powerful Approach to Multiple Testing. *J. R. Stat. Soc. Series B (Methodological)* **1995**, *57* (1), 289–300.

35. Altschul, S. F.; Gish, W.; Miller, W.; Myers, E. W.; Lipman, D. J. Basic Local Alignment Search Tool. *J. Mol. Biol.* **1990**, *215* (3), 403–410.

36. Demirkan, G.; Yu, K.; Boylan, J. M.; Salomon, A. R.; Gruppuso, P. A. Phosphoproteomic Profiling of In Vivo Signaling in Liver by the Mammalian Target of Rapamycin Complex 1 (MTORC1). *PLOS ONE* **2011**, *6* (6), e21729.

37. Harder, L. M.; Bunkenborg, J.; Andersen, J. S. Inducing Autophagy: A Comparative Phosphoproteomic Study of the Cellular Response to Ammonia and Rapamycin. *Autophagy* **2014**, *10* (2), 339–355.

38. Rigbolt, K. T.; Zarei, M.; Sprenger, A.; Becker, A. C.; Diedrich, B.; Huang, X.; Eiselein, S.; Kristensen, A. R.; Gretzmeier, C.; Andersen, J. S.; Zi, Z.; Dengjel, J. Characterization of Early Autophagy Signaling by Quantitative Phosphoproteomics. *Autophagy* **2014**, *10* (2), 356–371.

39. Wang, H.; Gau, B.; Slade, W. O.; Juergens, M.; Li, P.; Hicks, L. M. The Global Phosphoproteome of Chlamydomonas Reinhardtii Reveals Complex Organellar Phosphorylation in the Flagella and Thylakoid Membrane. *Mol. Cell Proteomics* **2014**, *13* (9), 2337–2353.

40. Ekim, B.; Magnuson, B.; Acosta-Jaquez, H. A.; Keller, J. A.; Feener, E. P.; Fingar, D. C. MTOR Kinase Domain Phosphorylation Promotes MTORC1 Signaling, Cell Growth, and Cell Cycle Progression. *Mol. Cell. Biol.* **2011**, *31* (14), 2787–2801.

41. Van Leene, J.; Han, C.; Gadeyne, A.; Eeckhout, D.; Matthijs, C.; Cannoot, B.; De Winne, N.; Persiau, G.; Van De Slijke, E.; Van de Cotte, B.; Stes, E.; Van Bel, M.; Storme, V.; Impens, F.; Gevaert, K.; Vandepoele, K.; De Smet, I.; De Jaeger, G. Capturing the Phosphorylation and Protein Interaction Landscape of the Plant TOR Kinase. *Nat. Plants* **2019**, *5* (3), 316–327.

42. Deragon, J.-M.; Bousquet-Antonelli, C. The Role of LARP1 in Translation and Beyond. *WIREs RNA* **2015**, *6* (4), 399–417.

43. Hsu, P. P.; Kang, S. A.; Rameseder, J.; Zhang, Y.; Ottina, K. A.; Lim, D.; Peterson, T. R.; Choi, Y.; Gray, N. S.; Yaffe, M. B.; Marto, J. A.; Sabatini, D. M. The MTOR-Regulated Phosphoproteome Reveals a Mechanism of MTORC1-Mediated Inhibition of Growth Factor Signaling. *Science* **2011**, *332* (6035), 1317–1322.

44. Yu, Y.; Yoon, S.-O.; Poulogiannis, G.; Yang, Q.; Ma, X. M.; Villén, J.; Kubica, N.; Hoffman, G. R.; Cantley, L. C.; Gygi, S. P.; Blenis, J. Phosphoproteomic Analysis Identifies Grb10 as an MTORC1 Substrate That Negatively Regulates Insulin Signaling. *Science* **2011**, *332* (6035), 1322–1326.

45. Kang, S. A.; Pacold, M. E.; Cervantes, C. L.; Lim, D.; Lou, H. J.; Ottina, K.; Gray, N. S.; Turk, B. E.; Yaffe, M. B.; Sabatini, D. M. MTORC1 Phosphorylation Sites Encode Their Sensitivity to Starvation and Rapamycin. *Science* **2013**, *341* (6144).

46. Hong, S.; Freeberg, M. A.; Han, T.; Kamath, A.; Yao, Y.; Fukuda, T.; Suzuki, T.; Kim, J. K.; Inoki, K. LARP1 Functions as a Molecular Switch for MTORC1-Mediated Translation of an Essential Class of MRNAs. *Elife* **2017**, *6*.

47. Fonseca, B. D.; Zakaria, C.; Jia, J.-J.; Graber, T. E.; Svitkin, Y.; Tahmasebi, S.; Healy, D.; Hoang, H.-D.; Jensen, J. M.; Diao, I. T.; Lussier, A.; Dajadian, C.; Padmanabhan, N.; Wang, W.; Matta-Camacho, E.; Hearnden, J.; Smith, E. M.; Tsukumo, Y.; Yanagiya, A.; Morita, M.; Petroulakis, E.; González, J. L.; Hernández, G.; Alain, T.; Damgaard, C. K. La-Related Protein 1 (LARP1) Represses Terminal Oligopyrimidine (TOP) MRNA Translation Downstream of MTOR Complex 1 (MTORC1). *J. Biol. Chem.* **2015**, *290* (26), 15996–16020.

48. Kim, S.; Kim, S. F.; Maag, D.; Maxwell, M. J.; Resnick, A. C.; Juluri, K. R.; Chakraborty, A.; Koldobskiy, M. A.; Cha, S. H.; Barrow, R.; Snowman, A. M.; Snyder, S. H. Amino Acid Signaling to MTOR Mediated by Inositol Polyphosphate Multikinase. *Cell Metab.* **2011**, *13* (2), 215–221.

49. Gwinn, D. M.; Shackelford, D. B.; Egan, D. F.; Mihaylova, M. M.; Mery, A.; Vasquez, D. S.; Turk, B. E.; Shaw, R. J. AMPK Phosphorylation of Raptor Mediates a Metabolic Checkpoint. *Mol. Cell* **2008**, *30* (2), 214–226.

50. Stretton, C.; Hoffmann, T. M.; Munson, M. J.; Prescott, A.; Taylor, P. M.; Ganley, I. G.; Hundal, H. S. GSK3-Mediated Raptor Phosphorylation Supports Amino-Acid-Dependent MTORC1-Directed Signalling. *Biochem. J.* **2015**, *470* (Pt 2), 207–221.

51. Yuan, H.-X.; Wang, Z.; Yu, F.-X.; Li, F.; Russell, R. C.; Jewell, J. L.; Guan, K.-L. NLK Phosphorylates Raptor to Mediate Stress-Induced MTORC1 Inhibition. *Genes Dev.* **2015**, *29* (22), 2362–2376.

52. Bang, S.; Kim, S.; Dailey, M. J.; Chen, Y.; Moran, T. H.; Snyder, S. H.; Kim, S. F. AMP-Activated Protein Kinase Is Physiologically Regulated by Inositol Polyphosphate Multikinase. *Proc. Natl. Acad. Sci. U.S.A.* **2012**, *109* (2), 616–620.

53. Bhat, R. V.; Shanley, J.; Correll, M. P.; Fieles, W. E.; Keith, R. A.; Scott, C. W.; Lee, C. M. Regulation and Localization of Tyrosine216 Phosphorylation of Glycogen Synthase Kinase-3beta in Cellular and Animal Models of Neuronal Degeneration. *Proc. Natl. Acad. Sci. U.S.A.* **2000**, *97* (20), 11074–11079.

54. Hughes, K.; Nikolakaki, E.; Plyte, S. E.; Totty, N. F.; Woodgett, J. R. Modulation of the Glycogen Synthase Kinase-3 Family by Tyrosine Phosphorylation. *EMBO J.* **1993**, *12* (2), 803–808.

55. Liu, H.; Remedi, M. S.; Pappan, K. L.; Kwon, G.; Rohatgi, N.; Marshall, C. A.; McDaniel, M. L. Glycogen Synthase Kinase-3 and Mammalian Target of Rapamycin Pathways Contribute to DNA Synthesis, Cell Cycle Progression, and Proliferation in Human Islets. *Diabetes* **2009**, *58* (3), 663–672.

56. Kamada, Y.; Funakoshi, T.; Shintani, T.; Nagano, K.; Ohsumi, M.; Ohsumi, Y. Tor-Mediated Induction of Autophagy via an Apg1 Protein Kinase Complex. *J. Cell Biol.* **2000**, *150* (6), 1507–1513.

57. Alers, S.; Löffler, A. S.; Wesselborg, S.; Stork, B. Role of AMPK-MTOR-Ulk1/2 in the Regulation of Autophagy: Cross Talk, Shortcuts, and Feedbacks. *Mol. Cell Biol.* **2012**, *32* (1), 2–11.

58. Cheong, H.; Yorimitsu, T.; Reggiori, F.; Legakis, J. E.; Wang, C.-W.; Klionsky, D. J. Atg17 Regulates the Magnitude of the Autophagic Response. *Mol. Biol. Cell* **2005**, *16* (7), 3438–3453.

59. Pérez-Pérez, M. E.; Couso, I.; Heredia-Martínez, L. G.; Crespo, J. L. Monitoring Autophagy in the Model Green Microalga Chlamydomonas Reinhardtii. *Cells* **2017**, *6* (4).

60. Allen, J. F. How Does Protein Phosphorylation Regulate Photosynthesis? *Trends Biochem. Sci.* **1992**, *17* (1), 12–17.

61. Rochaix, J.-D.; Lemeille, S.; Shapiguzov, A.; Samol, I.; Fucile, G.; Willig, A.; Goldschmidt-Clermont, M. Protein Kinases and Phosphatases Involved in the Acclimation of the Photosynthetic Apparatus to a Changing Light Environment. *Philos. Trans. R. Soc. Lond. B Biol. Sci.* **2012**, *367* (1608), 3466–3474.

62. Baginsky, S. Protein Phosphorylation in Chloroplasts – a Survey of Phosphorylation Targets. *J. Exp. Bot.* **2016**, *67* (13), 3873–3882.

63. Rantala, M.; Rantala, S.; Aro, E.-M. Composition, Phosphorylation and Dynamic Organization of Photosynthetic Protein Complexes in Plant Thylakoid Membrane. *Photochem. Photobiol. Sci.* **2020**, *19* (5), 604–619.

64. Pagliano, C.; Saracco, G.; Barber, J. Structural, Functional and Auxiliary Proteins of Photosystem II. *Photosynth. Res.* **2013**, *116* (2), 167–188.

65. Kukuczka, B.; Magneschi, L.; Petroutsos, D.; Steinbeck, J.; Bald, T.; Powikrowska, M.; Fufezan, C.; Finazzi, G.; Hippler, M. PGRL1-Mediated Cyclic Electron Flow Is Crucial for Acclimation to Anoxia and Complementary to Non-Photochemical Quenching in Stress Adaptation. *Plant Physiol.* **2014**.

66. Iwai, M.; Takizawa, K.; Tokutsu, R.; Okamuro, A.; Takahashi, Y.; Minagawa, J. Isolation of the Elusive Supercomplex That Drives Cyclic Electron Flow in Photosynthesis. *Nature* **2010**, *464* (7292), 1210–1213.

67. Bergner, S. V.; Scholz, M.; Trompelt, K.; Barth, J.; Gäbelein, P.; Steinbeck, J.; Xue, H.; Clowez, S.; Fucile, G.; Goldschmidt-Clermont, M.; Fufezan, C.; Hippler, M. STATE TRANSITION7-Dependent Phosphorylation Is Modulated by Changing Environmental Conditions, and Its Absence Triggers Remodeling of Photosynthetic Protein Complexes. *Plant Physiol.* **2015**, *168* (2), 615–634.

68. Reiland, S.; Finazzi, G.; Endler, A.; Willig, A.; Baerenfaller, K.; Grossmann, J.; Gerrits, B.; Rutishauser, D.; Gruissem, W.; Rochaix, J.-D.; Baginsky, S. Comparative Phosphoproteome Profiling Reveals a Function of the STN8 Kinase in Fine-Tuning of Cyclic Electron Flow (CEF). *Proc. Natl. Acad. Sci. U.S.A.* **2011**, *108* (31), 12955–12960.

69. Lemeille, S.; Turkina, M. V.; Vener, A. V.; Rochaix, J.-D. Stt7-Dependent Phosphorylation during State Transitions in the Green Alga Chlamydomonas Reinhardtii. *Mol. Cell Proteomics* **2010**, *9* (6), 1281–1295.

70. Finazzi, G.; Rappaport, F.; Furia, A.; Fleischmann, M.; Rochaix, J.-D.; Zito, F.; Forti, G. Involvement of State Transitions in the Switch between Linear and Cyclic Electron Flow in Chlamydomonas Reinhardtii. *EMBO Rep.* **2002**, *3* (3), 280–285.

71. Minagawa, J. State Transitions—The Molecular Remodeling of Photosynthetic Supercomplexes That Controls Energy Flow in the Chloroplast. *Biochim. Biophys. Acta Bioenerg.* **2011**, *1807* (8), 897–905.

72. Grieco, M.; Jain, A.; Ebersberger, I.; Teige, M. An Evolutionary View on Thylakoid Protein Phosphorylation Uncovers Novel Phosphorylation Hotspots with Potential Functional Implications. *J. Exp. Bot.* **2016**, *67* (13), 3883–3896.

73. Iwai, M.; Takahashi, Y.; Minagawa, J. Molecular Remodeling of Photosystem II during State Transitions in Chlamydomonas reinhardtii. *Plant Cell* **2008**, *20* (8), 2177–2189.

74. Turkina, M. V.; Blanco-Rivero, A.; Vainonen, J. P.; Vener, A. V.; Villarejo, A. CO2 Limitation Induces Specific Redox-Dependent Protein Phosphorylation in Chlamydomonas reinhardtii. *Proteomics* **2006**, *6* (9), 2693–2704.

75. Wagner, V.; Ullmann, K.; Mollwo, A.; Kaminski, M.; Mittag, M.; Kreimer, G. The Phosphoproteome of a Chlamydomonas Reinhardtii Eyespot Fraction Includes Key Proteins of the Light Signaling Pathway. *Plant Physiol.* **2008**, *146* (2), 772–788.

76. Finazzi, G.; Furia, A.; Barbagallo, R. P.; Forti, G. State Transitions, Cyclic and Linear Electron Transport and Photophosphorylation in Chlamydomonas Reinhardtii. *Biochim. Biophys. Acta Bioenerg.* **1999**, *1413* (3), 117–129.

77. Wang, S.; Li, Q.-P.; Wang, J.; Yan, Y.; Zhang, G.-L.; Yan, Y.; Zhang, H.; Wu, J.; Chen, F.; Wang, X.; Kang, Z.; Dubcovsky, J.; Gou, J.-Y. YR36/WKS1-Mediated Phosphorylation of PsbO, an Extrinsic Member of Photosystem II, Inhibits Photosynthesis and Confers Stripe Rust Resistance in Wheat. *Mol. Plant* **2019**, *12* (12), 1639–1650.

78. Puthiyaveetil, S.; Kirchhoff, H. A Phosphorylation Map of the Photosystem II Supercomplex C2S2M2. *Front. Plant Sci.* **2013**, *4*.

79. Munnik, T.; Vermeer, J. E. M. Osmotic Stress-Induced Phosphoinositide and Inositol Phosphate Signalling in Plants. *Plant Cell Environ.* **2010**, *33* (4), 655–669.

80. Munnik, T.; Testerink, C. Plant Phospholipid Signaling: “In a Nutshell.” *J. Lipid Res.* **2009**, *50* (Supplement), S260–S265.

81. Wang, X.; Devaiah, S. P.; Zhang, W.; Welti, R. Signaling Functions of Phosphatidic Acid. *Prog. Lipid Res.* **2006**, *45* (3), 250–278.

82. Lemtiri-Chlieh, F.; MacRobbie, E. A. C.; Webb, A. A. R.; Manison, N. F.; Brownlee, C.; Skepper, J. N.; Chen, J.; Prestwich, G. D.; Brearley, C. A. Inositol Hexakisphosphate Mobilizes an Endomembrane Store of Calcium in Guard Cells. *Proc. Natl. Acad. Sci. U.S.A.* **2003**, *100* (17), 10091–10095.

83. Roustan, V.; Bakhtiari, S.; Roustan, P.-J.; Weckwerth, W. Quantitative in Vivo Phosphoproteomics Reveals Reversible Signaling Processes during Nitrogen Starvation and Recovery in the Biofuel Model Organism Chlamydomonas Reinhardtii. *Biotechnol. Biofuels* **2017**, *10* (1), 280.

84. Croze, M. L.; Soulage, C. O. Potential Role and Therapeutic Interests of Myo-Inositol in Metabolic Diseases. *Biochimie* **2013**, *95* (10), 1811–1827.

85. Rupwate, S. D.; Rajasekharan, R. Plant Phosphoinositide-Specific Phospholipase C. *Plant Signal Behav.* **2012**, *7* (10), 1281–1283.

86. Rebecchi, M. J.; Pentyala, S. N. Structure, Function, and Control of Phosphoinositide-Specific Phospholipase C. *Physiol. Rev.* **2000**, *80* (4), 1291–1335.

87. Yeasmin, A. M.; Waliullah, T. M.; Kondo, A.; Kaneko, A.; Koike, N.; Ushimaru, T. Orchestrated Action of PP2A Antagonizes Atg13 Phosphorylation and Promotes Autophagy after the Inactivation of TORC1. *PLOS ONE* **2016**, *11* (12), e0166636.

88. Wong, P.-M.; Feng, Y.; Wang, J.; Shi, R.; Jiang, X. Regulation of Autophagy by Coordinated Action of MTORC1 and Protein Phosphatase 2A. *Nat. Comm.* **2015**, *6* (1), 8048.

89. Elam, C. A.; Wirschell, M.; Yamamoto, R.; Fox, L. A.; York, K.; Kamiya, R.; Dutcher, S. K.; Sale, W. S. An Axonemal PP2A B-Subunit Is Required for PP2A Localization and Flagellar Motility. *Cytoskeleton* **2011**, *68* (7), 363–372.

90. Chen, J.; Martin, B. L.; Brautigan, D. L. Regulation of Protein Serine-Threonine Phosphatase Type-2A by Tyrosine Phosphorylation. *Science* **1992**, *257* (5074), 1261–1264.

91. Boura, E.; Nencka, R. Phosphatidylinositol 4-Kinases: Function, Structure, and Inhibition. *Exp. Cell Res.* **2015**, *337* (2), 136–145.

92. Suer, S.; Sickmann, A.; Meyer, H. E.; Herberg, F. W.; Heilmeyer, L. M. G. Human Phosphatidylinositol 4-Kinase Isoform PI4K92. *Eur. J. Biochem.* **2001**, *268* (7), 2099–2106.

CHAPTER 5: Standard Operating Procedures for Protein Kinase Expression, Peptide Library Preparation and *in vitro* Kinase Screening

5.1 Introduction

High throughput *in vitro* approaches to delineate kinase-substrate relationships can vary in complexity and procedure based on the organism and kinase of interest. In the Hicks lab, we are interested in studying the kinases and their targets that are involved in the target of rapamycin (TOR) signaling pathway in photosynthetic organisms. One approach we use is a high throughput kinase screening method (Figure 5.1), where peptide targets of a kinase of interest are identified via mass spectrometry. This screening platform consists of four primary steps: generation of a kinase of interest, preparation of a substrate library from a cell lysate, screening, and analysis of the putative substrates. Screenings require a purified active kinase sample, which is either purified from its host organism or expressed using recombinant DNA technology. Library preparation must be optimized for each species of interest, including culturing and extraction conditions. When screening, cofactors and the concentrations of all of the components need to be optimized to maximize kinase activity. Additionally, after screening an enrichment method is required to concentrate putative substrates prior to analysis by LC-MS/MS. This chapter focuses on the standard operating procedures optimized and utilized in the *in vitro* screening of kinases from *Chlamydomonas*, specifically kinases suggested to be involved in the TOR signaling pathway, using a peptide substrate library. These procedures are used in Chapter 6, which describes the validation of this screening platform.

5.2 Recombinant Kinase Production

5.2.1 Selection of an Expression System

Protein purification is a critical step in most characterization techniques aimed at identifying a protein's function, structure, and interactions. For the kinases studied in this work, there are several characteristics that were considered when designing the expression system used to create active enzymes. Based on previous transcriptomic analysis[1], target of rapamycin (TOR) and ribosomal S6 kinase (S6K) as well as other kinases thought to be involved in TOR signaling are likely expressed at low levels, making it challenging to purify enough material from *Chlamydomonas* without the use of an overexpression system. While constitutive overexpression of genes in *Chlamydomonas* has been successfully implemented before[2], more traditional expression systems using *Escherichia coli* allow for higher protein yields in a shorter amount of time and are generally easier to culture. With this in mind, an inducible expression system in *E. coli* strain BL21(DE3) (New England Biolabs) was used to express fusion protein kinases with a glutathione S-transferase (GST) tag for affinity purification. This strain of *E. coli* uses the highly specific T7 RNA polymerase for selective overexpression of the protein of interest and is lacking the Lon protease to reduce enzymatic cleavage of the protein product[3]. The pGEX 6P-1 and pMAL vectors are both used in this work and contain the *tac* promoter, a synthetic combination promoter of the *lac* and *trp* operons[4] induced by the addition of isopropyl β-D-1-thiogalactopyranoside (IPTG), a nondegradable analog of allolactose. Induction of protein expression typically occurs when cultures are in exponential growth and translation is maximal.

The gene for each Chlamydomonas kinase was inserted to a pGEX 6P-1 vector (New England Biolabs, https://www.addgene.org/vector-database/2887/) that encodes for ampicillin resistance as well to allow for antibiotic-based selection. A sample vector, pAC1, which encodes

for the Chlamydomonas TOR extended kinase domain construct (CrTOR-EKD) is shown in Figure 5.2 along with a list of all of the Chlamydomonas kinase vector constructs in the Hicks lab.

Plasmids for the other *Chlamydomonas* protein kinases of interest, Glycogen Synthase Kinase 3 (GSK3) Phosphoinositide-dependent Protein Kinase 1 (PDK1), and S6K were commercially synthesized. However, unpublished work from the Umen lab (Danforth Center) fully sequenced CrS6K, and confirmed that a portion of the protein is missing in the original sequence included in the Chlamydomonas database available on Phytozome. For this work, this portion of sequence was added to the CrS6K plasmid construct for expression of the complete protein. This was done commercially by Biomatik with the original CrS6K vector and the missing portion as double stranded DNA synthesized by Genewiz. The full sequences of the synthesized Chlamydomonas proteins can be found in Figure 5.3, with the inserted portion of CrS6K highlighted.

The construction of an expression system for CrTOR was more challenging. One of the considerations when designing a recombinant expression system to overexpress a protein is the size of the expressed protein construct. Studies have shown that the probability of successful expression decreases considerably with constructs above 60 kDa due to problems with protein solubility, folding, and aggregation[5]. This is of great concern with the expression of Chlamydomonas TOR (CrTOR), which is 291 kDa in size and composed of 2691 amino acids (Cre09.g400553.t1.1). To address this issue, a construct was designed that contains only a portion of the protein corresponding to the kinase domain identified using the alignment of CrTOR to mammalian TOR (mTOR) via the Basic Local Alignment Search Tool (BLAST). While *in vitro* CrTOR activity has never been investigated using only the kinase domain,

previous work has shown recovery of TOR function in Arabidopsis TOR mutants with the expression of the a portion of the protein that includes the kinase domain and a portion of the FKBP12-rapamycin binding (FRB) domain[6]. Additionally, it has been shown when the kinase domain of CrTOR is heterlogously expressed and then immobilized, it has enough structural similarity to full-length CrTOR that it can bind and precipitate Chlamydomonas lethal with SEC13 protein 8 (CrLST8), a known component of TORC1, from a cell extract[7]. Based on this work, the corresponding section of CrTOR was identified, amplified by PCR from a Chlamydomonas cDNA library, digested and cloned into a pGEX6P-1 plasmid for expression in *E. coli* cells. This construct is referred to as the Chlamydomonas TOR Extended Kinase Domain (CrTOR-EKD) (Figure 5.3).

Arabidopsis pyruvate dehydrogenase kinase (AtPDK), a well-studied highly specific kinase, was used to validate this platform. A strain of *E. coli* already transformed with a pMAL vector encoding for AtPDK with a maltose binding protein (MBP) affinity tag and a β-lactamase gene to confer for ampicillin resistance was obtained from the Miernyk lab at the University of Missouri. With the use of a different vector and affinity tag, a unique set of parameters are used for the expression (5.2.4) and purification (5.2.7) of this protein.

5.2.2 Kinase Mutant Construction

For screening negative controls, we were interested in designing a construct that would allow for the control to be as similar to the active samples as possible, without any phosphorylation occurring. To do this, inactive kinase mutants were designed which can be expressed and purified alongside the active kinase. These inactive mutants were made using the Q5 Site Directed Mutagenesis Kit (New England Biolabs) with a single base pair substitution (Figure 5.4). In the conserved kinase domain of nearly all kinases, there is a conserved His-Arg-Asp

(HRD) motif, and it is well established that mutation of the Asp results in inhibition of any catalytic activity[8-12]. Based on the conserved kinase domains for each kinase of interest, DNA encoding for the HRD motif was identified (Figure 5.3) and non-overlapping primers were designed using NEBaseChanger and then synthesized by Integrated DNA Technologies (Table 5.1). The primers contain a single base change that modifies the aspartic acid of the HRD motif to an alanine on the forward primer. PCR is used to exponentially amplify the plasmid using the mutant primers and the Q5 Hot Start High-Fidelity DNA Polymerase. After PCR, the amplified DNA is added to the Kinase-Ligase-DpnI (KLD) enzyme mix for phosphorylation and ligation of the mutant plasmids as well as digestion of the parent template. After this the plasmids are transformed into competent *E. coli* cells, and colonies containing the plasmid are selected for using antibiotic resistance. Sequencing was done on the resulting plasmid to confirm correct substitution.

Day 1:

1. Streak the *E. coli* strain transformed with the corresponding plasmid construct you wish to mutate from a glycerol stock onto a lysogeny broth (LB) agar plate with ampicillin (made in the Hicks lab, see below) at a concentration of 100 µg/mL. Streak one quadrant of the plate at a time, using a fresh inoculation loop for each quadrant. The first quadrant is streaked from a small amount of the glycerol stock with each subsequent quadrant diluting from the previous with a single stroke from a fresh inoculation loop (Figure 5.5). Individual colonies typically for after 16 – 18 h incubation, so streaking after 3:00 pm is recommended for overnight incubation.
    a. When making LB agar plates, 500 mL of broth makes about 1 sleeve of plates (20-25 total).

i. Add 17.5 g of LB agar (BD Difco) to 500 mL MilliQ water in a 1 L small mouth media bottle.

ii. Autoclave media for 45 minutes and let cool in the hot water bath set to 51 °C for one h.

iii. Add 500 µL of 100 mg/mL ampicillin in water stock to the media. It is important to add the antibiotic after the media has cooled in the hot water bath to prevent degradation of the antibiotic.

iv. Open one sleeve of empty petri dishes in the biosafety cabinet and place them in stacks of 3-4 dishes based on how many you can pick up with a single hand.

v. Remove media from the water bath, wipe the bottle dry, and pour the media into the petri dishes starting with the bottom plate of each stack. Hold the rest of the stack and cover in one hand, and pour the media into the bottom dish so that the bottom of the plate is just covered (about 4-6 mm in thickness). Replace the cover and bottom of the next dish over the poured plate. Repeat this for each stack of plates until all of the media is poured. The last plate may need to be discarded if there is not sufficient media to pour a complete plate or if agar begins to solidify, resulting in lumps. Plates should be stacked in the corner of the hood to solidify overnight.

b. 100 mg/mL ampicillin stocks are made in bulk and stored in 1 mL aliquots at -20 °C.

i. Dissolve 1 g of ampicillin, sodium salt in 10 mL of MilliQ water. (Anhydrous ampicillin is not readily soluble in water without adjusting the pH.)

ii. Filter sterilize the stock by running it through a 0.22 µm syringe filter.

iii. Divide the stock into 1 mL aliquots and store them at -20 °C.

2. Label the plate with the corresponding strain, construct, date, and initials, and place in the stationary incubator at 37 °C overnight.

Day 2:

1. Remove plate from the incubator, seal with parafilm, and store at 4 °C after 16-18 h of incubation. Plates can be stored at 4 °C for up to two weeks.
2. After 3:00 pm, prepare a starter culture. Dispense 5 mL of LB into a 15 mL culture tube, using flame sterilization to minimize contamination, flaming the lid of the bottle and the pipette prior to collection of the media from the stock. Keep the culture capped between each step to minimize contamination.
    a. LB media is prepared in the Hicks lab. In a 500 mL small mouth bottle, add 12.5 g of LB broth powder to 500 mL MilliQ water. Stir until fully dissolved, place the cap on top of the bottle without tightening, and secure with a piece of autoclave tape. Autoclave for 45 min and store properly labeled in Kenan B328.
3. Add 5 µL of 100 mg/mL ampicillin in water stock into the culture tube.
4. Collect a single *E. coli* colony from the previously prepared LB plate using an autoclaved pipette tip. Insert this tip into the starter culture and pipette up and down several times to inoculate the culture. Cap the cultures to the first stopping point to allow airflow.
5. Incubate this culture overnight for 16-18 h at 37 °C, 240 rpm, positioned at an angle in an orbital shaker incubator to maximize aeration. The starter cultures should be cloudy after incubation, indicating adequate cell density.
6. Extract the plasmid DNA from this culture using the Qiagen QIAprep Spin Miniprep Kit following the manufacturers protocol.

7. Using a nanodrop microvolume spectrometer, measure the concentration of the extracted plasmid, and add Buffer EB from the Miniprep kit or 1mM TrisHCl, pH 8.5 to dilute the sample concentration to 10-25 ng of DNA per µL.
8. Using nuclease-free water, suspend the synthesized primers to a stock concentration of 100 µM, and then create a working stock of 10 µM for each primer using nuclease free water.
9. Using the manufacturer's protocol, perform site directed mutagenesis on the purified plasmid using the Q5 Site-Directed Mutagenesis kit with the following suggestions:
    a. Cycling conditions in the first step will vary depending on the melting temperature of the primers. Use the annealing temperature (T_a) recommended by NEBaseChanger when the primers were designed.
    b. Chemically competent cells are kept at -80 °C, and should be thawed on ice for 30 min prior to transformation with the KLD mix.
    c. Heat shock should be performed with the water bath set to 42 °C.
    d. Use LB + ampicillin plates for selection after transformation. These plates should be removed from the fridge and allowed to warm to room temperature for about an hour prior to plating.
    e. When plating, spread 800 µL across two selection plates (400 µL each) to increase likelihood of colonies forming.
10. After overnight incubation, the selection plates should have colonies present, which indicate successful transformation of the plasmid. The number of colonies can vary depending on the construct and success of the mutagenesis, from 3 to more than 50.

11. Select a single colony from a selection plate and prepare a starter culture from this colony as described above.
12. Use 500 µL of this starter culture to make a glycerol stock, and purify the plasmid from the remaining 4.5 mL using the Qiagen QIAprep Spin Miniprep Kit.
    a. To make a glycerol stock, combine 500 µL of culture with 500 µL 50% glycerol in a 2 mL screw top cryovial. Pipette mixture until fully incorporated. Label cryovial with plasmid name, construct and date before flash freezing with liquid nitrogen and storing at -80 °C.
13. Use this purified plasmid to confirm mutagenesis was successful by submitting a sample containing this plasmid and a sequencing primer to Genewiz for Sanger sequencing. (See the sample submission guidelines on the Genewiz website for more details.)
    a. The plasmid should be diluted with EB Buffer or 50 mM TrisHCl, pH 8.5 to a concentration that is dependent on the size of the plasmid (Table 5.2).
    b. Prepare your sequencing samples in 8-strip PCR tubes. Each sample should have 10 µL or plasmid and 5 µL of sequencing primer diluted to 5 pmol/µL.
    c. The sequencing primer should be 100-500 bp away from the mutation site either on the forward or reverse strand. For all of the *Chlamydomonas* kinases, primers already existed within the range needed to sequence across the mutation site. These were either designed to confirm insertion of the gene into the vector, confirmed the insertion of the missing portion of the CrS6K sequence, or were standard primers for the pGEX-6P-1 vector available for free from Genewiz that are added to the purified plasmid sample after it is received. These standard primers can be found on the

Genewiz website. If a primer needs to be designed, recommendations on design can be found on the Genewiz website.

d. Submit the sequencing samples to Genewiz no later than 3:00 pm on the Genewiz website. Place the PCR tubes and printed order information sheet into a sealed sandwich bag. Drop the sandwich bag into the Genewiz submission box, mounted to the wall outside room 3102 in Murray Hall. Sequencing results are typically available by 12:00 pm the next day via your Genewiz account.
e. Use SnapGene Viewer to open the sequence file and confirm the successful mutation of the base pair needed to create the mutant kinase construct.

5.2.3 *E. coli* Culturing

All steps are performed under reproducible conditions in Kenan B328, using sterile techniques as needed. All cultures are started from a frozen glycerol stock stored at -80 °C. For growth, a small amount of the stock is streaked onto a LB agar plate with ampicillin and incubated at 37 °C until visible single colonies are formed, typically overnight. The presence of ampicillin selects for colonies containing the plasmid encoding for the kinase of interest. These plates are stable for up to two weeks when sealed and stored at 4 °C.

Bacterial liquid starter cultures, each inoculated from a single agar colony, allow for more uniform growth across multiple large cultures than starting each culture separately from an agar colony. Cultures are incubated overnight (12-16 h) at 37 °C, shaking at 240 rpm in an incubator ensuring that the cultures have enough time to reach saturation so roughly the same number of cells are present in each culture. For this work, four starter cultures were used for each 1 L large culture to reduce the incubation time needed to reach mid-log growth phase.

Cultures for this work are grown by the liter in Fernbach flasks in terrific broth (TB; Research Products International), a highly enriched bacterial media made for high-density culturing. The cultures are inoculated with starter culture and ampicillin before incubation. For expression of AtPDK, glucose is also added to the cultures to minimize the production of amylase that may interfere with purification. Cultures are monitored via absorbance-based optical density until they reach mid-log phase, when the bacteria are adapted to their growth conditions, rapidly replicating, and not yet nutrient limited. For bacteria cultures, this is measured using optical density (OD_{600}), with a range of 0.4-0.8 being about mid-log phase. The total volume of bacterial culture needed for adequate protein yield, ideally >20 μg of expressed kinase to allow for multiple screenings with multiple replicates, varied greatly depending on the construct, but was generally achievable with 2 L of culture. AtPDK, CrGSK3, CrGSK3 D288A, CrPDK1, CrTOR-EKD, and CrTOR-EKD D239A all express well with yields typically > 1 mg protein per L of culture. CrPDK1 D151A, CrS6K, and CrS6K D812A have lower yields, but typically can express 10-50 μg of kinase per L of culture. This yield is generally dependent on protein toxicity and solubility[13], along with batch culturing conditions, which have been optimized here for the protein constructs of interest.

Day 1:

1. After 3:00 pm, streak the *E. coli* strain transformed with the corresponding plasmid construct from a glycerol stock onto an LB + ampicillin plate as described above (5.2.1 Day 1).
2. Label the plate with the corresponding strain, construct, date, and initials, and place in the stationary incubator at 37 °C overnight.

Day 2:

1. Remove plate from the incubator, seal with parafilm, and store at 4 °C after 16-18 h of incubation.
2. Prepare and autoclave TB in Fernbach flasks, 1 L per flask. To each flask add 5.2 g (4 mL) of glycerol. It is easiest to set the flask directly on the scale and dispense using a scoopula rather than measuring the glycerol by volume. Then add 1 L of MilliQ water to each flask and 47.6 g of TB powdered broth. Stir until dissolved, cover the mouth of the flask with aluminum foil and secure the foil to the flask with autoclave tape. Autoclave for 45 min and let cool overnight prior to use.
3. After 3:00 pm, prepare the starter cultures, 4 starters per L of large culture, as described above (5.2.1 Day 2).
    a. For expression of AtPDK only: Add 20 µL of 50% glucose stock to each starter culture.

Day 3:

1. To each Fernbach flask containing 1 L TB, add 1 mL of 100 mg/mL ampicillin.
2. For AtPDK expression only: Add 4 mL 50% glucose stock to each flask.
3. Add four 5 mL starter cultures to each flask.
4. Incubate the cultures at 37 °C, 240 rpm, monitoring their growth via optical density at 600 nm (OD_{600}) until mid-log growth is reached, typically OD_{600} 0.4-0.8 for BL21(DE3). This generally takes about 3 h.

5.2.4 Heterologous Protein Expression of Kinases

To optimize protein expression, additives are sometimes needed to improve protein yields, as they can improve solubility[14] or minimize proteolytic cleavage[15]. Optimized expression for the kinases of interest included the addition of a protease inhibitor, ε-aminocaproic acid (ε-ACA),

which improved protein yield. Additionally, optimization of IPTG concentration, expression temperature and expression time were performed to increase overall expression efficiency for these kinase constructs (Figure 5.6). To track the effectiveness of the expression and purification system, aliquots of the cultures are taken at each step in the process and analyzed via sodium dodecyl sulfate – polyacrylamide gel electrophoresis (SDS-PAGE). When specified, phosphate-buffered saline (PBS) contains 8 mM Na_2HPO_4, 2 mM KH_2PO_4, 2.7 mM KCl, and 137 mM NaCl dissolved in ultrapure water and adjusted to pH 7.4 using 1 M HCl.

Day 3:

1. After reaching mid-log phase, OD_{600} ~0.5-0.8, take a 30 µL pre-induction gel aliquot from each culture.
2. Add 1 mL of 1 M ε-ACA in water stock to each culture followed by 1 M IPTG in water stock. ε-ACA stock is stored at 4°C protected from light and is stable for up to a month. IPTG stocks are kept in 1 mL aliquots at -20 °C.
    a. For AtPDK add 300 µL IPTG stock, and for the *Chlamydomonas* kinase expression add 100 µL IPTG stock.
3. For expression of AtPDK, incubate cultures at 37 °C, 240 rpm for 4 hrs. Incubate induced *Chlamydomonas* kinase cultures at 10 °C, 240 rpm overnight.

Day 3/4:

1. After expression, take a 30 µL post-induction gel aliquot of each culture.
2. Transfer the cultures to 1 L centrifuge bottles, and pellet using centrifugation at 2300 x *g* and 4 °C for 10 min.
3. Decant the supernatant, treat with 10% bleach for 5-10 min, and dispose down the drain.

4. Resuspend each protein pellet in 10 mL of lysis buffer. For AtPDK, resuspend in amylose column buffer (20 mM Tris-HCl, pH 7.4, 200 mM NaCl, 1mM EDTA), and for the *Chlamydomonas* kinases resuspend in phosphate-buffered saline (PBS), pH 7.4. Combine samples into 50 mL conical tubes, one tube for every two cultures.
5. Flash freeze the cultures with liquid nitrogen and store at -80 °C.

5.2.5 *E. coli* Lysis and Soluble Protein Extraction

Many techniques exist for lysing cells, and generally Gram-negative bacteria are easier to lyse in comparison to Gram-positive bacteria[16]. With different expression systems, increasing protein yield while maintaining kinase activity dictates the selection of lysis techniques and parameters. Here, two methods are used in tandem to maximize protein extraction, chemical lysis with lysozyme and mechanical lysis with sonication, while keeping the cultures on ice to minimize protein denaturing. Additionally, the probe ultrasonicator used for lysis is pulsed with one-minute rest periods between sonication rounds to help reduce sample heating.

Day 1:

1. Defrost cell pellets in an ice-water bath.
2. Keeping the sample on ice, add 1 mg lysozyme per mL of sample, inverting the tube until the enzyme is dissolved.
3. Sonicate each sample using a probe ultrasonicator for 1 min with a 50% duty cycle a total of three times, resting for 1 min between each sonication while keeping the sample on ice.
4. Aliquot 20 µL for a total protein gel sample. The sample may be challenging to pipette due to its viscosity.

5. Split the samples evenly between two centrifuge tubes and centrifuge at 20,000 x *g* at 4° C for 30 min.
6. Combine the supernatants containing the soluble proteins for each sample into a 50 mL conical tube.
7. Aliquot 20 µL for a soluble protein gel sample.

5.2.6 Protein Purification of *Chlamydomonas* Kinases

Proteins can be separated and purified based on a number of characteristics including solubility, size, charge, and binding affinity[17]. One advantage of recombinant protein expression is the ability to express a fusion protein, adding a tag to the protein of interest for affinity purification. For these constructs, a glutathione S-transferase (GST) tag is included on the N-terminus of each protein, which can be used to purify the construct with a high level of specificity. In addition to being a tool for purification, GST tags can also promote greater expression and solubility due to its rapid folding and highly soluble nature[18]. GST is a 26 kDa protein that has a high binding affinity to glutathione, a tripeptide that is an oxidant in eukaryotes. Glutathione Sepharose 4B resin is composed of a glutathione ligand coupled to highly cross-linked agarose which allows for specific binding of GST and elution from the resin using a mild, nondenaturing buffer with high concentrations of reduced glutathione. This protocol uses a batch-style purification method, where resin is incubated with the sample and collected for washes and elution steps using centrifugation. This method is a quick way to purify proteins that requires minimal equipment.

Procedure:

1. If frozen, thaw soluble protein samples in an ice-water bath or at 4 °C.

2. Invert stock of Glutathione Sepharose 4B resin until resin is completely resuspended. Add 100 µL of resin solution for every 1 L of culture to a 2 mL tube. Centrifuge at 5,000 x *g*, 4 ºC for 5 min and remove supernatant.
3. Wash resin three times with 1 mL of PBS buffer, centrifuging at 5,000 x *g* 4 ºC for 5 min and remove the supernatant between each wash.
4. Use 1 mL of soluble protein sample to resuspend the resin. Transfer the resin back into the tube containing the remaining soluble protein. Rotate the sample end-over-end at 4 °C for at least 2 h.
5. Centrifuge at 5,000 x *g*, 4 °C for 5 min to pellet resin.
6. Remove the supernatant, resuspend resin in 1 mL fresh PBS buffer, and transfer to a 2 mL tube.
7. Centrifuge sample at 5,000 x *g* 4 °C for 5 min, discarding the supernatant. Wash the resin an additional 3 times with 1 mL fresh PBS buffer. Centrifuging after each wash step to collect the resin at the bottom of the tube.
8. Resuspend resin pellet in 300 µL Elution Buffer (50 mM Tris HCl, 10 mM reduced glutathione, pH 8.0) for every 100 µl resin. Rotate sample for 10 min end-over-end at 4°C. Centrifuge at 5,000 x *g,* 4°C for 5 min to pellet the resin and collect supernatant. Repeat twice with fresh Elution Buffer, combining all elutions.
9. Take 30 µL of elution to use as a gel sample. Add glycerol to the remaining elution at a concentration of 10-25% to keep sample stable. Store at 4°C until ready for buffer exchange and screening, within 24 hours of purification. Storage of the protein for a longer period of time or freezing of the sample causes protein degradation and impact the activity of the kinase.

5.2.7 AtPDK Affinity Purification

Amylose resin is an affinity matrix that can be used for the purification of fusion proteins with an MBP tag. Similar to GST, MBP is a large fusion tag, roughly 42 kDa in size that can also be useful for protein solubility. With amylose resin a hybrid approach between batch and column purifications is recommended for higher levels of specificity for smaller purification amounts. For this procedure, batch purification for incubating the resin and protein is combined with a gravity column washing and elution approach for the purification of AtPDK. All steps must be completed on ice or at 4°C to prevent protein degradation.

Procedure:

1. If frozen, thaw soluble protein samples in an ice-water bath or at 4 °C.
2. Invert stock of amylose resin until resin is completely resuspended. Add 100 μL of resin solution for every 5 mL of soluble protein into a 2 mL tube. Centrifuge at 5,000 x *g*, 4 °C for 5 min and remove supernatant.
3. Wash resin three times with 1 mL of amylose column buffer, centrifuging at 5,000 rpm, 4 °C for 5 min, removing the supernatant between each wash.
4. Use 1 mL of soluble protein sample to resuspend the resin. Transfer the resin back into the tube containing the remaining soluble protein. Rotate the sample end-over-end at 4 °C for at least 2 h.
5. Prepare one disposable 10 mL gravity flow Poly-prep column (Bio-Rad) for each liter of culture. Parafilm the top of a 50 mL conical tube and cut a small slit into the center of the film. Insert the disposable column through the slit in the parafilm and place the falcon tube into a cooler of ice.

6. Pour the soluble protein into the Poly-prep column(s) evenly. The soluble protein will flow through the column, collecting the resin with the bound protein.
7. After sample flows through leaving only a small amount of liquid above the resin bed, transfer the column to a new conical tube with parafilm.
8. Wash the resin column with 10 mL of fresh amylose column buffer leaving only a small amount of liquid above the resin bed.
9. Transfer the column to a new 15 mL conical tube and add 2 mL of elution buffer (amylose column buffer with 10 mM maltose). Allow the column to run dry and pool the elutions from all of the columns into one 15 mL conical tube.
10. Take 30 µL of elution to use as a gel sample. Add glycerol to the remaining elution at a concentration of 10-25% to keep sample stable. Store at 4 °C until ready for buffer exchange and screening, within 24 hours of purification. Storage of the protein for longer than this or freezing of the sample causes protein degradation and impacts the activity of the kinase.
11. Directly before screening, use a 10 kDa 4 mL MWCO filter to concentrate sample and buffer exchange into kinase screening buffer: 20 mM HEPES-KOH, pH 7.4, 5 mM $MgCl_2$ 1 mM dithiothreitol (DTT), 1x protease inhibitor cocktail (Roche) and 1x PhosSTOP phosphatase inhibitor (Roche). Concentrate the sample to ~0.5 mL volume per 1 L of culture originally expressed.
12. Measure the concentration of the kinase sample using a nanodrop microvolume spectrometer and adjust the concentration to ~0.5 mg/mL with additional screening buffer.

5.2.8 Confirmation via SDS-PAGE

After completion of protein expression and affinity purification, the gel samples taken at various points in the procedure can be run via SDS-PAGE to determine the effectiveness of the method and the overall purity of the final protein sample. With the varying concentrations and complexity of the protein samples, some dilution is necessary prior to analyzing these samples.

Procedure:

1. Thaw out gel samples from expression and purification.
2. Dilute total and soluble proteins 4-fold with water.
3. Prepare gel buffer by adding 10 µL 2-mercaptoethanol to 190 µL of 4x Laemmli buffer (Bio-Rad).
4. For each sample, aliquot 30 µL into a fresh tube and add 10 µL of gel buffer.
5. Heat samples on the heat block at 95°C for 5 min.
6. Use a 4-20% SDS-PAGE gel (Criterion gel by Bio-Rad recommended) for the separation. Rinse with ultrapure water and prepare the gel, loading it into the gel box.
7. Fill the box and upper gel compartment with SDS Running Buffer (0.25 M Tris Base, 1.92 M Glycine, 1% sodium dodecyl sulfate).
8. Load 40 µL of each gel sample into the lanes in the order that they were collected.
9. Load the remaining empty wells with 10 µL of gel buffer and each of the outer gel lanes with 5 µL of Precision Plus Dual Color Protein Standard (Bio-Rad).
10. Run the gel for 10 min at 100 V to allow the samples to migrate into the gel. Continue at 200 V for 30-40 min until the dye front reaches the bottom of the gel.
11. Rinse with ultrapure water and stain the gel with Coomassie dye (50% methanol, 10% acetic acid, 1 g/L bromophenol blue) for at least one hour.

12. Destain the gel using 50% methanol, 10% acetic acid until bands are clearly visible and image. A summary of the gel results for each construct can be seen in Figure 5.7 and full gel images are shown in Figure 5.8.

5.3 Substrate Library Preparation

Kinase screening requires the presence of a library of putative substrates to incubate with the kinase. For this work, a peptide library is prepared from a *Chlamydomonas* cell lysate to create a pool of potential substrates for a kinase of interest to phosphorylate. This creates a more biologically-relevant pool of substrates than using a library of synthesized peptides; the *in vivo* targets of the kinase of interest are likely to be present in the library. This library is prepared by digesting a protein extract of *Chlamydomonas*, followed by a dephosphorylation step to remove the endogenous phosphorylation present.

5.3.1 Algal Culturing

Since the isolation of Chlamydomonas by Gilbert Smith[19,20], a number of standard strains as well as mutants have been designed for laboratory purposes. The Chlamydomonas Resource Center (https://www.chlamycollection.org/) hosted at the University of Minnesota, Twin Cities serves as a repository for thousands of these strains including CC2895, the wild-type strain of choice for many experiments performed by the Hicks laboratory[21-24].

While the procedures for this culturing are similar to those used in the quantitative proteomics workflows implemented by the Hicks lab[21-24], there is less stringency needed for reproducible growth conditions. Liquid cultures are prepared in the biosafety cabinet and then grown on the bench top in Kenan B328. Although this growth area generally has more variability due to the exposure to temperature fluctuations and inconsistent overhead lighting, it allows for a higher volume of culturing for higher quantities of peptide library in each preparation. This

growth area is exposed to cool, white fluorescent bulbs that provide photosynthetically active radiation (PAR) between 400-700 nm at 50-100 μmol m^{-2} s^{-1} as measured by a PAR meter (Sun Systems) and constantly mixed on a platform shaker at 120 rpm. Cultures are usually grown in 1 L flasks, with room for up to 12 flasks on the benchtop shaker, though for ease of harvesting, cultures are usually grown with eight replicates at a time.

To help ensure even growth rates and to provide cells the opportunity to equilibrate to the growth conditions of liquid media, all cultures grown simultaneously are inoculated from a single starter culture that is grown and prepared beforehand. The cultures are mixotrophically grown with acetate as a carbon source provided in the Tris-acetate-phosphate (TAP)[25] media along with light exposure to maximize growth rate.

Day 1:

1. Measure 350 mL of liquid TAP media with a graduated cylinder and pour into an autoclaved 1 L Erlenmeyer flask with an aluminum foil lid.
2. Inoculate the culture with 3.5 mL of the starter culture.
3. Secure cultures on the shaker platform on the benchtop and shake at 120 rpm for 3-4 days.

Day 4:

1. After three days of growth, check that cultures have reached an OD_{750} ~0.4 corresponding approximately to mid-log phase growth. While cultures may be grown to a higher cell density, this is the point of harvest for most quantitative phosphoproteomic studies performed in the Hicks lab[17], making the peptide library prepared from these cultures more representative of the phosphoproteome analyzed in *in vivo* studies.

2. Harvest cultures by pouring into 1 L centrifuge bottles and centrifuging for 5 min at 2300 x *g* and 4°C before decanting the supernatant.
3. Resuspend the pellets in 5-10 mL of fresh TAP, transfer this to pre-weighed 15 mL conical tubes, and centrifuge again for 5 min at 3220 x *g* and 4°C.
4. Decant the supernatant and invert conical tubes on a paper towel to dry (~30 s) before replacing the cap and weighing the cell pellet.
5. Flash-freeze samples in liquid nitrogen and store pellets at -80 °C until ready for extraction.

5.3.2 Protein Extraction and Clean Up

Chlamydomonas, like many photosynthetic organisms, have a tough outer cell wall made up of complex glycoproteins that make protein extractions challenging[26]. For peptide library preparation, maximum protein yields are needed to ensure both library complexity and efficient extraction of potential substrates for kinase screening. With that in mind, this work uses two approaches to lysis, a chemical detergent-based extraction method as well as physical lysis using ultrasonication. The combination of these two methods produces protein yields greater than 10 mg protein/g fresh cell pellet weight. The lysis buffer consisted of 100 mM Tris, pH 8.0, 1% SDS, 1x cOmplete protease inhibitor (Roche) and 1x PhosSTOP phosphatase inhibitor (Roche). After lysis, a precipitation technique is used to remove small molecule contaminants from the lysate before protein quantitation. During lysis and clean up, samples are kept on ice to minimize protein degradation.

Procedure:

1. Resuspend cell pellets in 1 mL lysis buffer for every 0.1 g of wet cell pellet weight.

2. Transfer the samples to 2 mL Covaris ultrasonication vials and load into a 24 spot 2 mL microtube rack.
3. Sonicate cells using an E220 focused ultrasonicator (Covaris) in the UNC High Throughput Sequencing Center (https://www.med.unc.edu/genomics/, located in GSB 4th floor red pod). Set the water bath to 4 °C and sonicate for 3 min per tube with 200 cycles/burst, 100 W power and a 13% duty cycle.
4. After sonication, transfer the samples to 2 mL Eppendorf tubes and centrifuge at 16,000 x *g* and 4 °C for 10 min.
5. Transfer the clarified lysate into a 50 mL conical tube
6. Add 0.5 mL fresh lysis buffer to each 2 mL Eppendorf tube containing the remaining cellular debris and vortex until resuspended.
7. Centrifuge samples again for 10 min at 16,000 x *g*, 4 °C and combine with previous supernatant.
8. For each sample, separate lysate into multiple 50 mL conical tubes with a maximum of 10 mL per tube.
9. Precipitate proteins using 4x volume of cold 100 mM ammonium acetate in methanol. Vortex each sample briefly and incubate at -80 °C for four hours to overnight.
10. Centrifuge the samples for 5 min at 3220 x *g* to pellet precipitated proteins. Decant the resulting supernatant.
11. Perform two additional washes with fresh 100 mM ammonium acetate in methanol and an additional wash with 70% ethanol, each followed with centrifugation and decanting as described in step 10.

12. Dry pellets for about 5 min in the hood and then resolubilize in 1-2 mL 8 M urea, 100 mM Tris, pH 7.4 with repeated pipetting.
13. Incubate samples for 1 h at room temperature to solubilize.
14. Centrifuge samples at 3220 x *g* and 4°C for 5 min to pellet any insoluble protein. Combine supernatants from the same sample into one 15 mL conical tube.
15. Add an additional 0.5 mL 8 M urea, 100 mM Tris to each pellet, resuspend and repeat centrifugation. Combine with the supernatant from the previous resuspension.
16. Take a 10 µL aliquot of soluble protein and perform protein quantification using the CB-X protein assay (G-Biosciences) following the manufacturer's protocol. Normalize to ~2 mg protein / mL.
17. Store samples at -80 °C until ready for protein digestion.

5.3.3 Protein Digestion and C18-Clean Up

The overall workflow to this screening method is very similar to a bottom up proteomics analysis and requires reduction, alkylation, and digestion of the protein lysate. While this procedure can be scaled for any amount of protein, typical library preparation is performed in bulk; therefore, the specifics of this procedure are written with that in mind. Screening of a single kinase in triplicate including control samples requires 3 mg of digested protein, 500 µg peptide library each for the three replicates of kinase and control samples. With that in mind, typically 3-12 mg of protein is digested for substrate library depending on the number of screenings planned.

After digestion, various salts and detergents are present that need to be removed prior to screening to ensure optimal conditions for kinase activity. Sold-phase extraction (SPE) using C18 resin is a common purification technique for typical bottom-up proteomics that is also well-suited for these kinase screening experiments. In the Hicks laboratory, various C18 SPE

purification techniques are used depending on the amount of protein sample. For samples with smaller protein amounts in the range of a few micrograms, C18 ZipTips (Millipore) are used. The SPE resin is packed into a 10 µL micropipette tip and uses a micropipette for loading, washing, and eluting the sample. For larger amounts of protein, Sep-Pak C18 cartridges (Waters) are used, which range in size from 50 mg to 1 g of bed volume. The sample loading capacity for Sep-Pak C18 cartridges is estimated to be 1 mg of trypsin-digested proteome per 50 mg sorbent. For samples with > 1 mg digested proteome, both the sorbent weight and solvent volumes should be increased in proportion. For preparing a peptide library, typically a Sep-Pak C18 cartridge is used with either a 500 mg or 1 g bed volume depending on the amount of library digested. The procedure below is written for a bed volume of this size. The Hicks Laboratory owns a 24-position vacuum manifold (Phenomenex) that features 2-way stopcocks to secure SPE cartridges and allows for batch sample processing to minimize technical variability.

Procedure:

Reduction, Alkylation, and Digestion:

1. Thaw frozen samples to room temperature. There will be roughly 1.5 to 6 mL of sample from extraction above, depending on the total amount of library being prepared.
2. Prepare 1 mL of 500 mM DTT solution in 100 mM Tris, pH 8.0. Reduce proteins in the lysate by adding 20 µL of 500 mM DTT per 1 mL of protein sample.
3. Incubate the sample for 30 min at room temperature, rotating end-over-end.
4. While reducing the sample, prepare 2 mL of 500 mM iodoacetamide (IAM) solution in 100 mM Tris, pH 8.0, protecting the solution from light, as IAM is light-sensitive in solution.

5. After reduction of proteins, alkylation is performed by adding 80 µL of 500 mM IAM solution per 1 mL of protein sample.
6. Incubate the sample rotating end-over-end, protecting it from light for 30 min at room temperature.
7. Following alkylation, dilute the sample 5-fold using 100 mM Tris, pH 8.0 so the concentration of urea is less than 2 M, which is a requirement for effective protein digestion with trypsin. This will vary depending on the amount of library being prepared but is typically 5 to 30 mL total volume.
8. Digestion is performed overnight using Trypsin Gold (Promega) at a protease:protein concentration of 1:50 at room temperature. Add the corresponding amount of 0.5 µg/µL trypsin in 50 mM acetic acid stock solution to the sample and rotate end-over-end for at least 16 hours.
9. Quench the protein digestion by adding 20% trifluoroacetic acid (TFA) to a final concentration of about 0.2% or until the pH of the sample is less than 3.
10. Store samples at -80°C or proceed directly to C18 clean up.

SPE C-18 Clean Up:

1. Once samples are acidified and thawed as needed, centrifuge the sample for 5 min at maximum speed to pellet any precipitated protein.
2. Pre-elute 500 mg or 1 g Sep-Pak cartridge on the vacuum manifold with 5 mL of 80% acetonitrile, 0.1% TFA. Apply vacuum as needed to maintain a constant flow of about 1 drop per second. Leave a small amount of liquid visible at the top of the bed to ensure C18 resin does not dry out while performing the clean-up.

3. Equilibrate the cartridge with 10 mL of water with 0.1% TFA.
4. Load the peptide sample onto the column using only gravity flow, collecting the flow through in clean test tubes.
5. Re-apply this flow-through to the cartridge, this time using vacuum as needed at a rate of 1 drop per second.
6. Wash the cartridge with 10 mL of 0.1% TFA to remove any salts that may be non-specifically bound to the bed.
7. Finally, elute the peptides from the cartridge using 5 mL 80% acetonitrile, 0.1% TFA with gravity flow into 2 mL Eppendorf tubes. When cartridge is no longer eluting, apply increasing vacuum to the manifold until the bed is completely dried and all liquid is eluted from the column.
8. Freeze the elution and then dry using vacuum centrifugation. Resuspend peptides in each tube using 100 µL of 80% acetonitrile, 0.1% TFA and combine into a single tube. Refreeze and then dry using vacuum centrifugation.

5.3.4 Library Dephosphorylation

Using a peptide library prepared from a cell lysate means that there are likely post-translational modifications present, including endogenous phosphorylation. The presence of phosphorylation on these residues makes them more likely to be biologically significant, implying they could be important targets to include in the substrate library. To make these sites accessible to the kinase of interest during screening, this endogenous phosphorylation first needs to be removed. This work uses rAPid alkaline phosphatase (Bio-Rad), which removes phosphorylation from numerous phosphate esters including primary and secondary alcohols, saccharides, cyclic alcohols, phenols, and amines. Not all of the phosphorylation in the library

can be removed due to accessibility of the phosphorylation site to the phosphatase, but it serves to increase the number of phosphosites available to the kinase during the screening. Overnight incubation of the library with the phosphatase allows the maximum amount of dephosphorylation to occur.

Procedure:

1. Resuspend the peptide sample in 10 µL of 1x phosphatase buffer provided with the rAPid alkaline phosphatase for every 50 µg of peptide.
2. Add phosphatase to the sample at a ratio of 1 U (1 µL) phosphatase: 10 µg peptide.
3. Incubate the sample overnight at 37 °C in the Thermomixer (Eppendorf), rotating at 850 rpm.
4. Heat the sample at 75 °C for 5 min to inactivate the phosphatase.
5. Freeze the sample and dry via vacuum centrifugation. Glycerol is present in the stock of rAPid alkaline phosphatase, so sample will not dry completely.

5.4 Kinase Screening and Analysis

This screening platform is designed to help identify biologically-relevant putative substrates for kinases, but there are other more simplistic kinase assays designed to measure a kinase's activity[27-32]. While we have attempted to implement an absorbance-based assay in the Hicks lab, thus far we have been unsuccessful. Primarily, we have focused on implementation of the non-antibody phosphorylation detection reagent (pIMAGO) and the phosphatase-coupled universal kinase assay (R&D Systems) as a way to detect the phosphorylation of a substrate library from a kinase. Therefore, to ensure maximum activity of the kinase of interest without being able to directly measure its activity, screening is performed within 24 hours of purification of the kinase.

Screenings are typically performed in triplicate with three kinase samples and three control samples, which uses the inactive mutant form of the kinase. Although the library is dephosphorylated prior to screening, there is likely some amount of endogenous phosphorylation still present. To differentiate between this phosphorylation and phosphorylation that is a product of the kinase screening, an isotopic analog of ATP is used. This analog, which has been used previously for kinase screening[33], contains four ^{18}O's on the γ-phosphate group (Cambridge Isotope Laboratories). When this group is transferred by the kinase to the substrate, the resulting phosphorylation modification is 6 Da heavier than endogenous phosphorylation, which is referred to here as "heavy" phosphorylation, making the two modifications easily distinguishable via mass spectrometry.

After screening, a TiO_2 phosphopeptide enrichment step is needed prior to LC-MS/MS analysis to concentrate the kinase targets and remove non-substrate peptides. Glycerol is still present from the library dephosphorylation step, which needs to be removed using SPE prior to phosphopeptide enrichment to prevent clogging in the TiO_2 column. After enrichment, a final clean up step is performed to remove residual phthalic acid, an additive in the enrichment that helps to minimize non-specific binding of acidic residues to the TiO_2 resin.

5.4.1 Screening

When screening, a number of cofactors are included to help ensure the kinase is in its active form. Buffer is used to maintain a neutral pH, and glycerol is present from the kinase stock to help improve protein stability. A small concentration of DTT is included in the assay to create a reduced environment, which has been shown to improve kinase activity in *in vitro* assays[34,35], along with $MgCl_2$ as a metal cofactor. These conditions are based off of the screening conditions previously used for AtPDK, but the exact conditions needed for each kinase can vary depending

on the pH, cofactors, and other contributors needed for activity which may need to be optimized before activity is seen. Kinase activity in this assay can vary and false positives are often present. Replicate screenings facilitate statistical testing to identify significant substrates. Inactive mutants, such as those prepared for *Chlamydomonas* kinases, minimize the differences between the control and kinase screening samples to help keep false positives to a minimum.

Procedure:

1. Prepare 5 mL of 10x stock of the screening buffer: 200 mM HEPES-KOH, pH 7.4, 50 mM $MgCl_2$, 10 mM DTT.
2. Prepare the following stocks in 20 mM HEPES-KOH, pH 7.4:
    a. 5 mg/mL peptide library
    b. 10 mM $^{18}O_4$-ATP
    c. 0.5 mM kinase sample (see section 5.2.6).
3. Prepare control samples in triplicate with the following components in a 1.5 mL tube:
    a. 20 µL 10x screening buffer
    b. 20 µL 10 mM $^{18}O_4$-ATP
    c. 100 µL peptide library
    d. 56 µL Milli-Q water
    e. 4 µL inactive kinase mutant (for Chlamydomonas kinases) or 4 µL water for AtPDK.
4. Prepare kinase samples in triplicate using the same components as step 3 but add 4 µL of active kinase for step e.
5. Incubate screenings overnight at room temperature using the Thermomixer (Eppendorf) rotating at 850 rpm.
6. Store screenings at -80 °C until ready for C18 clean up.

7. Prior to C18 clean up, add 300 µL 0.1% TFA to each sample and check to confirm pH <3 prior to clean up.
8. Perform SPE clean up using a 50 mg Sep-Pak for each sample and the protocol used in 2.3.3 with solvent volumes reduced five times to accommodate smaller Sep-Pak volume (e.g. use 1 mL to pre-elute each column).
9. Dry down sample elutions using vacuum centrifugation and store at -80°C until ready for phosphopeptide enrichment.

5.4.2 Phosphopeptide Enrichment

The following protocol uses commercially available 1 mg TiO_2 phosphopeptide enrichment columns (GL Sciences). 500 µg of peptide library is enriched in this protocol, concentrating both the heavy phosphopeptides from the kinase screening and phosphopeptides that were not completely dephosphorylated in the peptide library. Each sample will require a 1 mg TiO_2 column, a centrifuge adaptor, 2 x 1.5 mL tubes, and 1 x 2 mL waste collection tube. All centrifugation steps in this procedure are performed at 1,000 x *g* at room temperature for 3 min unless otherwise noted. To remove any residual phthalic acid from the sample, C18 ZipTips (Millipore) are used to desalt the samples prior to LC-MS/MS. LC-MS grade solvents are used for all of the solutions used in these procedures.

Phosphopeptide Enrichment Procedure:

1. Prepare the following buffers:
    a. 20 mL of Buffer A: 80% acetonitrile, 1% TFA.
    b. 10 mL of Buffer B: 80% acetonitrile, 1% TFA, 25 mg/mL phthalic acid. This can be made by adding 300 mg of phthalic acid to 10 mL of Buffer A.

c. 5 mL of Buffer C: 20% acetonitrile, 5% aqueous ammonia.

2. Resuspend the samples in 70 µL Buffer B. Centrifuge the samples at 15,000 x *g* for 5 min to pellet any insoluble material to prevent tip clogging.
3. Pre-elute each column into a 2 mL waste collection tube by adding 50 µL of Buffer C and centrifuging.
4. Condition each column with 50 µL Buffer A twice and 50 µL Buffer B three times, centrifuging in the 2 mL waste collection tube for all steps.
5. Switch to a new 1.5 mL tube, apply sample to the column, and centrifuge for 3 - 5 min until all of the sample has run through the column.
6. Re-apply the flow-through to the column five times, centrifuging between each step.
7. Switch the column back to the 2 mL waste collection tube and wash the column with 50 µL Buffer B three times and 50 µL Buffer A twice, centrifuging between each step.
8. Switch the column to a new 1.5 mL tube and elute phosphopeptides with 50 µL of Buffer C. Repeat elution with an additional 50 µL of Buffer C, combining this elution with the previous. Dry the elutions using vacuum centrifugation and store at -80 °C until ready for ZipTip clean up.

C18 ZipTip Clean Up Procedure:

1. Prepare a 1 mL aliquot of acetonitrile, and 0.1% TFA in water.
2. For each sample prepare a 1.5 mL tube with 15 µL of 80% acetonitrile, 0.1% TFA to use for elution.
3. Resuspend each sample in 15 µL of 0.1% TFA and centrifuge at 15,000 x *g* for 5 min to pellet any insoluble material. Transfer the sample to a fresh 1.5 mL tube.

4. Attach a ZipTip to a 10 µL pipette set to 10 µL. Use a new ZipTip for each sample, making sure that no air is drawn through the tip during the procedure when pipetting up and down until the elution step by keeping a small volume of solvent above the bed of the column at all times.
5. Pre-elute the ZipTip by pipetting acetonitrile three times, discarding into waste each time.
6. Equilibrate the ZipTip with 0.1% TFA three times, discarding into waste each time.
7. Load the sample by pipetting up and down ten times, discarding the sample back into its tube each time.
8. Wash the ZipTip by pipetting up 0.1% TFA and discarding the waste. Repeat this five times for a total of six wash steps.
9. Elute the sample into the tube containing 80% acetonitrile, 0.1% TFA prepared in step two, pipetting up and down ten times. On the last elution, press the pipette all the way to the second stop to expel any remaining buffer from the tip before discarding the tip in the solid waste.
10. Dry samples using vacuum centrifugation.

5.4.3 LC-MS/MS Analysis

Phosphopeptide samples are resuspended in 20 µL of 5% acetonitrile/0.1%TFA. This resuspension volume allows for the desired injection loading level of 1 µg with an injection volume of about 2-4 µL. This loading can be hard to predict and may vary based on the promiscuity and activity of the kinase influencing the number of phosphopeptides that are enriched prior to LC-MS/MS. A 1 µL test injection should be performed to determine the appropriate loading level.

Configurations for the UPLC are listed in Table 5.3. Mobile phase A is water with 0.1% formic acid and mobile phase B is acetonitrile with 0.1% formic acid. Injections are made with a 5 µL/min flow rate for 3 min onto a Symmetry C_{18} trap column (100 Å, 5 µm, 180 µm x 20 mm, Waters) using 99% A. Samples are separated with a 300 nL/min flow rate on an HSS T3 C18 column (100 Å, 1.8 µm, 75 µm x 250 mm, Waters). Separation is performed in a gradient of 5-35% B over 90 min, followed by a ramp to 85% B in 5 min with a 5 min hold and a return to 5% B in 2 min with a re-equilibration time of 13 min, for a 120 min total run time.

The mass spectrometer is operated (Table 5.4) in positive polarity with a Nanospray Flex Ion Source (ThermoFisher) with a 2.1 kV spray voltage, 325 °C capillary temperature and S-lens RF level of 40. Lock masses of background polysiloxane ions are included. Full MS/DD-MS^2 scan type is used with a method duration of 120 min. During acquisition (Table 5.5) MS survey scans are performed in profile mode across 350-1600 *m/z* at 120,000 resolution (at *m/z* 200) with a 50 ms maximum IT and $3x10^6$ AGC target. The top 20 features with a +2 to +7 charge state above 5000 counts are selected. MS^2 scans are collected at 45,000 resolution with NCE at 32 until 100 ms maximum IT or $1x10^5$ AGC target. The dynamic exclusion window is set to 10 s and an isolation window of 0.7 *m/z* for precursor ions.

5.4.4 Data Processing

Following data acquisition, steps to align experimental runs, infer protein identifications, and provide quantitative information are necessary to identify putative kinase substrates. This is done using Progenesis QI for Proteomics (Nonlinear Dynamics) as discovery analysis software, Mascot Daemon (Matrix Science) for protein identification, and custom R scripts for data filtering. These scripts are adapted from the label-free quantitative workflow used by the Hicks Lab and are available via GitHub (https://github.com/hickslab/QuantifyR).

Procedure:

1. Create a new experiment in Progenesis QI for Proteomics (v 2.0, Waters). Make sure "Profile data" and "High resolution mass spectrometer" are selected.
2. Import acquired spectra, selecting the "Thermo(.raw)" file type.
3. Start automatic processing.
    a. Allow an alignment reference to be assigned automatically.
    b. Allow Progenesis to automatically align the runs and perform peak picking with the peak picking setting set to the maximum sensitivity under the peak picking limits tab of the parameters.
    c. Unselect the box labeled "Set up experiment design."
    d. Allow Progenesis to perform protein quantitation with default settings of "Relative Quantitation using Hi-N" and N set to 3 with protein grouping selected.
4. After automatic processing is complete, check to make sure all runs aligned and have an alignment score > 80%.
5. In the "Experiment Design Setup" stage, set up a "Between-subject Design" and select to group the runs manually.
    a. Select all of the control runs and add them to a condition.
    b. Select the remaining kinase runs and add them to a separate condition.
6. Complete the sections in Progenesis until the "Identify Peptides" stage. Select "Mascot" from the drop-down list of search programs, and then export the MS/MS spectra. This will create a merged peak list in a *.mgf file format.

7. Perform a Mascot database search using the parameters outlined below (Table 5.6). Upload the *.mgf file, select the appropriate parameter file, and name the task in the upper right corner, before submitting the search. The parameter file should include:
    a. The *Chlamydomonas reinhardtii* JGI v5.6 Phytozome database (https://phytozome-next.jgi.doe.gov/info/Creinhardtii_v5_6, 19,523 entries) appended with the entries from the NCBI chloroplast (BK000554.2, 68 entries) and mitochondrial (NC_001638.1, 8 entries) databases as well as the sequences for common laboratory contaminants (www.thegpm.org/cRAP, 116 entries).
    b. Select to perform a target decoy MS/MS search.
    c. Select trypsin specificity of up to two missed cleavages for enzyme.
    d. Use a peptide mass tolerance of 15 ppm, and a fragment mass tolerance of 0.02 Da.
    e. Include carbamidomethylation of cysteine as a fixed modification with acetylation at the protein N-terminus, oxidation of methionine, and heavy phosphorylation (18O-Phospho) of serine, threonine, and tyrosine included as variable modifications. This modification that is a custom modification added to the Hicks lab Mascot Daemon.
8. After completion of the search, adjust the false discovery rate to be less than 1% using the embedded Percolator algorithm[36], and export the search results as an *.xml.
9. Upload this file into Progenesis in the Identify Peptides tab for peak matching. After matching, remove identifications with a Mascot score less than 13 in the “Refine Identifications” stage.
10. Export the protein and peptide measurements for the enriched samples from the “Review Proteins” stage, using the default options.

11. In RStudio, create a new R script and copy the code under the "Phosphorylation" LFQ workflow from the Hicks Lab GitHub (https://raw.githubusercontent.com/hickslab/QuantifyR/master/workflow/Phospho-LFQ.R).
12. Set the working directory on line 21, selecting the folder where the protein and peptide measurement *.csv files are located. In this folder, add the *.fasta file for the corresponding database used to perform the Mascot search.
13. Make the following changes to the Process portion of the R script:
    a. On line 31 and 35, add in the name of the peptide and protein measurement file names, respectively.
    b. On line 42, add in the name of the database used to perform the Mascot search.
    c. On line 48, set the values to correspond with the peptide measurements file columns where the normalized abundance values are located.
    d. On lines 57 and 58, set the modification for the *filter* and *get_identifier* functions to "18O-Phospho".
14. Run the Process portion of the script and save the output to a *.csv file.
15. Make the following adjustments to the R script in the Analyze portion:
    a. Set the column indices for the control (a) and kinase (b) conditions. Adjust the names for these groups on line 87 and 89 to match the conditions and the comparison being performed.
    b. On line 99, set the number of nonzero values to 2.
16. Run the Analyze portion of the script through the *calculate_ttest* function and save the output to a *.csv file. This file can be opened in Excel and filtered by fold-change and *p*-

value to identify potential substrates of the kinase of interest (*i.e.* those heavy phosphopeptides that are significantly higher in abundance in the kinase samples when compared to the control).

17. Optional: Use the Volcano Plot under the Plot portion of the script to visualize the *p*-values and fold changes of the identified heavy phosphorylation sites.

5.5 Conclusions

Completion of all of the steps contained in this procedure typically takes 2-3 weeks in total. The peptide substrate library can be prepared in bulk well ahead of screening and stored in aliquots at -80 °C. A practice expression and purification that is then checked via SDS-PAGE is recommended prior to creation of a kinase sample that is then used for screening. With using freshly prepared kinase sample, it can be challenging to run a gel confirming successful purification prior to screening, so being comfortable with the procedure is important. Any new constructs that are expressed should have their sequences confirmed via MS prior to using them for any screening, particularly confirmation of the mutation site of any new inactive kinase mutants. Confirmation of correct substrate library preparation via MS is also recommended. The most challenging portions of this procedure is the timing associated with preparing the kinase sample directly before screening. Two full uninterrupted sequential lab days are needed for cell lysis, affinity purification, buffer exchange, and screening.

In the future, implementation of an easy kinase activity confirmation assay could ease the scheduling burden of this method and allow for more flexibility in the timing of the preparation of the kinase and screening samples. There appear to be challenges with the activity of the Chlamydomonas kinase constructs that may require additional optimization of the screening parameters to see detectable phosphorylation in this method. The availability of a simple way to

measure the activity of a given kinase construct would make this optimization significantly easier. Additionally, while batch-style purification is a quick and simple method for affinity purification, implementation of a chromatographic based approach with the use of Fast Protein Liquid Chromatography (FPLC) could provide a better purification with a higher protein yield. Automation of preparative chromatography could also allow for additional purification steps, such as implementation of size-exclusion to create a more purified sample. While there is room for improvements in this procedure, they provide a good basis for the heterologous expression and purification of kinases (and other enzymes) as well as creation of peptide libraries from cell lysates for screening of enzymes or other *in vitro* analyses.

5.6 Tables

Table 5.1 Plasmid size and concentration needed for Genewiz Sanger Sequencing.

DNA length including vector (kb)	Template concentration (ng/μL) in 10 μL	Template Total Mass (ng)
<6	~50	~500
6-10	~80	~800
>10	~100	~1,000

Table 5.2 Primers for plasmid mutagenesis for expression of inactive kinase mutants.

Primer Name	Target Gene	Function	Sequence	Melting Temp (°C)
MF014	CrTOR-EKD	Forward	5'-GGCCTGGGCGcCCGCCACCCC-3'	82
MF015	CrTOR-EKD	Reverse	5'-CAGGATGTAGCCCACCATGGACATGACGGC-3'	78
MF011	CrS6K	Forward	5'-GTTCATCGTGcTCTGAAACCG-3'	59
MF013	CrS6K	Reverse	5'-AATACCGCGTGAATGCAG-3'	63
MF009	CrGSK3	Forward	5'-TGTCATCGTGcTATTAAACCG-3'	56
MF010	CrGSK3	Reverse	5'-AATGCCCATTTTATGAATAC-3'	56
MF011	CrPDK1	Forward	5'-GTTCATCGTGcTCTGAAACCG-3'	59
MF012	CrPDK1	Reverse	5'-AACCTGTGCTTTACGCAG-3'	63

Table 5.3 Configuration for Waters M Class UPLC operation

UPLC system	Waters M Class
Mobile phase A	0.1% formic acid in water
Mobile phase B	0.1% formic acid in acetonitrile
Trap column	Waters Symmetry C18 (100 Å, 5 µm, 180 µm x 20 mm)
Trapping conditions	5 µL/min for 3 min 99% A and 1% B
Analytical column	Waters HSS T3 C18 (100 Å, 1.8 µm, 75 µm x 250 mm)
Flow rate	300 nL/min
Run time	120 min

Table 5.4 Hardware Configuration for Thermo Fisher Q Exactive HF-X MS Operation

MS system	Thermo Fisher Q Exactive HF-X
Ion source	Thermo Fisher Nanospray Flex Ion Source
Polarity	Positive
Spray voltage	2.1 kV
Capillary temperature	325 °C
S-lens RF level	40

Table 5.5 Method Parameters for Thermo Fisher Q Exactive HF-X MS Operation

Software	Xcalibur
MS1 survey scan	350-1600 m/z
MS1 resolution	120,000
MS1 maximum accumulation time	50 ms
MS1 AGC target	$3x10^6$
DDA selection criteria	Top 20 features +2 to +7 charge state >5000 counts
MS2 resolution	45,000
Normalized collision energy	32
MS2 maximum accumulation time	100 ms
MS2 AGC target	$1x10^5$
Dynamic exclusion window	10 s
Isolation window	0.7 *m/z*

Table 5.6 Screening Mascot search parameters

Database	JGI v5.6 Phytozome *Chlamydomonas reinhardtii* database appended with NCBI mitochondria and chloroplast database and common laboratory contaminants
MS/MS search	Target decoy enabled
Enzyme specificity	Trypsin, up to 2 missed cleavages
Peptide mass tolerance	15 ppm
Fragment mass tolerance	0.02 Da
Fixed modification	Carbamidomethylation (Cys)
Variable modifications	Acetylation (Protein N-term), Oxidation (Met), 18O-Phospho (Ser, Thr, Tyr)

5.7 Figures

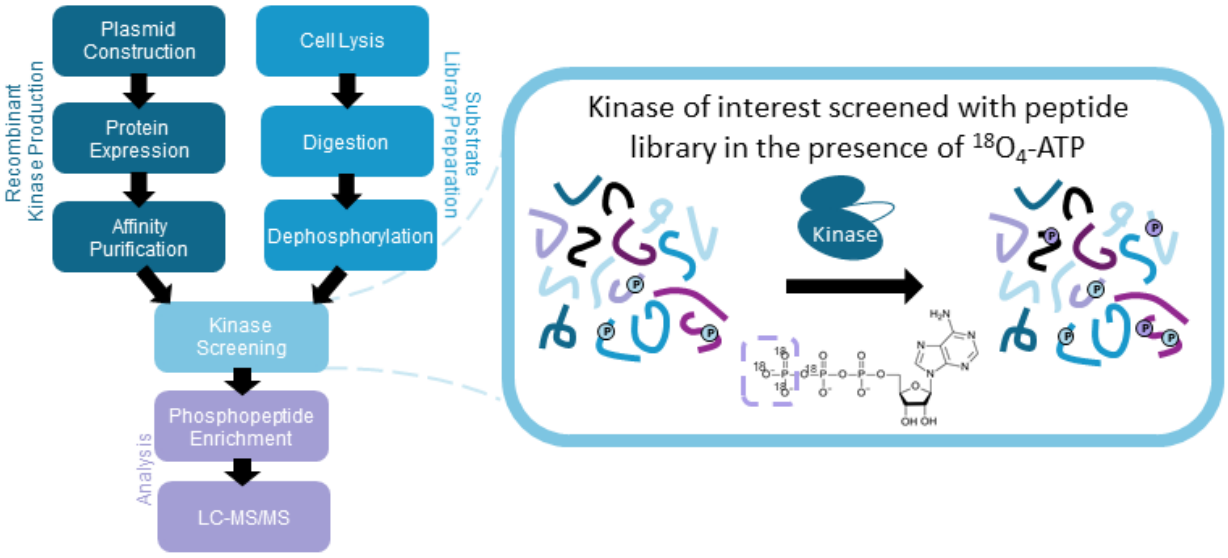

Figure 5.1 Overview of the high throughput kinase screening workflow. Briefly, a plasmid is designed that encodes for a fusion protein of the kinase of interest and an affinity purification tag. Active kinase sample is recombinantly produced by heterologous expression, and then affinity purified. A library of potential substrates is prepared from a cell lysate. The lysate is reduced, alkylated, and digested to form peptides. Then the library is dephosphorylated to remove most of the endogenous phosphorylation prior to screening. For kinase screening, the active kinase sample is combined with the prepared peptide and an isotopic analog of ATP. This analog has four 18-Oxygens on the γ-phosphate group, so the resulting phosphorylation event has three 18-Oxygens, making it 6 Da heavier than any endogenous phosphorylation that may be present. After screening, phosphopeptides are selectively enriched using TiO_2 before LC-MS/MS analysis.

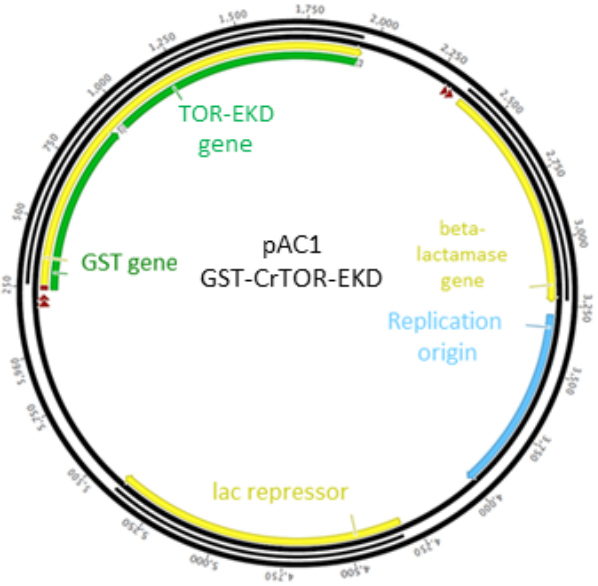

Plasmid Name	Construct	Plasmid Size (bp)	Gene size (bp)	Fusion protein weight (kDa)
pAC1	GST-CrTOR-EKD	5960	999	65.03
pCBxx70	GST-CrS6K	8194	3228	134.19
pCB128	GST-CrGSK3	6449	1479	81.99
pCB129	GST-CrPDK1	6239	1278	72.58
pMF010	GST-CrTOR-EKD D239A	5960	999	64.98
pMF011	GST-CrS6K D812A	8194	3228	134.14
pMF001	GST-CrGSK3 D288A	6449	1479	81.94
pMF002	GST-CrPDK1 D151A	6239	1278	72.54

Figure 5.2 Map of the pGEX-6P1 vector pAC1 with CrTOR-EKD sequence inserted. This plasmid encodes for the fusion protein GST-CrTOR-EKD as well as β-lactamase, which provides resistance to ampicillin for selection of cells transformed with the plasmid. pGEX vectors use the lac operon for induced expression of the fusion protein, so the lac repressor gene is encoded on the plasmid in addition to the replication origin. Similar plasmids were also constructed for CrS6K, CrGSK3, and CrPDK1.

>Cre13.g579200.t1.2 | Ribosomal protein S6 kinase (CrS6K)
MPTLNPSAAEFNPTKWASAAKSGQQHNQQQHTHHKNAGASAPASAHPVAS
GHGPAKPPQEADFPALGGAAANVAAAGGNQAPGAKSWKNVAGPAQTAAAP
VAAAPAQAPRPASAAPAAPPANAWPLLGEAGRANGHHPPPPAGHPQQQQT
APARAPLMVPQGRFPGAGAPPPPQPNGARGAKQQPQHAPPPPPPPAGQAG
AGTAGAPPTQHQQQGGRKAQQQQQQQQQQQHQQNGRSSLKPAFDGLAQQA
AVNALTGSGGARGGASAGTAAAPHTTPGAAGPTPFGTTAAQAPPAGFHVN
PTSAAAAAAAAAAAASTTTPTGKAPGAKPTRKASPLTAALNNAGSGGGGGG
GSSAENSNHNSPRRGPGGAANGHGHGPKPSHPPSSSATPIPARGGRMAPL
VPPSPGGGGGGGGGGGGGAHTLSPGSGSAASSSAAITPSMPIAIRSRGSR
QQLTMVEVMEAEEDEERSRRIQQRRDGKAAAEAAAAVAAAAPPGAAKGGA
AAPPAAPAGAAGAAAGAGGGKGVGAGPGGRALQAGPHEESMTFEEQFDTH
SQASRTSSIASRPSEALSYNISGDQPDGAAIAAAAAAAAAALELNGGSPS
ASDGGAAAAAAGRLDEAMVEAASDHAGGGDGASGDLLLREAQLEMEVDGP
VSCPQLHGTEEAAKRAEAVAAAAHIEPFVPPGKVGPQDFEMLRVVGQGAF
GKVFQVMHKATKTIYAMKVMRKERILQRDHSEYVRSERDLLTAVVHPYIV
TLRFSFQTPTKLYLVLDFLNGGHLFFNLYRQGVFSEDVARLYTAEIVLAI
SYLHSRGIVHRDLKPENVLLDNEGHVRLTDFGLAKGNMGCEQSRTNSFIG
TMEYMAPEIIEAKGHGKAVDWWSTGILMYEMLCGVPPFRAKSRQALQQQI
ATGKVKYPKFLSTDSQSLLKGLLIRDPNKRLGAGADGSAAVKRHAFFKSI
NWAKLEARQIESKFKPTVTCNMDIGNFDKIWTDQPAVDSPCGTPTVASLG
RFDGFTYVAPCFLGTEQGAAAMAGVAATAQAAVDAVAAAAAAIAAAGGAA
GGAAAPPPPPAVEGAAAVAVGAAGH*

>Cre11.g467568.t1.1 | 3\'-phosphoinositide-dependent protein kinase 1 (PDK1)
MASEEGLRDREQQEGYRAPRVTLTIKDFDVLGRIGDGSFSTVFLARQKQS
GKQYAIKMMNKHLVMRNKMVEYIKNERFILDKFDDAGIAKLHFTFQDPDN
LYMGMEYCAGGELYEQINKRGRLPLEAVRFYAAEVVLILEYLRKAQVVHR
DLKPENLLLSGDGHLKLIDFGSARAFFLPAAEKPPGKQRATSFVGTAEYV
SPEVLLNAPLSYPADLWALGCMIYQMIVGRPPFKAASEYLTFQKITDREF
AYPGDPGYNADGEPDDEEGGEEEEEEAGGKEGKAEGGAAAVEAAAQREGA
DAEAAAAGGEGAGSSSGAGTGGGGGGLGAAGKVPKLRGPVVYPDDARDLT
DRLLTMEPAARIGAEDMAELRAHPFFAGVDWAALRAGPAPPYLPPRVPGA
PGSDGGYEEGLDWELTSLVRDAAES*

Legend:
Kinase Domain
HRD Motif
Inserted S6K Sequence

>Cre12.g511850.t1.2 | Glycogen Synthase Kinase 3 (GSK3)
MKARGVLSRSLRNICGALGPCATKLFKTHSLTFRNANGDPRLSLLRQGRV
HPSSHIRPLRSTAPQRPHSAWTPVLDLRVAQVAMSASVANPAQQPSVSGN
DLQQGMKELNIKDKDDEAGSSKAQQNAATAEIFEGRLIEGDLKTGGHVLS
ASSGTGASRQTYNYSTDRVVGNGSFGVVFQATCLETGETVAIKKVLQDKR
FKNRELQIMKLVDHPNIVKLKHCFYSHTDKDETYLHLVLEFVPDTVYRIS
KHYAKNNQRMPNLFVKLYAYQMCRALNSIHKMGICHRDIKPQNLLVNTET
HQLKLCDFGSAKVLVKGEPNISYICSRYYRAPELIFGATDYTSAIDVWSV
GCVLAELLLGQPLFPGESGVDQLVEIIKVLGTPTREEINAMNPNYTEFKF
PQIKAHPWTKVFSKRMPPDAVDLVSKLLQYAPQKRMTAVQAMTHPFFDEL
RDPATRLPNGRALPPLFNWLPGELDEVPADIVRKLQPVAKAS*

>Cre09.g400553.t1.1 Trp2210-Trp2691 | Target of Rapamycin - Extended Kinase Domain (CrTOR-EKD)
WDLYYHVFKRINKQLHSLTTLELQYVSPALVRAQGLELAVPGTYIAGEPL
VTIAAFAPQLHVISSKQRPRKLTIHGGDGAEYMFLLKGHEDLRQDERVMQ
LFGLVNTMLAHDRITAERDLSIARYAVIPLSPNSGLIGWVPNCDTLHALI
REYREARKIPLNWEHRLMLGMAPDYDHLTVIQKVEVFEYALDSTSGEDLH
KVLWLKSRNSEVWLDRRTNYTRSAAVMSMVGYILGLGDRHPSNLMLDRYS
GKLLHIDFGDCFEASMNREKFPEKVPFRLTRMMIKAMEVSGIEGNFRTTC
ENVMRVLRSNKESVTAMLEAFVHDPLINWRLLNTTEAATEAALARTDGGG
GGGGHMDGPGGHPGGRDALGGGGGGAGGGGGGDPGAMPSPPRRETREKEL
KEAFVNLGDANEVLNTRAVEVMKRMSDKLMGRDYAPELCVGGGSGASGME
PDSVPAQVGRLINMAVNHENLCQSYIGWCPFW*

Figure 5.3 The sequences for CrS6K, CrPDK1, CrTOR-EKD, and CrGSK3. The kinase domains for each protein are underlined, and the conserved HRD domains are bolded and highlighted in blue.

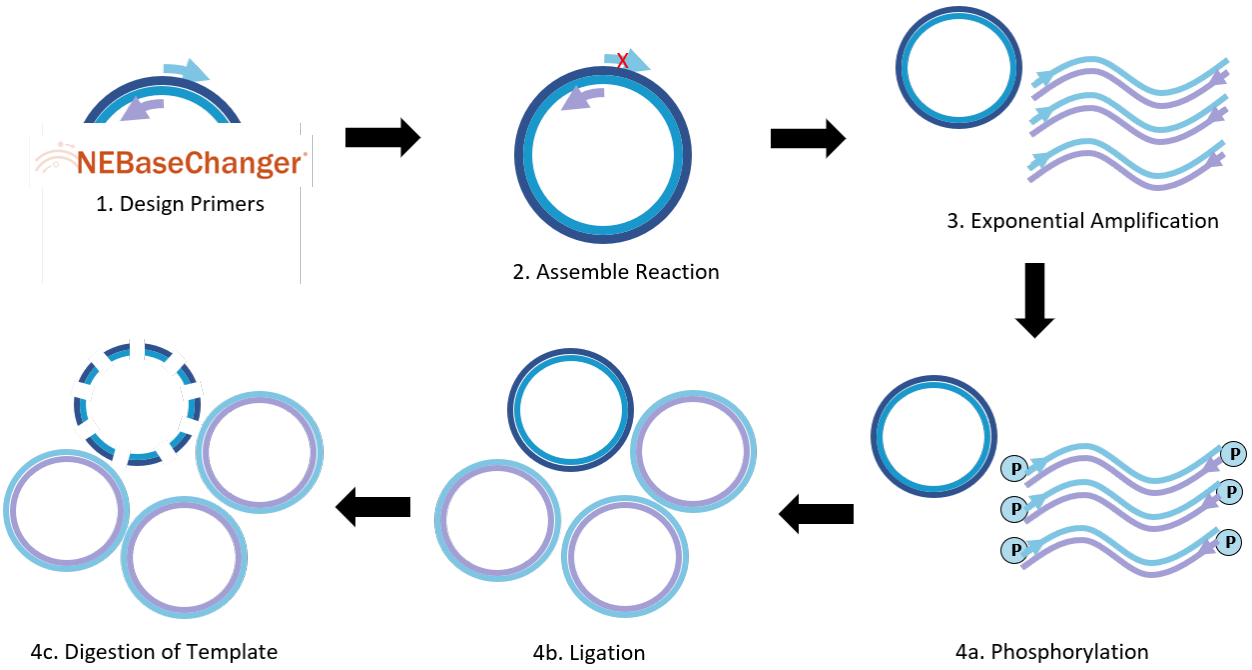

Figure 5.4 Overview of the creation of inactive kinase mutants using the Q5 site-directed mutagenesis kit. NEBaseChanger was used to design non-overlapping primers that contain a single base change that modifies the aspartic acid of the HRD motif to an alanine on the forward primer. PCR is used to exponentially amplify the plasmid using the mutant primers and the Q5 Hot Start High-Fidelity DNA Polymerase. After PCR, the amplified DNA is added to the Kinase-Ligase-DpnI (KLD) enzyme mix for phosphorylation and ligation of the mutant plasmids as well as digestion of the parent template. After this the plasmids are transformed into competent *E. coli* cells, and colonies containing the plasmid are selected for using antibiotic resistance. Sequencing was done on the resulting plasmid to confirm correct substitution.

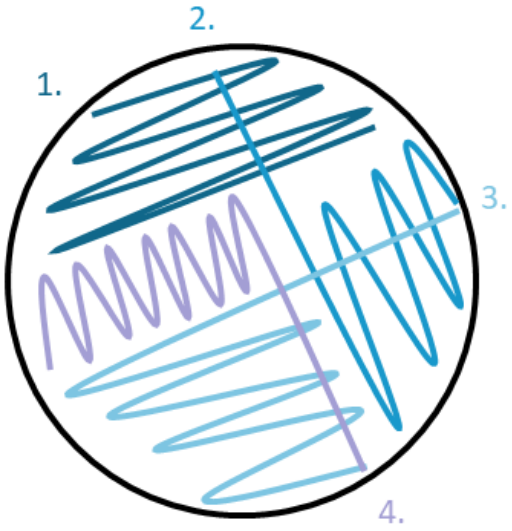

Figure 5.5 Streaking format for *E. coli* plates to allow for growth of individual colonies. Plates are streaked one quadrant at a time, as denoted by the numbering and color coding, with each quadrant using a fresh inoculation loop. The first quadrant is streaked from a small amount of the glycerol stock with each subsequent quadrant diluting from the previous with a single stroke with the fresh inoculation loop.

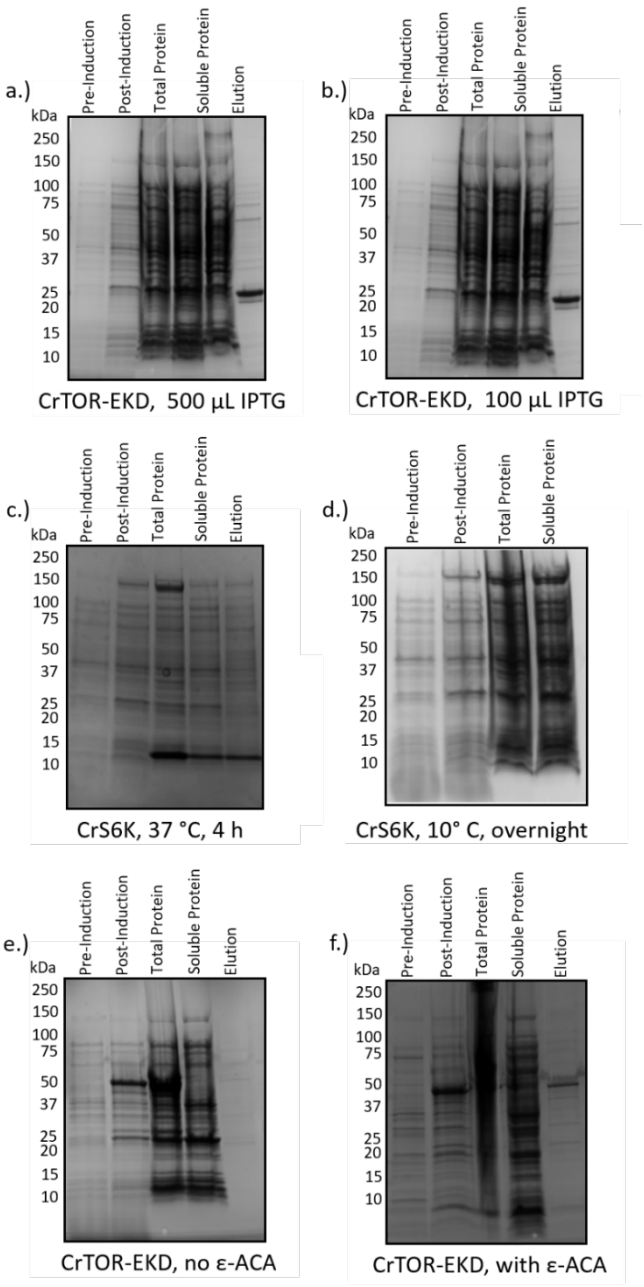

Figure 5.6 Gel results of optimization of kinase expression and purification. Expression of CrTOR-EKD with 500 µL 1 M IPTG stock a.) vs 100 µL 1 M IPTG stock b.) showed no apparent difference in total purified protein abundance. Expression of CrS6K at 37 °C for 4 h c.) vs at 10 °C overnight d.). Little to no soluble CrS6K was seen when expressed at a higher temperature, but appeared to be slightly higher in concentration when expressed for longer at a lower temperature. Expression of CrTOR-EKD without e.) and with f.) ε-ACA. More CrTOR-EKD is seen in the elution when ε-ACA is added.

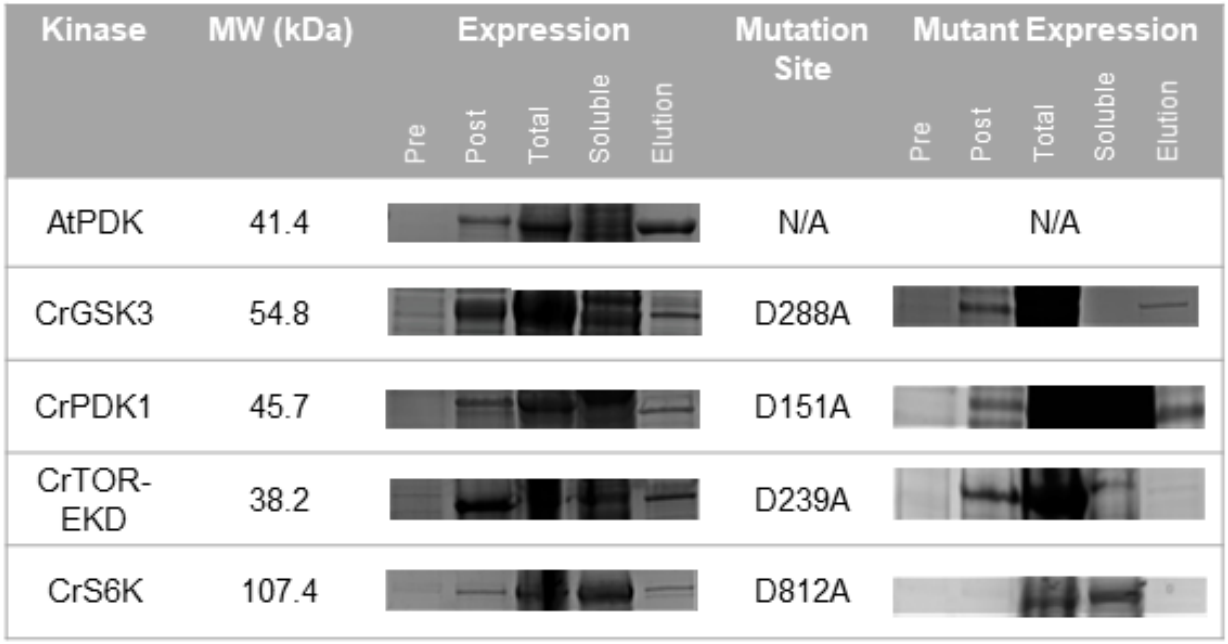

Figure 5.7 Expression results of the kinase constructs and their corresponding mutants, where relevant. Expression was monitoring using SDS-PAGE, with gel samples taken before and after expression, after lysis, and before and after purification. LC-MS/MS confirmed expression of all of the constructs, but CrTOR-EKD D239A and CrS6K D812A in particular were challenging to express, with no visible band present in the elution samples.

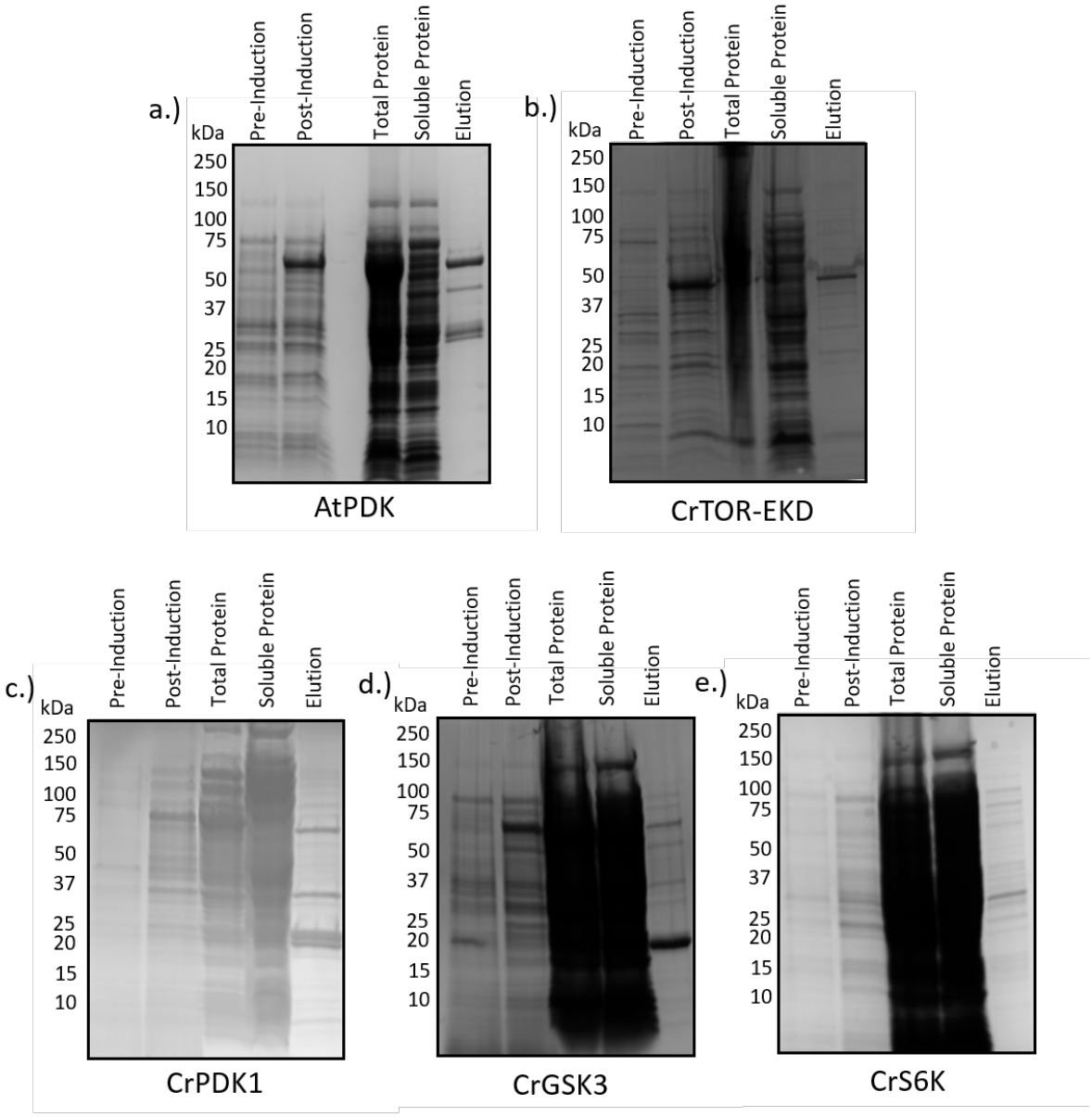

Figure 5.8 Full gel expression results for the kinase screening constructs. Expression was monitored using SDS-PAGE, with gel samples taken before and after expression, after lysis, and before and after purification. a.) Gel results of AtPDK expression. There is some evidence of partial expression of the construct based on the presence of multiple bands in the elution. b.) Gel results of CrTOR-EKD expression. c.) Gel results of CrPDK1 expression. A large band is seen at the molecular weight corresponding to the GST tag. This could be due to partial expression of the fusion protein, cleavage of the tag from CrPDK1 after expression, or enrichment of endogenous GST. d.) Gel results of CrGSK3 expression. Similar to CrPDK1, a large band is seen at the molecular weight corresponding to GST. e.) Gel results of CrS6K expression.

REFERENCES

1. Zones, J. M.; Blaby, I. K.; Merchant, S. S.; Umen, J. G. High-Resolution Profiling of a Synchronized Diurnal Transcriptome from Chlamydomonas reinhardtii Reveals Continuous Cell and Metabolic Differentiation. *Plant Cell* **2015**, *27* (10), 2743–2769.

2. Huang, L.-F.; Lin, J.-Y.; Pan, K.-Y.; Huang, C.-K.; Chu, Y.-K. Overexpressing Ferredoxins in Chlamydomonas reinhardtii Increase Starch and Oil Yields and Enhance Electric Power Production in a Photo Microbial Fuel Cell. *Int. J. Mol. Sci.* **2015**, *16* (8), 19308–19325.

3. Studier, F. W.; Moffatt, B. A. Use of Bacteriophage T7 RNA Polymerase to Direct Selective High-Level Expression of Cloned Genes. *J. Mol. Biol.* **1986**, *189* (1), 113–130.

4. de Boer, H. A.; Comstock, L. J.; Vasser, M. The Tac Promoter: A Functional Hybrid Derived from the Trp and Lac Promoters. *Proc. Natl. Acad. Sci. U.S.A.* **1983**, *80* (1), 21–25.

5. Protein Production and Purification. *Nat. Methods* **2008**, *5* (2), 135–146.

6. Ren, M.; Qiu, S.; Venglat, P.; Xiang, D.; Feng, L.; Selvaraj, G.; Datla, R. Target of Rapamycin Regulates Development and Ribosomal RNA Expression through Kinase Domain in Arabidopsis. *Plant Physiol.* **2011**, *155* (3), 1367–1382.

7. Díaz-Troya, S.; Florencio, F. J.; Crespo, J. L. Target of Rapamycin and LST8 Proteins Associate with Membranes from the Endoplasmic Reticulum in the Unicellular Green Alga Chlamydomonas reinhardtii. *Eukaryot. Cell* **2008**, *7* (2), 212–222.

8. Skamnaki, V. T.; Owen, D. J.; Noble, M. E.; Lowe, E. D.; Lowe, G.; Oikonomakos, N. G.; Johnson, L. N. Catalytic Mechanism of Phosphorylase Kinase Probed by Mutational Studies. *Biochem.* **1999**, *38* (44), 14718–14730.

9. Gibbs, C. S.; Zoller, M. J. Rational Scanning Mutagenesis of a Protein Kinase Identifies Functional Regions Involved in Catalysis and Substrate Interactions. *J. Biol. Chem.* **1991**, *266* (14), 8923–8931.

10. Madhusudan; Akamine, P.; Xuong, N.-H.; Taylor, S. S. Crystal Structure of a Transition State Mimic of the Catalytic Subunit of CAMP-Dependent Protein Kinase. *Nat. Struct. Biol.* **2002**, *9* (4), 273–277.

11. Adams, J. A. Kinetic and Catalytic Mechanisms of Protein Kinases. *Chem. Rev.* **2001**, *101* (8), 2271–2290.

12. Oruganty, K.; Talathi, N. S.; Wood, Z. A.; Kannan, N. Identification of a Hidden Strain Switch Provides Clues to an Ancient Structural Mechanism in Protein Kinases. *Proc. Natl. Acad. Sci. U.S.A.* **2013**, *110* (3), 924–929.

13. Rosano, G. L.; Ceccarelli, E. A. Recombinant Protein Expression in Escherichia coli: Advances and Challenges. *Front. Microbiol.* **2014**, *5*.

14. Prasad, S.; Khadatare, P. B.; Roy, I. Effect of Chemical Chaperones in Improving the Solubility of Recombinant Proteins in Escherichia Coli. *Appl. Environ. Microbiol.* **2011**, *77* (13), 4603–4609.

15. Goldberg, A. L. Effects of Protease Inhibitors on Protein Breakdown and Enzyme Induction in Starving Escherichia Coli. *Nat. New Biol.* **1971**, *234* (45), 51–52.

16. Liu, Y.; Schulze-Makuch, D.; de Vera, J.-P.; Cockell, C.; Leya, T.; Baqué, M.; Walther-Antonio, M. The Development of an Effective Bacterial Single-Cell Lysis Method Suitable for Whole Genome Amplification in Microfluidic Platforms. *Micromachines (Basel)* **2018**, *9* (8).

17. Berg, J. M.; Tymoczko, J. L.; Stryer, L. The Purification of Proteins Is an Essential First Step in Understanding Their Function. *Biochemistry.* 5th edition*;* W.H. Freeman, New York, NY, USA; **2002**.

18. Frangioni, J. V.; Neel, B. G. Solubilization and Purification of Enzymatically Active Glutathione S-Transferase (PGEX) Fusion Proteins. *Anal. Biochem.* **1993**, *210* (1), 179–187.

19. Smith, G. M. The Nature of Sexuality in Chlamydomonas. *Am. J. Bot.* **1946**, *33* (8), 625–630.

20. Smith, G. M.; Regnery, D. C. Inheritance of Sexuality in Chlamydomonas reinhardi. *Proc. Natl. Acad. Sci. U.S.A.* **1950**, *36* (4), 246–248.

21. Werth, E. G.; McConnell, E. W.; Gilbert, T. S. K.; Couso Lianez, I.; Perez, C. A.; Manley, C. K.; Graves, L. M.; Umen, J. G.; Hicks, L. M. Probing the Global Kinome and Phosphoproteome in Chlamydomonas reinhardtii via Sequential Enrichment and Quantitative Proteomics. *Plant J* **2017**, *89* (2), 416–426.

22. McConnell, E. W.; Werth, E. G.; Hicks, L. M. The Phosphorylated Redox Proteome of Chlamydomonas reinhardtii: Revealing Novel Means for Regulation of Protein Structure and Function. *Redox Biol.* **2018**, *17*, 35–46.

23. Werth, E. G.; McConnell, E. W.; Lianez, I. C.; Perrine, Z.; Crespo, J. L.; Umen, J. G.; Hicks, L. M. Investigating the Effect of Target of Rapamycin Kinase Inhibition on the Chlamydomonas reinhardtii Phosphoproteome: From Known Homologs to New Targets. *New Phytol.* **2019**, *221* (1), 247–260.

24. Ford, M. M.; Smythers, A. L.; McConnell, E. W.; Lowery, S. C.; Kolling, D. R. J.; Hicks, L. M. Inhibition of TOR in Chlamydomonas reinhardtii Leads to Rapid Cysteine Oxidation Reflecting Sustained Physiological Changes. *Cells* **2019**, *8* (10), 1171.

25. Gorman, D. S.; Levine, R. P. Cytochrome f and Plastocyanin: Their Sequence in the Photosynthetic Electron Transport Chain of Chlamydomonas reinhardtii. *Proc. Natl. Acad. Sci. U.S.A.* **1965**, *54* (6), 1665–1669.

26. Imam, S. H.; Buchanan, M. J.; Shin, H. C.; Snell, W. J. The Chlamydomonas Cell Wall: Characterization of the Wall Framework. *J. Cell Biol.* **1985**, *101* (4), 1599–1607.

27. Xu, X.; Liu, X.; Nie, Z.; Pan, Y.; Guo, M.; Yao, S. Label-Free Fluorescent Detection of Protein Kinase Activity Based on the Aggregation Behavior of Unmodified Quantum Dots. *Anal. Chem.* **2011**, *83* (1), 52–59.

28. Hastie, C. J.; McLauchlan, H. J.; Cohen, P. Assay of Protein Kinases Using Radiolabeled ATP: A Protocol. *Nat. Protocols* **2006**, *1* (2), 968–971.

29. Shults, M. D.; Janes, K. A.; Lauffenburger, D. A.; Imperiali, B. A Multiplexed Homogeneous Fluorescence-Based Assay for Protein Kinase Activity in Cell Lysates. *Nat. Methods* **2005**, *2* (4), 277–284.

30. Lesaicherre, M.-L.; Uttamchandani, M.; Chen, G. Y. J.; Yao, S. Q. Antibody-Based Fluorescence Detection of Kinase Activity on a Peptide Array. *Bioorganic Med. Chem. Lett.* **2002**, *12* (16), 2085–2088.

31. Wu, Z. L. Phosphatase-Coupled Universal Kinase Assay and Kinetics for First-Order-Rate Coupling Reaction. *PLoS ONE* **2011**, *6* (8), e23172-.

32. Iliuk, A. B.; Tao, W. A. Universal Non-Antibody Detection of Protein Phosphorylation Using PIMAGO. *Curr. Protoc. Chem. Biol.* **2015**, *7* (1), 17–25.

33. Xue, L.; Wang, P.; Cao, P.; Zhu, J.; Tao, W. A. Identification of Extracellular Signal-Regulated Kinase 1 (ERK1) Direct Substrates Using Stable Isotope Labeled Kinase Assay-Linked Phosphoproteomics. *Mol. Cell Proteomics* **2014**, *13* (11), 3199–3210.

34. Beullens, M.; Vancauwenbergh, S.; Morrice, N.; Derua, R.; Ceulemans, H.; Waelkens, E.; Bollen, M. Substrate Specificity and Activity Regulation of Protein Kinase MELK. *J. Biol. Chem.* **2005**, *280* (48), 40003–40011.

35. Charter, N. W.; Kauffman, L.; Singh, R.; Eglen, R. M. A Generic, Homogenous Method for Measuring Kinase and Inhibitor Activity via Adenosine 5'-Diphosphate Accumulation. *J. Biomol. Screen* **2006**, *11* (4), 390–399.

36. Käll, L.; Canterbury, J. D.; Weston, J.; Noble, W. S.; MacCoss, M. J. Semi-Supervised Learning for Peptide Identification from Shotgun Proteomics Datasets. *Nat. Methods* **2007**, *4* (11), 923–925.

CHAPTER 6: Developing an *in vitro* Platform for Investigating TOR Pathway Kinase-Substrate in *Chlamydomonas reinhardtii*

6.1 Introduction

Since the discovery of glycogen phosphorylase activation via phosphorylation by Fisher and Krebs over 60 years ago[1,2] the regulation of enzymes through phosphorylation has been extensively studied. In plants, reversible protein phosphorylation and dephosphorylation by kinases and phosphatases, respectively, has been shown to control signal transduction pathways that regulate many essential cellular activities including the cell cycle[3], metabolism[4], and stress response[5]. Despite the importance of phosphorylation in cell regulation, kinase-substrate relationships are not well characterized. While it is estimated that 30% of eukaryotic proteins are targets of phosphorylation[6], less than 3% of phosphorylation events detected in humans are linked to a specific kinase experimentally[7] and even fewer for plant model organisms. This lack of information is due in part to the large scale of these signaling networks, particularly in photosynthetic organisms. *Arabidopsis thaliana,* a model plant species, has an estimated 942 kinases[8], nearly double the number predicted in humans[9], and over 55,000 phosphorylation sites[10–12], while *Chlamydomonas reinhardtii*, a model photosynthetic microalgal organism, has an estimated 355 kinases[13] with 18,000 potential phosphorylation sites[14]. The prevalence, importance, and complexity of phosphorylation signaling in phototrophs drives the interest in studying kinase-substrate relationships using high-throughput screening approaches.

In plants, strategies that have been implemented to identify substrates for kinases include two-hybrid screening, tandem affinity purification, and *in vitro* screening processes[15]. Both two-

hybrid screening and tandem affinity purification rely on capturing the protein-protein interaction of a kinase and its substrate, which can be challenging with substrates of weak affinity. This makes *in vitro* processes appealing alternatives as they allow for targeted screenings without restrictions to kinase type based on the formation of strong enzyme-substrate complexes. *In vitro* approaches in plants usually involve the creation of a library of potential substrates, either intact proteins or smaller peptides, that are then incubated with a kinase of interest. This library can be either (1) synthesized or (2) derived from the organism of interest. In the case of (1), synthetic peptide libraries are designed to have amino acids held fixed at a specific position relative to the potential site of phosphorylation to identify conserved substrate sequence motifs for a kinase of interest[16,17]. The library is incubated with an active form of the kinase obtained either through heterologous expression or purification from its native organism. Synthetic peptide libraries allow for control of substrate abundance, and are easily modified for bead-, surface-, and polymer-based enrichment techniques. However, these screening methods can be laborious because they involve library synthesis, and screening may not result in physiologically relevant motifs or target phosphosites or reveal any unpredicted substrate motifs, contributing to the movement toward naturally produced substrate libraries[18–22]. With (2), a substrate library produced from the kinase's endogenous organism, targets for the kinase are likely to be present either intact in the case of a protein library or in peptidyl form, and screening these libraries can provide potential protein substrate targets that can then be validated. However, substrate abundances in these libraries are hard to control with concentrations of potential substrates being dependent on expression levels at the time of harvest and varying by several orders of magnitude. While a protein library derived from an organism of interest provides a higher level of protein specificity, allowing for specificity factors such as distal docking sites and

scaffold proteins, peptidyl libraries can often simplify the screening process. Dephosphorylation of endogenous phosphorylation is more complete with peptide libraries than protein libraries, creating more potential targets for the kinase. Additionally, protein libraries can contain additional active kinases that need to be inhibited prior to screening to minimize false positives phosphorylation events.

This work presents validation of an *in vitro* kinase screening approach to identify potential substrates for kinases in *C. reinhardtii,* and preliminary screening results of the *Chlamydomonas* Target of Rapamycin (CrTOR) kinase. This screening platform, which is explained in detail in Chapter 5, uses a peptide substrate library created from a proteome extracted from the organism of interest along with an isotopic analog of ATP to identify targets of a kinase of interest by mass spectrometry (Figure 5.1). This is adapted from previous work showing the use of protein and peptide lysates as substrate libraries for peptide screenings[18–22] with additional label-free quantitative proteomic strategies implemented to prioritize target substrates and minimize false positive identifications. While this platform is adaptable to any source of purified kinase, the kinases were heterologously expressed in *E. coli* and affinity purified using a protein fusion tag for this work. The peptide library was prepared from a *C. reinhardtii* protein digest, and dephosphorylated using rAPid alkaline phosphatase, a commercially produced recombinant enzyme, to remove the majority of endogenous phosphorylation prior to screening. The purified kinase along with the peptide library were incubated with γ-$^{18}O_4$-ATP, which resulted in a "heavy" phosphorylation on the target substrate that contains three Oxygen-18's, making it 6 Da heavier than endogenous phosphorylation. With this mass shift, heavy phosphorylation is easily differentiated from any remaining endogenous phosphorylation by mass spectrometry. Herein, validation experiments use the well-studied pyruvate dehydrogenase kinase from *Arabidopsis*

thaliana (AtPDK) to demonstrate that this platform can successfully identify its known phosphorylation site from the E1α subunit of the pyruvate dehydrogenase complex (AtPDCe1α)[23].

Once the platform is validated, the workflow is applied to investigation of the *Chlamydomonas* TOR pathway. TOR is a serine/threonine kinase conserved in most eukaryotes that has been shown to be a master regulator, and responsible for many cellular signaling pathways involved in metabolism, stress response, response to nutrients, and anabolic functions[24]. It has been shown that TOR signaling in fungi and animals comes from two protein complexes, TORC1 and TORC2[25]. In photosynthetic organisms only homologs of TORC1 have been identified[26], and the exact targets and functions of TOR are not well characterized[27,28]. Based on what is known about mammalian TOR (mTOR), a number of components of the TOR pathway can be predicted in *Chlamydomonas* (Figure 6.1)[29], including ribosomal S6 kinases (S6Ks) which are known direct targets of TOR across many plant and animal species. While both mammalian systems and Arabidopsis have two S6K genes, only one homolog of S6K has been identified in *Chlamydomonas* (CrS6K, Cre13.g579200.t1.2)[30]. Studies in other organisms including human cells lines[31], *Arabidopsis*[32], rice[32], and yeast[33] have identified a Thr in the hydrophobic motif of S6Ks that is a direct target of TOR and an additional Ser that is known to be TOR-mediated, though its exact regulatory mechanism is less established[30]. These two potential phosphorylation sites are also conserved in CrS6K (Thr1006 and Ser989), but are not confirmed as CrTOR targets.

This work shows the successful validation of our *in vitro* screening platform with *Arabidopsis thaliana* (AtPDK) along with the results from the preliminary screening of a fusion protein construct containing the kinase domain of CrTOR (referred to as CrTOR-EKD, see 5.2.1

for details). This includes screenings against digests of heterologously expressed CrS6K, a synthetic peptide containing the conserved TOR-targeted S6K phosphosite and a *Chlamydomonas* peptide library. Constructs of other kinases in the TOR pathway were designed (highlighted in Figure 6.1), but are not included in the preliminary results here. A full list of these kinase constructs, expression and purification conditions can be found in Chapter 5. While a phosphorylation site was not identified on CrS6K in any of the screenings, one potential target peptide was identified from acidic ribosomal protein P2 (Cre02.g143050.t1.2), which may have a role in controlling ribosomal performance or specificity. However, when CrTOR was screened against a synthetic peptide of the same sequence, this activity was not observed.

6.2 Materials and Methods

6.2.1 Bacterial Expression and Purification of AtPDK

A thorough procedure including troubleshooting tips for the methods included here can be found in Chapter 5. *E. coli* cells strain BL21(DE3) transformed with a pMAL DNA vector construct encoding for AtPDK with a MBP fusion protein tag was provided the Miernyk lab from the University of Missouri. Cells were stored as a frozen glycerol stock at -80 °C. Cells were taken from the glycerol stock and grown on a lysogeny broth (LB) agar plate supplemented with 100 µg/mL ampicillin at 37 °C until single colonies were visible. 40 mL of starter culture were prepared in 5 mL aliquots of LB supplemented with 100 µg/mL ampicillin and 2% glucose. Each 5 mL aliquot was inoculated with cells from a single colony on the LB agar plate. These starter cultures were incubated overnight at 37 °C and 240 rpm, giving the cultures adequate time to reach saturation. AtPDK was expressed as 2 1 L cultures from Terrific Broth (TB) supplemented with 100 µg/mL ampicillin and 2% glucose. Cultures were inoculated with cells from 20 mL of starter culture and grown at 37 °C and 240 rpm, monitoring cell density until

mid-log growth was reached, an OD_{600} of approximately 0.5. Stock aminocaproic acid (ε – ACA) solution was added to a final concentration of 1 mM followed by induction with 300 μM IPTG. Cultures were incubated at 37 °C and 240 rpm for 4 h, before cells were harvested via centrifugation, resuspended in 20 mL of amylose column buffer (20 mM Tris-HCl, pH 7.4, 200 mM NaCl, 1 mM EDTA) and combined. The resuspension was then flash frozen and stored at -80 °C.

The sample was thawed in an ice-water bath, and then lysozyme was added at a concentration of 1 mg/mL. The sample was then sonicated using a probe ultrasonicator (Heat Systems) for 1 min with a 50% duty cycle a total of three times, resting for 1 min between each sonication, keeping the sample on ice. The lysate was collected by centrifuging to remove cell debris and insoluble components.

400 μL of amylose resin was washed three times with amylose column buffer before it was added to the cell lysate. The lysate and resin were incubated for 2 h at 4 °C, rotating end over end. Two 50 mL conical tubes were parafilmed over the top and a slit was cut in the center. A Poly-prep column (Biorad) was inserted through the slit so it was suspended in the conical tube and the conical tube was placed on ice. The lysate and resin were poured evenly into the two columns, and the liquid was allowed to flow through the column until a small volume was left above the resin bed. The resin was washed with 10 mL fresh amylose column buffer before bound proteins were eluted in 2 mL elution buffer, amylose column buffer with 10 mM maltose. Samples were stored at 4 °C overnight. The elution was concentrated and buffer exchanged into 20 mM HEPES-KOH with 1x protease inhibitor cocktail (Roche) and 1x PhosSTOP phosphatase inhibitor (Roche) to a final volume of ~0.5 mL. Kinase sample concentration was measured

using a NanoDrop 1000 microvolume spectrometer (ThermoFisher) and adjusted to a concentration of 0.5 mg/mL.

6.2.2 Design of CrTOR Constructs

When using a recombinant host to overexpress a protein, the success of expression is limited by the size of the protein construct. Studies have shown that the probability of successful expression decreases considerably with constructs above 60 kDa due to problems with protein solubility, folding, and aggregation[34]. This is a concern with the expression of CrTOR, which is over 290 kDa in size and composed of almost 2700 amino acids. To address this issue, a construct was designed that contains only a portion of the protein corresponding to the kinase domain identified using the alignment of CrTOR to mammalian TOR (mTOR) via BLAST[35]. While CrTOR activity has never been investigated using only the kinase domain, previous work has shown recovery of TOR function in Arabidopsis TOR (AtTOR) knockout mutants when the strain is complemented with a portion of AtTOR that includes the kinase domain and part of the FKBP12-rapamycin binding (FRB) domain[36]. Additionally, it has been shown when the kinase domain of CrTOR is heterlogously expressed and then immobilized, it has enough structural similarity to full-length CrTOR that it can bind and precipitate Chlamydomonas lethal with SEC13 protein 8 (CrLST8), a known component of TORC1, from a cell extract[37]. Based on this work, the corresponding section of CrTOR was identified, amplified by PCR from a Chlamydomonas cDNA library, digested and cloned into a pGEX6P-1 plasmid for expression in *E. coli* cells. This construct is referred to as the Chlamydomonas TOR extended kinase domain (CrTOR-EKD).

To help reduce the number of false positives that may arise during screening, an inactive mutant form of CrTOR-EKD was used as the negative control for this assay. This mutant was

created using a single amino acid substitution of Asp to Ala in the CrTOR-EKD construct, resulting in the TOR-EKD D239A inactive mutant. The aspartic acid selected for mutation is part of the conserved HRD motif in the kinase domain of TOR that is directly involved in the transfer of the γ-phosphate group from ATP to the target substrate[38]. Mutation at this amino acid results in an inactive domain that is still structurally similar to CrTOR-EKD. Inactive mutants were designed for the other constructs of known TOR pathway kinases. Information on these mutants and gel results confirming their expression can be found in Chapter 5.

6.2.3 Creation of CrTOR-EKD Construct

CrTOR-EKD construct was created through collaboration with Soon Goo Lee (current affiliation: UNC-W). A cDNA fragment of 999 bp length containing the kinase domain and a portion of the FRB domain of Chlamydomonas TOR was amplified from Chlamydomonas mRNA by RT-PCR using the primers 5′-TGGGACCTGTACTACCACGTC-3′ and 5′-GAGCAGGCGCCAGTTGATGAG-3′ obtained from the Crespo lab from previous work studying the CrTOR kinase domain[37]. The PCR amplified cDNA fragment was cloned into the pCR-Blunt II-TOPO cloning vectors (Invitrogen), followed by subcloning into the pGEX-6P-1 expression vector containing a GST tag (GE Healthcare).

6.2.4 Creation of Inactive CrTOR-EKD D239A Mutant Construct

The vector encoding for CrTOR-EKD was mutated using the Q5 Site-Directed Mutagenesis Kit (New England Biolabs) using the manufacturers protocol. Briefly, NEBaseChanger (New England Biolabs) was used to design a forward primer (5’-GGCCTGGGCG**c**CCGCCACCCC-3’) with a single bp substitution to mutate the Asp239 to Ala239 and a reverse primer (5’-CAGGATGTAGCCCACCATGGACATGACGGC-3’). These primers were synthesized by IDT DNA and resuspended in nuclease-free water to a concentration of 10 μM. 12.5 μL Q5 Hot Start

High-Fidelity 2x Master Mix, 1.25 µL of each primer, 1 µL of template DNA and 9 µL nuclease free water were added to a PCR tube. The reagents were mixed and the tube was cycled in a Mastercycler Nexus PCR Cycler (Eppendorf) using the conditions described in the manufacturer's protocol. Following this, 1 µL of this sample was added to a fresh PCR tube along with 5 µL 2X kinase-ligase-Dpn1 (KLD) Reaction Buffer, 1 µL 10X KLD Enzyme Mix and 3 µL nuclease-free water. The reagents were mixed and incubated at room temperature for 5 min.

A tube of NEB 5-alpha competent *E. coli* cells were thawed on ice. 5 µL of the sample from the KLD reaction was added to the tube of thawed cells. The tube was flicked five times to mix and then placed on ice for 30 seconds. The tube was then transferred to a 42 °C hot water bath and heat shocked for 30 seconds. The sample was then placed on ice for 5 min, followed by the addition of 950 µL SOC into the tube. The tube was then incubated at 37 °C, 250 rpm for 60 minutes, before 100 µL of cells were removed and spread onto a selection plate of LB agar with 100 µg/mL ampicillin and incubated overnight at 37 °C. A single colony from this plate was inoculated into 5 mL LB with 100 µg/mL ampicillin and the liquid culture was incubated overnight at 37°C, 240 rpm. From this culture a glycerol stock was made and plasmid was purified from 1 mL of culture using the Qiagen Plasmid Purification kit. This plasmid was sequenced by Genewiz to confirm the mutation with the primer 5'-CTCCGCTATCGCTACGTGAC-3', which anneals across the multiple cloning site of the vector. Additional plasmid was then purified and transformed into BL21(DE3) competent cells (New England Biolabs) using the sample procedure and a glycerol stock of this strain was made.

6.2.5 Synthesis of the CrS6K Construct

A pUC57 vector encoding for the CrS6K sequence provided by the Chlamydomonas database from Phytozome (v5.5) was synthesized by Biomatik. This sequence was then spliced into the pGEX-6P-1 vector. Double-stranded DNA encoding for the missing portion of the CrS6K gene was synthesized by IDT DNA and this was inserted into the pGEX-6P-1 vector containing the original gene sequence by Biomatik. Sequencing of the new plasmid (Genewiz) using the primer 5'-CAATACCGCGTGAATGCAG-3' confirmed the insertion and the new plasmid was transformed into BL21(DE3) competent cells as previously described.

6.2.6 Bacterial Expression and Purification of CrTOR Constructs

E. coli cells strain BL21(DE3) transformed with pGEX-6P-1 plasmids encoding for CrTOR-EKD, CrTOR-EKD D239A, and CrS6K were taken from glycerol stocks and grown on a lysogeny broth (LB) agar plate supplemented with 100 µg/mL ampicillin at 37 °C until single colonies were visible. 120 mL of starter culture were prepared in 5 mL aliquots of LB supplemented with 100 µg/mL ampicillin for each construct. Each 5 mL aliquot was inoculated with cells from a single colony on the LB agar plate. These starter cultures were incubated overnight at 37 °C and 240 rpm, giving the cultures adequate time to reach saturation. The kinases were expressed as 6 1 L cultures from Terrific Broth (TB) supplemented with 100 µg/mL ampicillin. Each culture was inoculated with cells from 20 mL of starter culture and grown at 37 °C and 240 rpm, monitoring cell density until mid-log growth was reached, an OD_{600} of approximately 0.5. Stock aminocaproic acid (ε – ACA) solution was added to a final concentration of 1 mM followed by induction with 100 µM IPTG. Cultures were incubated at 10 °C and 240 rpm overnight, before cells were harvested via centrifugation, resuspended in 10 mL

of PBS, pH 7.4 per L of culture and combined by construct. The resuspension was then flash frozen and stored at -80 °C.

CrS6K was lysed and purified first, with CrTOR-EKD and CrTOR-EKD D239A being lysed and purified directly before screening to minimize free-thaw cycles. The samples were thawed in an ice-water bath, and then lysozyme was added at a concentration of 1 mg/mL. The sample was then sonicated using a probe ultrasonicator (Heat Systems) for 1 min with a 50% duty cycle a total of three times, resting for 1 min between each sonication, keeping the sample on ice. The lysate was collected by centrifuging to remove cell debris and insoluble components.

600 µL of Glutathione Sepharose 4B resin was used to purify each construct. The resin was washed three times with PBS before it was added to the cell lysate. For all steps, resin is collected via centrifugation at 5,000 x *g*, 4 °C for 5 min. The lysate and resin were incubated for 2 h at 4 °C, rotating end over end. The resin was then collected via centrifugation, washed three times with PBS, and then each resin pellet was resuspended in 300 µL Elution Buffer (50 mM Tris HCl, 10 mM reduced glutathione, pH 8.0). The sample was rotated end over end at 4 °C for 10 min. The resin was collected via centrifugation and the elution was collected. This was repeated twice with fresh elution buffer, and all elutions were combined and stored at 4 °C.

For CrTOR-EKD and CrTOR-EKD D239A, the elution was concentrated and buffer exchanged into 20 mM HEPES-KOH with 1x protease inhibitor cocktail (Roche) and 1x PhosSTOP phosphatase inhibitor (Roche) to a final volume of ~0.5 mL. Kinase sample concentration was measured using a NanoDrop 1000 microvolume spectrometer (ThermoFisher) and adjusted to a concentration of 0.5 mg/mL.

6.2.7 Synthesis of Peptide Targets

Peptides were synthesized via semi-automated flow chemistry by the Wommack laboratory at High Point University using an instrument built in-house[39]. Synthesis used 200 mg of 2-chlorotrityl chloride resin (200-400 mesh) pre-loaded with the C-terminal amino acid (0.80 mmol/g). Fmoc-protected amino acids (1 mmol) were solubilized in 2.5 mL of fresh 0.38 M hexafluorophosphate benzotriazole tetramethyl uranium in dimethylformamide (DMF). Rapid Fmoc solid-phase peptide chemistry began after the instrument was prepared with appropriate levels of DMF for washing (40 mL per residue) and 20% piperidine in DMF for Fmoc deprotection (7 mL per residue), heating the water bath to 60 ºC for immersion of the sealed reactor, programing the pump flow rate to 20 mL/min, and assembling the reactor containing pre-weighed resin. To activate the amino acid solutions for coupling, 450 µL of *N*,*N*-diisopropylethylamine (or 250 µL with His, Cys, or Trp) was added and gently mixed. After syringe pump administration of the activated coupling solution at 6 mL/min, the resin was immediately washed at 20 mL/min with DMF for 20 sec, Fmoc deprotected with 20% piperidine in DMF for 30 sec, and washed with DMF for 1 min. Following the coupling and deprotection of the final amino acid, the reactor was disassembled and the resin-bound peptide was eluted with a 10 min incubation at 60 ºC using 10 mL of 94% TFA/4% triisopropylsilane/2% H2O. The crude peptide solution was filtered and the volume was reduced to 5 mL under N_2 gas. The crude peptide solution was cooled to 4 ºC before precipitating with cold diethyl ether. Following centrifugation at 3,000 rpm for 10 min at 4 ºC to collect the crude peptide precipitate, the white solid was resuspended in cold diethyl ether and the centrifugation was repeated. The pellet was dried *in vacuo* to deliver crude peptide. Each synthesized peptide was resuspended in 20 mM HEPES-KOH, pH 7.4 to a final concentration of 1 µg/µL, except for the peptide

GRFDGF**T**YVAPCF, which was resuspended in 20% acetonitrile, 80% 20 mM HEPES-KOH, pH 7.4.

6.2.8 Preparation of *Chlamydomonas* Peptide Library

Chlamydomonas peptide library was generated using a protocol similar to previous work[40]. Briefly, *Chlamydomonas* strain CC-2289 6145c mt- (Chlamydomonas Resource Center) cultures were maintained photoheterotrophically on Tris-acetate-phosphate (TAP) agar plates. A culture was grown to mid-log phase (OD_{750} 0.3-0.5) before 3.5 mL of this culture were inoculated into 350 mL TAP in 1 L Erlenmeyer flasks. Four 350 mL cultures were grown photoheterotrophically to mid-exponential phase (OD_{750} 0.5) under constant light conditions of 39 μmol photons/m^2s at 25 °C and at an orbital rotational speed 120 rpm on a VWR International model 1000 standard orbital shaker. Once grown, cultures were harvested via centrifugation at 3220 x *g*, 4 °C for 5 min. The supernatant was discarded and then pellets were flash frozen in liquid nitrogen and stored at -80 °C.

Frozen cell pellets were lysed in 4 mL of buffer containing 100 mM Tris, pH 8.0, 1% sodium dodecyl sulfate, 1x cOmplete EDTA-free protease inhibitor cocktail (Roche), and 1x PhosSTOP phosphatase inhibitor cocktail (Roche). Cell were lysed via sonication using an E220 focused ultrasonicator (Covaris) for 180 s at 200 cycles/burst, 100 W power, and 13% duty cycle. After sonication, samples were centrifuged at 15,000 x *g* for 10 min at 4 °C and the supernatant was collected. The cell pellet was resuspended in 1 mL of fresh lysis buffer, incubated for 30 min at 4 °C, and centrifuged again. Supernatants were combined and proteins were precipitated using four volumes of cold 100 mM ammonium acetate in methanol, incubating overnight at -80 °C. Proteins were pelleted by centrifugation at 3220 x *g* for 5 min and washed twice with fresh 100 mM ammonium acetate in methanol. Proteins were allowed to dry for 5 min before resuspension

in 2 mL 8 M urea in 100 mM Tris, pH 8.0. All samples were combined and protein concentration was measured using the CB-X Protein assay (G-Biosciences,) according to the manufacturer's protocol.

Protein thiols were reduced using 10 mM dithiothreitol at room temperature for 30 min followed by alkylation with 40 mM iodoacetamide for 45 min at room temperature while protected from light. Samples were diluted 5-fold after alkylation with 100 mM Tris, pH 8.0 to reduce the concentration of urea to 1.6 M. Samples were then digested with Trypsin Gold (Promega) at a 1:50 enzyme:protein ratio overnight at room temperature, rotating end-over-end. The digestion was quenched with 20% trifluoroacetic acid (TFA, Fisher Scientific) to a final concentration of 0.4% TFA and a pH < 3.0.

After digestion, samples were desalted using 50 mg/1.0 mL Sep-Pak C18 cartridges (Waters) using a vacuum manifold (Phenomenex). Resin was pre-eluted with 1 mL 80% acetonitrile, 0.1% TFA and then equilibrated with 2 mL 0.1% TFA at a flow rate of ~1 drop/s. Samples were first centrifuged at 3220 x *g* for 5 min to pellet undigested protein before loading onto the cartridges using gravity flow. Samples were then reloaded once, and cartridges were washed with 2 mL of 0.1% TFA followed by elution of the peptides in 1.5 mL of 80% acetonitrile, 0.1% TFA. The samples were then dried by vacuum centrifugation.

6.2.9 Preparation of CrS6K Digests

After affinity purification, the CrS6K sample was precipitated using four volumes of cold 100 mM ammonium acetate in methanol, incubating for 1 h at -80 °C. Proteins were pelleted by centrifugation at 3220 x *g* for 5 min and washed twice with fresh 100 mM ammonium acetate in methanol. Proteins were allowed to dry for 5 min before resuspension in 0.5 mL 4 M urea in 100 mM Tris, pH 8.0. Protein concentration was measured using the CB-X Protein assay (G-

Biosciences) according to the manufacturer's protocol, and 5 mg were aliquoted from the sample.

Protein thiols were reduced using 10 mM dithiothreitol at room temperature for 30 min followed by alkylation with 40 mM iodoacetamide for 45 min at room temperature while protected from light. Samples were diluted 4-fold after alkylation with 100 mM Tris, pH 8.0 to reduce the concentration of urea to 1 M. Samples were digested with Trypsin Gold (Promega) at a 1:50 enzyme:protein ratio overnight at room temperature, rotating end-over-end. The digestion was quenched with 20% trifluoroacetic acid (TFA, Fisher Scientific) to a final concentration of 0.4% TFA and a pH < 3.0. For Glu-C S6K digest, additional CrS6K digest was prepared as described above, except resuspension was performed with 4 M urea, 100 mM phosphate buffer, pH 7.4, and dilution was performed with 100 mM phosphate buffer, pH 7.4 to a urea concentration of 1 M. The sample was then digested overnight with Glu-C (sequencing grade, Sigma Aldrich) at 37 °C with an enzyme:protein ratio of 1:50.

Sample digestion was quenched with the addition of 20% TFA until samples reached a pH < 3.0. After this, samples were desalted using 50 mg/1.0 mL Sep-Pak C18 cartridges as described in Section 6.2.8, and dried to completeness.

6.2.10 Kinase Screening Assay

10x screening buffer was prepared with 50 mM $MgCl_2$, and 10 mM DTT in 20 mM HEPES-KOH, pH 7.4. Peptide library and CrS6K digests were resuspended at a concentration of 10 mg/mL in 20 mM HEPES-KOH, pH 7.4. 10 mM aliquots of $^{18}O_4$-ATP were made in 20 mM HEPES-KOH, pH 7.4.

Kinase screening was performed in triplicate at 25 °C overnight with a 100 µL per sample volume. Each sample had 1 mM $^{18}O_4$-ATP, 20 µg of target peptide with 1 µg kinase were used

for synthetic peptide screens, and 500 µg digested CrS6K or peptide library with 2 µg of kinase for other screens. Triplicate control samples were also prepared and incubated overnight with no kinase added for the AtPDK controls and CrTOR-EKD D239A used in the CrTOR-EKD screening controls.

6.2.11 Phosphopeptide Enrichment

Phosphopeptide enrichment was performed on each sample as previously described using 1 mg Titansphere Phos-TiO_2 kit spin columns (GL Sciences)[40,41]. Following each step in the enrichment, columns were centrifuged at 1000 x *g* for 5 min until dry. Columns were pre-eluted with 50 µL 20% acetonitrile, 5% aqueous ammonia, and the equilibrated with 50 µL 80% acetonitrile, 1% TFA twice, and 50 µL 80% acetonitrile, 1% TFA with 25 mg/ml phthalic acid three times. Samples were resuspended in 70 µL of 80% acetonitrile, 1% TFA with 25 mg/mL phthalic acid, and then centrifuged at 15,000 x *g* for 5 min to pellet any precipitant and prevent column clogging. Samples were loaded onto the column a total of five times, reapplying the flow through after each centrifugation step. Columns were then washed using 50 µL 80% acetonitrile, 1% TFA with 25 mg/mL phthalic acid twice, and 50 µL 80% acetonitrile, 1% TFA three times. Phosphopeptides were eluted in 50 µL 20% acetonitrile, 5% aqueous ammonia twice, for a total of 100 µL of elution. Samples were then dried using vacuum centrifugation.

Following phosphopeptide enrichment, samples were desalted using 0.6 µL C_{18} ZipTips (MilliporeSigma). After drying, samples were resuspended in 15 µL 0.1 TFA and centrifuged for 5 min at 15,000 x *g* to remove any precipitant and prevent tip clogging. Tips were first pre-eluted three times with 10 µL of 80% acetonitrile, 0.1% TFA, followed by equilibration with 10 µL 0.1% TFA three times. The samples were then loaded on the tip by passing the phosphopeptides through ten times. Following loading, the tips were then washed six times with 10 µL of 0.1%

TFA and the eluted by passing 15 µL of 80% acetonitrile, 0.1% TFA through the tip ten times. The samples were then dried down using vacuum centrifugation.

6.2.12 LC-MS/MS

Samples were resuspended in 5% ACN, 0.1% TFA to a concentration of 0.2 µg/µL for library/digest samples and 20 ng/µL for synthetic peptide samples. Samples were analyzed using an Acquity M-Class UPLC system (Waters) coupled to a Q Exactive HF-X Hybrid Quadrupole Orbitrap mass spectrometer (ThermoFisher) via a Nanospray Flex Ion Source (ThermoFisher) with a spray voltage of 2.1 kV, except for samples of AtPDK screens against GHSLADPDELR, which were analyzed using a nanoAcquity (Waters) coupled to a TripleTOF 5600 mass spectrometer (AB Sciex). For all samples, mobile phase A was water with 0.1% formic acid and mobile phase B was ACN with 0.1% formic acid. 1 µL of each sample was injected with a 5 µL/min flow rate for 3 min onto a Symmetry C_{18} trap column (100 Å, 5 µm, 180 µm x 20 mm, Waters). Samples were separated with a 0.3 µL/min flow rate on an HSS T3 C18 column (100 Å, 1.8 µm, 75 µm x 250 mm, Waters). Library/digest samples separation used a gradient of 5-35% B over 90 min, followed by a ramp to 85% B in 5 min with a 5 min hold and a return to 5% B in 2 min with a re-equilibration time of 13 min, for a 120 min total run time. Synthetic peptide sample separation used a ramp of 5%−50% B over 30 min instead, for a 60 min total run time.

For most samples, the mass spectrometer was operated in positive polarity with a 2.1 kV spray voltage, 325°C capillary temperature and S-lens RF level of 40. Lock masses of background polysiloxane ions were included. Full MS/DD-MS^2 scan type was used. MS survey scan was performed in profile mode across 350-1600 Da at 120,000 resolution with a 50 ms maximum IT and $3x10^6$ AGC target. The top 20 features with a +2 to +7 charge state above 5000 counts were selected. MS^2 scans were collected at 45,000 resolution with NCE at 32 until 100 ms

maximum IT or $1x10^5$ AGC target. The dynamic exclusion window was set to 10 s and an isolation window of 0.7 *m/z* for precursor ions. For AtPDK screens against GHSLADPDELR, the mass spectrometer was operated in positive-ion, high-sensitivity mode with the MS survey spectrum using a mass range of 350−1600 Da in 250 ms and information-dependent acquisition (IDA) of MS/MS data. The first 20 features above 150 counts with a charge state of +2 to +5 were fragmented using rolling collision energy (±5%). Auto calibration was performed every eight samples with a BSA tryptic digest. The mass spectrometry proteomics data and supplemental tables have been deposited to the ProteomeXchange Consortium via the PRIDE partner repository[42] and can be accessed with the Identifier PXD023453 (Username: reviewer_pxd023453@ebi.ac.uk, Password: OsGKUzTy).

6.2.13 Data Analysis

For peptide screening samples, peak areas were measured using Analyst (AB Sciex) or Xcaliber (ThermoFisher). Individual samples were converted to peak lists (*.mgf) for database searching using the MSConvertGUI (ProteoWizard) with the following settings: peakPicking, vendor MS level 1-2; remove extra zero samples; HCD activation; threshold count of 5000 most intense peaks. The peaklist was uploaded into Mascot (Matrix Science, version 2.5.1) and database searching was performed against the *E. coli* BL21(DE3) Uniprot database (https://www.uniprot.org/proteomes/UP000002032, 4,156 entries) with appended target peptide and kinase sequences. Sequences for common laboratory contaminants (www.thegpm.org/cRAP, 116 entries) were also included in the database. A target decoy MS/MS search was performed with trypsin specificity with up to two missed cleavages, a peptide mass tolerance of 15 ppm, and a fragment mass tolerance of 0.02 Da. Carbamidomethylation of cysteine was included as a fixed modification with oxidation of methionine, and heavy phosphorylation ($P^{18}O_3$) of serine,

threonine, and tyrosine included as variable modifications. After completion of the search, the false discovery rate was adjusted to be less than 1% using the embedded Percolator algorithm, and matches were exported.

For library/digest screenings, the acquired spectral files (*.raw) were uploaded into Progenesis QI for Proteomics (Nonlinear Dynamics, Waters) for label-free quantification. An automatically assigned reference spectrum was used to align the total ion chromatograms and a peak picking sensitivity was set to the maximum of 5. Alignment was validated with a score >90%, and replicates were grouped based on sample type before being exported as a combined peak list (*.mgf). The peaklist was uploaded into Mascot (Matrix Science, version 2.5.1) and database searching was performed against the *Chlamydomonas reinhardtii* JGI v5.6 Phytozome database (https://phytozome-next.jgi.doe.gov/info/Creinhardtii_v5_6, 19,523 entries) appended with the entries from the NCBI chloroplast (BK000554.2, 68 entries) and mitochondrial (NC_001638.1, 8 entries) databases for peptide library screenings. CrS6K digest screenings were searched against *E. coli* BL21(DE3) database with appended target peptide and kinase sequences. Sequences for common laboratory contaminants (www.thegpm.org/cRAP, 116 entries) were also included in the databases. A target decoy MS/MS search was performed with trypsin or Glu-C specificity with up to two missed cleavages, a peptide mass tolerance of 15 ppm, and a fragment mass tolerance of 0.02 Da. Carbamidomethylation of cysteine was included as a fixed modification with acetylation at the protein N-terminus, oxidation of methionine, and heavy phosphorylation ($P^{18}O_3$) of serine, threonine, and tyrosine included as variable modifications. After completion of the search, the false discovery rate was adjusted to be less than 1% using the embedded Percolator algorithm, and matches were exported and reuploaded

into Progenesis for peak matching. After matching, identifications with a Mascot score less than 13 were removed before exporting protein/peptide measurements.

Data were parsed using custom R scripts designed for phosphoproteomic data (https://github.com/hickslab/QuantifyR). Groups in the peptide measurements data were reduced to satisfy the principle of parsimony, removing duplicated and matched peptides with identical sequence, modifications, and score. These were represented by the protein accession with the highest number of unique peptides, which was found in the protein measurements data, else the protein with the highest confidence score assigned via Progenesis. For identical features with differing peptide identifications, duplicates were reduced to the peptide with the highest Mascot ion score. These results were filtered for only peptides containing heavy phosphorylation. Identifiers were created for each of these features by joining the protein accession for each peptide to the amino acid and location of the site(s) of modification in the protein sequence. The data were then reduced to only unique identifiers by summing all of the contributing peak features which may come from different charge states, missed cleavages, and the presence of additional variable modifications. The peptide with the highest Mascot score in each group represented the corresponding identifier. Identifiers were then removed if they did not have at least one condition where 2/3 replicates had nonzero values for their Progenesis-normalized abundances. These abundances were $\log_2$-transformed and imputation was applied to assign missing values. Statistical significance was calculated using a two-tailed, equal variance *t*-test and fold-change was calculated from the difference of the mean abundance values between conditions. Observations with a *p*-value <0.05 and a $\log_2$-transformed fold change of ± 1 were considered significantly changing.

6.3 Results and Discussion

6.3.1 Platform Validation

6.3.1.1 AtPDK Screening with Synthetic Target Peptide

To confirm successful expression and purification of active AtPDK, screening was first performed using a synthetic peptide corresponding to the sequence of the tryptic peptide containing the target phosphorylation site from AtPDCe1α (YHGH**S**MSDPGSTYR). AtPDK was incubated with the target peptide in the presence of γ-$^{18}O_4$-ATP and then analyzed via LC-MS/MS. Extracted ion chromatograms (XICs) confirmed that the unphosporylated target peptide was present in all samples and that the heavy phosphorylated peptide was only present in the kinase samples (Figure 6.2a). While phosphopeptides are generally found to have worse ionization efficiency than there unphosphorylated counterparts, the difference appears to be relatively small when using electrospray ionization[43], allowing for a rough comparison of the abundances to conservatively estimate phosphorylation efficiency of the kinase. Comparing the summed peak areas of the unphosphorylated and phosphorylated peptides (Table 6.1) shows that only about 1-1.5% of the present peptide was phosphorylated by AtPDK but this suggests the kinase is active.

To further validate the activity of AtPDK, the kinase samples were searched using Mascot against a custom database containing the AtPDCe1α sequence, including heavy phosphorylation as a variable modification on serine, threonine, and tyrosine residues. In the search results (Table 6.S1), the target peptide was identified in its unmodified, oxidized, and phosphorylated states and phosphorylation was localized to the serine (Ser5) targeted by AtPDK (Figure 6.2b). This localization was confirmed based on the presence of the y8 and y9 ions and a Mascot delta localization score of 27.7 between Ser 5 and Ser7. Additionally, neutral loss from the

phosphorylation was identified as an $H_3PO^{18}O_3$, characteristic of a β-elimination reaction rarely seen in phosphotyrosine fragmentation[44], preferencing phosphorylation on Ser5 over Tyr1.

6.3.1.2 AtPDK Screening with Peptide Library

For platform validation, the synthetic target peptide was spiked into a *C. reinhardtii* digest peptide library at a physiologically-relevant concentration (100 ng in a 500 µg library) to ensure target identification in the presence of a more complex library. After screening, the samples were enriched for phosphopeptides and analyzed via LC-MS/MS. A label-free quantitative proteomic workflow, and statistical testing using custom R scripts adapted from the QuantifyR LFQ phosphorylation workflow (https://github.com/hickslab/QuantifyR) was used to perform a *t*-test between the control and kinase samples, giving a list of potential target substrates that were significantly more abundant in the kinase samples. A total of 37 peptides were identified with heavy phosphorylation, six of which were significantly more abundant in the kinase samples (Figure 6.3a, Table 6.S2). One of these was the synthetic AtPDCe1α target peptide, which was 3.75x more abundant in the kinase samples. Again, the phosphorylation event was successfully localized using MS^2 fragmentation (Figure 6.3b). This confirms that this platform can screen an active kinase and identify its potential target substrates.

The other five peptides shown to be significantly more abundant in the kinase samples may also be targets of phosphorylation of AtPDK from the *C. reinhardtii* peptide library. One of these identified peptides was GH**S**LADPDELR, which was found to be 20.5x more abundant in the kinase samples. This peptide is from the *C. reinhardtii* homolog of the PDCe1α subunit (CrPDCe1α, Cre02.g099850.t1.1), and when the sequences of AtPDCe1α and CrPDCe1α were aligned using BLAST[35], a 56% positive alignment was seen between the two homologs, with the two peptides found in the screening aligning with one another (Figure 6.4). The two peptides

have four conserved amino acids, Gly and His at the -2 and -1 positions, and Asp and Pro at the +3 and +4 positions, with two additional residues that are similar, suggesting that this peptide could also be a target of phosphorylation by AtPDK. However, when AtPDK was screened against a synthetic version of this peptide, XICs did not show the presence of a heavy phosphopeptide in the kinase samples (Figure 6.5, Table 6.2), showing that this substrate identification was most likely a false positive. This implies that AtPDK has a high level of selectivity and has a consensus motif more specific than the conserved amino acids found between this potential target and the known tryptic substrate from AtPDCe1α.

6.3.2 Screening of CrTOR-EKD

6.3.2.1 CrTOR-EKD Screening with Tryptic CrS6K Digest

With the validation of the screening approach successful, it was applied to identification of CrTOR targets using the CrTOR-EKD construct. For a more targeted screening approach, instead of screening against a full Chlamydomonas peptide library, CrTOR-EKD was first screened against CrS6K, which is suspected to be a direct target of TOR based on homology. A vector construct encoding for CrS6K was synthesized commercially based on the corrected CrS6K from the Umen lab (Danforth Center) (see corrected sequence in Figure 5.3). Their unpublished work confirmed that a portion of the protein is missing in the original sequence included in the Chlamydomonas database available on Phytozome. For this work, this portion of sequence was added to the CrS6K plasmid construct for expression of the complete protein and the sequence for S6K included in the customized database was updated accordingly. Using this vector construct, CrS6K was heterologously expressed, purified, and then digested using trypsin. This tryptic digest was used as a substrate library for screening CrTOR-EKD.

A total of 41 peptides were identified with heavy phosphorylation, two from CrS6K while the remaining 39 were from *E. coli* protein contaminants that were digested along with CrS6K during peptide library preparation (Figure 6a, Table 6.S3). Of these heavy phosphopeptides, one from *E. coli* was found to be significantly more abundant in the CrTOR-EKD samples when compared to the CrTOR-EKD D239A control samples (Figure 6a). This peptide is not a biologically relevant target of CrTOR, and not found in any protein in the *Chlamydomonas* database. While it could provide information on TOR consensus motif specificity, additional target peptides would be needed to establish a putative motif.

6.3.2.2 CrTOR-EKD Screening with Glu-C CrS6K Digest

Tryptic digestions are often used in bottom-up proteomic experiments because it typically produces a large number of small peptides within the mass range of most high resolution mass spectrometers[45]. However, like many proteins, not all portions of CrS6K are produce reasonably sized tryptic peptides. Specifically, Thr1006, the conserved residue that is known to be a target of TOR in other organisms, is part of a 6.4 kDa C-terminal peptide that is likely too large to be easily ionized. Containing no Arg and Lys residues and only one His, this peptide is likely to have low charge states that are outside of the mass range of many mass analyzers. As a result, it was not detected in the previous screening. In an attempt to obtain coverage on this site and determine if it is a target of CrTOR, CrS6K was digested with Glu-C instead of trypsin, which produces a peptide containing Thr1006 that is 1.4 kDa in size.

When CrTOR-EKD was screened against the Glu-C CrS6K digest, 3779 peptides were identified, 10 of which had heavy phosphorylation modifications (Table 6.S4). However, the peptide containing Thr1006 was only identified in its unphosphorylated form, no heavy phosphopeptides were identified from CrS6K, and none of the identified phosphopeptides were

found to be significantly changing in the kinase samples when compared to the control (Figure 6b). The other phosphorylation site known to be regulated by TOR in mammalian cells [31] is also conserved in CrS6K, Ser1003, but the corresponding Glu-C digest peptide was not detected in these data.

Additionally, a synthetic peptide was produced containing the target Thr1006 with six residues of the CrS6K sequence on either side, GRFDGF**T**YVAPCF. This peptide was screened against CrTOR-EKD in the presence of heavy ATP, but the phosphorylated form of the peptide was not identified, suggesting the kinase did not have activity against the Thr1006 target or that the kinase construct is not active. (Figure 6.7, Table 6.3).

6.3.2.3 CrTOR-EKD Screening with *Chlamydomonas* Peptide Library

When CrTOR-EKD was screened against a *Chlamydomonas* tryptic peptide library, a total of 19 heavy phoshopeptides were identified, with only one peptide significantly higher in abundance in the CrTOR-EKD samples when compared to the CrTOR-EKD D239A control samples (Table 6.S5, Figure 6.8a). This peptide is from acidic ribosomal protein P2 (Cre02.g143050.t1.2), and phosphorylation was identified on the tryptic peptide containing Ser44 (LI**S**ELEGK, FC: 1.78). While this protein has never been identified as a target of TOR phosphorylation, ribosomal P proteins are known to be regulated via phosphorylation[46–49], with the p-protein complex of eukaryotic ribosomes thought to assist in the elongation phase of translation when in its active, multiply phosphorylated form[50]. While the exact role of this phosphorylation site is unknown, it could aid the p-protein complex through either increased activity or additional specificity, but more work is needed to determine its exact role. TOR is known to regulate translation through phosphorylation of S6K and indirectly ribosomal protein S6 (RPS6)[29], but this result suggests that TOR may have additional ribosomal targets.

In an attempt to validate the phosphorylation site identified as a potential target on acidic ribosomal protein P2, a synthetic version of the tryptic peptide containing the target was made and screened against CrTOR-EKD in the presence of heavy ATP. However, XICs did not show the presence of any phosphorylation, so this protein has not been validated and is either no a direct substrate of CrTOR, or this further suggests that the CrTOR-EKD construct is not active. (Figure 6.8b, Table 6.4). However, further studies are required to determine the exact cause of inactivity seen from CrTOR-EKD.

6.4 Conclusions and Future Directions

While this in vitro screening approach was able to successfully identify phosphorylation of the target peptide of AtPDK, the platform was not successful in identifying potential substrates of CrTOR. This could be due to a number of issues, but the inactivity of the CrTOR-EKD is likely a contributing factor.

Heterologous expression and purification of active enzymes, and kinases in particular, can be challenging. Many kinases suffer from poor solubility, incorrect folding or aggregation when expressed in prokaryotic hosts [51]. Previous work has shown that the kinase domain of CrTOR, when heterologously expressed as a fusion protein with MBP, is still able to bind CrLST8 *in vitro* which would imply that the construct is structurally folded enough for this interaction to occur[37]. However, CrTOR-EKD is a fusion protein with a different tag, GST, but this is s known for acting as a chaperone for protein folding and can help with solubility[52]. The successful purification of CrTOR-EKD suggests that the fusion GST tag is folded correctly to the extent that it is able to properly able to bind glutathione, and the construct appears to be soluble. However, further investigation is needed to determine the structure of the CrTOR-EKD construct and whether the GST fusion tag helps in the solubility and folding, or if the bulky tag interferes

with the activity of the kinase. This construct, like many fusion proteins, encodes for a site-specific protease recognition sequence that could allow for the tag to be removed prior to screening.

This screening platform is designed to help identify biologically-relevant putative substrates for kinases, but there are other more simplistic kinase assays designed to measure a kinase's activity[53–58]. While we have attempted to implement an absorbance-based assay in the Hicks lab to confirm construct activity prior to screening, thus far we have been unsuccessful. Primarily, we have focused on implementation of the non-antibody phosphorylation detection reagent (pIMAGO) and the phosphatase-coupled universal kinase assay (R&D Systems) as a way to detect the phosphorylation of a substrate library from a kinase. CrTOR is particularly challenging to screen for activity because there is not a confirmed phosphorylation target that can be used as a positive control. While CrS6K would be an obvious candidate given its homology with the known direct target of mTOR, no phosphorylation has ever been detected in in vivo experiments perturbing TOR activity via phosphoproteomics[40].

Another factor of concern for heterologous kinase expression is the potential for heterogeneous auto-phosphorylation, where the kinase can phosphorylate itself at different sites as expression occurs decreasing the activity of the kinase[51]. To address this, kinases are often partially or completed dephosphorylated in vitro and then a particular phosphoform is purified using chromatography. Alternatively, a phosphatase can be co-expressed along with the kinase, increasing the yield of the non-phosphorylated form of the kinase.

Successful screening of CrTOR-EKD and the other kinases selected from the TOR signaling pathway will require additional optimization of expression, purification, and screening parameters necessary to ensure each construct is active. This may require techniques to

determine the structural characteristics of the constructs under different conditions as well as mapping of the modifications needed to ensure kinase activity. This approach will likely be most successful in cases where a known kinase substrate can be used to identify changes in activity and will be challenging to implement in the absence of a known substrate.

In addition to these proposed improvements to kinase activity, adaptations of the substrate library used in screening may help improve identification of putative substrates. While the work herein used a lysate of *Chlamydomonas* cells grown under favorable conditions for library creation, implementation of a stressor such as nutrient deprivation or chemical treatment could provide a unique library derived from the expression levels of the proteome under stressed conditions. This could increase the concentration of substrates of interest, particularly for kinases like TOR, which are known to regulate nutrient and stress response. Additionally, the peptide substrate library could be pre-enriched for phosphopeptides prior to dephosphorylation[18]. This pool of peptides represents a subset of potentially more biologically relevant targets as they are found endogenously in their phosphorylated form. These adaptations to the substrate pool along with further kinase expression and screening optimization could create a platform that is more amenable for screening TOR in addition to Chlamydomonas kinases. The combination of this *in vitro* work with *the in vivo* studies of earlier chapters, could provide a thorough investigation of the Chlamydomonas TOR signaling pathway, providing insight into a complex, but essential regulatory network.

6.5 Tables

Table 6.1 XIC peak areas and percent phosphorylation from AtPDK screening with synthetic target peptide YHGHSMSDPSTYR.

	Unphosphorylated			Phosphorylated			Total Peak Areas		Percent Phos.
Sample	+2	+3	+4	+2	+3	+4	Unphos.	Phos.	
Control 1	6.87 E+10	2.08 E+11	1.03 E+10	3.61 E+06	3.13 E+07	1.35 E+06	2.87 E+11	3.62 E+07	0.01%
Control 2	1.30 E+11	3.37 E+11	1.46 E+10	1.38 E+08	9.51 E+08	1.68 E+08	4.82 E+11	1.26 E+09	0.26%
Control 3	8.35 E+10	2.41 E+11	1.11 E+10	1.02 E+08	8.37 E+08	1.34 E+08	3.36 E+11	1.07 E+09	0.32%
Kinase 1	1.33 E+11	3.51 E+11	1.42 E+10	9.51 E+08	5.49E +09	1.72 E+08	4.98 E+11	6.62 E+09	1.31%
Kinase 2	1.45 E+11	3.63 E+11	1.45 E+10	1.42 E+09	7.35 E+09	1.42 E+08	5.23 E+11	8.91 E+09	1.68%
Kinase 3	1.28 E+11	3.54 E+11	1.44 E+10	9.81 E+08	5.25 E+09	1.36 E+08	4.96 E+11	6.36 E+09	1.27%

Table 6.2 XIC peak areas and percent phosphorylation from AtPDK screening with synthetic target peptide GHSLADPDELR.

	Unphosphorylated		Phosphorylated		Total Peak Areas		Percent Phos.
Sample	+2	+3	+2	+3	Unphos.	Phos.	
Control 1	3.29E+08	2.14E+08	2.13E+06	0.00E+00	5.43E+08	2.13E+06	0.391%
Control 2	3.45E+08	1.11E+08	1.12E+05	8.76E+04	4.56E+08	2.00E+05	0.044%
Control 3	3.21E+08	2.10E+08	9.97E+04	5.95E+04	5.31E+08	1.59E+05	0.030%
Kinase 1	3.32E+08	2.14E+08	8.99E+04	9.42E+04	5.46E+08	1.84E+05	0.034%
Kinase 2	3.04E+08	2.02E+08	1.13E+05	1.30E+05	5.06E+08	2.43E+05	0.048%
Kinase 3	2.73E+08	1.84E+08	1.19E+05	9.81E+04	4.57E+08	2.17E+05	0.048%

Table 6.3 XIC peak areas and percent phosphorylation from CrTOR-EKD screening with synthetic target peptide GRFDGFTYVAPCF.

	Sample	Control 1	Control 2	Control 3	Kinase 1	Kinase 2	Kinase 3
Unphosphorylated	+1	2.13E+10	1.98E+10	1.95E+10	1.96E+10	1.92E+10	2.05E+10
	+2	4.05E+11	3.92E+11	3.74E+11	3.69E+11	3.76E+11	4.08E+11
	+3	1.28E+07	9.16E+06	5.62E+06	1.01E+07	1.20E+07	8.87E+06
	+4	1.56E+05	9.85E+04	1.17E+06	2.43E+06	1.59E+06	3.95E+05
Phosphorylated	+1	0.00E+00	3.94E+05	1.22E+06	0.00E+00	0.00E+00	0.00E+00
	+2	1.36E+09	1.51E+09	1.40E+09	1.11E+09	9.98E+08	1.39E+09
	+3	3.83E+07	4.28E+07	3.13E+07	4.16E+07	3.79E+07	3.58E+07
	+4	1.50E+06	2.59E+06	2.58E+06	2.94E+06	3.74E+06	3.51E+06
Total Areas	Unphos.	4.27E+11	4.12E+11	3.93E+11	3.88E+11	3.95E+11	4.28E+11
	Phos.	1.40E+09	1.55E+09	1.43E+09	1.16E+09	1.04E+09	1.43E+09
	Percent Phos.	0.33%	0.38%	0.36%	0.30%	0.26%	0.33%

Table 6.4 XIC peak areas and percent phosphorylation from CrTOR-EKD screening with synthetic target peptide LISELEGK.

	Unphosphorylated		Phosphorylated		Total Peak Areas		Percent Phos.
Sample	+1	+2	+1	+2	Unphos.	Phos.	
Control 1	4.08E+11	1.12E+12	8.40E+07	7.25E+08	1.52E+12	8.09E+08	0.053%
Control 2	3.76E+11	1.02E+12	5.33E+07	4.65E+08	1.40E+12	5.18E+08	0.037%
Control 3	3.99E+11	1.10E+12	4.67E+07	4.52E+08	1.50E+12	4.99E+08	0.033%
Kinase 1	3.97E+11	1.09E+12	4.68E+07	4.35E+08	1.49E+12	4.82E+08	0.032%
Kinase 2	3.81E+11	1.07E+12	2.70E+07	2.42E+08	1.46E+12	2.69E+08	0.019%
Kinase 3	3.68E+11	1.01E+12	2.43E+07	2.32E+08	1.38E+12	2.56E+08	0.019%

6.6 Figures

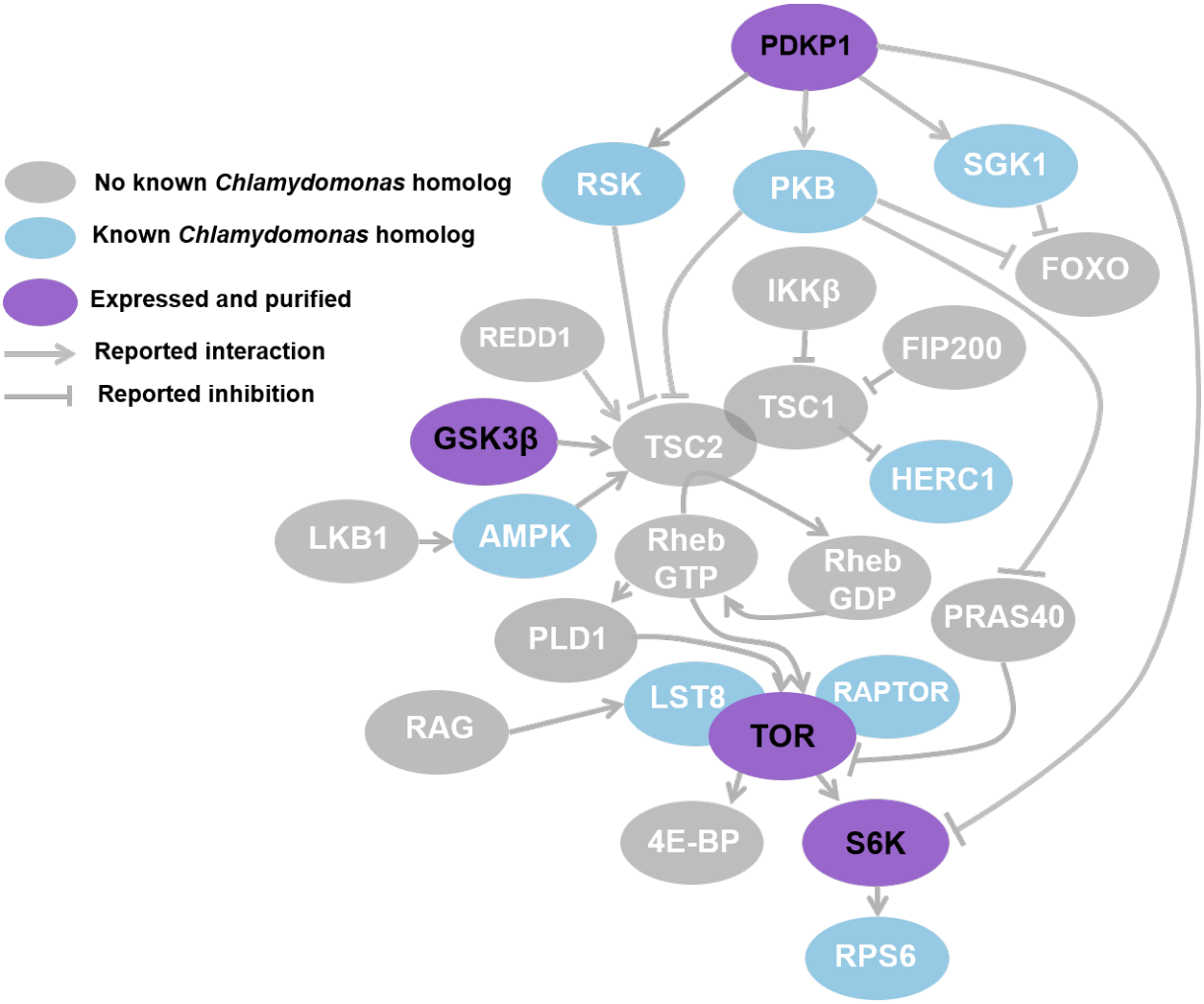

Figure 6.1 The TOR kinase signaling pathway based on homology from mammalian TOR. Proteins with known homologs in *Chlamydomonas* are blue, and the kinases with constructs made for this screening work are in purple.

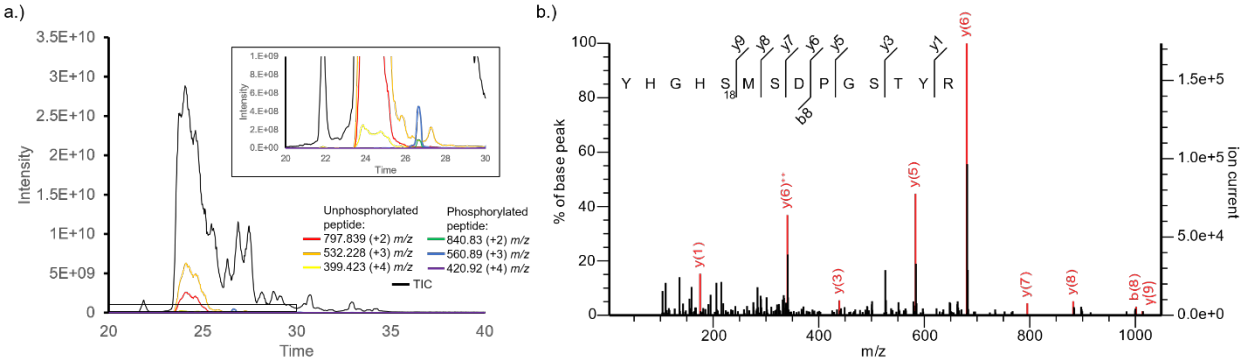

Figure 6.2 Results of screening AtPDK with synthetic peptide target, YHGHSMSDPSTYR. a.) TIC of screening sample and XICs of unphosphorylated and phosphorylated peptide *m/z*'s. b.) MS^2 of target phosphopeptide with localization of the phosphorylation on Ser5.

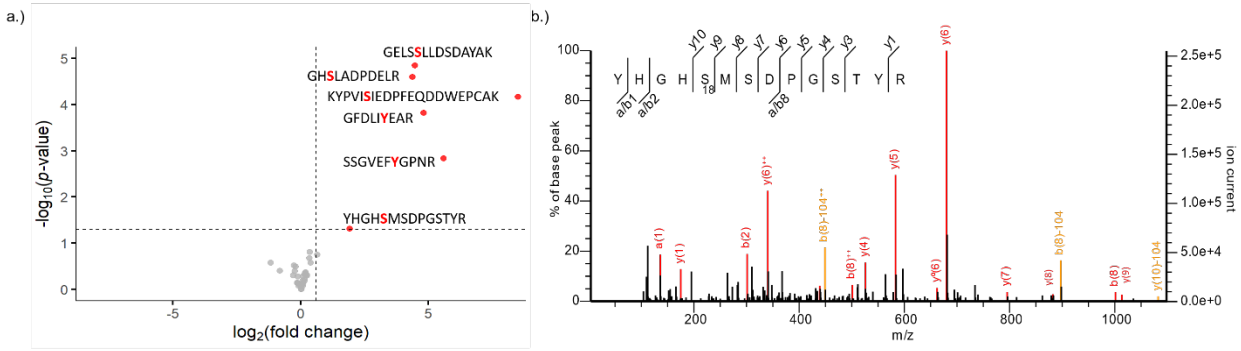

Figure 6.3 Screening results of AtPDK with *C. reinhardtii* peptide library and synthetic target peptide spike-in. a.) After performing a *t*-test between the kinase and control samples, six phosphopeptides were found to be significantly more abundant in the kinase samples (red), including the target peptide YHGHSMSDPGSTYR. b.) MS^2 of target phosphopeptide with localization of the phosphorylation on Ser5.

```
Score:223 bits(569), Expect:5e-73,
Method:Compositional matrix adjust.,
Identities:130/347(37%), Positives:196/347(56%), Gaps:26/347(7%)

AtPDCe1α  64   FYKLMYKMRRMEIAADMMYKAKFIRGFCHLYDGQEAVLTGIEAAITLKDSIITSYRDHCQ  123
               +Y ++      E+ A M Y+ K   GF HLY GQEAV +G+   +   D ++++YRDH
CrPDCe1α  118  YYDMVLGREFEEMCAQMYYRGKMF-GFVHLYSGQEAVSSGVIRQLRQDDYVVSTYRDHVH  176

AtPDCe1α  124  HVSRGGSIVSLMAELMGKQEGATKGLGGSMHIYNRKNNFYGGNGIVGAQIPLGAGIALAH  183
                +S+G S   +MAEL GK+ G  +G GGSMH+++ K    GG   +G  IP+G G A
CrPDCe1α  177  ALSKGVSAREVMAELFGKKTGCCRGQGGSMHMFSAKAGVLGGYAFIGEGIPVGLGAAFQS  236

AtPDCe1α  184  KYKGE-------PHVCITMYGDGAANQGQKYEALNMAGLWNLPAIFVCENNHYGMGTAEW  236
               KY+ +         V  + +GDG  N GQ YE+LNMA L+ LP IFV ENN + +G +
CrPDCe1α  237  KYRRDVLGDEKADSVTCSFFGDGTCNVGQFYESLNMAALYKLPHIFVVENNLWAIGMSHL  296

AtPDCe1α  237  RAAKS------PNFYTRGDY--IPGIKVDGMDVLAV----KNAVAFAKAYALANGPIVME  284
               RA  S      P+ Y +G    +PG+ VDGMDVL V    K A+  A+      GP ++E
CrPDCe1α  297  RATASTAGDQDPHIYKKGPAFGMPGVLVDGMDVLKVHQVAKEAIERARR---GEGPTLIE  353

AtPDCe1α  285  MDTYRYHGHSMSDPGSTYRTRDEINAMRTERDPIERVKRLLLNNGV-DPADLKKIDKEVK  343
                +TYR+ GHS++DP    R+++E  A    RDPI ++K+ +++NG+   AD+K ++ +V
CrPDCe1α  354  AETYRFRGHSLADP-DELRSKEE-KAKWLARDPIPQLKKYMIDNGLASEADIKALEDKVA  411

AtPDCe1α  344  KEVDDAVEQAKQGQIPPLHWLWRNMYAEPLGAGMRGVLPAEYHVPAF  390
               + V+D V+ A +   P    L  N++A+P G G+       Y +P F
CrPDCe1α  412  EVVEDCVKFADESPKPERGQLLENVFADPRGFGIAEDGRYRYQMPGF  458
```

Figure 6.4 BLASTp results of AtPDCe1α and CrPDCe1α with target phosphopeptides identified in AtPDK screening highlighted in red along with their matching/similar residues.

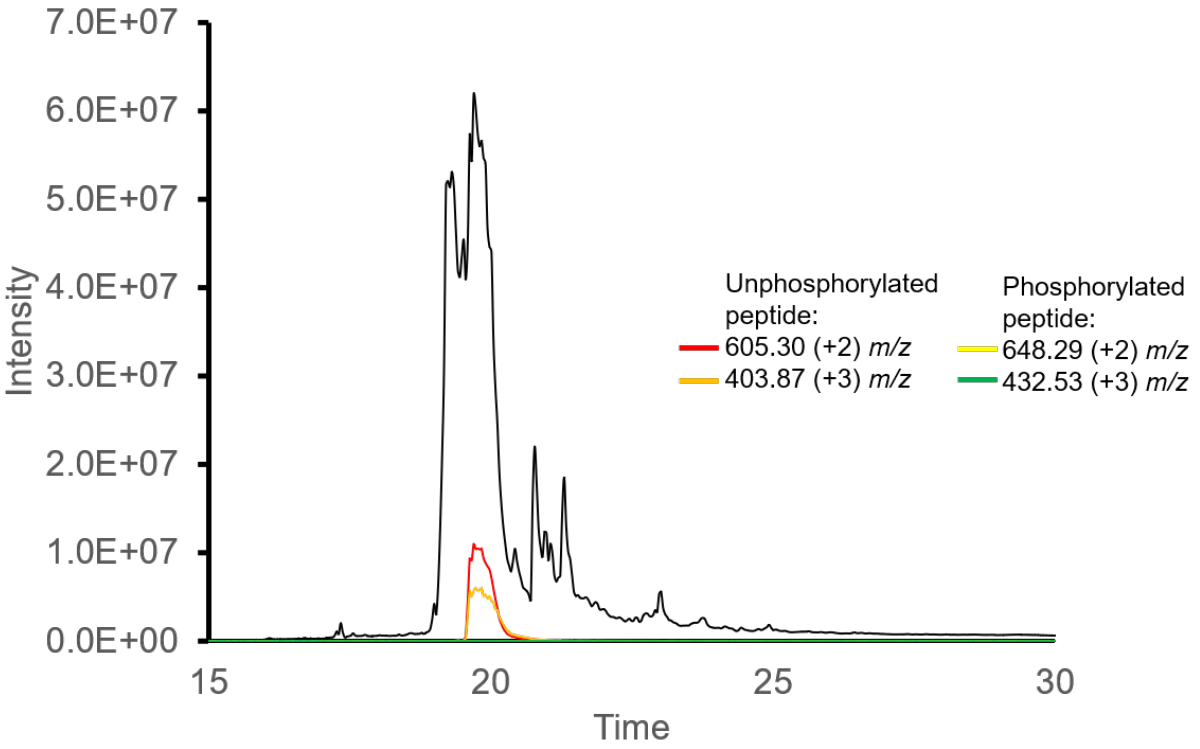

Figure 6.5 Results of screening AtPDK with synthetic peptide target, GHSLADPDELR. TIC of screening sample and XICs of unphosphorylated and phosphorylated peptide *m/z*'s.

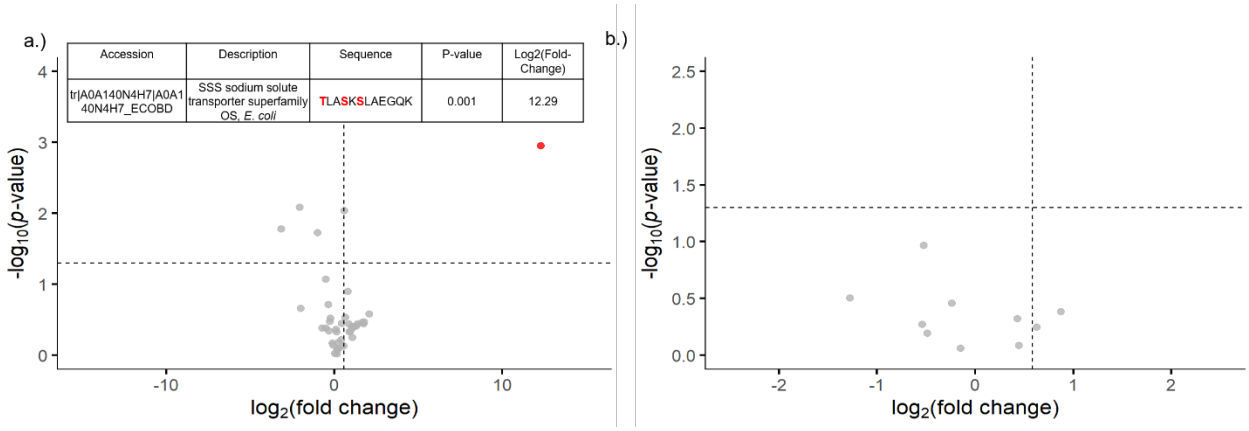

Figure 6.6 CrTOR-EKD screening results against CrS6K. a.) CrTOR-EKD screened against a CrS6K tryptic digest. No peptides from CrS6K were identified as being phosphorylated by CrTOR-EKD, but one peptide target from an *E. coli* protein was identified (red). b.) CrTOR-EKD screened against a Glu-C S6K digest. No peptides were identified as being phosphorylated by CrTOR-EKD.

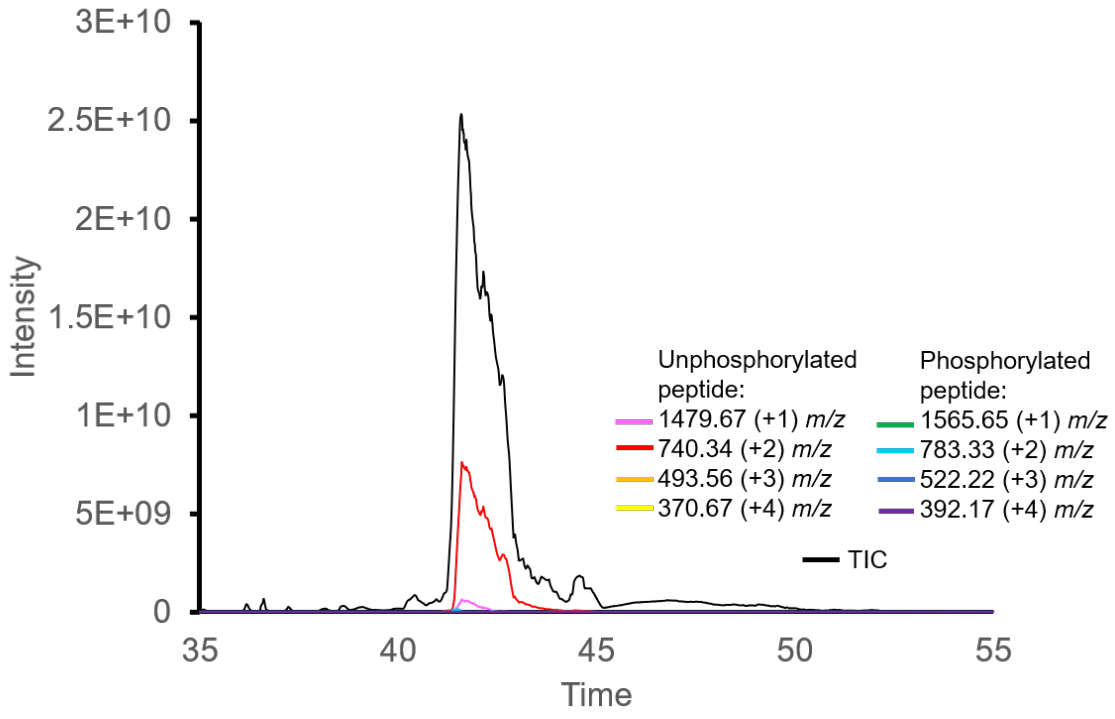

Figure 6.7 Results of screening CrTOR-EKD with synthetic peptide target, GRFDGFTYVAPCF. TIC of screening sample and XICs of unphosphorylated and phosphorylated peptide *m/z*'s.

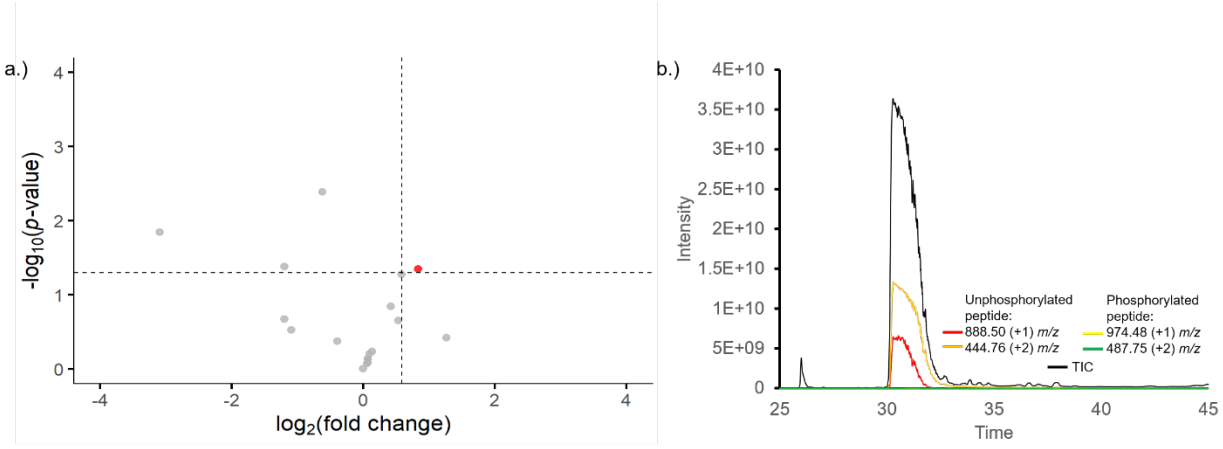

Number	Accession	Description	Sequence	P-value	Log2(Fold-Change)
1	Cre02.g143050.t1.2	Acidic ribosomal protein P2	LISELEGK	0.045	0.832

Figure 6.8 CrTOR-EKD screening results. a.) Screening CrTOR-EKD with *Chlamydomonas* peptide library. One peptide from acidic ribosomal protein P2 was identified as a potential target of CrTOR (red). b.) Screening of CrTOR-EKD against synthetic peptide LISELEGK. TIC of screening sample and XICs of unphosphorylated and phosphorylated peptide *m/z*'s.

REFERENCES

1. Krebs, E. G.; Fischer, E. H. Phosphorylase Activity of Skeletal Muscle Extracts. *J. Biol. Chem.* **1955**, *216* (1), 113–120.

2. Fischer, E. H.; Krebs, E. G. Conversion of Phosphorylase b to Phosphorylase a in Muscle Extracts. *J. Biol. Chem.* **1955**, *216* (1), 121–132.

3. Inzé, D.; De Veylder, L. Cell Cycle Regulation in Plant Development. *Annu. Rev. Genet.* **2006**, *40*, 77–105.

4. Polge, C.; Thomas, M. SNF1/AMPK/SnRK1 Kinases, Global Regulators at the Heart of Energy Control? *Trends Plant Sci.* **2007**, *12* (1), 20–28.

5. Rampitsch, C.; Bykova, N. V. The Beginnings of Crop Phosphoproteomics: Exploring Early Warning Systems of Stress. *Front. Plant Sci.* **2012**, *3*, 144.

6. Pinna, L. A.; Ruzzene, M. How Do Protein Kinases Recognize Their Substrates? *Biochim. Biophys. Acta Mol. Cell Res.* **1996**, *1314* (3), 191–225.

7. Newman, R. H.; Hu, J.; Rho, H.-S.; Xie, Z.; Woodard, C.; Neiswinger, J.; Cooper, C.; Shirley, M.; Clark, H. M.; Hu, S.; Hwang, W.; Jeong, J. S.; Wu, G.; Lin, J.; Gao, X.; Ni, Q.; Goel, R.; Xia, S.; Ji, H.; Dalby, K. N.; Birnbaum, M. J.; Cole, P. A.; Knapp, S.; Ryazanov, A. G.; Zack, D. J.; Blackshaw, S.; Pawson, T.; Gingras, A.-C.; Desiderio, S.; Pandey, A.; Turk, B. E.; Zhang, J.; Zhu, H.; Qian, J. Construction of Human Activity-Based Phosphorylation Networks. *Mol. Syst. Biol.* **2013**, *9*, 655.

8. Zulawski, M.; Schulze, G.; Braginets, R.; Hartmann, S.; Schulze, W. X. The Arabidopsis Kinome: Phylogeny and Evolutionary Insights into Functional Diversification. *BMC Genomics* **2014**, *15*, 548.

9. Manning, G.; Whyte, D. B.; Martinez, R.; Hunter, T.; Sudarsanam, S. The Protein Kinase Complement of the Human Genome. *Science* **2002**, *298* (5600), 1912–1934.

10. Heazlewood, J. L.; Durek, P.; Hummel, J.; Selbig, J.; Weckwerth, W.; Walther, D.; Schulze, W. X. PhosPhAt: A Database of Phosphorylation Sites in Arabidopsis Thaliana and a Plant-Specific Phosphorylation Site Predictor. *Nucleic Acids Res.* **2008**, *36* (Database issue), D1015–D1021.

11. Durek, P.; Schmidt, R.; Heazlewood, J. L.; Jones, A.; MacLean, D.; Nagel, A.; Kersten, B.; Schulze, W. X. PhosPhAt: The Arabidopsis Thaliana Phosphorylation Site Database. An Update. *Nucleic Acids Res.* **2010**, *38* (Database issue), D828–D834.

12. Zulawski, M.; Braginets, R.; Schulze, W. X. PhosPhAt Goes Kinases—Searchable Protein Kinase Target Information in the Plant Phosphorylation Site Database PhosPhAt. *Nucleic Acids Res.* **2013**, *41* (Database issue), D1176–D1184.

13. Wheeler, G. L.; Miranda-Saavedra, D.; Barton, G. J. Genome Analysis of the Unicellular Green Alga Chlamydomonas Reinhardtii Indicates an Ancient Evolutionary Origin for Key Pattern Recognition and Cell-Signaling Protein Families. *Genetics* **2008**, *179* (1), 193–197.

14. Wang, H.; Gau, B.; Slade, W. O.; Juergens, M.; Li, P.; Hicks, L. M. The Global Phosphoproteome of Chlamydomonas Reinhardtii Reveals Complex Organellar Phosphorylation in the Flagella and Thylakoid Membrane. *Mol. Cell Proteomics* **2014**, *13* (9), 2337–2353.

15. Jha, S. K.; Malik, S.; Sharma, M.; Pandey, A.; Pandey, G. K. Recent Advances in Substrate Identification of Protein Kinases in Plants and Their Role in Stress Management. *Curr. Genomics* **2017**, *18* (6), 523–541.

16. Huang, Y.; Houston, N. L.; Tovar-Mendez, A.; Stevenson, S. E.; Miernyk, J. A.; Randall, D. D.; Thelen, J. J. A Quantitative Mass Spectrometry-Based Approach for Identifying Protein Kinase Clients and Quantifying Kinase Activity. *Anal. Biochem.* **2010**, *402* (1), 69–76.

17. Vlad, F.; Turk, B. E.; Peynot, P.; Leung, J.; Merlot, S. A Versatile Strategy to Define the Phosphorylation Preferences of Plant Protein Kinases and Screen for Putative Substrates. *Plant J.* **2008**, *55* (1), 104–117.

18. Wang, P.; Hsu, C.-C.; Du, Y.; Zhu, P.; Zhao, C.; Fu, X.; Zhang, C.; Paez, J. S.; Macho, A. P.; Tao, W. A.; Zhu, J.-K. Mapping Proteome-Wide Targets of Protein Kinases in Plant Stress Responses. *Proc. Natl. Acad. Sci. U.S.A.* **2020**, 201919901.

19. Xue, L.; Wang, P.; Cao, P.; Zhu, J.; Tao, W. A. Identification of Extracellular Signal-Regulated Kinase 1 (ERK1) Direct Substrates Using Stable Isotope Labeled Kinase Assay-Linked Phosphoproteomics. *Mol. Cell Proteomics* **2014**, *13* (11), 3199–3210.

20. Xue, L.; Wang, W.-H.; Iliuk, A.; Hu, L.; Galan, J. A.; Yu, S.; Hans, M.; Geahlen, R. L.; Tao, W. A. Sensitive Kinase Assay Linked with Phosphoproteomics for Identifying Direct Kinase Substrates. *Proc. Natl. Acad. Sci. U.S.A.* **2012**, *109* (15), 5615–5620.

21. Xue, L.; Arrington, JustineV.; Tao, W. A. Identification of Direct Kinase Substrates via Kinase Assay-Linked Phosphoproteomics. In *Phospho-Proteomics*; von Stechow, L., Stechow, L. von, Eds.; Methods in Molecular Biology; Springer New York, 2016; pp 263–273.

22. Hsu, C.-C.; Arrington, J. V.; Xue, L.; Tao, W. A. Identification of Plant Kinase Substrates Based on Kinase Assay-Linked Phosphoproteomics. In *Kinase Signaling Networks*; Tan, A.-C., Huang, P. H., Eds.; Methods in Molecular Biology; Springer: New York, NY, 2017; pp 327–335.

23. Thelen, J. J.; Miernyk, J. A.; Randall, D. D. Pyruvate Dehydrogenase Kinase from Arabidopsis Thaliana: A Protein Histidine Kinase That Phosphorylates Serine Residues. *Biochem. J.* **2000**, *349* (Pt 1), 195–201.

24. Ren, M.; Venglat, P.; Qiu, S.; Feng, L.; Cao, Y.; Wang, E.; Xiang, D.; Wang, J.; Alexander, D.; Chalivendra, S.; Logan, D.; Mattoo, A.; Selvaraj, G.; Datla, R. Target of Rapamycin Signaling Regulates Metabolism, Growth, and Life Span in Arabidopsis. *Plant Cell* **2012**, *24* (12), 4850–4874.

25. Loewith, R.; Jacinto, E.; Wullschleger, S.; Lorberg, A.; Crespo, J. L.; Bonenfant, D.; Oppliger, W.; Jenoe, P.; Hall, M. N. Two TOR Complexes, Only One of Which Is Rapamycin Sensitive, Have Distinct Roles in Cell Growth Control. *Mol. Cell* **2002**, *10* (3), 457–468.

26. Crespo, J. L.; Díaz-Troya, S.; Florencio, F. J. Inhibition of Target of Rapamycin Signaling by Rapamycin in the Unicellular Green Alga Chlamydomonas Reinhardtii. *Plant Physiol.* **2005**, *139* (4), 1736–1749.

27. Zhang, Y.; Persson, S.; Giavalisco, P. Differential Regulation of Carbon Partitioning by the Central Growth Regulator Target of Rapamycin (TOR). *Mol. Plant* **2013**, *6* (6), 1731–1733.

28. Xiong, Y.; Sheen, J. The Role of Target of Rapamycin Signaling Networks in Plant Growth and Metabolism1. *Plant Physiol.* **2014**, *164* (2), 499–512.

29. van Dam, T. J. P.; Zwartkruis, F. J. T.; Bos, J. L.; Snel, B. Evolution of the TOR Pathway. *J. Mol. Evol.* **2011**, *73* (3–4), 209–220.

30. Yaguchi, M.; Ikeya, S.; Kozaki, A. The Activation Mechanism of Plant S6 Kinase (S6K), a Substrate of TOR Kinase, Is Different from That of Mammalian S6K. *FEBS Lett.* **2020**, *594* (4), 776–787.

31. Magnuson, B.; Ekim, B.; Fingar, D. C. Regulation and Function of Ribosomal Protein S6 Kinase (S6K) within MTOR Signalling Networks. *Biochem. J.* **2012**, *441* (1), 1–21.

32. Yaguchi, M.; Kozaki, A. Plant S6 Kinases Do Not Require Hydrophobic Motif Phosphorylation for Activity in Yeast Lacking Ypk3. *FEBS Lett.* **2018**, *592* (4), 610–620.

33. González, A.; Shimobayashi, M.; Eisenberg, T.; Merle, D. A.; Pendl, T.; Hall, M. N.; Moustafa, T. TORC1 Promotes Phosphorylation of Ribosomal Protein S6 via the AGC Kinase Ypk3 in Saccharomyces Cerevisiae. *PLoS ONE* **2015**, *10* (3), e0120250.

34. Protein Production and Purification. *Nat. Methods* **2008**, *5* (2), 135–146.

35. Altschul, S. F.; Gish, W.; Miller, W.; Myers, E. W.; Lipman, D. J. Basic Local Alignment Search Tool. *J. Mol. Biol.* **1990**, *215* (3), 403–410.

36. Ren, M.; Qiu, S.; Venglat, P.; Xiang, D.; Feng, L.; Selvaraj, G.; Datla, R. Target of Rapamycin Regulates Development and Ribosomal RNA Expression through Kinase Domain in Arabidopsis. *Plant Physiol.* **2011**, *155* (3), 1367–1382.

37. Díaz-Troya, S.; Florencio, F. J.; Crespo, J. L. Target of Rapamycin and LST8 Proteins Associate with Membranes from the Endoplasmic Reticulum in the Unicellular Green Alga Chlamydomonas Reinhardtii. *Eukaryot. Cell* **2008**, *7* (2), 212–222.

38. Bayliss, R.; Fry, A.; Haq, T.; Yeoh, S. On the Molecular Mechanisms of Mitotic Kinase Activation. *Open Biol. 2* (11), 120136.

39. Simon, M. D.; Heider, P. L.; Adamo, A.; Vinogradov, A. A.; Mong, S. K.; Li, X.; Berger, T.; Policarpo, R. L.; Zhang, C.; Zou, Y.; Liao, X.; Spokoyny, A. M.; Jensen, K. F.; Pentelute, B. L. Rapid Flow-Based Peptide Synthesis. *ChemBioChem* **2014**, *15* (5), 713–720.

40. Werth, E. G.; McConnell, E. W.; Lianez, I. C.; Perrine, Z.; Crespo, J. L.; Umen, J. G.; Hicks, L. M. Investigating the Effect of Target of Rapamycin Kinase Inhibition on the Chlamydomonas reinhardtii Phosphoproteome: From Known Homologs to New Targets. *New Phytol.* **2019**, *221* (1), 247–260.

41. Werth, E. G.; McConnell, E. W.; Gilbert, T. S. K.; Couso Lianez, I.; Perez, C. A.; Manley, C. K.; Graves, L. M.; Umen, J. G.; Hicks, L. M. Probing the Global Kinome and Phosphoproteome in Chlamydomonas reinhardtii via Sequential Enrichment and Quantitative Proteomics. *Plant J* **2017**, *89* (2), 416–426.

42. Vizcaíno, J. A.; Côté, R. G.; Csordas, A.; Dianes, J. A.; Fabregat, A.; Foster, J. M.; Griss, J.; Alpi, E.; Birim, M.; Contell, J.; O'Kelly, G.; Schoenegger, A.; Ovelleiro, D.; Pérez-Riverol, Y.; Reisinger, F.; Ríos, D.; Wang, R.; Hermjakob, H. The Proteomics Identifications (PRIDE) Database and Associated Tools: Status in 2013. *Nucleic Acids Res.* **2013**, *41* (D1), D1063–D1069.

43. Steen, H.; Jebanathirajah, J. A.; Rush, J.; Morrice, N.; Kirschner, M. W. Phosphorylation Analysis by Mass Spectrometry: Myths, Facts, and the Consequences for Qualitative and Quantitative Measurements. *Mol. Cell. Proteomics* **2006**, *5* (1), 172–181.

44. Potel, C. M.; Lemeer, S.; Heck, A. J. R. Phosphopeptide Fragmentation and Site Localization by Mass Spectrometry: An Update. *Anal. Chem.* **2019**, *91* (1), 126–141.

45. Laskay, Ü. A.; Lobas, A. A.; Srzentić, K.; Gorshkov, M. V.; Tsybin, Y. O. Proteome Digestion Specificity Analysis for Rational Design of Extended Bottom-up and Middle-down Proteomics Experiments. *J. Proteome Res.* **2013**, *12* (12), 5558–5569.

46. Carroll, A. J. The Arabidopsis Cytosolic Ribosomal Proteome: From Form to Function. *Front. Plant Sci.* **2013**, *4*.

47. Zambrano, R.; Briones, E.; Remacha, M.; Ballesta, J. P. G. Phosphorylation of the Acidic Ribosomal P Proteins in Saccharomyces Cerevisiae: A Reappraisal. *Biochem.* **1997**, *36* (47), 14439–14446.

48. Pérez-Méndez, A.; Raúl, A.; Briones, E.; Sánchez-de-Jiménez, E. Characterization of Ribosomal Protein Phosphorylation in Maize Axes during Germination. *Plant Sci.* **1993**, *94* (1), 71–79.

49. Vard, C.; Guillot, D.; Bargis, P.; Lavergne, J.-P.; Reboud, J.-P. A Specific Role for the Phosphorylation of Mammalian Acidic Ribosomal Protein P2. *J. Biol. Chem.* **1997**, *272* (32), 20259–20262.

50. Szick, K.; Springer, M.; Bailey-Serres, J. Evolutionary Analyses of the 12-KDa Acidic Ribosomal P-Proteins Reveal a Distinct Protein of Higher Plant Ribosomes. *Proc. Natl. Acad. Sci. U.S.A.* **1998**, *95* (5), 2378–2383.

51. Bhoir, S.; Shaik, A.; Thiruvenkatam, V.; Kirubakaran, S. High Yield Bacterial Expression, Purification and Characterisation of Bioactive Human Tousled-like Kinase 1B Involved in Cancer. *Sci. Rep.* **2018**, *8* (1), 4796.

52. Harper, S.; Speicher, D. W. Purification of Proteins Fused to Glutathione S-Transferase. *Methods Mol. Biol.* **2011**, *681*, 259–280.

53. Xu, X.; Liu, X.; Nie, Z.; Pan, Y.; Guo, M.; Yao, S. Label-Free Fluorescent Detection of Protein Kinase Activity Based on the Aggregation Behavior of Unmodified Quantum Dots. *Anal. Chem.* **2011**, *83* (1), 52–59.

54. Hastie, C. J.; McLauchlan, H. J.; Cohen, P. Assay of Protein Kinases Using Radiolabeled ATP: A Protocol. *Nat. Protocols* **2006**, *1* (2), 968–971.

55. Shults, M. D.; Janes, K. A.; Lauffenburger, D. A.; Imperiali, B. A Multiplexed Homogeneous Fluorescence-Based Assay for Protein Kinase Activity in Cell Lysates. *Nat. Methods* **2005**, *2* (4), 277–284.

56. Lesaicherre, M.-L.; Uttamchandani, M.; Chen, G. Y. J.; Yao, S. Q. Antibody-Based Fluorescence Detection of Kinase Activity on a Peptide Array. *Bioorganic & Medicinal Chemistry Letters* **2002**, *12* (16), 2085–2088.

57. Wu, Z. L. Phosphatase-Coupled Universal Kinase Assay and Kinetics for First-Order-Rate Coupling Reaction. *PLoS ONE* **2011**, *6* (8), e23172-.

58. Iliuk, A. B.; Tao, W. A. Universal Non-Antibody Detection of Protein Phosphorylation Using PIMAGO. *Curr. Protoc. Chem. Biol.* **2015**, *7* (1), 17–25.

CHAPTER 7: Conclusions and Future Directions

7.1 Conclusions

Despite the known importance of TOR and its regulatory mechanisms in mammalian cells, there is still limited understanding of its role in stress signaling and nutrient response in phototrophs. The work presented in this dissertation focused on investigation of TOR pathway regulation via post-translational modifications in *Chlamydomonas*. Specifically, we focused on identifying points of regulation of various cellular processes via TOR-modulated reversible oxidation and phosphorylation, using inhibition studies combined with label-free quantitative proteomics as well as *in vitro* kinase screening assays to identify modification sites under the regulation of TOR.

With its role as a model photosynthetic organism for studying algal biological processes, there is growing interest in elucidation of *Chlamydomonas* signaling networks. Previous work in the Hicks lab established OxRAC as an indirect method of identifying reversibly oxidized cysteines[1], which was implemented to discern oxidative pathways after TOR inhibition (Chapter 2). After treating *Chlamydomonas* with the TOR inhibitor AZD8055, OxRAC was combined with label-free proteomics to identify oxidation sites regulated by TOR. We identified 401 proteins with significant changes in oxidation on 510 peptides following TOR inhibition. These differences mirrored characterized physiological changes, supporting the role of reversible oxidation in TOR regulation of TAG production, protein translation, carbohydrate catabolism and photosynthesis.

TOR is a conserved kinase and phosphorylation is one of the most prevalent regulatory PTMs, thus motivating the study of this signaling mechanism in *Chlamydomonas* and other organisms. To this end, we presented a comprehensive label-free workflow for accurate and reproducible phosphoproteomic quantification (Chapter 3). With this method, we identified 3595 phosphosites from 1775 phosphoproteins with a median CV of 21% across three technical replicates. This workflow was then applied to delineate the coordination between TOR and InsP signaling (Chapter 4). Using *vip1-1*, a mutant strain lacking the VIP1 protein responsible for InsP7 and InsP8 synthesis, phosphorylation differences were compared to wild-type *Chlamydomonas*. Rapamycin was used to assess differential phosphorylation with TOR inhibition in the two strains to investigate the intersection of TOR regulatory pathways and InsP signaling. With its hypersensitivity to rapamycin treatment, we hypothesized there would be stark differences in TOR-regulated phosphorylation between the two strains. Of the 3,986 phosphopeptides identified, 217 and 1,029 were found to be significantly changing in wild-type and *vip1-1*, respectively, with rapamycin treatment. From these data, it is clear that several crucial processes have TOR signaling points that are dependent on VIP1 including autophagy and photosynthesis.

In addition to the quantitative work investigating TOR *in vivo*, an *in vitro* screening approach was validated and implemented in an attempt to identify the direct targets of TOR. A detailed procedure is delineated for the heterologous expression and purification of kinases, creation of a *Chlamydomonas* peptide library, kinase screening, phosphopeptide enrichment, and LC-MS/MS analysis including method modification options and troubleshooting tips (Chapter 5). Validation of this platform with AtPDK showed successful identification of the corresponding known target tryptic peptide from AtPDCe1α upon screening (Chapter 6). However, screening of a CrTOR-

EKD construct did not successfully reveal any putative *in vivo* targets of TOR phosphorylation. This may be due to a lack of activity from the CrTOR-EKD construct, and more work is needed to optimize the expression and purification parameters needed to obtain a concentrated, active form of CrTOR.

Combined, the work shared in Chapters 2 and 4 highlights the importance of TOR in algal signaling and provided valuable information on the regulatory modifications under TOR control. They also lay the framework for future work including validation of identified sites and analysis of other mutant strains.

7.2 Future Directions

The label-free PTM-based work presented here takes a broad look at the PTM-level changes regulated by TOR. While this is useful to identify regulatory points and provide context to TOR signaling mechanisms, further studies are needed to validate specific sites and identify the physiological impact of these PTMs. In Chapter 2, differential reversible oxidation following TOR inhibition was quantified, but the exact oxidation modifications (*e.g.,* disulfide bond, sulfenic acid, etc.) are lost in this enrichment method. Adaptations of this method exist that allow for selective enrichment of certain reversible oxidation modifications, including *S*-nitrosylation [2,3], *S*-glutathionylation [4,5], and *S*-acylation[6] that could allow for more insight into the role of the TOR regulated sites identified in this work. Previous work has shown that there is only a small overlap between the thiols targeted by each form of reversible oxidation[7], implying that each form may have its own unique regulatory roles. Selective enrichment could provide insight into what these roles may be based on the sites identified. The methods for the selective enrichment of nitrosylation, glutathionylation and acylation would be relatively easy to incorporate into the OxRAC platform as they are resin-assisted capture-based methods similar to what was presented

here, but selective enrichments have not been developed for all reversible cysteine modifications. Additionally, the Thiopropyl Sepharose 6B resin used in this work is no longer commercially available, requiring the additional step of synthesizing the thiol resin prior to use[8].

With proteomic data, there is a trend whereby authors are required to include some orthogonal validation that supports the results obtained via mass spectrometry, most typically using a western blot approach with antibodies specific to a given protein [9]. While these experiments are relatively straight forward when assessing global proteomic changes, it can be more challenging when assessing PTM-level changes, particularly for reversible oxidation modifications. However, the use of phospho-specific antibodies has become more common for validation of phosphoproteomic studies, allowing for quantification of changes in the relative abundance of a given phosphorylation site [10,11].

As shown by the phosphoproteomic work performed in *vip1-1*, the use of mutant strains can provide insight into how TOR regulates different biological processes or how different signaling networks interact with one another. For *Chlamydomonas*, a library of insertional mutants (called the CLiP library, https://www.chlamylibrary.org/) was created[12,13] and is available through the Chlamydomonas Resource Center. The mutant strains require confirmation of gene disruption prior to use, but a number of TOR pathway-related mutants are available including insertions in LARP, S6K, and GSK3. Expansion of our investigation of TOR signaling in *Chlamydomonas* into some of these mutant strains may help to delineate the roles of the altered proteins with respect to TOR and how they help regulate biological processes.

The size and relatively low abundance of CrTOR and its related proteins, present a challenge in identifying the proteins that associated with CrTOR[14], whether it be associations to form a complex or as a target of phosphorylation. However, in addition to *in vitro* screening

methods, there are other approaches that could be helpful in the investigation of TOR's interactions. Previous work has localized CrTOR to regions adjacent to the plasmid membrane and membranous structures[15]. Implementing isolation steps where cytosolic proteins, including CrTOR, are separated from organelle proteins such as those in the chloroplast[16] or nucleus[17], could act as an enrichment and improve coverage on CrTOR and its interactors. In addition to these isolation strategies, the Hicks laboratory is currently optimizing a procedure for *in vitro* crosslinking of protein complexes using affinity-labeled MS-cleavable crosslinkers[18]. This technique would allow for proteomic digestion followed by enrichment of crosslinked peptides that still retains the crosslinker intact until cleaved in MS^2, so interactions across multiple complexes can be identified in a single sample. This crosslinking could preserve the interactions of the TORC1 complex, including potential phosphorylation targets. When combined with sample fractionation, this could allow for the enrichment and depth of coverage needed to identify CrTOR and its interactors. While the work shared in the previous chapters highlights the importance of TOR in algal signaling and provided valuable information on the regulatory modifications under TOR control, many avenues of discovery remain and can build upon the knowledge obtained in this work.

REFERENCES

1. McConnell, E. W.; Werth, E. G.; Hicks, L. M. The Phosphorylated Redox Proteome of Chlamydomonas reinhardtii: Revealing Novel Means for Regulation of Protein Structure and Function. *Redox Biol.* **2018**, *17*, 35–46.

2. Forrester, M. T.; Thompson, J. W.; Foster, M. W.; Nogueira, L.; Moseley, M. A.; Stamler, J. S. Proteomic Analysis of S-Nitrosylation and Denitrosylation by Resin-Assisted Capture. *Nat. Biotechnol.* **2009**, *27* (6), 557–559.

3. Su, D.; Shukla, A. K.; Chen, B.; Kim, J.-S.; Nakayasu, E.; Qu, Y.; Aryal, U.; Weitz, K.; Clauss, T. R. W.; Monroe, M. E.; Camp, D. G.; Bigelow, D. J.; Smith, R. D.; Kulkarni, R. N.; Qian, W.-J. Quantitative Site-Specific Reactivity Profiling of S-Nitrosylation in Mouse Skeletal Muscle Using Cysteinyl Peptide Enrichment Coupled with Mass Spectrometry. *Free Radic. Biol. Med.* **2013**, *57*, 68–78.

4. Su, D.; Gaffrey, M. J.; Guo, J.; Hatchell, K. E.; Chu, R. K.; Clauss, T. R. W.; Aldrich, J. T.; Wu, S.; Purvine, S.; Camp, D. G.; Smith, R. D.; Thrall, B. D.; Qian, W.-J. Proteomic Identification and Quantification of S-Glutathionylation in Mouse Macrophages Using Resin-Assisted Enrichment and Isobaric Labeling. *Free Radic. Biol. Med.* **2014**, *67*, 460–470.

5. Lind, C.; Gerdes, R.; Hamnell, Y.; Schuppe-Koistinen, I.; von Löwenhielm, H. B.; Holmgren, A.; Cotgreave, I. A. Identification of S-Glutathionylated Cellular Proteins during Oxidative Stress and Constitutive Metabolism by Affinity Purification and Proteomic Analysis. *Arch. Biochem. Biophys.* **2002**, *406* (2), 229–240.

6. Forrester, M. T.; Hess, D. T.; Thompson, J. W.; Hultman, R.; Moseley, M. A.; Stamler, J. S.; Casey, P. J. Site-Specific Analysis of Protein S-Acylation by Resin-Assisted Capture. *J. Lipid Res.* **2011**, *52* (2), 393–398.

7. Gould, N.; Doulias, P.-T.; Tenopoulou, M.; Raju, K.; Ischiropoulos, H. Regulation of Protein Function and Signaling by Reversible Cysteine S-Nitrosylation. *J. Biol. Chem.* **2013**, *288* (37), 26473–26479.

8. Axen, R.; Drevin, H.; Carlsson, H. Preparation of Modified Agarose Gels Containing Thiol Groups. *Acta Chem. Scan.* **1975**, *29b*, 471–474.

9. Handler, D. C.; Pascovici, D.; Mirzaei, M.; Gupta, V.; Salekdeh, G. H.; Haynes, P. A. The Art of Validating Quantitative Proteomics Data. *Proteomics* **2018**, *18* (23), 1800222.

10. Fuhrmann, J.; Subramanian, V.; Thompson, P. R. Synthesis and Use of a Phosphonate-Amidine to Generate an Anti-Phosphoarginine Specific Antibody. *Angew Chem. Int. Ed. Engl.* **2015**, *54* (49), 14715–14718.

11. Ren, S.; Yang, M.; Li, Y.; Zhang, F.; Chen, Z.; Zhang, J.; Yang, G.; Yue, Y.; Li, S.; Ge, F.; Wang, S. Global Phosphoproteomic Analysis Reveals the Involvement of

Phosphorylation in Aflatoxins Biosynthesis in the Pathogenic Fungus Aspergillus Flavus. *Sci. Rep.* **2016**, *6*.

12. Li, X.; Zhang, R.; Patena, W.; Gang, S. S.; Blum, S. R.; Ivanova, N.; Yue, R.; Robertson, J. M.; Lefebvre, P. A.; Fitz-Gibbon, S. T.; Grossman, A. R.; Jonikas, M. C. An Indexed, Mapped Mutant Library Enables Reverse Genetics Studies of Biological Processes in Chlamydomonas reinhardtii. *Plant Cell* **2016**, *28* (2), 367–387.

13. Li, X.; Patena, W.; Fauser, F.; Jinkerson, R. E.; Saroussi, S.; Meyer, M. T.; Ivanova, N.; Robertson, J. M.; Yue, R.; Zhang, R.; Vilarrasa-Blasi, J.; Wittkopp, T. M.; Ramundo, S.; Blum, S. R.; Goh, A.; Laudon, M.; Srikumar, T.; Lefebvre, P. A.; Grossman, A. R.; Jonikas, M. C. A Genome-Wide Algal Mutant Library and Functional Screen Identifies Genes Required for Eukaryotic Photosynthesis. *Nat. Genetics* **2019**, *51* (4), 627–635.

14. Zones, J. M.; Blaby, I. K.; Merchant, S. S.; Umen, J. G. High-Resolution Profiling of a Synchronized Diurnal Transcriptome from Chlamydomonas reinhardtii Reveals Continuous Cell and Metabolic Differentiation. *Plant Cell* **2015**, *27* (10), 2743–2769.

15. Díaz-Troya, S.; Florencio, F. J.; Crespo, J. L. Target of Rapamycin and LST8 Proteins Associate with Membranes from the Endoplasmic Reticulum in the Unicellular Green Alga Chlamydomonas reinhardtii. *Eukaryot. Cell* **2008**, *7* (2), 212–222.

16. Yang, M.; Jiang, J.-P.; Xie, X.; Chu, Y.-D.; Fan, Y.; Cao, X.-P.; Xue, S.; Chi, Z.-Y. Chloroplasts Isolation from Chlamydomonas reinhardtii under Nitrogen Stress. *Front. Plant Sci.* **2017**, *8*.

17. Winck, F. V.; Kwasniewski, M.; Wienkoop, S.; Mueller-Roeber, B. An Optimized Method for the Isolation of Nuclei from Chlamydomonas reinhardtii (Chlorophyceae). *J. Phycol.* **2011**, 2, 333-340.

18. Yu, C.; Kandur, W.; Kao, A.; Rychnovsky, S.; Huang, L. Developing New Isotope-Coded Mass Spectrometry-Cleavable Cross-Linkers for Elucidating Protein Structures. *Anal. Chem.* **2014**, 86(4), 2099-2106.